

MAGMATIC HISTORY OF LAVAS FROM KĪLAUEA VOLCANO, HAWAII AND
SOUTH PAGAN VOLCANO, NORTHERN MARIANA ISLANDS

A DISSERTATION SUBMITTED TO THE GRADUATE DIVISION OF THE
UNIVERSITY OF HAWAII IN PARTIAL FULFILLMENT OF THE
REQUIREMENTS FOR THE DEGREE OF

DOCTOR OF PHILOSOPHY
IN
GEOLOGY AND GEOPHYSICS
MAY 2010

By
Jared P. Marske

Thesis Committee:

Michael Garcia, Chairperson
Eric Hellebrand
Aaron Pietruszka
Scott Rowland
David Muenow

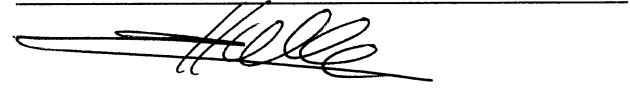
We certify that we have read this dissertation and that, in our opinion, it is satisfactory in scope and quality as a dissertation for the degree of Doctor of Philosophy in Geology and Geophysics.


DISSERTATION COMMITTEE


Chairperson









“May all your trails be crooked, winding, lonesome, dangerous, leading to the most amazing view...where something strange and more beautiful and more full of wonder than your deepest dreams waits for you.”
-Edward Abbey

“Civilization exists by geological consent, subject to change without notice.”
-Will Durant

“I choose to live, not just exist”
-James Hetfield

ACKNOWLEDGEMENTS

I want to extend my sincerest thanks to my graduate advisors Michael Garcia and Aaron Pietruszka for their guidance, support, and dedication over the past 7 years. I want to thank my Mom, Dad, and Brother Gearz for their love and support over these many years. Many thanks to my dissertation committee members Eric Hellebrand, David Muenow, and Scott Rowland for their support, enthusiasm, and constructive reviews. Much appreciation goes out to my collaborators Marc Norman, Michael Rhodes, and Frank Trusdell for their helpful contributions to my dissertation. I want to extend a big mahalo to Dale Burns, Barry Hanan, Brian Jicha, Chad Shishido, Kyle Taniguchi, Michael Vollinger, and Joan Willis for their assistance in sample preparation and analyses. Thank you to Julie Herring, Game McGimsey, Maurice Sako, Daisy Wheeler, and the CNMI hazards personnel for their assistance during the Pagan Island fieldwork. I want to acknowledge a number of institutes (Hawaiian Volcano Observatory, National Science Foundation, and the Smithsonian Institute) for their helpful assistance. I am grateful for my officemates and husband, Wendy Stovall, Rebecca Carey, Carrie Brugger, Heidi Hansen, Anette von der Handt, Lisa Petrochilos, and Owen Neill for helping me stay sane over the years. I want to extend a special thank you to Angelo Bernardino, Adam Johnson, Francois Paquay, and Thomas Shea (a.k.a. The Horsemen) with whom, I have shared some of the best moments of my life. Finally, my warmest aloha goes out to all of my fellow graduate students who have made a positive impact on me both personally and professionally. You guys rock!

ABSTRACT

Petrologic and geochemical time-series studies of active volcanoes yield valuable insight into the crustal processes (e.g., crystal fractionation and accumulation, and crustal assimilation) and mantle source and melting variations (e.g., mantle source heterogeneity, and melt production, extraction, and transportation). This dissertation is composed of three main projects related to the magmatic history of lavas from Kīlauea Volcano, Hawai'i and South Pagan Volcano, Northern Mariana Islands. These volcanoes are highly active providing an excellent opportunity to investigate the magmatic processes that operate in both intra-plate (Kīlauea) and island-arc (South Pagan) settings over timescales of hours to thousands of years. Here, I present a comprehensive petrologic evaluation of: (1) 1998-2005 Pu'u 'Ō'ō lavas from Kīlauea's east rift zone (Chapter 1); (2) Quaternary to Holocene lavas from two volcanoes in South Pagan (Chapter 2); and (3) Historical (1790-1980 A.D.) Kīlauea rift lavas (Chapter 3) using Pb, Sr, and Nd isotope ratios, major and trace element abundances, olivine compositions, and petrographic data. Chapter 1 discusses the compositional evolution of 1998-2005 Pu'u 'Ō'ō lavas and the implications for the nature and scale of mantle source heterogeneity within the Hawaiian plume. Chapter 2 examines the chemistry of stratigraphically-controlled southern Pagan lavas to assess and identify the slab contributions (fluid and sediment components) involved in arc magma genesis, determine the nature and extent of mantle partial melting, and evaluate crustal magmatic processes beneath Mariana volcanoes. Chapter 3 investigates the temporal geochemical variations of historical Kīlauea rift lavas to examine the petrogenetic relationship between summit and rift parental magmas, evaluate the magmatic link between the summit and rift zones, and determine the timescales of magma transport, mixing, and differentiation processes within the shallow plumbing system.

TABLE OF CONTENTS

ACKNOWLEDGEMENTS.....	i
ABSTRACT.....	v
LIST OF TABLES.....	viii
LIST OF FIGURES.....	ix

Chapter 1: Geochemical Variations during Kīlauea 's Pu‘u ‘Ō‘ō Eruption reveal a fine-scale mixture of mantle heterogeneities within the Hawaiian Plume

1.1 Abstract.....	1
1.2 Introduction.....	2
1.3 Results.....	6
1.3.1 Overview of the Pu‘u ‘Ō‘ō eruption.....	6
1.3.2 Petrography.....	7
1.3.3 Olivine composition.....	9
1.3.4 Whole-rock analytical methods.....	12
1.3.5 Geochemistry of 1998-2005 Pu‘u ‘Ō‘ō lavas.....	26
1.4 Discussion.....	29
1.4.1 Crustal magmatic processes during the eruption.....	29
1.4.2 Temporal compositional variations.....	30
1.4.3 Pu‘u ‘Ō‘ō source characteristics.....	33
1.4.3.1 A lithospheric source component for Pu‘u ‘Ō‘ō lavas?.....	33
1.4.3.2 A third mantle source for the Pu‘u ‘Ō‘ō eruption.....	35
1.4.3.3 A pyroxenite source for Pu‘u ‘Ō‘ō lavas?.....	39
1.4.4 Small-scale mantle heterogeneity.....	40
1.4.5 Chemical structure of the Hawaiian plume.....	42
1.5 Conclusions.....	45

Chapter 2: Geochemistry of southern Pagan Island lavas, Mariana Arc: The role of subduction zone processes

2.1 Abstract.....	47
2.2 Introduction.....	48
2.3 Results.....	51
2.3.1 Pagan geology and sampling.....	51
2.3.2 Analytical methods.....	54
2.3.3 Major element chemistry.....	64
2.3.4 Trace element chemistry.....	64
2.3.5 Pb, Sr, and Nd isotope ratio variations.....	67
2.4 Discussion.....	68
2.4.1 Magmatic differentiation.....	68
2.4.2 The role of slab contributions.....	71
2.4.2.1 Aqueous fluid component.....	71
2.4.2.2 Sediment component.....	75
2.4.3 Mantle source and melting model for Mariana lavas.....	80
2.4.4 Dynamics of the partial melting processes beneath Pagan.....	89
2.5 Conclusions.....	91

Chapter 3: Evolution of Kīlauea Volcano's shallow magmatic plumbing system: a geochemical perspective from historical rift lavas (1790-1980 A.D.)

3.1 Abstract.....	93
3.2 Introduction.....	94
3.3 Results.....	102
3.3.1 Overview of Kīlauea’s historical rift zone eruptions.....	102
3.3.2 Analytical methods	104
3.3.3 Sampling	115
3.3.4 Whole-rock geochemistry.....	116
3.3.5 Temporal and spatial compositional variations	119
3.4 Discussion.....	124
3.4.1 Magma mixing vs. crystal fractionation in rift zone magmas	124
3.4.2 Magmatic plumbing network beneath Kīlauea volcano	127
3.4.2.1 1790-1923 eruptive interval.....	128
3.4.2.2 1955-1968 eruptive interval.....	133
3.4.2.3 1969-1974 eruptive interval.....	140
3.4.2.4 1974-1979 eruptive interval.....	144
3.5 Summary of magmatic processes in Kīlauea’s rift zones	146
APPENDIX.....	148
A.1 Individual Sr isotope ratios for Pu‘u ‘Ō‘ō lavas	148
A.2 Pagan sample locations	149
A.3 Kīlauea rift sample locations.....	150
A.4 Kīlauea rift sample labels.....	151
A.5 1919-20 Mauna Iki sample locations.....	151
REFERENCES	152

LIST OF TABLES

Table 1.1 Modal mineralogy of representative 1998-2005 Pu‘u ‘Ō‘ō lavas	8
Table 1.2 Microprobe analyses of olivine cores from 1998-2005 Pu‘u ‘Ō‘ō lavas.....	10
Table 1.3 Whole-rock XRF analyses of 1998-2005 Pu‘u ‘Ō‘ō lavas.....	13
Table 1.4 ICP-MS analyses of 1998-2005 Pu‘u ‘Ō‘ō lavas.....	22
Table 1.5 Pb, Sr and Nd isotope data for Pu‘u ‘Ō‘ō lavas.....	25
Table 2.1 Whole-rock XRF analyses of southern Pagan lavas.....	56
Table 2.2 ICP-MS trace element analyses of southern Pagan lavas.....	61
Table 2.3 Pb, Sr, and Nd isotopic data for southern Pagan lavas	63
Table 2.4 Mineral/melt partition coefficients for the mass-balance model calculations..	73
Table 2.5 Representative results of the REE melting model for Mariana lavas.....	82
Table 2.6 Summary of REE melt model results..	86
Table 3.1 Whole-rock XRF analyses of historical Kīlauea rift lavas.....	105
Table 3.2 ICP-MS trace element analyses of Kīlauea rift lavas..	111
Table 3.3 Pb, Sr, and Nd isotopic data for Kīlauea rift lavas..	114

LIST OF FIGURES

Figure 1.1 Location map of the Pu‘u ‘Ō‘ō eruption flow field.....	3
Figure 1.2 Olivine chemistry for 1998-2005 lavas.....	11
Figure 1.3 Whole-rock MgO variation diagrams for Pu‘u ‘Ō‘ō lavas.....	27
Figure 1.4 Trace element variation diagrams for Pu‘u ‘Ō‘ō lavas.....	28
Figure 1.5 Temporal geochemical variations during the Pu‘u ‘Ō‘ō eruption.....	31
Figure 1.6 $^{206}\text{Pb}/^{204}\text{Pb}$ vs. $^{87}\text{Sr}/^{86}\text{Sr}$ isotope ratios for Pu‘u ‘Ō‘ō lavas.....	34
Figure 1.7 Ba/Ce vs. $^{87}\text{Sr}/^{86}\text{Sr}$ for Pu‘u ‘Ō‘ō lavas.....	37
Figure 1.8 $^{206}\text{Pb}/^{204}\text{Pb}$ and $^{87}\text{Sr}/^{86}\text{Sr}$ vs. MgO-normalized SiO_2 contents for Pu‘u ‘Ō‘ō lavas.....	41
Figure 1.9 Hypothetical cross-section of the lithosphere and the upper part of the Hawaiian plume beneath Kīlauea and Mauna Loa.....	44
Figure 2.1 Location map of the Northern Mariana Islands.....	49
Figure 2.2 Simplified geologic map of southern Pagan Island.....	53
Figure 2.3 Whole-rock MgO variation diagrams for Pagan lavas.....	65
Figure 2.4 Normalized trace element patterns for Pagan lavas.....	66
Figure 2.5 Trace element ratio-ratio plots for Pagan lavas.....	69
Figure 2.6 Temporal geochemical variations of South Pagan and CVR lavas.....	72
Figure 2.7 Plots of $^{206}\text{Pb}/^{204}\text{Pb}$ vs. $^{208}\text{Pb}/^{204}\text{Pb}$ and $^{143}\text{Nd}/^{144}\text{Nd}$ ratios for Pagan lavas.....	74
Figure 2.8 SiO_2 vs. CaO/ Al_2O_3 , Sr/La, TiO ₂ /Y, and Eu/Eu* for Mariana lavas.....	76
Figure 2.9 Sc/Y vs. CaO/ Al_2O_3 for South Pagan, and CVR lavas.....	77
Figure 2.10 Nb/Zr vs. $^{208}\text{Pb}/^{204}\text{Pb}$ and Th/Nb vs. $^{143}\text{Nd}/^{144}\text{Nd}$ for Pagan lavas.....	79
Figure 2.11 Mass-balance REE melting model results for a representative South Pagan sample.....	85
Figure 2.12 SiO_2 vs. the estimated amount of crystallization and accumulation for Mariana lavas.....	88
Figure 2.13 Incompatible trace element ratios vs. the amount of sediment addition to the mantle source and the degree of partial melting for selected Mariana arc lavas.....	90
Figure 3.1 Location map of historical SWRZ, ERZ, and summit eruptions.....	95
Figure 3.2 Graphic summary of the historical eruptive activity at Kīlauea volcano.....	98
Figure 3.3 Temporal variation in Nb/Y and $^{206}\text{Pb}/^{204}\text{Pb}$ ratios for Kīlauea historical rift and summit lavas.....	100
Figure 3.4 Whole-rock MgO variation diagrams for historical Kīlauea rift and summit lavas.....	117
Figure 3.5 Trace-element geochemical variations for historical Kīlauea rift and summit lavas.....	120
Figure 3.6 Plots of $^{206}\text{Pb}/^{204}\text{Pb}$ vs. $^{208}\text{Pb}/^{204}\text{Pb}$ and $^{87}\text{Sr}/^{86}\text{Sr}$ ratios for historical Kīlauea rift and summit lavas.....	121
Figure 3.7 Temporal geochemical variations for Kīlauea rift and summit lavas between 1968 and 1983.....	125
Figure 3.8 Plots of $^{206}\text{Pb}/^{204}\text{Pb}$ vs. $^{208}\text{Pb}/^{204}\text{Pb}$ ratios for historical Kīlauea rift and summit lavas.....	131
Figure 3.9 Hypothetical cross-section of Kīlauea’s upper magmatic plumbing system.....	138

CHAPTER 1
GEOCHEMICAL VARIATIONS DURING KĪLAUEA'S PU'U 'Ō'Ō ERUPTION
REVEAL A FINE-SCALE MIXTURE OF MANTLE HETEROGENEITIES WITHIN
THE HAWAIIAN PLUME

1.1 Abstract

Long-term geochemical monitoring of lavas from the ongoing 25-year-old Pu'ū 'Ō'Ō eruption allows us to probe the crustal and mantle magmatic processes beneath Kīlauea volcano in unparalleled detail. Here we present new Pb, Sr, and Nd isotope ratios, major and trace element abundances, olivine compositions, and petrographic data for Pu'ū 'Ō'Ō lavas erupted from 1998-2005. Olivine fractionation and accumulation are important crustal processes for the eruption, with minor clinopyroxene fractionation observed in the most recent lavas. Small, yet systematic variations in $^{87}\text{Sr}/^{86}\text{Sr}$ and incompatible trace element ratios, and MgO-normalized major element abundances document rapid changes in the parental magma composition delivered to Pu'ū 'Ō'Ō. Recent (1998-2003) lavas display a systematic temporal evolution towards an intermediate area between the compositional fields of historical Kīlauea and Mauna Loa lavas. At least three distinct mantle source components are required to explain the overall isotopic and chemical variability of Pu'ū 'Ō'Ō lavas. Two of these source components observed in pre-1998 Pu'ū 'Ō'Ō lavas have similar Pb, Sr, and Nd isotope ratios, although one underwent a recent (<8 ka) small-degree melting event and became depleted in incompatible trace elements. This recently depleted component was an increasingly important source for lavas erupted between 1985-1998. The third component is a hybrid mixture of nearly equal portions Kīlauea- and Mauna Loa-like mantle source compositions. It was progressively tapped in greater amounts from 1998 to 2003 and then subsequently decreased. The increasing importance of the hybrid source can be explained if melt pathways migrated from an area within Kīlauea's typical melting region (important for the 1985-

1998 lavas) towards Mauna Loa, where a similar proportion of Kīlauea- and Mauna Loa-like mantle components might exist. The Pu‘u ‘Ō‘ō data suggest that Kea and Loa mantle components are distributed on a fine-scale within the Hawaiian plume, and both are present beneath Kīlauea volcano. Based on the geochemical and isotopic variations during the Pu‘u ‘Ō‘ō eruption, the estimated volume for Kīlauea and Mauna Loa compositional heterogeneities is <10-35 km³.

1.2 Introduction

Time-series studies of geochemical variations during long-lived eruptions or eruptive sequences provide valuable insights into the magmatic processes within active volcanoes (e.g., Arenal, Costa Rica, Bolge et al., 2006; Etna, Italy, Rizzo et al., 2006; Grímsvötn, Iceland, Sigmarsson et al., 1992; Parícutin, Mexico, Wilcox, 1954; McBirney et al., 1987; Piton de la Fournaise, Réunion Island, Vlastelic et al., 2005). These studies provide a detailed view of the crustal- and mantle-related magmatic processes occurring on short time scales (days to years). Kīlauea volcano, located on the island of Hawai‘i (Fig. 1.1), has frequently erupted (averaging ~25 million cubic meters per year; Macdonald et al., 1983; Sutton et al., 2003) during the past 200 years making it an ideal location to investigate temporal variations in lava chemistry that are related to changes in mantle source compositions and melting conditions within the Hawaiian plume.

Previous seismic and petrologic studies suggest that Kīlauea magmas originate from partial melting at mantle depths >60-80 km within the upper Hawaiian plume (e.g., Eaton and Murata, 1960; Watson and McKenzie, 1991; Tilling and Dvorak, 1993). Rapid melt extraction from the mantle source region into chemically isolated channels (e.g., McKenzie, 1985; Williams and Gill, 1989) is probably the dominant melt transport mechanism beneath Kīlauea because it provides a relatively large amount of melt for sustained, high volume eruptions such as Pu‘u ‘Ō‘ō (Pietruszka et al., 2006). After accumulating, these melts are thought to ascend through a primary

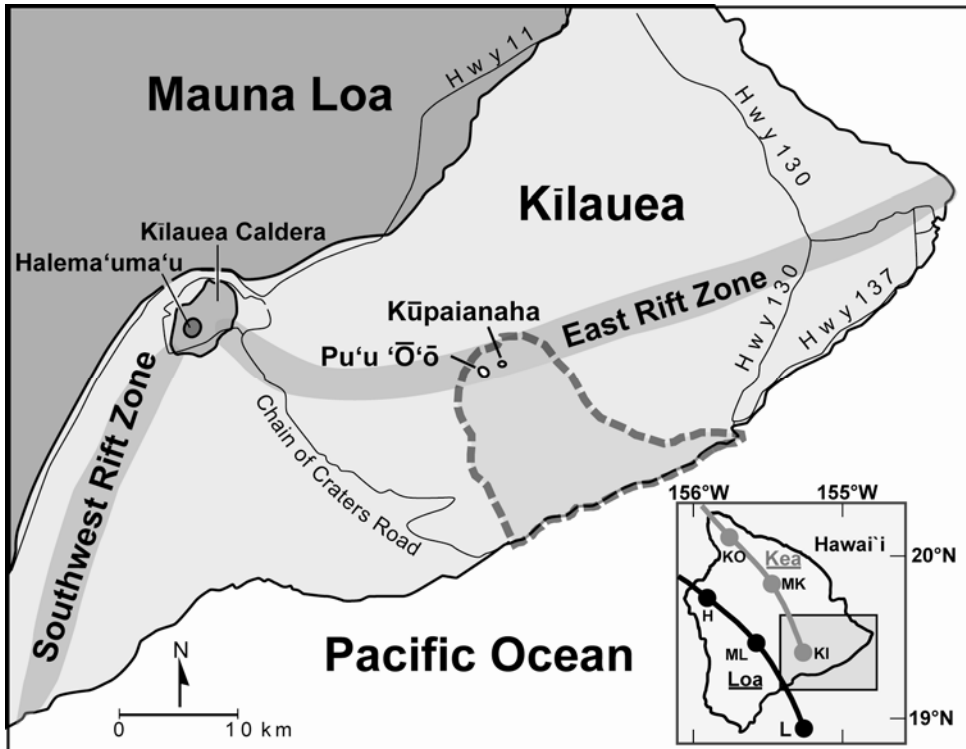


Fig. 1.1 Location map of the Pu'u Ō'ō eruption flow field (dashed outline) on the East Rift Zone of Kīlauea volcano, Hawai'i (after Mittelstaedt and Garcia, 2007). Lava erupted from two primary vents: the Pu'u Ō'ō cone between 1983-1986 and 1992-2007 (episodes 4-47, 50-53, and 55), and at Kūpaianaha between 1986-1992 (episode 48 and 49). The inset map shows the distribution of Loa (H: Hualālai, ML: Mauna Loa, L: Lō'ihī) and Kea (KO: Kohala, MK: Mauna Kea, KI: Kīlauea) volcanoes.

conduit delivering magma to Kīlauea's shallow (2-6 km deep) magma reservoir, and may subsequently erupt in the summit caldera or feed the volcano's two rift zones (e.g., Tilling and Dvorak, 1993; Wright and Klein, 2006).

The Pu'u Ō'ō eruption is the longest sustained (25+ years) and most voluminous (~3 km³ erupted lava) historical eruption of Kīlauea volcano (Garcia et al., 2000; Heliker and Mattox, 2003). Pu'u Ō'ō magmas are thought to partially bypass the summit reservoir (based on the rapid variations in incompatible trace element ratios for Pu'u Ō'ō lavas compared with Kīlauea summit lavas) before intruding Kīlauea's East Rift Zone to feed a shallow (<3 km depth) magma reservoir system beneath the Pu'u Ō'ō cone (Garcia et al., 1996; Shamberger and Garcia, 2006). Since the start of the eruption in January 1983, there have been small but systematic variations in the Pb, Sr and O isotope ratios and major and trace element abundances of Pu'u Ō'ō lavas. These fluctuations provide an unprecedented opportunity to document the crustal processes (e.g., crystal fractionation and accumulation, and crustal assimilation) and mantle source and melting variations (e.g., mantle source heterogeneity, and melt production, extraction, and transportation) within the Hawaiian plume on a time scale of months to years (e.g., Garcia et al., 1989, 1992, 1996, 1998, 2000; Putirka, 1997; Thornber, 2001, 2003; Pietruszka et al., 2006).

Two different length scales of mantle heterogeneity within the Hawaiian plume have been recognized based on the distinct isotopic variations of individual volcanoes. Large-scale heterogeneity has been proposed based on the persistent intershield geochemical differences of Hawaiian volcanoes over tens to hundreds of thousands of years (e.g., Frey and Rhodes, 1993; Chen et al., 1996), and the long-term differences in Pb isotope ratios (Tatsumoto, 1978; Abouchami et al., 2005) along two NW-trending loci of volcanoes (Fig. 1.1): northeastern 'Kea' trend (e.g., Kīlauea) and southwestern 'Loa' trend (e.g., Mauna Loa). The Kea end member is defined by higher ²⁰⁶Pb/²⁰⁴Pb and ¹⁴³Nd/¹⁴⁴Nd and lower ⁸⁷Sr/⁸⁶Sr and is predominately observed in lavas from Kīlauea, Mauna Kea, West Maui, Haleakalā, and East Moloka'i volcanoes (Stolper

et al., 1996; DePaolo et al., 2001; Blichert-Toft et al., 2003; Eisele et al., 2003). The Loa end member is defined by higher $^{87}\text{Sr}/^{86}\text{Sr}$ and lower $^{143}\text{Nd}/^{144}\text{Nd}$ and $^{206}\text{Pb}/^{204}\text{Pb}$ and is mostly observed in lavas from Mauna Loa, Hualālai, Lana‘i, Kaho‘olawe, West Moloka‘i and Ko‘olau volcanoes (Hauri, 1996; Lassiter and Hauri, 1998; Abouchami et al., 2005; Fekiacova et al., 2007; Xu et al., 2007).

Individual volcanoes (e.g., Kīlauea and Mauna Loa) also record isotopic variations over shorter time scales (years to centuries) that are attributed to partial melting of small-scale compositional heterogeneities within the plume (e.g., Frey and Rhodes, 1993; Kurz et al., 1995; Rhodes and Hart, 1995; Pietruszka and Garcia, 1999a; Marske et al., 2007). Estimates for the size and shape of small-scale heterogeneities range from vertical streaks that are several tens to hundreds of kilometers long (e.g., Farnetani et al., 2002; Eisele et al., 2003; Abouchami et al., 2005) to heterogeneous blobs set in a compositionally distinct matrix (e.g., Frey and Rhodes, 1993; Rhodes and Hart, 1995; Blichert-Toft et al., 2003). A range of vertical length scales for these compositional heterogeneities from 6.5-160 km (Blichert-Toft et al., 2003) to 0.06-12 km (Kurz et al., 2004) have been estimated based on isotopic fluctuations recorded in 550-180 ka Mauna Kea lavas. In contrast, the presence of a pancake-shaped heterogeneity (>18 km wide and <5-10 km thick) has been inferred based on systematic Pb, Sr and Nd isotopic fluctuations in young prehistoric (<2.6 ka) Kīlauea and Mauna Loa lavas (Marske et al., 2007). Unlike these previous studies that document the size of mantle heterogeneities on a scale of hundreds to thousands of years, the Pu‘u ‘Ō‘ō eruption offers an opportunity to probe the finer-scale compositional variations related to distinctive mantle sources on very short time scales (months to years). Here we provide a comprehensive petrologic evaluation of the most recent (1998-2005) Pu‘u ‘Ō‘ō lavas using petrography, olivine and whole-rock chemistry, and Pb, Sr, and Nd isotope ratios, and discuss the compositional evolution of these lavas and their implications for the nature and scale of mantle source heterogeneity within the Hawaiian plume.

1.3 Results

1.3.1 Overview of the Pu‘u ‘Ō‘ō eruption

The onset of the eruption (episode 1) in January 1983, began with intermittent fire fountaining along an 8-km-long fissure system in the middle of Kīlauea’s East Rift Zone (Wolfe et al., 1987; Garcia et al., 1989; Fig. 1.1). During episodes 2 and 3, activity was localized to a 1 km section of the fissure system. A central vent, Pu‘u ‘Ō‘ō, was the focus of effusion for episodes 4-47 (June 1983-June 1986). These episodes were generally short-lived (5-100 h) with variable (10-400 m) lava fountaining heights (Garcia et al., 1992; Heliker and Mattox, 2003). In July 1986, the primary vent migrated 3 km downrift from the Pu‘u ‘Ō‘ō cone to the Kūpaianaha lava shield (Fig. 1.1). This shift coincided with a change in eruptive style from episodic, fire-fountaining events to nearly continuous and gentle effusion (Garcia et al., 1996). Kūpaianaha was the site of nearly continuous lava effusion (episode 48 and 49) until February 1992 when activity shifted back to Pu‘u ‘Ō‘ō. From February 1992 to January 1997 (episodes 50-53), a shield 60 m high and 1.3 km in diameter was built at Pu‘u ‘Ō‘ō (Heliker et al., 1998). On January 29, 1997, the lava lake inside the Pu‘u ‘Ō‘ō shield suddenly drained, and a 22-hour eruption (episode 54) occurred 2-4 km uprift (Harris et al., 1997; Thornber et al., 2003).

Following a 24-day hiatus, episode 55 began, marking the longest (1997-2007) and most voluminous ($\sim 1.6 \text{ km}^3$) effusive interval for this eruption. Episode 55 activity displayed nearly continuous eruption of lava (except for infrequent 1-4 day pauses) from vents on the south and west flanks of the Pu‘u ‘Ō‘ō cone (Garcia et al., 2000; Heliker and Mattox, 2003). The most significant event during episode 55 occurred on September 12, 1999 when magma-induced earthquake swarms and surficial deflation of the Pu‘u ‘Ō‘ō cone were followed by intrusion of magma into the upper East Rift Zone of Kīlauea (Nakata et al., 2000). An 11-day hiatus followed as magma supplying the Pu‘u ‘Ō‘ō cone was temporally diverted to the upper rift zone. Episode 55 ended after a one day eruption (episode 56) that occurred ~ 6 km uprift of the Pu‘u ‘Ō‘ō cone

in mid-June 2007 (Poland et al., 2008). Following a two week pause, lava effusion resumed in early July 2007, and as of April 2008, lava continues to erupt from a vent 2 km downrift of the Pu‘u ‘Ō‘ō cone.

1.3.2 Petrography

A majority of samples studied here were collected in a molten state and most were quenched in water. The sample label (e.g., 17-Aug-01) is the date it was collected, and in nearly all cases, within a day of when it was erupted. The vast majority of the 1998-2005 Pu‘u ‘Ō‘ō lavas petrographically studied are glassy, strongly vesicular, friable and aphyric to moderately olivine-phyric (<3 vol. % phenocrysts; Table 1.1). Olivine is almost always the only phenocryst in these samples and is usually small (~0.5-1 mm in diameter), euhedral and undeformed with spinel and glass inclusions. Olivine is somewhat less common (~1 vol. %) in the 1998-2005 lavas compared to those from the preceding six years of eruptive activity but similar in abundance to lavas erupted from the Kūpaianaha vent (1986-1992; Garcia et al., 1996). The total olivine abundance (phenocrysts and microphenocrysts) generally correlates with whole-rock MgO content, although it can vary ~4 vol. % for a given MgO (Table 1.1). Clinopyroxene phenocrysts are rare in the 1998-2005 Pu‘u ‘Ō‘ō lavas, yet microphenocrysts of clinopyroxene (up to 3 vol. %) are present in almost all of these lavas (Table 1.1). In contrast, clinopyroxene is absent or rare (<1 vol. %) in earlier Pu‘u ‘Ō‘ō lavas (except in the more evolved 1983 lavas; Garcia et al., 1989).

Clinopyroxene crystals are small (0.1-0.3 mm) and commonly display sector zoning. Plagioclase microphenocrysts occur in most of the 1998-2005 Pu‘u ‘Ō‘ō lavas, although they are usually rare (<1 vol. %; Table 1.1) and small (0.1-0.2 mm wide laths). Plagioclase is less common in earlier erupted Pu‘u ‘Ō‘ō lavas (except for the lavas from episodes 1-10 and 54, which were affected by magma mixing in Kīlauea’s East Rift Zone (Garcia et al., 1989, 1992, 2000; Thornber et al., 2003). The groundmass of the 1998-2005 lavas generally consists of honey-brown glass or black

Table 1.1 Modal mineralogy of representative 1998-2005 Pu'u 'Ō'ō lavas. All values are in vol. % and are based on 500 point counts/sample, without vesicles. Phenocrysts (ph) are >0.5 mm long; microphenocrysts (mph) are 0.1-0.5 mm long. Matrix contains glass and crystals <0.1 mm long.

Sample	Whole-rock	Olivine		Clinopyroxene		Plagioclase	Matrix
	MgO (wt. %)	ph	mph	ph	mph	mph	
21-Jan-98	7.96	0.6	3.6	0.0	0.0	0.0	95.8
13-Feb-99	7.41	0.6	3.4	0.0	1.4	0.2	94.4
19-Jun-99	8.17	0.9	2.5	0.0	0.1	0.0	96.5
11-Aug-99	6.85	0.0	2.0	0.0	0.4	0.6	97.0
27-Oct-99	7.98	0.6	3.8	0.0	0.2	0.4	95.0
4-Jan-00	9.54	3.0	3.2	0.0	1.2	0.8	91.8
21-Jun-00	7.23	2.5	0.6	0.0	1.7	0.6	94.6
4-Aug-00	8.29	2.8	2.6	0.0	1.4	1.0	92.2
8-Apr-01	7.93	1.9	3.7	<0.1	2.8	0.2	91.4
29-Sep-01	6.69	0.0	1.9	0.0	2.0	1.1	95.0
12-Apr-02	8.03	2.8	3.0	0.0	3.0	0.4	90.8
20-Aug-02	8.11	1.6	2.8	0.6	3.0	0.2	91.6
21-Nov-02	7.39	0.6	1.0	0.0	<0.1	0.0	98.4
12-Mar-03	7.53	2.4	2.8	0.0	1.0	0.2	93.6
29-Aug-03	6.87	0.6	1.6	<0.1	0.8	0.2	96.8
15-Jan-04	7.18	1.6	0.6	<0.1	3.0	0.6	94.2
23-Jul-04	6.97	0.6	0.6	0.0	3.0	1.4	94.4
31-Oct-04	6.90	1.8	3.0	0.0	1.4	0.8	93.0
6-Feb-05	7.03	0.8	2.0	0.0	0.8	0.8	95.6
23-Jun-05	6.85	1.0	1.6	0.0	0.4	0.2	96.8

cryptocrystalline material with microlites (<0.1 mm) of plagioclase, clinopyroxene, olivine, and spinel.

1.3.3 Olivine composition

A five spectrometer Cameca SX-50 electron microprobe with SAMx automation was used for the olivine analyses at the University of Hawai'i using techniques described by Garcia et al. (2000). Olivine compositions (Table 1.2) were determined for 175 olivine crystals from 19 lavas erupted between 1998-2005 that span a wide compositional range (whole-rock MgO contents of 6.7 to 9.5 wt. %). All of the analyzed olivine crystals are unzoned or normally zoned with up to 3% forsterite (Fo) variation from core to rim. The forsterite content of the olivine cores range from 76.5 to 86.0% (Fig. 1.2) with phenocrysts and microphenocrysts overlapping in composition. The average Fo content is ~81.0%, which is similar to lavas from the previous six years and somewhat lower than olivines in the earlier lavas (1986-1992) erupted from the Kūpaianaha vent (~82.5% on average; Garcia et al., 1996, 2000). The NiO and CaO contents in the olivines are moderate (Table 1.2) indicating crystallization at crustal depths from somewhat fractionated parental magmas (e.g., Garcia et al., 2002).

Olivines in the 1998-2005 lavas typically have Fo compositions that are in equilibrium with their whole-rock Mg#, particularly for lavas with lower Mg# (<58; Fig. 1.2). Most samples with Mg# >58 have olivine compositions that plot below the equilibrium field, especially the sample with the highest Mg# (4-Aug-00; Fig. 1.2). The higher Mg# lavas probably accumulated olivine, which is consistent with their higher abundance of this mineral (e.g., 4-Aug-00 contains the highest olivine content; Table 1.1). The highest measured forsterite content of olivine within the 1998-2005 lavas (Fo₈₆) occurs in a sample with an intermediate Mg#, 21-Jan-98 (Table 1.2). This olivine, like all of the other crystals, shows no signs of deformation. Thus, it is probably

Table 1.2 Microprobe analyses of olivine cores from 1998-2005 Pu'u 'Ō'ō lavas. Values are the average of three spot analyses per sample. All oxides concentrations are in wt. %.

Sample	SiO ₂	FeO	NiO	MgO	CaO	Total	Fo	Mg#
21-Jan-98	38.89	17.14	0.22	42.46	0.26	98.98	81.5	58.9
	39.16	16.73	0.21	43.01	0.25	99.37	82.1	
	39.74	13.28	0.35	45.64	0.20	99.22	86.0	
13-Feb-99	39.36	18.03	0.18	41.86	0.27	99.64	80.5	57.3
	39.11	16.76	0.22	43.26	0.24	99.59	82.1	
	39.64	15.94	0.26	43.88	0.25	99.96	83.1	
19-Jun-99	39.28	17.22	0.19	42.85	0.25	99.48	81.6	59.4
	39.53	16.96	0.22	42.97	0.26	99.95	81.9	
11-Aug-99	39.13	17.51	0.19	42.40	0.26	99.49	81.2	55.6
	39.27	17.13	0.22	42.79	0.26	99.67	81.7	
	39.31	16.19	0.21	43.45	0.22	99.38	82.7	
4-Jan-00	38.78	17.82	0.16	42.29	0.28	99.34	80.9	62.6
	38.86	17.50	0.21	42.57	0.28	99.42	81.3	
	39.04	17.29	0.19	42.92	0.27	99.72	81.6	
21-Jun-00	38.92	17.82	0.16	42.33	-	99.51	80.9	56.9
	38.95	17.59	0.17	42.55	-	99.51	81.2	
	39.29	17.24	0.18	43.08	-	100.04	81.7	
4-Aug-00	38.72	17.42	0.18	42.47	0.30	99.10	81.3	59.8
	38.69	17.37	0.16	42.59	0.27	99.07	81.4	
8-Apr-01	38.55	19.41	0.16	41.26	0.25	99.64	79.1	58.8
	38.68	18.34	0.16	42.08	0.26	99.53	80.4	
	38.76	17.12	0.20	43.24	0.25	99.57	81.8	
29-Sep-01	38.43	21.55	0.12	39.44	-	99.83	76.5	54.7
	38.88	18.68	0.14	41.62	-	99.61	79.9	
	39.05	17.81	0.18	42.55	-	99.87	81.0	
12-Apr-02	38.87	18.02	0.18	42.26	0.25	99.57	80.7	59.0
	39.10	17.28	0.18	42.75	0.23	99.54	81.5	
	39.45	15.57	0.23	44.04	0.22	99.51	83.4	
20-Aug-02	39.25	17.95	0.23	42.42	0.27	100.13	80.8	59.1
	39.11	17.68	0.20	42.68	0.26	99.94	81.1	
	39.42	16.35	0.20	43.57	0.25	99.79	82.6	
21-Nov-02	39.11	17.99	0.19	42.54	0.25	100.09	80.8	57.1
	39.05	17.43	0.20	42.67	0.27	99.62	81.4	
	39.14	16.86	0.21	43.32	0.25	99.78	82.1	
12-Mar-03	39.26	17.60	0.21	42.35	0.26	99.69	81.1	57.5
	39.08	17.38	0.17	42.27	0.26	99.15	81.3	
	39.02	17.14	0.21	42.46	0.26	99.09	81.5	
29-Aug-03	40.06	17.95	0.16	40.89	0.34	99.41	80.2	55.3
	39.77	17.46	0.19	41.62	0.27	99.30	80.9	
	39.92	17.33	0.14	41.83	0.25	99.46	81.1	
23-Jul-04	39.70	18.44	0.18	41.44	0.26	100.02	80.0	55.9
	39.79	17.80	0.22	41.96	0.26	100.04	80.8	
	39.43	17.45	0.20	41.89	0.25	99.22	81.1	
31-Oct-04	38.35	18.83	0.19	41.52	0.29	99.17	79.7	55.6
	38.67	18.68	0.23	41.73	0.30	99.61	79.9	
6-Feb-05	38.18	19.26	0.19	41.51	0.33	99.48	79.3	56.1
	38.94	18.64	0.17	41.59	0.27	99.62	79.9	
	39.16	17.07	0.28	42.95	0.27	99.73	81.8	
23-Jun-05	38.50	19.03	0.23	41.12	0.30	99.19	79.4	55.4
	38.85	18.08	0.23	42.00	0.28	99.45	80.5	
	38.92	16.94	0.28	42.95	0.27	99.36	81.9	

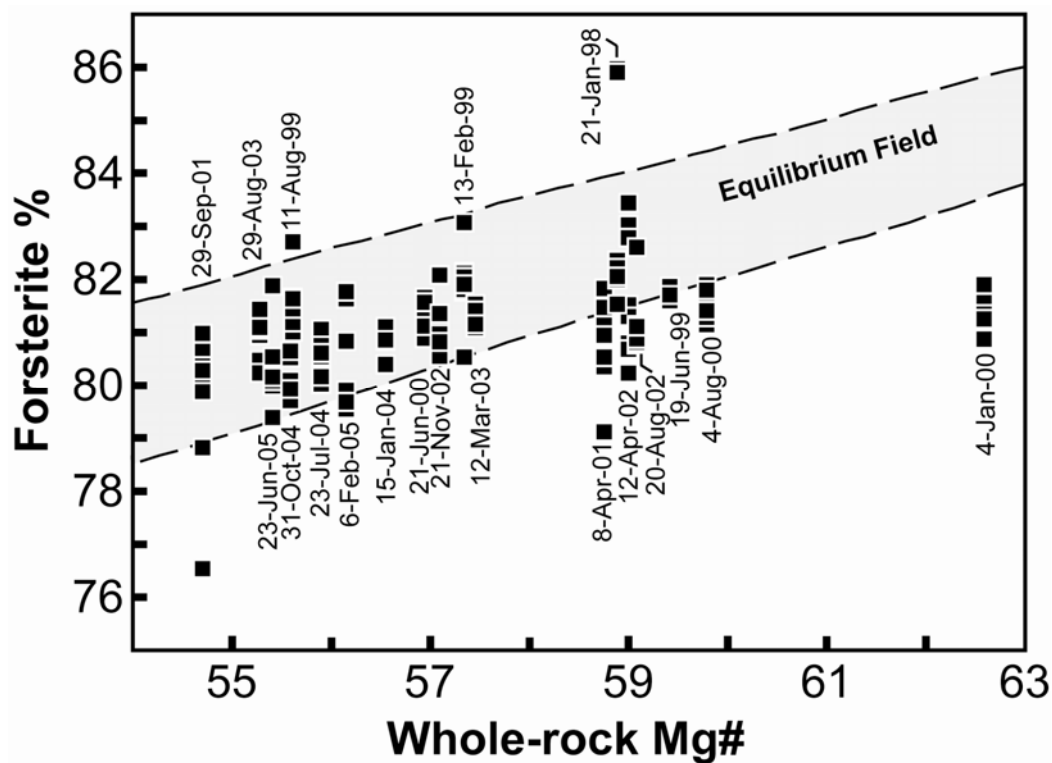


Fig. 1.2 Olivine chemistry for 1998-2005 lavas. Representative whole-rock Mg# $[(\text{Mg}/\text{Mg} + \text{Fe}^{2+}) * 100]$ plotted against olivine core forsterite content (Fo %). The Mg# is calculated assuming 90% of the total iron is Fe^{2+} , which is consistent with measurements on Kilauea lavas (e.g., Moore and Ault, 1965; Byers et al., 1985; Rhodes and Vollinger, 2005). The date with each set of olivine data is the sample number. The diagonal field is the shallow pressure (1 atm) equilibrium field for basaltic magma ($\text{Fe}/\text{Mg } K_d = 0.30 \pm 0.03$; Roeder and Emslie, 1970; Ulmer, 1989). Lava samples that plot below the equilibrium field (e.g., 4-Jan-00) have probably experienced olivine accumulation.

indicative of the parental magma composition for recent Pu‘u ‘Ō‘ō lavas (Mg# ~59; Fig. 1.2), consistent with estimates for previous Pu‘u ‘Ō‘ō lavas (Garcia et al., 2000).

1.3.4 Whole-rock analytical methods

Eighty-two new Pu‘u ‘Ō‘ō lava samples erupted between 1998-2005 were analyzed for major and trace element (Rb, Sr, Y, Nb, Zr, Zn, Ni, Cr, V, Ba, and Ce) abundances over a seven-year period using X-ray fluorescence spectrometry (XRF) at the University of Massachusetts (Table 1.3). The Kīlauea basaltic standard BHVO-1 (n=13) and in-house reference material K1919 (n=13) were collected from the same flow, and were run as internal controls for major and trace element abundances during this period, respectively (Table 1.3). All Pu‘u ‘Ō‘ō samples presented here were analyzed in the same XRF laboratory using the same calibration procedures. Thus, any long-term analytical drift in the major and trace element abundances is expected to be relatively minor. Details of methods used and estimates of analytical precision for the XRF analyses are given in Rhodes (1996) and Rhodes and Vollinger (2004).

In addition, 27 samples were analyzed over a one-week period for Sc, V, Cr, Co, Ni, Cu, Zn, Sr, Cs, Rb, Ba, Th, U, Nb, Zr, Hf, Y, and rare-earth element abundances using inductively coupled plasma mass spectrometry (ICP-MS) at the Australian National University (Table 1.4). The Kīlauea rock standard BHVO-2 (n=2) was analyzed with these samples. Analytical methods and estimates of precision for the ICP-MS trace element analyses are given in Table 1.4 and Norman et al. (1998). Prior to both XRF and ICP-MS analyses, the Pu‘u ‘Ō‘ō lava samples were washed in an ultrasonic bath of deionized water for 10-20 minutes, hand picked (30-100 g) to remove any rare altered rock chips, and powdered in a tungsten carbide swing mill for the XRF analyses and an agate mill for the ICP-MS analyses.

Fourteen Pu‘u ‘Ō‘ō lavas erupted between 1998-2005 were analyzed for Pb and Nd isotope ratios (Table 1.5) using a Nu Plasma multi-collector inductively coupled plasma mass

Table 1.3 Whole-rock XRF analyses of 1998-2005 Pu'u Ō'ō lavas. *Fe₂O₃ is total iron. Day is the number of days since the start of the Pu'u Ō'ō eruption on Jan. 3, 1983. Oxide abundances are in wt %; trace element contents are in ppm. Samples 17-Jan-98, 11-May-98, and 07-Sep-98 are from Garcia *et al.* (2000). Between 1998-2005, K1919 (n=13) and BHVO-1 (n=13) were analyzed by XRF for major and trace element abundances, respectively.

Sample	17-Jan-98	11-May-98	25-Jun-98	7-Sep-98	14-Nov-98
Day	5493	5607	5652	5726	5794
SiO ₂	50.16	50.21	50.54	50.26	50.30
TiO ₂	2.282	2.316	2.393	2.353	2.345
Al ₂ O ₃	12.70	12.80	13.36	12.98	12.99
Fe ₂ O ₃ *	12.48	12.40	11.98	12.32	12.21
MnO	0.18	0.17	0.17	0.17	0.18
MgO	9.26	9.10	7.52	8.65	8.38
CaO	10.42	10.40	10.95	10.58	10.65
Na ₂ O	2.21	2.10	2.22	2.24	2.20
K ₂ O	0.402	0.405	0.416	0.406	0.409
P ₂ O ₅	0.215	0.221	0.232	0.224	0.229
Total	100.31	100.13	99.77	100.16	99.87
Y	23.2	23.5	24.4	23.7	24.0
Sr	297	301	316	306	308
Rb	7.0	7.1	6.8	7.5	6.4
Nb	11.7	12.2	12.4	12.4	12.1
Zr	139	142	142	145	140
Ni	146	168	95	145	133
Cr	519	549	465	493	489
V	273	274	289	278	283
Zn	115	115	112	115	113
Ba	96	99	100	97	101
Ce	28	26	30	30	27
Sample	13-Feb-99	13-Mar-99	13-Apr-99	25-Apr-99	19-Jun-99
Day	5885	5913	5944	5956	6011
SiO ₂	50.58	50.17	50.11	50.47	50.30
TiO ₂	2.400	2.344	2.281	2.325	2.324
Al ₂ O ₃	13.37	13.07	12.79	13.10	13.07
Fe ₂ O ₃ *	12.14	12.29	12.45	12.17	12.29
MnO	0.17	0.17	0.17	0.18	0.17
MgO	7.41	8.08	9.03	8.16	8.17
CaO	10.91	10.67	10.42	10.65	10.64
Na ₂ O	2.34	2.30	2.27	2.11	2.28
K ₂ O	0.416	0.406	0.393	0.404	0.402
P ₂ O ₅	0.235	0.229	0.224	0.225	0.228
Total	99.98	99.70	100.13	99.77	99.87
Y	24.4	23.9	23.2	24.1	23.7
Sr	315	306	299	307	305
Rb	7.2	7.3	7.1	6.6	7.3
Nb	12.5	12.3	11.9	12.0	12.1
Zr	146	143	140	139	143
Ni	89	120	141	111	119
Cr	385	449	499	450	440
V	281	276	270	286	275
Zn	113	114	114	114	114
Ba	97	96	94	99	99
Ce	32	29	28	29	28

Table 1.3 (Continued)

Sample	14-Jul-99	11-Aug-99	27-Oct-99	20-Nov-99	29-Dec-99
Day	6036	6064	6141	6165	6204
SiO ₂	50.36	50.66	50.33	50.34	50.39
TiO ₂	2.340	2.398	2.320	2.333	2.325
Al ₂ O ₃	13.10	13.38	13.02	13.13	13.04
Fe ₂ O ₃ *	12.28	12.04	12.26	12.22	12.28
MnO	0.17	0.17	0.17	0.18	0.17
MgO	8.03	6.85	7.98	7.69	7.87
CaO	10.70	10.98	10.64	10.73	10.65
Na ₂ O	2.31	2.33	2.36	2.37	2.30
K ₂ O	0.402	0.415	0.400	0.402	0.404
P ₂ O ₅	0.229	0.232	0.227	0.224	0.227
Total	99.92	99.45	99.71	99.61	99.66
Y	23.9	24.8	23.8	24.0	24.1
Sr	308	316	307	308	306
Rb	7.4	7.0	6.7	6.9	6.7
Nb	12.2	12.6	12.1	12.3	12.0
Zr	143	148	143	144	143
Ni	109	73	105	87	96
Cr	425	327	406	371	404
V	277	281	277	273	276
Zn	114	113	114	113	113
Ba	96	90	88	86	83
Ce	30	29	31	29	29
Sample	4-Jan-00	19-Feb-00	26-Mar-00	8-Apr-00	6-May-00
Day	6210	6256	6292	6305	6333
SiO ₂	49.72	50.27	50.83	50.71	50.83
TiO ₂	2.217	2.275	2.336	2.388	2.355
Al ₂ O ₃	12.46	12.87	13.14	13.37	13.22
Fe ₂ O ₃ *	12.56	12.36	12.21	11.98	12.14
MnO	0.18	0.18	0.18	0.18	0.18
MgO	9.54	8.55	7.97	7.10	7.65
CaO	10.14	10.50	10.75	11.01	10.80
Na ₂ O	2.24	2.17	2.21	2.36	2.16
K ₂ O	0.378	0.386	0.398	0.408	0.397
P ₂ O ₅	0.217	0.222	0.225	0.230	0.226
Total	99.64	99.79	100.24	99.73	99.95
Y	23.1	23.7	23.8	24.5	24.0
Sr	292	299	303	309	304
Rb	6.4	6.7	6.4	6.7	6.8
Nb	11.5	11.6	12.0	12.1	11.9
Zr	136	138	140	143	140
Ni	140	111	102	76	90
Cr	489	440	419	348	372
V	261	270	272	280	272
Zn	113	114	113	114	113
Ba	97	98	100	91	89
Ce	24	27	29	27	26

Table 1.3 (Continued)

Sample	6-Jun-00	21-Jun-00	14-Jul-00	4-Aug-00	12-Oct-00
Day	6364	6379	6402	6423	6492
SiO ₂	50.71	51.01	50.50	50.77	51.00
TiO ₂	2.306	2.361	2.253	2.288	2.311
Al ₂ O ₃	12.91	13.33	12.74	12.93	13.09
Fe ₂ O ₃ *	12.24	12.04	12.40	12.28	12.18
MnO	0.18	0.18	0.18	0.18	0.18
MgO	8.24	7.23	8.84	8.29	7.85
CaO	10.60	10.88	10.36	10.56	10.70
Na ₂ O	2.21	2.31	2.18	2.17	2.18
K ₂ O	0.390	0.405	0.387	0.390	0.408
P ₂ O ₅	0.222	0.228	0.220	0.224	0.225
Total	100.00	99.98	100.07	100.10	100.12
Y	23.7	24.4	23.3	23.9	23.8
Sr	300	308	292	299	302
Rb	6.6	6.6	6.2	6.4	6.6
Nb	11.7	12.2	11.3	11.7	11.7
Zr	138	143	135	138	139
Ni	107	80	135	112	100
Cr	419	354	469	416	387
V	271	282	268	276	276
Zn	113	113	115	113	114
Ba	85	88	83	93	84
Ce	28	29	29	28	29
Sample	24-Dec-00	8-Jan-01	27-Jan-01	16-Feb-01	11-Mar-01
Day	6565	6580	6599	6619	6642
SiO ₂	50.75	51.01	50.69	51.02	50.83
TiO ₂	2.348	2.349	2.360	2.361	2.369
Al ₂ O ₃	13.21	13.23	13.30	13.26	13.25
Fe ₂ O ₃ *	12.04	12.14	12.16	12.23	12.21
MnO	0.18	0.18	0.18	0.18	0.18
MgO	7.39	7.55	7.56	7.66	7.53
CaO	10.75	10.76	10.79	10.78	10.76
Na ₂ O	2.48	2.23	2.22	2.20	2.25
K ₂ O	0.402	0.400	0.402	0.403	0.405
P ₂ O ₅	0.229	0.229	0.260	0.230	0.229
Total	99.78	100.08	99.91	100.32	100.01
Y	24.4	24.2	24.3	24.4	24.4
Sr	308	307	308	307	310
Rb	6.7	6.5	6.5	6.6	6.8
Nb	12.1	12.0	12.1	12.1	12.0
Zr	143	142	139	142	144
Ni	87	89	87	93	93
Cr	355	357	357	361	346
V	280	279	283	281	284
Zn	114	114	113	114	115
Ba	87	91	94	91	93
Ce	29	27	29	30	28

Table 1.3 (Continued)

Sample	8-Apr-01	27-Apr-01	24-May-01	7-Jul-01	15-Jul-01
Day	6670	6689	6716	6760	6768
SiO ₂	50.91	50.61	50.57	50.20	50.82
TiO ₂	2.340	2.371	2.359	2.340	2.397
Al ₂ O ₃	13.12	13.26	13.21	13.19	13.41
Fe ₂ O ₃ *	12.26	12.17	12.20	12.15	12.16
MnO	0.18	0.18	0.17	0.17	0.17
MgO	7.93	7.53	7.55	7.36	7.03
CaO	10.70	10.81	10.71	10.66	10.81
Na ₂ O	2.11	2.18	2.23	2.89	2.11
K ₂ O	0.399	0.404	0.399	0.400	0.406
P ₂ O ₅	0.228	0.227	0.228	0.230	0.231
Total	100.18	99.73	99.62	99.59	99.54
Y	24.1	24.2	24.4	24.5	24.8
Sr	306	308	308	310	313
Rb	6.7	6.3	6.6	6.7	6.8
Nb	12.1	11.9	12.1	12.3	12.2
Zr	141	139	143	144	145
Ni	103	91	94	91	83
Cr	371	376	366	357	337
V	286	277	284	287	287
Zn	115	112	115	114	115
Ba	94	95	93	91	91
Ce	28	28	31	33	30
Sample	29-Sep-01	13-Oct-01	3-Nov-01	12-Jan-02	9-Feb-02
Day	6844	6858	6879	6949	6977
SiO ₂	51.19	50.82	50.81	50.55	50.79
TiO ₂	2.454	2.390	2.384	2.330	2.338
Al ₂ O ₃	13.69	13.35	13.34	13.02	13.11
Fe ₂ O ₃ *	12.20	12.23	12.21	12.26	12.31
MnO	0.18	0.17	0.17	0.17	0.17
MgO	6.69	7.29	7.25	8.03	7.90
CaO	10.95	10.75	10.74	10.64	10.68
Na ₂ O	2.13	2.03	1.98	2.05	2.03
K ₂ O	0.418	0.404	0.401	0.390	0.391
P ₂ O ₅	0.236	0.230	0.230	0.223	0.224
Total	100.14	99.66	99.52	99.66	99.94
Y	24.8	24.5	24.3	23.8	24.2
Sr	319	312	312	303	305
Rb	6.7	6.4	6.6	6.4	6.4
Nb	12.6	12.2	12.1	11.9	11.8
Zr	148	145	145	140	140
Ni	69	88	83	106	103
Cr	283	324	332	403	376
V	283	282	280	280	276
Zn	114	115	120	115	115
Ba	88	88	90	92	90
Ce	32	29	29	29	29

Table 1.3 (Continued)

Sample	27-Mar-02	5-Apr-02	12-Apr-02	5-Jun-02	16-Jun-02
Day	7023	7032	7039	7093	7104
SiO ₂	50.95	50.84	50.83	50.88	50.84
TiO ₂	2.379	2.340	2.322	2.340	2.346
Al ₂ O ₃	13.32	13.21	13.07	13.19	13.21
Fe ₂ O ₃ *	12.21	12.20	12.29	12.29	12.32
MnO	0.17	0.17	0.17	0.18	0.18
MgO	7.42	7.79	8.03	7.96	7.73
CaO	10.72	10.71	10.66	10.66	10.67
Na ₂ O	1.95	2.05	2.00	2.13	2.15
K ₂ O	0.395	0.389	0.385	0.394	0.392
P ₂ O ₅	0.229	0.225	0.224	0.227	0.226
Total	99.74	99.92	99.98	100.25	100.06
Y	24.4	24.1	23.9	24.3	24.3
Sr	311	306	304	305	307
Rb	6.5	6.3	6.4	6.4	6.2
Nb	12.0	11.9	11.7	11.7	11.8
Zr	144	141	140	141	142
Ni	87	94	100	99	93
Cr	333	379	404	379	357
V	279	275	272	277	278
Zn	115	114	114	115	114
Ba	93	94	89	91	93
Ce	30	28	29	30	28
Sample					
Day	12-Jul-02	31-Jul-02	6-Aug-02	20-Aug-02	27-Sep-02
SiO ₂	7130	7149	7155	7169	7207
TiO ₂	50.90	50.92	51.01	50.82	50.74
Al ₂ O ₃	2.407	2.374	2.384	2.337	2.352
Fe ₂ O ₃ *	13.47	13.34	13.33	13.09	13.25
MnO	12.19	12.25	12.25	12.37	12.24
MgO	0.18	0.18	0.18	0.18	0.17
CaO	7.09	7.46	7.51	8.11	7.47
Na ₂ O	10.80	10.70	10.73	10.62	10.68
K ₂ O	2.19	2.06	2.24	2.15	2.15
P ₂ O ₅	0.406	0.396	0.401	0.390	0.392
Total	0.234	0.230	0.232	0.225	0.232
Y	99.87	99.91	100.27	100.29	99.68
Sr	25.0	24.7	24.6	24.2	24.4
Rb	315	312	310	306	308
Nb	6.6	6.5	6.3	6.5	6.7
Zr	12.2	12.0	12.1	11.8	12.0
Ni	146	144	144	142	143
Cr	79	87	86	103	88
V	328	343	347	374	354
Zn	280	280	281	273	279
Ba	115	116	115	115	114
Ce	92	92	95	97	96

Table 1.3 (Continued)

Sample	19-Oct-02	21-Nov-02	11-Jan-03	11-Feb-03	12-Mar-03
Day	7229	7262	7313	7344	7373
SiO ₂	50.96	50.72	50.76	50.75	50.78
TiO ₂	2.381	2.352	2.372	2.367	2.354
Al ₂ O ₃	13.33	13.20	13.36	13.31	13.21
Fe ₂ O ₃ *	12.20	12.23	12.17	12.16	12.23
MnO	0.18	0.18	0.18	0.18	0.18
MgO	7.13	7.39	7.29	7.50	7.62
CaO	10.75	10.68	10.73	10.72	10.66
Na ₂ O	2.15	2.17	2.22	2.25	2.19
K ₂ O	0.394	0.391	0.394	0.398	0.392
P ₂ O ₅	0.238	0.230	0.231	0.230	0.229
Total	99.71	99.54	99.69	99.85	99.84
Y	24.5	24.5	24.7	24.6	24.5
Sr	311	308	311	308	308
Rb	6.8	6.4	6.8	6.5	6.9
Nb	12.2	12.1	12.1	11.8	12.0
Zr	144	143	144	139	143
Ni	79	91	82	83	91
Cr	351	377	348	346	357
V	285	283	285	281	279
Zn	114	150	115	115	115
Ba	92	91	91	92	95
Ce	30	60	29	30	30
Sample	12-Apr-03	28-Jun-03	31-Jul-03	29-Aug-03	19-Sep-03
Day	7404	7481	7514	7543	7564
SiO ₂	50.79	50.73	50.70	50.87	50.65
TiO ₂	2.380	2.376	2.350	2.385	2.340
Al ₂ O ₃	13.34	13.42	13.22	13.43	13.17
Fe ₂ O ₃ *	12.15	12.14	12.23	12.19	12.21
MnO	0.18	0.18	0.18	0.18	0.18
MgO	7.20	7.08	7.42	7.08	7.44
CaO	10.75	10.78	10.69	10.77	10.67
Na ₂ O	2.22	2.30	2.24	2.34	2.25
K ₂ O	0.397	0.401	0.389	0.401	0.389
P ₂ O ₅	0.231	0.234	0.227	0.235	0.226
Total	99.62	99.63	99.62	99.86	99.50
Y	24.7	24.8	24.3	24.7	24.2
Sr	313	315	309	312	307
Rb	6.7	6.8	6.7	6.6	6.5
Nb	12.4	12.4	12.0	12.4	11.9
Zr	145	145	142	145	142
Ni	79	77	84	78	89
Cr	335	321	342	336	354
V	280	286	281	286	282
Zn	114	115	114	115	115
Ba	95	103	95	101	98
Ce	27	26	29	28	29

Table 1.3 (Continued)

Sample	9-Oct-03	15-Jan-04	1-Mar-04	16-Mar-04	23-Apr-04
Day	7584	7682	7728	7743	7781
SiO ₂	50.87	50.82	50.83	50.77	50.83
TiO ₂	2.379	2.410	2.415	2.413	2.418
Al ₂ O ₃	13.27	13.48	13.38	13.34	13.45
Fe ₂ O ₃ *	12.15	12.10	12.11	12.09	12.23
MnO	0.18	0.17	0.18	0.18	0.18
MgO	7.45	7.16	7.20	7.17	7.13
CaO	10.78	10.81	10.86	10.85	10.85
Na ₂ O	2.25	2.27	2.27	2.28	2.28
K ₂ O	0.398	0.404	0.405	0.402	0.408
P ₂ O ₅	0.231	0.235	0.235	0.234	0.236
Total	99.94	99.85	99.88	99.73	100.00
Y	24.7	24.9	24.9	24.9	24.9
Sr	311	313	314	314	314
Rb	6.6	6.6	6.7	6.7	6.6
Nb	12.0	12.0	12.2	12.2	12.2
Zr	141	142	144	143	143
Ni	82	78	79	79	77
Cr	346	309	309	304	293
V	285	287	288	289	282
Zn	114	115	114	114	112
Ba	98	94	92	91	93
Ce	28	28	31	31	30
Sample	2-Jun-04	7-Jun-04	23-Jul-04	10-Aug-04	15-Oct-04
Day	7821	7826	7872	7890	7956
SiO ₂	50.75	50.92	51.00	50.71	50.97
TiO ₂	2.423	2.436	2.439	2.361	2.417
Al ₂ O ₃	13.51	13.56	13.68	13.33	13.44
Fe ₂ O ₃ *	12.11	12.12	12.11	12.04	12.14
MnO	0.18	0.18	0.17	0.17	0.17
MgO	7.04	6.99	6.97	7.46	7.24
CaO	10.83	10.82	10.83	10.90	10.91
Na ₂ O	2.28	2.30	2.24	2.31	2.30
K ₂ O	0.421	0.417	0.420	0.405	0.424
P ₂ O ₅	0.234	0.239	0.238	0.225	0.232
Total	99.75	99.98	100.1	99.91	100.24
Y	25.0	25.2	25.1	24.2	24.8
Sr	317	318	319	309	315
Rb	6.7	6.6	6.5	6.2	6.5
Nb	12.4	12.3	12.4	11.9	12.3
Zr	144	144	143	137	141
Ni	77	75	75	87	80
Cr	280	262	250	351	287
V	288	286	290	280	283
Zn	114	114	114	112	116
Ba	100	97	96	94	94
Ce	31	32	34	30	31

Table 1.3 (Continued)

Sample	31-Oct-04	4-Dec-04	31-Jan-05	6-Feb-05	23-Feb-05
Day	7972	8006	8064	8070	8087
SiO ₂	50.85	50.94	50.98	50.81	50.80
TiO ₂	2.448	2.483	2.492	2.417	2.437
Al ₂ O ₃	13.51	13.64	13.63	13.47	13.52
Fe ₂ O ₃ *	12.14	12.13	12.23	12.09	12.13
MnO	0.18	0.18	0.18	0.18	0.18
MgO	6.90	6.68	6.69	7.03	6.98
CaO	10.85	10.86	10.85	10.91	10.86
Na ₂ O	2.39	2.37	2.44	2.36	2.42
K ₂ O	0.424	0.433	0.425	0.415	0.418
P ₂ O ₅	0.234	0.239	0.239	0.231	0.232
Total	99.93	99.96	100.16	99.91	99.98
Y	25.2	25.5	25.5	24.7	25.1
Sr	319	322	320	315	317
Rb	6.7	6.6	6.5	6.3	6.5
Nb	12.5	12.4	12.5	12.2	12.4
Zr	144	145	144	140	141
Ni	75	67	69	78	77
Cr	243	218	217	270	255
V	294	293	288	288	289
Zn	116	116	115	113	114
Ba	100	100	100	93	94
Ce	31	32	32	32	34
Sample	4-Mar-05	24-Mar-05	22-Apr-05	23-Jun-05	16-Jul-05
Day	8096	8116	8145	8207	8230
SiO ₂	50.71	50.79	50.96	50.76	50.86
TiO ₂	2.409	2.395	2.422	2.451	2.450
Al ₂ O ₃	13.42	13.42	13.52	13.58	13.56
Fe ₂ O ₃ *	12.08	12.12	12.17	12.14	12.15
MnO	0.18	0.17	0.18	0.17	0.17
MgO	7.07	7.28	7.18	6.85	6.94
CaO	10.90	10.92	10.94	10.83	10.87
Na ₂ O	2.35	2.35	2.38	2.54	2.46
K ₂ O	0.418	0.408	0.413	0.417	0.411
P ₂ O ₅	0.229	0.230	0.232	0.235	0.230
Total	99.77	100.08	100.4	99.97	100.1
Y	24.9	25.5	25.5	25.9	25.9
Sr	315	315	315	319	318
Rb	6.6	6.5	6.3	6.5	6.5
Nb	12.4	12.7	12.7	13.0	12.9
Zr	140	146	146	150	148
Ni	91	86	83	77	82
Cr	280	298	277	247	269
V	287	289	283	291	282
Zn	114	115	114	116	115
Ba	95	100	101	104	100
Ce	33	32	29	30	28

Table 1.3 (Continued)

Sample	8-Aug-05	23-Sep-05	22-Oct-05	19-Nov-05	26-Dec-05
Day	8253	8299	8328	8356	8393
SiO ₂	50.89	50.94	50.85	50.87	50.84
TiO ₂	2.430	2.439	2.437	2.422	2.432
Al ₂ O ₃	13.52	13.63	13.62	13.51	13.47
Fe ₂ O ₃ *	12.05	12.14	12.12	12.05	12.07
MnO	0.18	0.17	0.17	0.18	0.18
MgO	6.91	6.96	6.98	7.19	7.09
CaO	10.79	10.84	10.80	10.85	10.83
Na ₂ O	2.50	2.41	2.42	1.93	2.06
K ₂ O	0.415	0.418	0.413	0.403	0.405
P ₂ O ₅	0.230	0.233	0.229	0.228	0.231
Total	99.92	100.18	100.04	99.63	99.61
Y	26.0	25.7	25.8	25.4	25.8
Sr	318	316	315	315	315
Rb	6.5	6.6	6.9	6.3	6.1
Nb	13.0	12.9	12.9	12.7	12.6
Zr	148	148	147	146	147
Ni	79	83	82	87	86
Cr	259	256	255	286	276
V	291	289	290	291	291
Zn	116	115	115	115	116
Ba	102	105	104	105	97
Ce	32	30	28	28	29
Sample	K1919 avg.	± 2σ	BHVO-1 avg.	± 2σ	
Day	—	—	—	—	
SiO ₂	49.88	0.24	—	—	
TiO ₂	2.797	0.03	—	—	
Al ₂ O ₃	13.63	0.19	—	—	
Fe ₂ O ₃ *	12.04	0.07	—	—	
MnO	0.17	0.007	—	—	
MgO	6.63	0.24	—	—	
CaO	11.39	0.04	—	—	
Na ₂ O	2.38	0.32	—	—	
K ₂ O	0.548	0.012	—	—	
P ₂ O ₅	0.292	0.006	—	—	
Total	99.75	—	—	—	
Y	—	—	25.1	0.3	
Sr	—	—	380	7	
Rb	—	—	9.2	0.5	
Nb	—	—	18.6	0.4	
Zr	—	—	177	8	
Ni	—	—	114	2	
Cr	—	—	297	3	
V	—	—	293	6	
Zn	—	—	112	2	
Ba	—	—	129	8	
Ce	—	—	40	2	

Table 1.4 ICP-MS analyses of 1998-2005 Pu‘u ‘Ō‘ō lavas. Day is the number of days since the start of the Pu‘u ‘Ō‘ō eruption on Jan. 3, 1983; values are in ppm. BHVO-2 (n=2) was analyzed as an internal standard for these analyses.

Sample	Day	Rb	Cs	Ba	La	Ce	Pr	Nd	Sm	Eu	Gd	Tb
17-Jan-98	5493	6.8	0.070	93.4	10.2	26.4	3.90	18.3	5.05	1.72	5.31	0.85
11-May-98	5607	7.0	0.072	95.8	10.3	26.8	3.96	18.5	5.10	1.71	5.36	0.85
7-Sep-98	5726	7.1	0.076	98.2	10.6	27.4	4.03	18.9	5.21	1.78	5.47	0.88
13-Feb-99	5885	7.3	0.073	99.4	10.7	27.7	4.09	19.1	5.26	1.80	5.62	0.89
19-Jun-99	6011	7.1	0.073	97.3	10.5	27.2	4.01	18.8	5.20	1.77	5.46	0.88
27-Oct-99	6141	6.9	0.070	96.8	10.5	27.1	3.99	18.8	5.11	1.77	5.52	0.88
19-Feb-00	6256	6.7	0.068	93.3	10.2	26.2	3.86	18.2	5.00	1.74	5.34	0.86
21-Jun-00	6379	6.7	0.065	93.9	10.2	26.2	3.83	18.3	4.97	1.73	5.43	0.87
12-Oct-00	6492	6.8	0.067	95.8	10.5	26.8	3.95	18.6	5.09	1.79	5.55	0.89
8-Jan-01	6580	6.9	0.070	95.9	10.5	26.7	3.97	18.7	5.10	1.78	5.53	0.88
8-Apr-01	6670	7.0	0.070	100	10.8	28.0	4.15	19.5	5.27	1.81	5.70	0.90
7-Jul-01	6760	6.9	0.069	98.4	10.6	27.6	4.07	19.1	5.20	1.79	5.65	0.89
13-Oct-01	6858	6.9	0.069	98.4	10.6	27.6	4.08	19.2	5.18	1.79	5.70	0.89
9-Feb-02	6977	6.6	0.067	93.1	10.1	26.1	3.86	18.1	4.95	1.71	5.39	0.85
5-Jun-02	7093	6.7	0.069	95.5	10.3	26.8	3.96	18.7	5.12	1.75	5.59	0.87
20-Aug-02	7169	6.7	0.070	95.9	10.3	26.8	3.96	18.7	5.15	1.79	5.48	0.89
21-Nov-02	7262	6.6	0.066	93.7	10.1	26.2	3.88	18.4	5.05	1.76	5.50	0.88
12-Apr-03	7404	6.9	0.071	98.0	10.6	27.4	4.04	19.1	5.28	1.83	5.68	0.90
19-Sep-03	7564	6.9	0.070	97.1	10.5	27.2	4.03	18.6	5.30	1.82	5.69	0.90
15-Jan-04	7682	7.1	0.073	99.3	10.7	27.8	4.10	19.4	5.31	1.86	5.69	0.92
23-Apr-04	7781	7.1	0.071	98.7	10.7	27.7	4.09	19.2	5.26	1.82	5.70	0.91
7-Jun-04	7826	7.4	0.078	103	11.2	29.0	4.28	20.0	5.47	1.89	6.00	0.94
15-Oct-04	7956	7.1	0.070	98.4	10.7	27.6	4.09	19.1	5.27	1.80	5.69	0.91
31-Jan-05	8064	7.5	0.076	104	11.2	29.0	4.30	20.1	5.55	1.89	5.92	0.95
22-Apr-05	8145	7.1	0.072	100	10.9	28.2	4.19	19.6	5.42	1.83	5.83	0.92
8-Aug-05	8253	7.2	0.073	102	11.0	28.4	4.18	19.8	5.46	1.85	5.87	0.93
In-house basaltic reference material (Kīlauea Volcano)												
BHVO-2	—	9.2	0.106	129	14.8	36.7	5.27	23.9	6.02	2.02	6.11	0.94
±2σ	—	0.2	0.006	2.0	0.2	0.1	0.01	0.01	0.11	0.001	0.14	0.02

Table 1.4 (Continued)

Sample	Day	Dy	Ho	Er	Yb	Lu	Th	Y	Nb	Hf	U	Pb
17-Jan-98	5493	4.88	0.93	2.28	1.93	0.275	0.81	23.8	12.0	3.42	0.260	1.01
11-May-98	5607	4.90	0.93	2.31	1.95	0.273	0.83	24.1	12.4	3.49	0.265	1.07
7-Sep-98	5726	4.92	0.95	2.33	1.97	0.286	0.84	24.3	12.6	3.55	0.278	1.04
13-Feb-99	5885	5.07	0.97	2.38	2.02	0.288	0.86	25.1	12.9	3.59	0.277	1.05
19-Jun-99	6011	5.00	0.96	2.34	1.99	0.281	0.84	24.9	12.7	3.59	0.271	1.04
27-Oct-99	6141	4.95	0.96	2.34	2.00	0.278	0.80	24.3	12.4	3.52	0.260	1.00
19-Feb-00	6256	4.86	0.95	2.29	1.98	0.277	0.80	23.8	12.1	3.44	0.259	1.07
21-Jun-00	6379	4.90	0.95	2.31	2.00	0.278	0.80	24.0	12.1	3.44	0.261	0.98
12-Oct-00	6492	5.06	0.98	2.42	1.99	0.282	0.81	24.7	12.3	3.52	0.261	1.04
8-Jan-01	6580	5.03	0.98	2.38	2.03	0.283	0.81	24.7	12.4	3.56	0.265	0.98
8-Apr-01	6670	5.20	1.00	2.45	2.08	0.287	0.85	25.1	12.6	3.65	0.282	1.00
7-Jul-01	6760	5.07	0.99	2.43	2.03	0.284	0.83	24.8	12.4	3.59	0.273	0.99
13-Oct-01	6858	5.09	0.99	2.42	2.05	0.282	0.83	24.7	12.4	3.58	0.264	0.97
9-Feb-02	6977	4.86	0.95	2.29	1.94	0.273	0.78	23.7	11.7	3.40	0.261	0.93
5-Jun-02	7093	5.01	0.96	2.39	2.02	0.276	0.80	24.4	12.1	3.50	0.266	0.96
20-Aug-02	7169	5.08	0.98	2.41	2.02	0.286	0.78	24.3	12.2	3.54	0.269	0.95
21-Nov-02	7262	4.99	0.97	2.38	1.99	0.282	0.78	24.1	11.9	3.48	0.257	0.93
12-Apr-03	7404	5.21	1.01	2.46	2.07	0.290	0.81	25.0	12.4	3.62	0.270	0.98
19-Sep-03	7564	5.16	1.00	2.44	2.05	0.286	0.81	25.1	12.4	3.56	0.271	0.97
15-Jan-04	7682	5.22	1.02	2.51	2.10	0.293	0.83	25.2	12.6	3.67	0.268	1.00
23-Apr-04	7781	5.13	1.00	2.42	2.04	0.287	0.83	25.2	12.7	3.61	0.267	1.00
7-Jun-04	7826	5.37	1.04	2.52	2.14	0.300	0.87	26.3	13.3	3.77	0.284	1.02
15-Oct-04	7956	5.12	1.00	2.41	2.01	0.282	0.83	25.1	12.7	3.61	0.275	1.01
31-Jan-05	8064	5.31	1.05	2.50	2.13	0.294	0.88	26.2	13.4	3.78	0.279	1.06
22-Apr-05	8145	5.17	1.01	2.46	2.06	0.291	0.86	25.2	12.9	3.68	0.278	1.02
8-Aug-05	8253	5.30	1.01	2.49	2.09	0.295	0.84	25.5	12.8	3.65	0.281	1.01
Hawaiian Rock Standard (Kīlauea Volcano)												
BHVO-2	—	5.18	0.98	2.35	1.92	0.275	1.25	24.4	18.0	4.17	0.408	1.68
±2σ	—	0.09	0.01	0.02	0.01	0.003	0.02	0.5	0.6	0.04	0.008	0.04

Table 1.4 (Continued)

Sample	Day	Zr	Sr	Sc	V	Cr	Co	Ni	Cu	Zn	Ga
17-Jan-98	5493	139	313	30.8	264	432	52.6	171	120	105	18.9
11-May-98	5607	141	317	30.5	266	446	52.0	178	119	103	18.8
7-Sep-98	5726	143	322	30.8	268	449	49.3	149	120	103	18.9
13-Feb-99	5885	146	331	31.7	278	380	45.5	100	126	102	19.4
19-Jun-99	6011	145	327	31.4	277	440	50.5	137	122	104	19.2
27-Oct-99	6141	141	318	31.1	266	389	48.0	118	123	103	19.2
19-Feb-00	6256	138	309	30.7	261	418	50.3	133	121	106	18.8
21-Jun-00	6379	138	312	30.8	264	374	48.7	115	121	101	19.0
12-Oct-00	6492	142	318	31.9	268	364	47.8	103	123	109	19.5
8-Jan-01	6580	144	320	31.3	269	354	47.2	99	123	111	19.4
8-Apr-01	6670	144	325	31.4	270	302	45.4	89	124	104	19.9
7-Jul-01	6760	142	320	31.4	267	342	46.3	96	122	104	19.7
13-Oct-01	6858	142	320	31.3	266	347	47.2	105	121	105	19.6
9-Feb-02	6977	135	306	30.6	256	417	51.5	140	114	102	18.6
5-Jun-02	7093	139	315	30.6	262	347	47.5	108	117	101	19.1
20-Aug-02	7169	139	314	30.4	260	325	47.7	108	119	103	19.2
21-Nov-02	7262	137	309	31.0	260	409	48.2	114	116	104	18.9
12-Apr-03	7404	143	322	31.2	267	306	44.7	82	122	103	19.7
19-Sep-03	7564	143	322	31.5	268	341	47.9	98	124	107	19.9
15-Jan-04	7682	145	326	31.1	270	287	44.5	83	120	102	19.6
23-Apr-04	7781	146	327	31.6	271	297	45.8	91	122	105	19.9
7-Jun-04	7826	153	341	32.4	281	261	46.0	85	127	108	20.7
15-Oct-04	7956	145	327	31.7	272	304	45.0	90	120	104	19.9
31-Jan-05	8064	153	342	32.0	281	214	44.3	77	126	107	20.4
22-Apr-05	8145	147	329	31.8	273	267	46.0	93	123	107	20.1
8-Aug-05	8253	147	331	31.8	273	255	45.1	89	124	106	20.2
Hawaiian Rock Standard (Kīlauea Volcano)											
BHVO-2 avg.	—	169	388	31.2	278	282	42.9	115	121	99	20.0
±2σ	—	3	9	1.0	9	10	2.2	6	6	4	0.5

Table 1.5 Pb, Sr and Nd isotope data for Pu‘u ‘Ō‘ō lavas. The Pb, Sr and Nd isotope ratios of the samples were measured over two periods of time. The 1998-2004 Pu‘u ‘Ō‘ō lavas were analyzed at the same time as the Kīlauea samples presented by Marske et al. (2007), whereas the 2005 lavas, a new dissolution of Kil1919 (an in-house reference material collected from the same flow as K1919, BHVO-1, and BHVO-2) and the re-analyzed 1989-1995 lavas in Table A.1 in the appendix [previously studied by Garcia et al. (1996, 2000) and Pietruszka et al. (2006)] were analyzed subsequently by MC-ICP-MS (for Pb and Nd isotopes) and TIMS (for Sr isotopes). Analytical details relevant to the 1998-2004 samples are presented in Marske et al. (2007). The following analytical details apply to the other samples, unless otherwise noted. Pb isotope ratios were corrected for instrumental mass fractionation using the measured isotope ratio of Tl (SRM 997) added to the sample compared to an assumed $^{205}\text{Tl}/^{203}\text{Tl}=2.3889$ for this standard from Thirlwall (2002). The average Tl-corrected value for NBS981 Pb (n=5) was $^{206}\text{Pb}/^{204}\text{Pb}=16.9434\pm 15$ (2 σ), $^{207}\text{Pb}/^{204}\text{Pb}=15.5019\pm 16$ (2 σ), and $^{208}\text{Pb}/^{204}\text{Pb}=36.7298\pm 42$ (2 σ). All of the Pb isotopic data are reported relative to the NBS 981 Pb standard values of Galer & Abouchami (1998): $^{206}\text{Pb}/^{204}\text{Pb}=16.9405$, $^{207}\text{Pb}/^{204}\text{Pb}=15.4963$, and $^{208}\text{Pb}/^{204}\text{Pb}=36.7219$. Sr and Nd isotope ratios were corrected for instrumental mass fractionation relative to $^{86}\text{Sr}/^{88}\text{Sr}=0.1194$ and $^{146}\text{Nd}/^{144}\text{Nd}=0.7219$, respectively. The average measured values for Sr and Nd standards were $^{87}\text{Sr}/^{86}\text{Sr}=0.710246\pm 17$ (2 σ ; n=18) for SRM987 (by TIMS) and $^{143}\text{Nd}/^{144}\text{Nd}=0.512103\pm 7$ (2 σ ; n=6) for Ames Nd (by MC-ICP-MS). All Sr and Nd isotopic data are reported relative to constant standard values for SRM987 ($^{87}\text{Sr}/^{86}\text{Sr}=0.710250$) and Ames Nd ($^{143}\text{Nd}/^{144}\text{Nd}=0.512130$). After correcting to this value for Ames Nd, a single analysis of the La Jolla Nd standard as an unknown gave $^{143}\text{Nd}/^{144}\text{Nd}=0.511845$. The estimated reproducibility ($\pm 2\sigma$) for all of the data is based on multiple analyses of the La Jolla Nd standard and the Kil1919 rock in-house material by Marske et al. (2007). Uncertainties of the individual Sr analyses are based on the $\pm 2\sigma_m$ (n>4) of replicate analyses of each sample reported in Table A.1 in the appendix and in Garcia et al. (1996, 2000) and Pietruszka et al. (2006). Total procedural blanks were negligible compared to the amount of sample used (>0.6 g) and the concentrations of Pb, Sr, and Nd in the samples.

Sample	$^{206}\text{Pb}/^{204}\text{Pb}$	$^{207}\text{Pb}/^{204}\text{Pb}$	$^{208}\text{Pb}/^{204}\text{Pb}$	$^{87}\text{Sr}/^{86}\text{Sr}$	$^{143}\text{Nd}/^{144}\text{Nd}$	ϵ_{Nd}
7-Sep-98	18.4107	15.4727	38.0752	0.703601 \pm 6	0.512956	+6.21
13-Feb-99	18.4124	15.4736	38.0764	0.703616 \pm 6	0.512944	+5.97
27-Oct-99	18.4018	15.4726	38.0687	0.703622 \pm 9	0.512948	+6.04
19-Feb-00	18.4072	15.4712	38.0720	0.703634 \pm 7	0.512944	+5.97
21-Jun-00	18.4067	15.4704	38.0688	0.703644 \pm 7	0.512947	+6.04
8-Jan-01	18.4116	15.4721	38.0737	0.703639 \pm 12	0.512946	+6.01
7-Jul-01	18.4137	15.4719	38.0729	0.703626 \pm 9	0.512943	+5.95
9-Feb-02	18.4139	15.4707	38.0691	0.703637 \pm 8	0.512940	+5.89
20-Aug-02	18.4152	15.4722	38.0719	0.703639 \pm 5	0.512945	+5.98
12-Apr-03	18.4161	15.4726	38.0715	0.703641 \pm 5	0.512953	+6.14
15-Jan-04	18.4154	15.4719	38.0694	0.703632 \pm 7	0.512946	+6.01
7-Jun-04	18.4146	15.4716	38.0680	0.703623 \pm 7	0.512943	+5.95
31-Jan-05	18.4170	15.4735	38.0752	0.703624 \pm 5	0.512955	+6.19
8-Aug-05	18.4119	15.4727	38.0699	0.703622 \pm 10	0.512953	+6.14
In-house basaltic reference material (Kīlauea Volcano)						
Kil1919	18.6562	15.4903	38.2092	0.703477	0.512973	+6.53

spectrometer (MC-ICP-MS) at San Diego State University (SDSU). Strontium isotope ratios were measured using this MC-ICP-MS and/or a VG Sector 54 thermal ionization mass spectrometer (TIMS) at SDSU to compare the results of the two instruments. Additionally, six lavas erupted from 1989-1998 (Garcia et al., 1992, 1996, 2000) were reanalyzed for Sr isotope ratios from the original dissolutions using TIMS to improve the analytical precision for these samples (Table A.1). A detailed overview of the analytical methods used in this study is given in Marske et al. (2007). Additional details pertinent to this study are presented in Table 1.5.

1.3.5 Geochemistry of 1998-2005 Pu‘u ‘Ō‘ō lavas

The 1998-2005 Pu‘u ‘Ō‘ō lavas are compositionally similar to earlier lavas from this eruption (Fig. 1.3). For example, their MgO contents (6.7-9.8 wt. %) lie within the range of 1985-1998 lavas (6.7-10.1 wt. %, excluding mixed and evolved lavas from episode 54). However, small, but significant short-term (years) variations in major element abundances (at a given MgO) are evident in these lavas (Fig. 1.3). Similar variations have been observed for historical Kīlauea summit lavas and were related to changes in parental magma composition (e.g., Wright, 1971; Garcia et al., 2003). Overall, Pu‘u ‘Ō‘ō lavas have become progressively lower in CaO/Al₂O₃ ratios and incompatible element (TiO₂ and K₂O) contents, and higher in SiO₂ abundances (at a given MgO content) during the eruption (even if more differentiated samples with <7.2 wt. % MgO are excluded; Fig. 1.3). At a given MgO content, the total variation of Fe₂O₃* (i.e., total iron), Al₂O₃, and Na₂O abundances (not shown) for the 1998-2005 lavas lie within the compositional field of previous lavas. The high SiO₂ and low CaO, TiO₂, and K₂O contents, and CaO/Al₂O₃ ratios of the recent lavas expand the known compositional range for historical Kīlauea lavas towards historical Mauna Loa lavas (Fig. 1.3).

The relatively low abundances and ratios of incompatible elements (e.g., Nb and La/Sm) in 1998-2005 lavas form trends that partially overlap with 1989-1997 Pu‘u ‘Ō‘ō lavas, but also

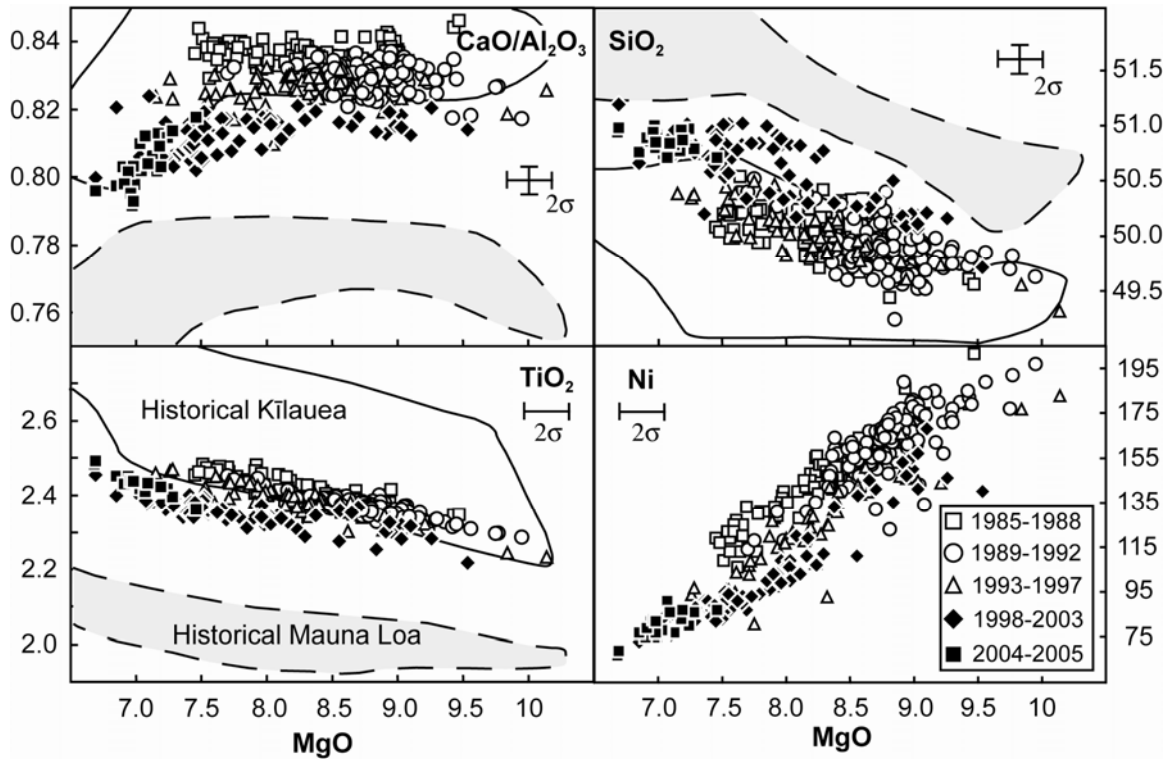


Fig. 1.3 Whole-rock MgO variation diagrams for Pu'u Ō'ō lavas, historical Kīlauea (Garcia et al., 2003), and historical Mauna Loa (Rhodes and Hart, 1995) lavas. The Pu'u Ō'ō lavas are grouped according to eruption date (see inset for symbols). The new 1998-2005 Pu'u Ō'ō data (solid symbols) from Table 1.3 are plotted with previous data (open symbols) from Garcia et al. (1992, 1996, 2000). These groups were further subdivided to better resolve the systematic geochemical changes, and to emphasize the rapid temporal changes during the eruption. Mixed and/or evolved Pu'u Ō'ō lavas (episodes 1-29 and 54) are not shown in this and subsequent figures. All values are in wt. % (except CaO/Al₂O₃). The 2σ error bars are shown in the corner of each plot unless they are smaller than the size of the symbols.

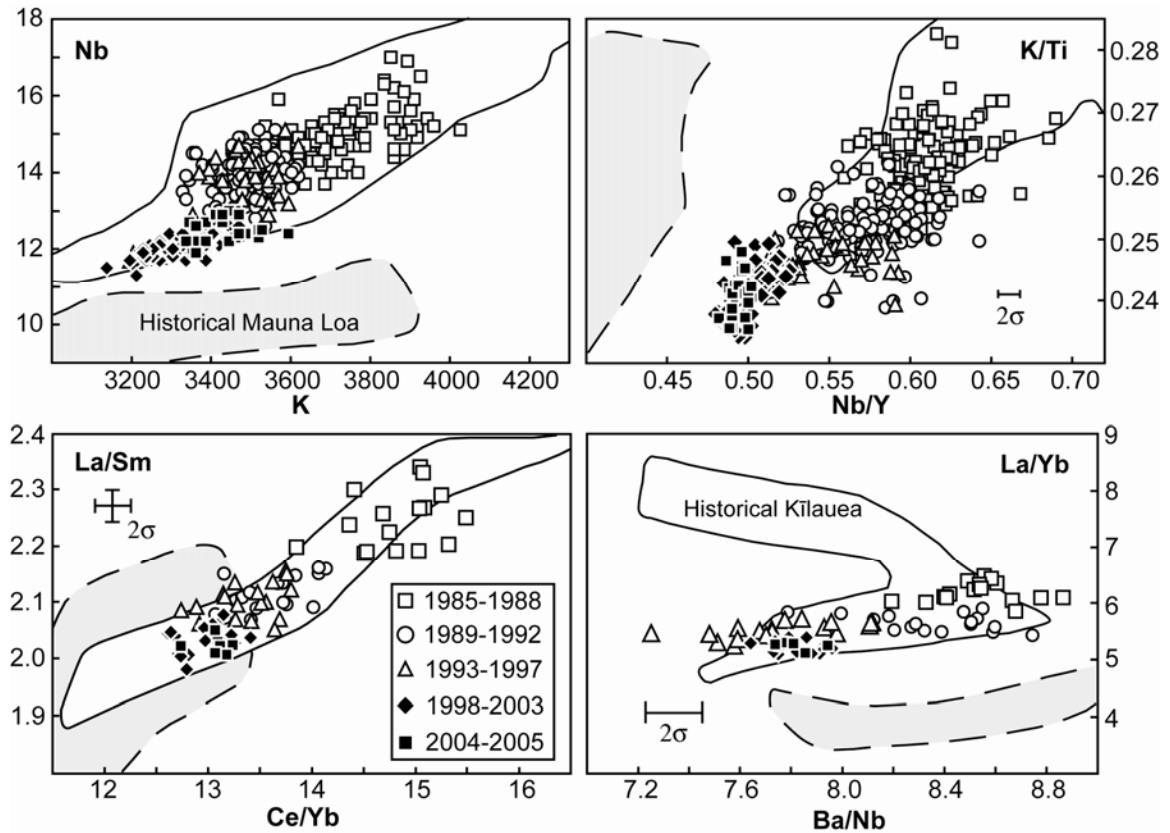


Fig. 1.4 Trace element variation diagrams for Pu'u Ō'ō lavas. The compositional fields of historical Kīlauea (Pietruszka and Garcia, 1999a; Garcia et al., 2003) and Mauna Loa (Rhodes and Hart, 1995; J.M. Rhodes, unpublished data, 2008) lavas are also plotted. The 2σ error bars are shown in the corner of each plot unless they are smaller than the size of the symbols. The values are in ppm except for the ratios. Estimates for the analytical precision of Pu'u Ō'ō lavas analyzed (by ICP-MS) prior to this study can be found in Garcia et al. (1996, 2000). Kil1919 and BHVO-2 come from the same lava flow. Pu'u Ō'ō ICP-MS trace element data from previous studies were corrected by normalizing the average Kil1919 in-house material ($n=11$) used for 1985-1998 Pu'u Ō'ō lavas to the BHVO-2 standard values for this study. Although the Kil1919 and BHVO-2 differ by 0.3 wt. % MgO, if this was due to olivine control (as expected) the maximum difference in the incompatible trace element concentrations would be 0.7%, which is within analytical uncertainty of the ICP-MS data (Norman et al., 1998).

expand the compositional range to the lowest values observed during the eruption (Fig. 1.4). Recent Pu‘u ‘Ō‘ō lavas continue the overall temporal decrease in highly to moderately incompatible trace element ratios (i.e., La/Yb) and abundances (i.e., Nb and Ba) since the early part of the eruption (Figs 1.4 and 1.5). These trace element abundances and ratios of the recent lavas, like the major element contents, extend the Pu‘u ‘Ō‘ō compositional range toward the field of historical Mauna Loa lavas (Fig. 1.4).

The $^{87}\text{Sr}/^{86}\text{Sr}$ ratios of the 1998-2005 lavas (0.70360-0.70364) are higher than previous Pu‘u ‘Ō‘ō lavas (0.70357-0.70360). In contrast, Pb (Figs 1.5 and 1.6) and Nd isotope ratios are within the range of previous lavas. However, the 1998-2005 lavas make a small, yet distinctive trend in $^{206}\text{Pb}/^{204}\text{Pb}$ vs. $^{87}\text{Sr}/^{86}\text{Sr}$ that expands the isotopic range for this eruption (Fig. 1.6).

Unlike the major and trace element chemistry, these Pb and Sr isotope variations trend towards an area between the compositional fields of Kīlauea and Mauna Loa (rather than directly towards the field of Mauna Loa lavas). Furthermore, this trend does not project towards a Hawaiian mantle end member (e.g., Kea or Loa) or towards the known isotopic composition of any other Hawaiian volcano.

1.4 Discussion

1.4.1 Crustal magmatic processes during the eruption

Olivine fractionation plays a dominant role in controlling the compositional variations in Hawaiian lavas (e.g., Powers, 1955; Wright, 1971). The importance of olivine crystallization in Pu‘u ‘Ō‘ō lavas is evident from their wide range of MgO contents (5.6-10.1 wt. %), and the presence of normally zoned olivine phenocrysts (Garcia et al., 1996, 2000). Shallow magma mixing between stored rift magmas and ‘fresh’ MgO-rich magma(s) was important process that controlled the composition of lavas erupted before February 1985 (episode 1-29; Garcia et al., 1992), and during episode 54 in January 1997 (Garcia et al., 2000; Thornber et al., 2003). Most

(~93%) Pu‘u ‘Ō‘ō lavas (excluding evolved lavas from episodes 1-29 and 54) have >7.2 wt. % MgO suggesting that the variation in the major element abundances of these lavas is primarily related to olivine fractionation and/or accumulation (i.e., olivine control; Wright, 1971). However, the MgO and Ni abundances of the Pu‘u ‘Ō‘ō lavas have systematically decreased (with much scatter) since the eruption location shifted in early 1992 from the Kūpaianaha vent to the Pu‘u ‘Ō‘ō cone (Figs 1.3 and 1.5), suggesting that Pu‘u ‘Ō‘ō magmas are becoming increasingly differentiated with time. Clinopyroxene fractionation has become an increasingly important process for 1998-2005 lavas. For example, there is a greater abundance of clinopyroxene microphenocrysts in the 1998-2005 lavas (up to 3 vol. %; Table 1.1) compared to earlier erupted Pu‘u ‘Ō‘ō lavas (<1 vol. % or absent), and ~50% of the most recent lavas (2004-2005) have differentiated beyond olivine control (<7.2 wt. % MgO; Fig. 1.5).

Olivine accumulation has also affected some Pu‘u ‘Ō‘ō lava compositions based on the low Fo contents of some olivines compared to their whole-rock Mg# (Fig. 1.2). For example, the maximum MgO difference for two olivine-controlled 1998-2005 lavas (23-Jul-04; 7.0 wt. % MgO and 4-Jan-00; 9.5 wt. % MgO) with similar olivine Fo contents (81-82%; Fig. 1.2) can be explained by the accumulation of ~6.1 vol. % olivine. This is consistent with the 5% greater modal abundance of olivine phenocrysts in sample 4-Jan-00 compared to 23-Jul-04, and the position of sample 4-Jan-00 to the right of the equilibrium field on Fig. 1.2. All of the 2003-2005 lavas analyzed have Fo contents in equilibrium with their bulk compositions (Fig. 1.2).

1.4.2 Temporal compositional variations

Pu‘u ‘Ō‘ō lavas display systematic temporal variations of MgO-normalized major element abundances, ratios of highly to moderately incompatible trace elements (e.g., La/Yb), highly

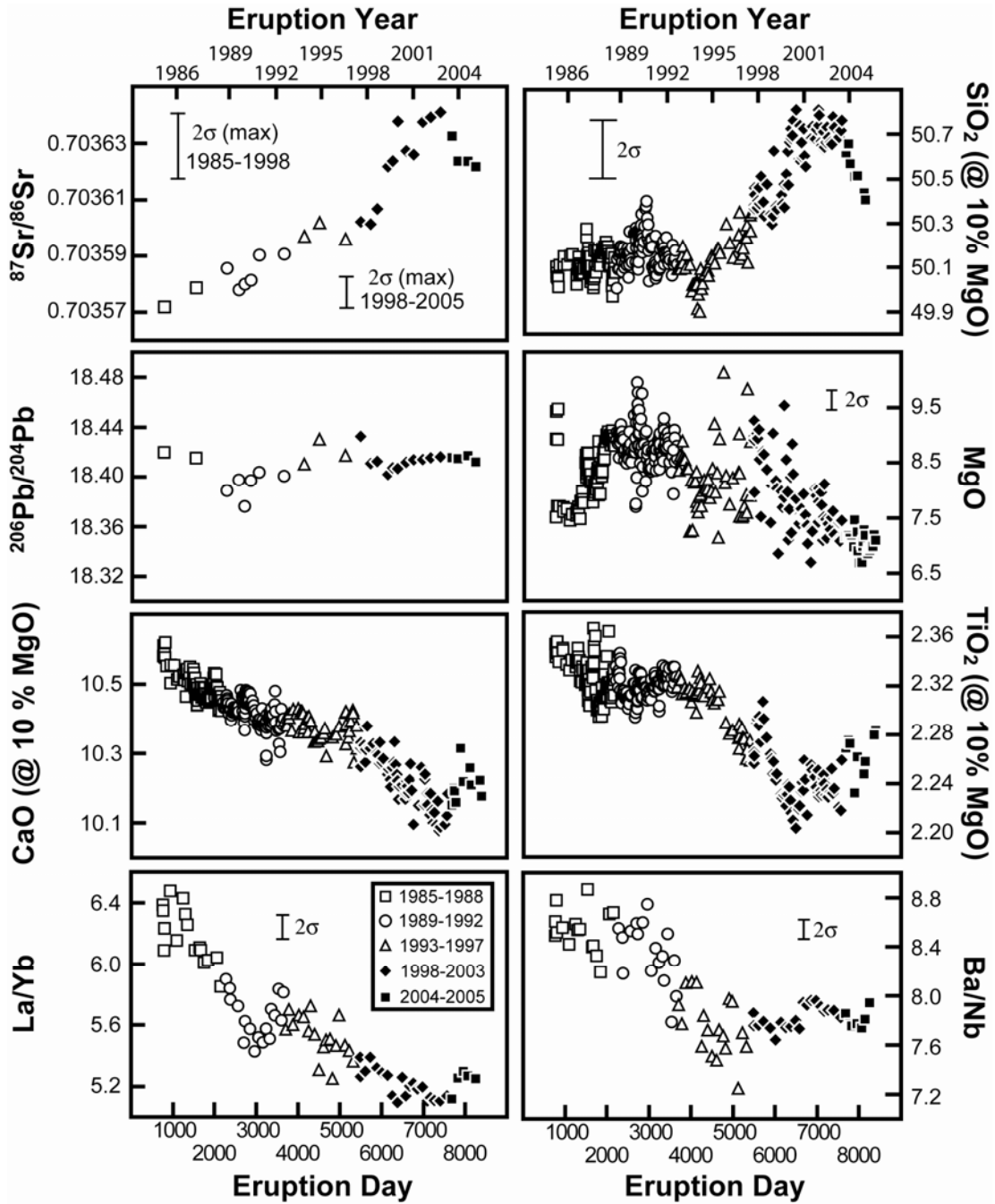


Fig. 1.5 Temporal geochemical variations during the Pu'u Ō'ō eruption. The 1985-1998 Pu'u Ō'ō lava data are from Garcia et al. (1992, 1996, 2000). SiO₂, CaO, and TiO₂ were normalized to 10 wt. % MgO (the most primitive lava erupted from Pu'u Ō'ō; Garcia et al., 2000) by the addition of equilibrium composition olivine (98.5%) and spinel (1.5%) in 0.5 mol. % steps (Garcia et al., 2003; Rhodes and Vollinger, 2005). Pu'u Ō'ō lavas with <7.2 wt. % MgO may have crystallized minerals other than olivine (e.g., clinopyroxene and plagioclase) and were not included in the olivine normalization procedure. The 2σ error bars are shown in the corner of each plot unless they are smaller than the size of the symbols. The maximum 2σ error bars are presented in the Sr isotope panel for lavas erupted between 1985-1998 and 1998-2005. The individual ⁸⁷Sr/⁸⁶Sr analytical uncertainties for each sample (presented in Table 1.5) are typically smaller than the maximum 2σ error bar.

incompatible trace element ratios (e.g., Ba/Nb), and Pb and Sr isotope ratios (Fig. 1.5). At least three distinct end-member magma compositions may be delineated based on correlated temporal changes among some MgO-normalized major element abundances, and incompatible trace element and Sr isotope ratios: (1) 1985-1998 (day ~760-5500), (2) 1998-2003 (day ~5501-7400), and (3) 2003-2005 (day ~7401-8400). Magma mixing affected the composition of lavas erupted before February 1985 (days 1-745; Garcia et al., 1992) and during episode 54 in January 1997 (day 5141; Garcia et al., 2000; Thornber et al., 2003) and these lavas were excluded from the plots.

The SiO₂ temporal trend for Pu'u Ō'ō lavas inversely correlates with the temporal variations of CaO and TiO₂ (Fig. 1.5). Between ~1985-1998, MgO-normalized major element abundances display relatively flat (SiO₂) and slightly decreasing (CaO and TiO₂) trends. However, lavas erupted between ~1998 to 2003 display changes in slope with significant increases and decreases in these abundances, respectively, until mid-2003 (Fig. 1.5). Following a compositional reversal in mid-2003, the MgO-normalized SiO₂ abundances have decreased whereas CaO and TiO₂ contents have increased. In contrast, Al₂O₃ and Fe₂O₃ contents (not shown) have remained nearly constant.

Pu'u Ō'ō lavas also display systematic fluctuations in incompatible trace element ratios that correlate with the major element changes (Fig. 1.5). Between ~1985 to 1998 there are small, but significant decreases in some ratios of incompatible trace elements until day ~5500. Between ~1998-2003 these incompatible trace element ratios display flattening (e.g., La/Yb) or nearly constant (e.g., Ba/Nb) temporal trends. Some ratios of highly over moderately incompatible trace elements (e.g., La/Yb) record a small compositional reversal in mid-2003, followed by a small increase similar to the reversal recorded by the normalized major element abundances (Fig. 1.5).

The ⁸⁷Sr/⁸⁶Sr ratios of Pu'u Ō'ō lavas gradually increased between ~1985-1998, before a sharper increase occurred in 1998 (day ~5500). This shift coincided with the significant

increases in MgO-normalized SiO₂ abundances and decreases in the CaO and TiO₂ abundances (Fig. 1.5). The ⁸⁷Sr/⁸⁶Sr ratios increased to the highest observed values for this eruption in mid-2003, and reversed from 2003-2005. This is also analogous to the reversals of MgO-normalized major element abundances and incompatible trace element ratios (Fig. 1.5). In contrast, the Pb and Nd isotope ratios have remained relatively constant since 1985 (relative to analytical error), especially for the 1998-2005 lavas (Fig. 1.5; Table 1.5).

In summary, three distinct end-member compositions are important during the Pu‘u ‘Ō‘ō eruption. First, an early end member (~1985) has relatively low ⁸⁷Sr/⁸⁶Sr ratios and MgO-normalized SiO₂ abundances and high CaO and TiO₂ abundances and incompatible trace element ratios (e.g., Ba/Nb or La/Yb). Second, a later end member (~1998) from a recently depleted source (Pietruszka et al., 2006) has slightly higher ⁸⁷Sr/⁸⁶Sr and MgO-normalized SiO₂ contents, yet lower incompatible trace element ratios and CaO and TiO₂ abundances. Third, the most recent end-member composition (~2003) displays the highest ⁸⁷Sr/⁸⁶Sr ratios and MgO-normalized SiO₂ abundances, and lowest abundances of CaO and TiO₂ and ratios of incompatible trace elements for the eruption.

1.4.3 Pu‘u ‘Ō‘ō source characteristics

1.4.3.1 *A lithospheric source component for Pu‘u ‘Ō‘ō lavas?*

Magmas originating from partial melting within the Hawaiian plume can be compositionally modified at shallower depths by the assimilation of hydrothermally altered oceanic crust (e.g., Eiler et al., 1996) or lower gabbroic crust (e.g., Gaffney et al., 2004), or by partial melting the upper ambient mantle (lithospheric or asthenosphere) beneath Hawai‘i (e.g., Tatsumoto, 1978; Chen and Frey, 1985; Stille et al., 1986; Lassiter et al., 1996). However, it is unlikely that crustal assimilation or melting of the upper ambient mantle significantly modified the chemical signature of Pu‘u ‘Ō‘ō lavas. Pu‘u ‘Ō‘ō lavas erupted between 1983-1986 have relatively low δ¹⁸O

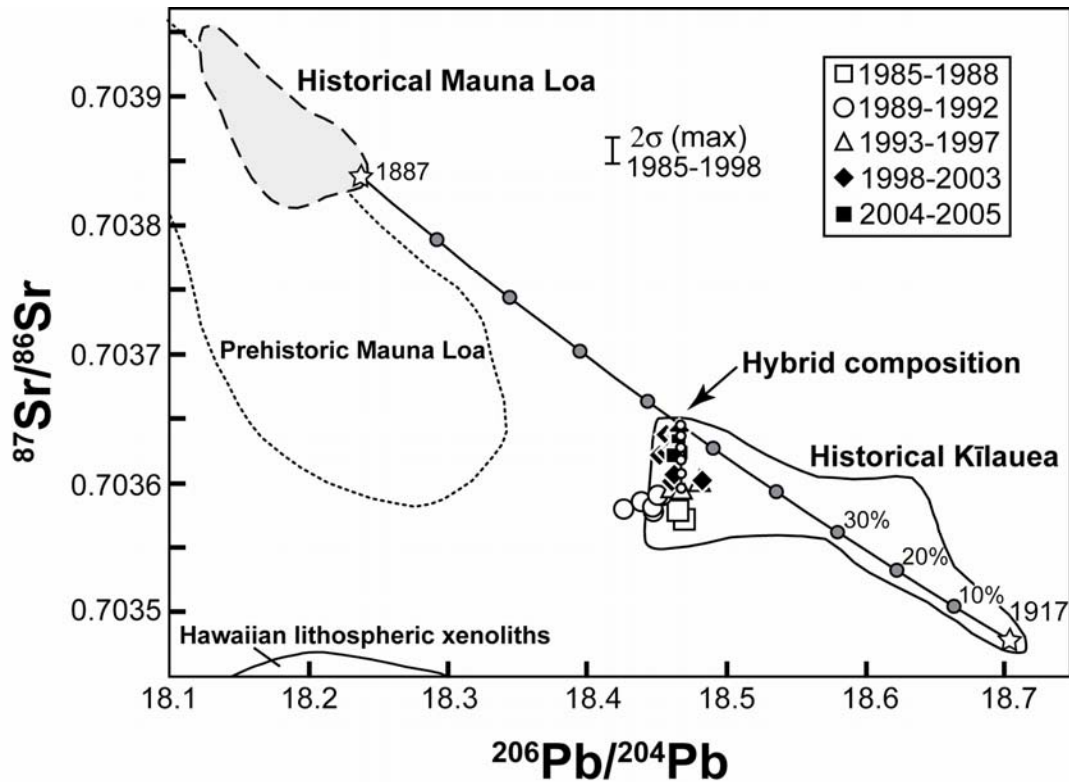


Fig. 1.6 $^{206}\text{Pb}/^{204}\text{Pb}$ vs. $^{87}\text{Sr}/^{86}\text{Sr}$ isotope ratios for Pu'ū Ō'ō lavas compared with historical Kīlauea, and prehistoric and historical Mauna Loa lavas. Data sources: Garcia et al. (1992, 1996, 2000) for 1985-1998 Pu'ū Ō'ō lavas; Pietruszka and Garcia (1999a) and Abouchami et al. (2005) for historical Kīlauea lavas; Kurz and Kammer (1991), Kurz et al. (1995), Rhodes and Hart (1995), Wanless et al. (2006), and Marske et al. (2007) for historical and prehistoric Mauna Loa lavas. The compositional fields of Pacific mid-oceanic ridge basalts ($^{206}\text{Pb}/^{204}\text{Pb} = 18.24\text{-}19.48$ and $^{87}\text{Sr}/^{86}\text{Sr} = 0.70264\text{-}0.70367$; King et al., 1993; Fekiacova et al., 2007) and most Hawaiian lithospheric xenoliths ($^{206}\text{Pb}/^{204}\text{Pb} = 17.58\text{-}18.38$ and $^{87}\text{Sr}/^{86}\text{Sr} = 0.70271\text{-}0.70347$; Okano and Tatsumoto, 1996; Lassiter and Hauri, 1998) lie off the figure (below the isotopic fields of Kīlauea and Mauna Loa). Mixing lines between 1917 A.D. Kīlauea and 1887 A.D. Mauna Loa lavas (line with gray circles) and between a Pu'ū Ō'ō sample (10-Jan-1997) and a hybrid source (line with small open circles) containing a 55:45 proportion of the historical Kīlauea and Mauna Loa compositions are shown. The Pb abundances assumed for the mixing model are 1 ppm for Kīl1917 ($^{206}\text{Pb}/^{204}\text{Pb} = 18.653$, $^{87}\text{Sr}/^{86}\text{Sr} = 0.703478$) and 10-Jan-1997 ($^{206}\text{Pb}/^{204}\text{Pb} = 18.417$, $^{87}\text{Sr}/^{86}\text{Sr} = 0.703596$) based on the average Pb concentrations in Table 1.4, and 0.9 ppm Pb for the 1887 Mauna Loa ($^{206}\text{Pb}/^{204}\text{Pb} = 18.187$, $^{87}\text{Sr}/^{86}\text{Sr} = 0.703838$) lava. The Sr concentrations in the mixing end members are from Pietruszka and Garcia (1999a) for the 1917 Kīlauea lava (389 ppm Sr), Rhodes and Hart (1995) for 1887 Mauna Loa lava (275 ppm Sr), and Garcia et al. (2000) for the 10-Jan-1997 lava (307 ppm Sr). The maximum 2σ error bars are presented for 1985-1998 lavas. The 2σ error bars for 1998-2005 Pb and Sr isotope ratios are smaller than the size of the symbol.

groundmass values (4.6-5.0‰) that are in disequilibrium with their olivine phenocrysts, suggesting these early magmas interacted with shallow wall rock in the rift zone just prior to eruption (Garcia et al., 1998). The switch in eruptive style from episodic lava fountaining to near continuous effusion in 1986, led to a marked reduction or elimination of contamination based on higher $\delta^{18}\text{O}$ groundmass values (5.0-5.3‰) in equilibrium with olivines in the 1986-1998 lavas (Garcia et al., 1998). Furthermore, the 1998-2003 Pu‘u ‘Ō‘ō lavas record systematic temporal increases in $^{87}\text{Sr}/^{86}\text{Sr}$ ratios and relatively constant $^{206}\text{Pb}/^{204}\text{Pb}$ ratios (Fig. 1.6) that trend away from the compositional fields of lithospheric mantle xenoliths from Salt Lake Crater, O‘ahu (Okano and Tatsumoto, 1996) and Hualālai volcano, Hawai‘i (Lassiter and Hauri, 1998), and Cretaceous Pacific mid-oceanic ridge basalts near Hawai‘i (e.g., Ocean Drilling Program Site 843; King et al., 1993; Fekiacova et al., 2007).

Historical Kīlauea summit lavas have relatively low $\delta^{18}\text{O}$ isotope values that are attributed to <5-12% contamination of parental magmas with altered country rock from both Kīlauea and Mauna Loa (Garcia et al., 2008). The overall increase of Sr isotopes in Pu‘u ‘Ō‘ō lavas could potentially be explained if a more typical Kīlauea parental magma (e.g., 1993-1997 Pu‘u ‘Ō‘ō lavas) progressively assimilated a roughly constant (55:45) mixture of older Kīlauea and Mauna Loa basement rocks (Fig. 1.6). However, this would require ~100% contamination because the Pu‘u ‘Ō‘ō lava with the highest $^{87}\text{Sr}/^{86}\text{Sr}$ ratio overlaps with the composition of the 55:45 Kīlauea-Mauna Loa assimilant. These combined observations suggest that melt interaction with the upper mantle, crust, or volcanic edifice beneath Kīlauea is minimal for recent Pu‘u ‘Ō‘ō lavas.

1.4.3.2 A third mantle source for the Pu‘u ‘Ō‘ō eruption

At least three distinct mantle source components are required to explain the compositional variability of Pu‘u ‘Ō‘ō lavas (Fig. 1.7). The 1985-1998 Pu‘u ‘Ō‘ō lavas originated from at least

two distinct source components with similar Kīlauea-like Pb, Sr, and Nd isotopic compositions but different incompatible element abundances and ratios (Garcia et al., 2000). One component with higher MgO-normalized CaO and TiO₂ abundances and incompatible trace element ratios (e.g., Ba/Ce or La/Yb), was important during the early part of the eruption (~1985; Figs 1.5 and 1.7), following the period of magma mixing during episodes 1-29. The temporal decreases among ²³⁰Th-²³⁸U and ²²⁶Ra-²³⁰Th disequilibria, incompatible trace element ratios (e.g., Th/U or Nd/Sm), and some normalized major element abundances in lavas from 1985-2001 (Fig. 1.5) suggest a second mantle component was tapped (Pietruszka et al., 2006). This ‘recently depleted’ component is thought to have formed <8 ka (based on modeling of ²²⁶Ra-²³⁰Th-²³⁸U disequilibria) by the removal of melt from Kīlauea’s source region within the Hawaiian plume, causing it to become depleted in incompatible trace elements (Pietruszka et al., 2006). A progressive increase in the proportion of the recently depleted component is indicated by the temporal trends between 1985-1998 (Figs 1.5 and 1.7; Garcia et al., 2000; Pietruszka et al., 2006).

The systematic geochemical variations from 1998-2003 (Figs 1.5-1.7) require a third component that was increasingly tapped during this time interval. Based on the temporal increases of some highly incompatible trace element ratios (e.g., Ba/Th) in lavas erupted from 1999-2001, Pietruszka et al. (2006) suggested that Pu‘u ‘Ō‘ō lavas are derived in greater proportions of a source component similar to historical Mauna Loa lavas. However, simple mixing of melt from a Mauna Loa-like source (with relatively low ²⁰⁶Pb/²⁰⁴Pb and high ⁸⁷Sr/⁸⁶Sr) with an earlier Pu‘u ‘Ō‘ō composition (i.e., the recently depleted component) cannot explain the increase in ⁸⁷Sr/⁸⁶Sr ratios at relatively constant ²⁰⁶Pb/²⁰⁴Pb ratios between 1998-2003 (Fig. 1.6).

Rhodes et al. (1989) proposed that magma from Mauna Loa may periodically invade Kīlauea’s plumbing system. Pre-mixing nearly equal proportions of historical Kīlauea- and Mauna Loa-like magmas prior to eruption could potentially explain the trends of recent Pu‘u ‘Ō‘ō lavas (Figs 1.6 and 1.8). Although this pre-mixing could occur in the Kīlauea’s ~2-3 km³ summit

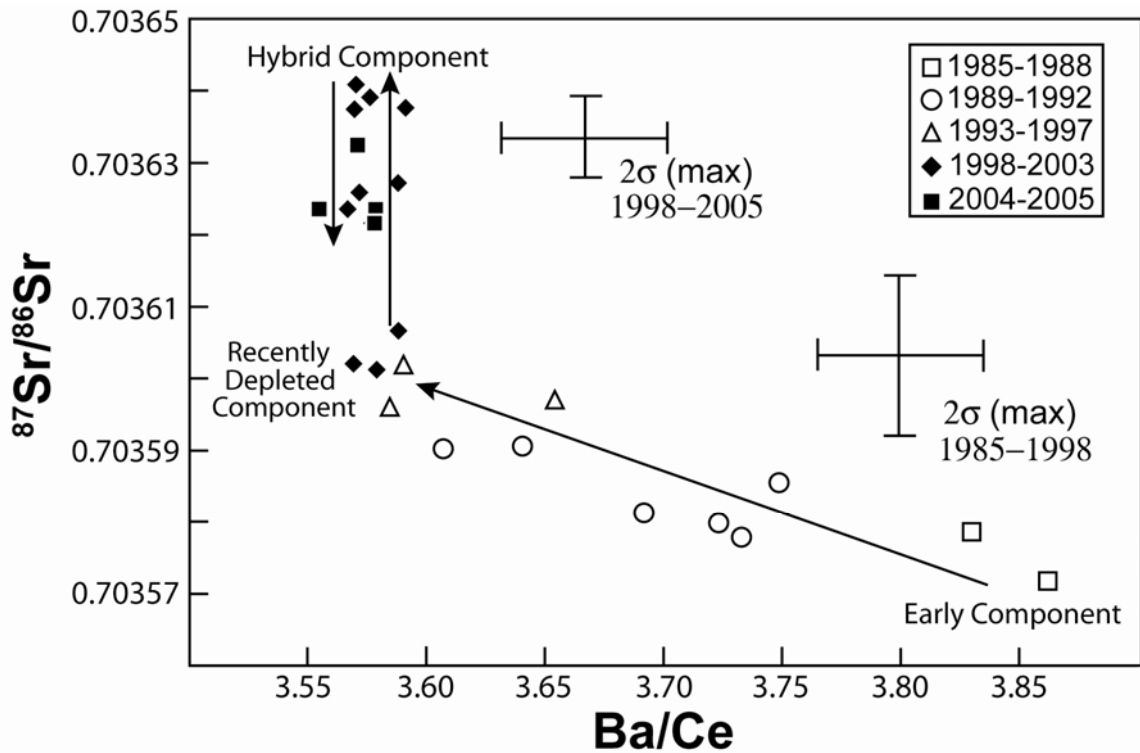


Fig 1.7 Ba/Ce vs. $^{87}\text{Sr}/^{86}\text{Sr}$ for Pu'u Ō'ō lavas. The 1985-1998 Pu'u Ō'ō lava data are from Garcia et al. (1992, 1996, 2000). At least three distinct mantle sources (termed the early, recently depleted and hybrid components) are required to explain the chemical variability during the Pu'u Ō'ō eruption. The maximum 2σ error bar is presented for 1985-1998 and 1998-2005 lavas (Sr isotopes only). Historical Mauna Loa lavas display a lower Ba/Ce range (2.6-3.5; J.M. Rhodes, unpublished data, 2008), with higher Sr isotope values (>0.70375 ; Rhodes and Hart, 1995).

reservoir (Pietruszka and Garcia, 1999b), the rapid compositional changes in Pu‘u ‘Ō‘ō lavas are inconsistent with mixing in this reservoir (Garcia et al., 1996). No other suitable crustal reservoir is known to accommodate this magma mixing. Thus, crustal magma mixing is an unlikely explanation for the 1998-2003 Pu‘u ‘Ō‘ō compositional variations. Instead, these recent lavas can be explained if they were derived from a mixture of Mauna Loa- and Kīlauea-like mantle sources that subsequently melted. This hybrid source represents a new component for the eruption.

Historical lavas from Kīlauea and Mauna Loa volcano provide an important window to the present-day composition and distribution of mantle components in the Hawaiian plume (e.g., Rhodes and Hart, 1995; Pietruszka and Garcia, 1999a). Consequently, the origin of the recent Pu‘u ‘Ō‘ō lavas is discussed below in terms of mixing between the mantle source components defined by historical lavas from these two volcanoes (rather than the more extreme end-member isotopic compositions observed in Ko‘olau and Mauna Kea lavas). The proportions of Kīlauea and Mauna Loa components in the hybrid source can be estimated from compositional mixing trends (Figs 1.6 and 1.8). The 1917 Kīlauea lava was chosen as an end member because it has the highest $^{206}\text{Pb}/^{204}\text{Pb}$ and $^{143}\text{Nd}/^{144}\text{Nd}$ and lowest $^{87}\text{Sr}/^{86}\text{Sr}$ ratios among olivine-controlled historical Kīlauea lavas (Pietruszka and Garcia, 1999a). Although a range of historical Mauna Loa lavas would make reasonable isotopic end members for this calculation, the 1887 Mauna Loa lava (Rhodes and Hart, 1995) was selected because it creates a suitable mixing trend on the plots of MgO-normalized major elements vs. $^{206}\text{Pb}/^{204}\text{Pb}$ and $^{87}\text{Sr}/^{86}\text{Sr}$ (Fig. 1.8). The 10-Jan-1997 Pu‘u ‘Ō‘ō sample was chosen to represent the recently depleted Kīlauea source component because it has the lowest ratios of highly incompatible trace elements (e.g., Ba/Nb or Ba/Rb) for this eruption. Mixing trends between the 1917 Kīlauea (55%) and 1887 Mauna Loa (45%) lavas (Figs 1.6 and 1.8) pass within analytical error of the 2001-2003 Pu‘u ‘Ō‘ō lavas (i.e., the samples with

the highest $^{87}\text{Sr}/^{86}\text{Sr}$ and MgO-normalized SiO_2 values). Therefore, this 55:45 Kīlauea-Mauna Loa composition might be a good estimate of the hybrid source.

This mixing model suggests that the melt contribution from the recently depleted source component decreased starting in early 1998 as melt derived from the hybrid source was tapped in greater proportions until mid-2003 (Figs 1.7 and 1.8). Following the mid-2003 compositional reversal, the lavas display chemical and isotopic variations that overlap with the compositional fields of the 1998-2003 lavas (Figs 1.3-1.8) indicating a diminishing importance for the hybrid component since 2003.

1.4.3.3 A pyroxenite source for Pu‘u ‘Ō‘ō lavas?

Partial melting of a heterogeneous plume source containing a mixture of peridotite and ancient recycled oceanic crust \pm sediment (pyroxenite or eclogite) has become a common explanation for the chemical and isotopic variations in Hawaiian lavas (e.g., Hauri, 1996; Lassiter and Hauri, 1998; Blichert-Toft et al., 1999; Takahashi and Nakajima, 2002; Gaffney et al., 2005; Sobolev et al., 2005, 2007; Herzberg, 2006). For example, Ko‘olau lavas, with relatively high $^{87}\text{Sr}/^{86}\text{Sr}$ (~ 0.7044) and SiO_2 (~ 53 -55 wt. %), are explained by melting ancient recycled oceanic crust within the Hawaiian plume (Hauri, 1996; Lassiter and Hauri, 1998; Blichert-Toft et al., 1999; Huang and Frey, 2005; Fekiacova et al., 2007). Further support for a pyroxenite source within the Hawaiian plume comes from modeling compositional variations of lavas during long-lived eruptions, including Pu‘u ‘Ō‘ō (Reiners, 2002). This model predicts the continuous SiO_2 increases and CaO decreases could be explained if Pu‘u ‘Ō‘ō lavas originated from a mixed pyroxenite-peridotite source with different solidi.

The temporal increases in $^{87}\text{Sr}/^{86}\text{Sr}$ ratios and SiO_2 abundances (normalized to 10 wt. % MgO) in the 1998-2003 lavas (Fig. 1.5) could be evidence for increased melting of an eclogite or pyroxenite lithology (i.e., recycled oceanic crust) in the Hawaiian plume. However, an increasing

contribution of this source lithology during the eruption is unlikely for the following reasons: (1) the MgO-normalized SiO₂ trend is relatively flat prior to 1998, increased from 1998 to 2003, and has decreased since mid-2003. Moreover, the CaO trend has increased since mid-2003. Both trends are inconsistent with a simple mixed lithology source (e.g., Reiners, 2002); and (2) the Ni abundances of the lavas have progressively decreased (at a given MgO) from ~1992 to 2005 (Fig. 1.3). Because Ni is highly compatible in olivine relative to clinopyroxene (e.g., Sobolev et al., 2005), the decreases in Ni content suggest that recent Pu‘u ‘Ō‘ō lavas originated from a peridotite source that became more olivine-rich and/or clinopyroxene-poor with time. A peridotite source is also supported by the positive correlation between ²²⁶Ra-²³⁰Th and ²³⁰Th-²³⁸U disequilibria of 1985-2001 Pu‘u ‘Ō‘ō lavas (Pietruszka et al., 2006).

1.4.4 Small-scale mantle heterogeneity

The timing of the temporal inflections of the ⁸⁷Sr/⁸⁶Sr ratios in the Pu‘u ‘Ō‘ō lavas may be used to help constrain the scale of heterogeneity within Kīlauea’s melting region. The steady increase in the ⁸⁷Sr/⁸⁶Sr ratios between 1998 (day ~5500) and 2003 (day ~7400) suggests the proportion of the hybrid component progressively increased during this period. The lack of significant changes in the volume of magma stored in the shallow summit reservoir beneath Kīlauea during prolonged (months to years) historical Kīlauea rift eruptions (i.e., Mauna Ulu and Pu‘u ‘Ō‘ō) suggest the magma supply rate is similar to lava effusion rate (Tilling et al., 1987; Dvorak and Dzurisin, 1993; Denlinger, 1997). Assuming the magma supply rate is approximately equal to the lava effusion rate (~0.13 km³/yr; Sutton et al., 2003) for the Pu‘u ‘Ō‘ō eruption, the total volume of melt extracted from Kīlauea’s source region from 1998-2003 (~1900 days) was ~0.7 km³. This estimate probably represents the maximum volume of melt derived from the hybrid source during this period. If 100% of the recently depleted and hybrid components was being tapped at the temporal inflections in 1998 and 2003, respectively, melt from the hybrid source might represent

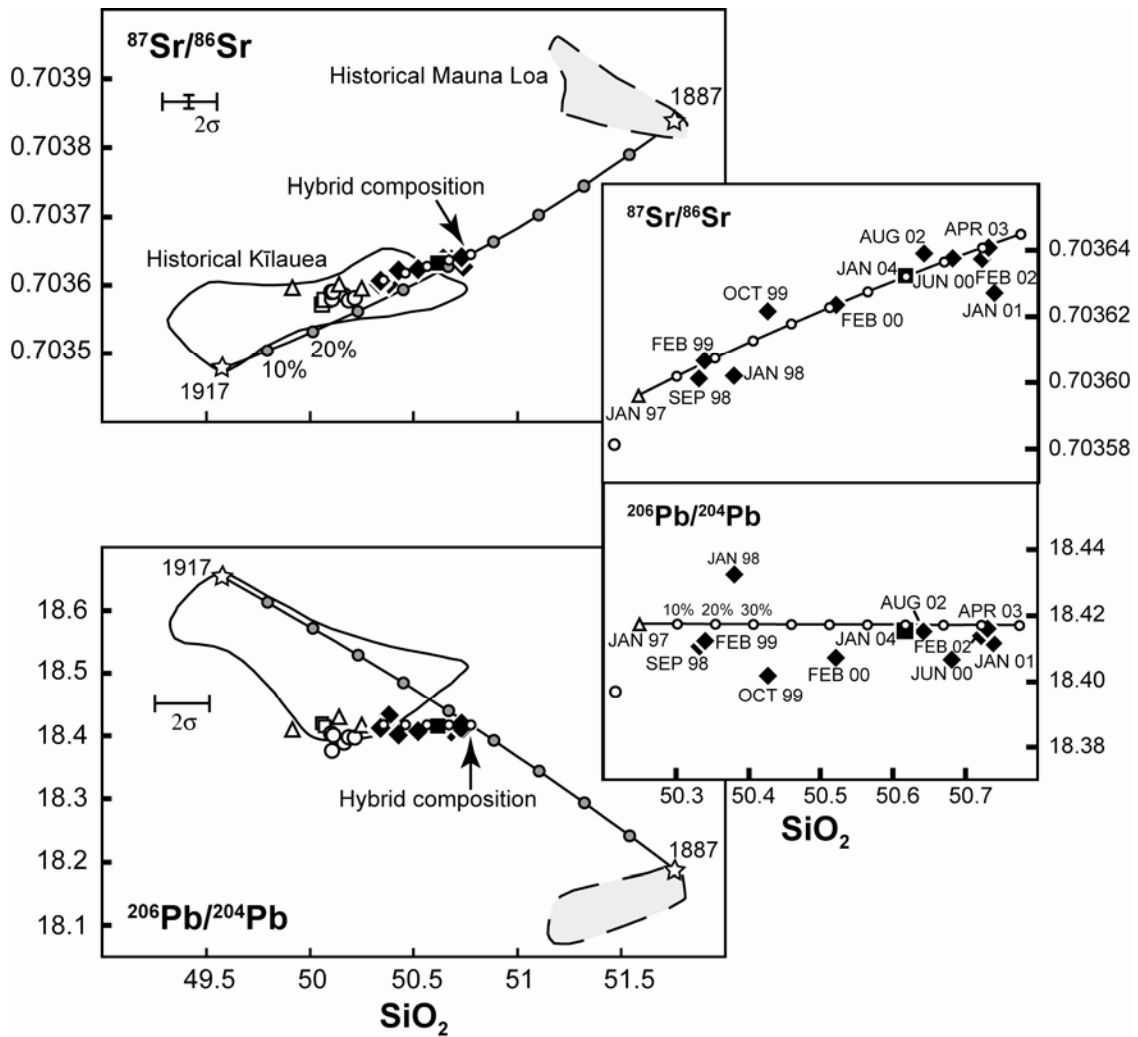


Fig. 1.8 $^{206}\text{Pb}/^{204}\text{Pb}$ and $^{87}\text{Sr}/^{86}\text{Sr}$ vs. MgO-normalized SiO_2 abundances for Pu'u Ō'ō, and historical Kīlauea and Mauna Loa lavas. Data sources: Garcia et al. (1992, 1996, 2000) for 1985-1998 Pu'u Ō'ō lavas; Pietruszka and Garcia (1999a), Garcia et al. (2003), and Abouchami et al. (2005) for historical Kīlauea lavas; Rhodes and Hart (1995) for historical Mauna Loa lavas. Mixing lines between a Pu'u Ō'ō sample (10-Jan-1997) and a hybrid composition containing a 55:45 proportion of historical Kīlauea (i.e., 1917 A.D.) and Mauna Loa (i.e., 1887 A.D.) compositions are shown. Mixing model details are listed in the caption of Fig. 1.6. The 2σ error bar applies to 1985-1998 ($^{206}\text{Pb}/^{204}\text{Pb}$ and $^{87}\text{Sr}/^{86}\text{Sr}$ ratios) and 1985-2005 (SiO_2 contents) lavas. The 2σ error bars for 1998-2005 Pb and Sr isotope ratios on the main plots are smaller than the size of the symbols.

~50% of the total lava volume erupted from 1998 to 2003 (~0.35 km³). Models for tholeiitic basalt production within the Hawaiian plume suggest that the melt-zone porosity within Kīlauea's source region is ~2-3% (Sims et al., 1999, Pietruszka et al., 2001). Thus, if melt tapped from 1998-2003 represents ~2-3% of the total volume from which it was extracted, then the volume of the source region that supplied melt during this period would be ~10-35 km³.

The 1998-2003 lavas plot within analytical error along the mixing line from the recently depleted source (10-Jan-1997) towards the hybrid component (Figs 1.6 and 1.8). If these recent lavas are derived from a hybrid mantle source containing a mixture of Kīlauea and Mauna Loa components, then the size of these components must be significantly smaller than the volume of the source region that was tapped from 1998-2003 (<10-35 km³). Thus, the Kīlauea and Mauna Loa mantle components that make up the hybrid component are thought to be mixed on a fine-scale.

1.4.5 Chemical structure of the Hawaiian plume

The long-term geographical and compositional differences among Hawaiian shield volcanoes have been related to the distribution of large-scale heterogeneities in a radially (Lassiter et al., 1996; Bryce et al., 2005), asymmetric (Abouchami et al., 2005) or irregularly zoned (Kurz et al., 2004) Hawaiian plume. For example, Kīlauea and Mauna Loa volcanoes have erupted geochemically distinct lavas for most of their known eruptive history, suggesting that the source components of these volcanoes (i.e., Kea and Loa) have remained compositionally distinct [except for some young prehistoric (A.D. 900-1400) Kīlauea and Mauna Loa lavas; Marske et al., 2007] over a time scale of thousands of years (e.g., large-scale heterogeneity; Frey and Rhodes, 1993; Abouchami et al., 2005). However, the recent Pu'u Ō'ō compositional trends suggest that both Kīlauea- and Mauna Loa-like components are present within Kīlauea's source region with a

spatial distribution capable of creating the rapid fluctuation towards the hybrid composition on a time scale of years.

To explain the recent trend of Pu‘u ‘Ō‘ō lavas towards the hybrid composition we propose a model with large-scale compositional heterogeneity (e.g., Lassiter et al., 1996; DePaolo et al., 2001; Bryce et al., 2005) that is gradational across the Hawaiian plume (black to white shading in Fig. 1.9a). On a finer scale, Kīlauea- and Mauna Loa-like heterogeneities (<10-35 km³) are assumed to be present (within the enlarged circles in Fig. 1.9a), but vary in relative abundance depending on location within the Hawaiian plume. For example, the darker zonation within Kīlauea’s typical source region contains more Kīlauea heterogeneities, and vice versa for the whiter zone below Mauna Loa. Similarly, the intermediate gray zone located between these two volcanoes represents a source with approximately equal amounts of Kīlauea- and Mauna Loa-like compositions (Fig. 1.9a).

Resolving the spatial distribution of these small-scale compositional heterogeneities (<10-35 km³) is problematic given the wide range in estimates for the size of Kīlauea’s melting region. These estimates vary from a ~55 km thick region near the central axis of the plume (Watson and McKenzie, 1991) to a thickness of <5-10 km (Marske et al., 2007). The maximum radius of this melting region is probably ~17 km (i.e., half the distance between the summits of Kīlauea and Mauna Loa; Pietruszka et al., 2001). Estimates for the rates of mantle melting in the Hawaiian plume range from >0.0005 to >0.03 kg m⁻³ yr⁻¹ (Cohen et al., 1993; Hemond et al., 1994; Sims et al., 1999; Pietruszka et al., 2001). Even the highest melting rates would require melting over a voluminous mantle source region (~8500 km³; Pietruszka et al., 2006) to account for the vigorous lava effusion rate during the Pu‘u ‘Ō‘ō eruption (~0.13 km³/yr; Sutton et al., 2003). Tapping such a large melting region would probably homogenize the melts derived from the three distinct sources for this eruption. Instead, the compositional variability of Pu‘u ‘Ō‘ō

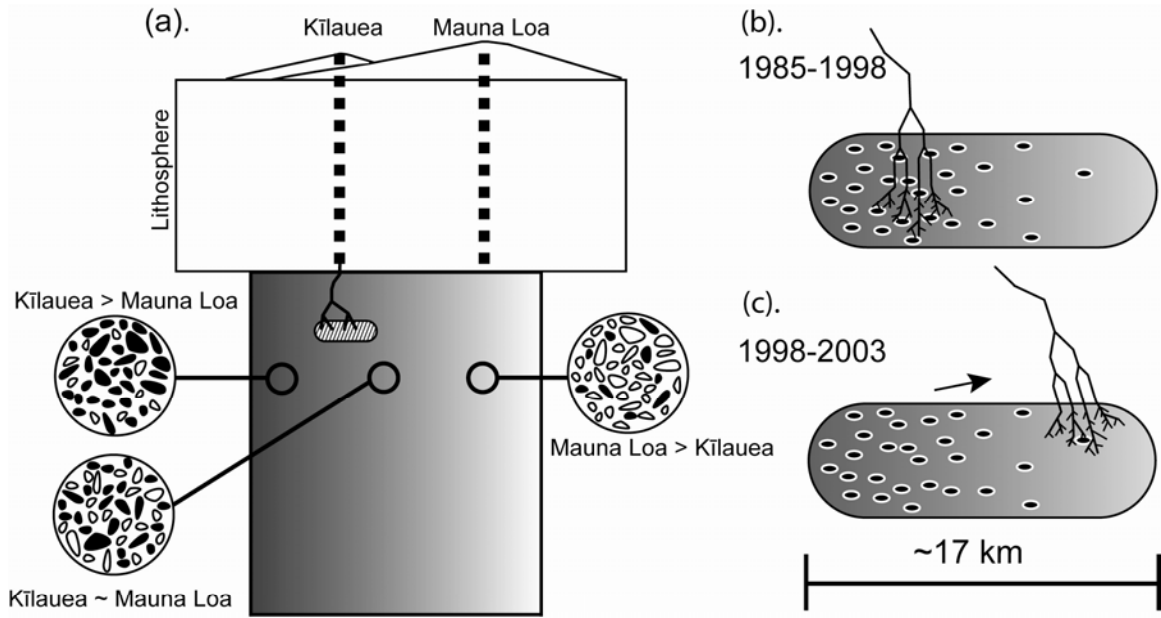


Fig. 1.9 Hypothetical cross-section of the lithosphere and the upper part of the Hawaiian plume beneath Kīlauea and Mauna Loa. (a.) The long-term compositional differences among Hawaiian shield volcanoes are illustrated with black to white gradation representing large-scale compositional heterogeneity within the plume (e.g., Lassiter et al., 1996, Kurz et al., 2004, Abouchami et al., 2005, Bryce et al., 2005). Superimposed on this large-scale heterogeneity are small-scale heterogeneities ($<10\text{-}35\text{ km}^3$; blobs within the enlarged circles) that reflect a predominance of Kīlauea (black) and Mauna Loa (white) components beneath these volcanoes. An isotopically distinct plume matrix (white area between the blobs) is also thought to be present in the plume based on the Pb, Sr and Nd isotopic evidence for at least three components within the Hawaiian plume (e.g., West and Leeman, 1987; Eiler et al., 1996; Hauri, 1996). The matrix is a schematic representation and other geometries of the three mantle components are possible (e.g., three isotopically distinct blobs or streaks with no matrix). Melt extraction via chemically isolated channels (inverted tree structures) may be the primary mechanism to withdraw melt from Kīlauea's melting region [striped region in (a.)] into the volcano's primary magma conduit (thick dashed black line; Pietruszka et al., 2006). (b.) and (c.) are enlargements of Kīlauea's melting region. The small-scale heterogeneities from (a.) are not shown in (b.) and (c.) for simplicity, yet are assumed to be present. Between 1985-1998 (b.), the recently depleted source (black ovals) was an important component in Kīlauea's melting region. The importance of the Kīlauea-Mauna Loa hybrid component (gray zone) that was progressively tapped from 1998-2003 can be explained if the melt channels migrated towards Mauna Loa while possibly extracting melt at shallower depths (c.).

lavas could be preserved if compositionally distinct melts are extracted into chemically isolated channels and efficiently transported to the surface (Pietruszka et al., 2006).

The melting region beneath Hawaiian volcanoes is predicted to be zoned with higher degrees of partial melting (and higher melt productivity) in a relatively thin zone near the top of the melting region (Watson and McKenzie, 1991). Thus, melt extraction would probably be more effective if it occurred laterally over a thinner (i.e., ~5-10 km thick; Marske et al., 2007) region. As melt migrates into channels to supply the Pu‘u ‘Ō‘ō eruption, it must be extracted from more distal areas to sustain the flow of melt to the surface, otherwise the melt supply would become exhausted (Pietruszka et al., 2006). In this context, we propose that the systematic geochemical trends toward the hybrid composition from 1998-2003 could be explained if melt pathways migrated from an area within Kīlauea’s typical melting region dominated by the early and recently depleted component (black ovals; Fig. 1.9b) towards Mauna Loa, where more Mauna Loa-like components would be expected (Fig. 1.9c). In contrast, the MgO-normalized SiO₂ abundances are thought to be controlled by the depth of partial melting (e.g., Hirose and Kushiro, 1993; Kushiro, 1996; Longhi, 2002). Thus, the temporal increase in normalized SiO₂ abundances in 1998-2003 lavas could also be explained if melt production and segregation occurred at progressively shallower depths (e.g., Stolper et al., 2004) during this interval (Figs 1.9b and 1.9c). This model for a fine-scale mixture of compositionally distinct mantle heterogeneities (i.e., Kīlauea and Mauna Loa components) within the Hawaiian plume is consistent with the presence of both Kea and Loa compositions in young prehistoric (A.D. 900-1400) Kīlauea and Mauna Loa lavas (Marske et al., 2007), and in the melt inclusions of East Maui lavas (Ren et al., 2006).

1.5 Conclusions

The Pu‘u ‘Ō‘ō eruption is exceptional among historical eruptions for its long duration (25+ years) and compositional variability. Pu‘u ‘Ō‘ō lavas erupted from 1985 to 1998 are thought to have

originated from at least two distinct source components with similar isotopic compositions, although one was more depleted in incompatible trace elements by a recent (<8 ka) melting event in the Hawaiian plume. Post-1998 Pu‘u ‘Ō‘ō lavas record small but distinctive variations of MgO-normalized major element abundances, and Sr isotope and incompatible trace element ratios (compared to earlier erupted lavas) that require a third source component. Lavas erupted between 1998-2003 display a temporal geochemical evolution toward an intermediate area between the compositional fields of historical Kīlauea and Mauna Loa lavas. Based on mixing models, the 1998-2003 Pu‘u ‘Ō‘ō lavas trend towards a hybrid mantle source composition made of roughly equal proportions of Kīlauea- and Mauna Loa-like components. The contribution from a recently depleted Kīlauea component decreased starting in early 1998 as the volcano tapped greater proportions of a hybrid component until mid-2003. The systematic geochemical trends toward this hybrid composition can be explained if melt pathways migrated from an area within Kīlauea’s melting region (important for 1985-1998 lavas) towards Mauna Loa, where an equal mixture of Kīlauea- and Mauna Loa-like components may exist. The presence of Kīlauea (i.e., Kea) and Mauna Loa (i.e., Loa) components (<10-35 km³) in Pu‘u ‘Ō‘ō lavas suggests both of these components are present as a fine-scale mixture in Kīlauea’s source region.

CHAPTER 2

GEOCHEMISTRY OF SOUTHERN PAGAN ISLAND LAVAS, MARIANA ARC: THE ROLE OF SUBDUCTION ZONE PROCESSES

2.1 Abstract

New major and trace element compositions, and Pb, Sr, and Nd isotopic ratios of Quaternary lavas from two adjacent volcanoes [South Pagan and the Central Volcanic Region (CVR)] located on Pagan Island allow us to investigate the mantle source (i.e., slab components) and melting dynamics within the Mariana intra-oceanic arc. Geologic mapping reveals two main eruptive sequences, pre-caldera (<780-9.4 ka) and post-caldera (<9.4 ka) stages for South Pagan, whereas the eruptive history of the older CVR is poorly constrained. Olivine, clinopyroxene, titanomagnetite, and plagioclase fractionation, plagioclase accumulation, and magma mixing are important crustal processes for the southern Pagan lavas. Geochemical and isotopic variations indicate that South Pagan, CVR, and Mt. Pagan lavas originated from compositionally distinct parental magmas due to variations in slab contributions (sediment and aqueous fluid) to the mantle wedge, and the extent of partial melting beneath these volcanoes. A mixing model based on Pb and Nd isotopic ratios suggests that the average sediment contribution to CVR (~2.0%) and South Pagan (~1.8%) lavas is slightly higher than Mt. Pagan (~1.4%) lavas. These estimates lie within the range of sediment-poor Guguan (~1.3%) and sediment-rich Agrigan (~2.2%) lavas for the Mariana arc. Melt modeling of Mariana lavas demonstrates that the saucer-shaped normalized rare-earth element (REE) patterns observed in some arc lavas can arise from partial melting of a mixed mantle-sediment source, and do not require amphibole interaction or fractionation to depress the middle REE abundances of the lavas. The modeled degree of mantle partial melting for Agrigan (2-5%), Pagan (3-7%), and Guguan (9-15%) volcanoes correlates with indicators of fluid addition (e.g., Ba/Th and Ba/La). This relationship suggests that the fluid flux

to the mantle wedge is the dominant control on the extent of partial melting beneath Mariana arc volcanoes. A decrease in the amount of fluid addition (lower Ba/Th and Ba/La) and extent of melting (higher Sm/Yb), and increase in the sediment contribution (higher Th/Nb, La/Sm, Nb/Zr, and $^{208}\text{Pb}/^{204}\text{Pb}$) from Mt. Pagan to South Pagan could reflect cross-arc melting variations within the Mariana arc. These variations might reflect a decrease in the fluid component (and the extent of melting) and/or an increase in the amount of subducted sediment due to the sampling of melts from increasing depth in the subduction zone. A significantly larger range in the sediment content of Mt. Pagan versus South Pagan lavas suggests that the length scale of compositional heterogeneity in the mantle wedge is small with respect to the distance between their summits (~10 km).

2.2 Introduction

Magma generation at subduction zones is one of the most important yet enigmatic geologic processes on Earth. Subduction zone magmatism involves the transfer of chemical components from the subducted slab into the mantle wedge, a process that modifies the mantle composition and triggers melting (e.g., Gill 1981). Two main slab-derived components, commonly characterized as sediment or sediment melts and aqueous fluid, are responsible for much of the compositional variation in arc lavas based on high precision isotopic and trace element studies (e.g., Elliott et al., 1997; Plank and Langmuir, 1998; Stern et al., 2003; Tollstrup and Gill, 2005; Shaw et al., 2008). Arc magmas generated at continental convergent margins can also be modified by crustal assimilation (e.g., Andean, Stern and Kilian, 1996; Alaska-Aleutian, George et al., 2003; Cascade, Jicha et al., 2008) obscuring slab-related geochemical signatures in the lavas. In contrast, intra-oceanic convergent margins (i.e., Izu-Bonin-Mariana arcs) are ideal locations to study the processes that operate within the mantle wedge because the compositional

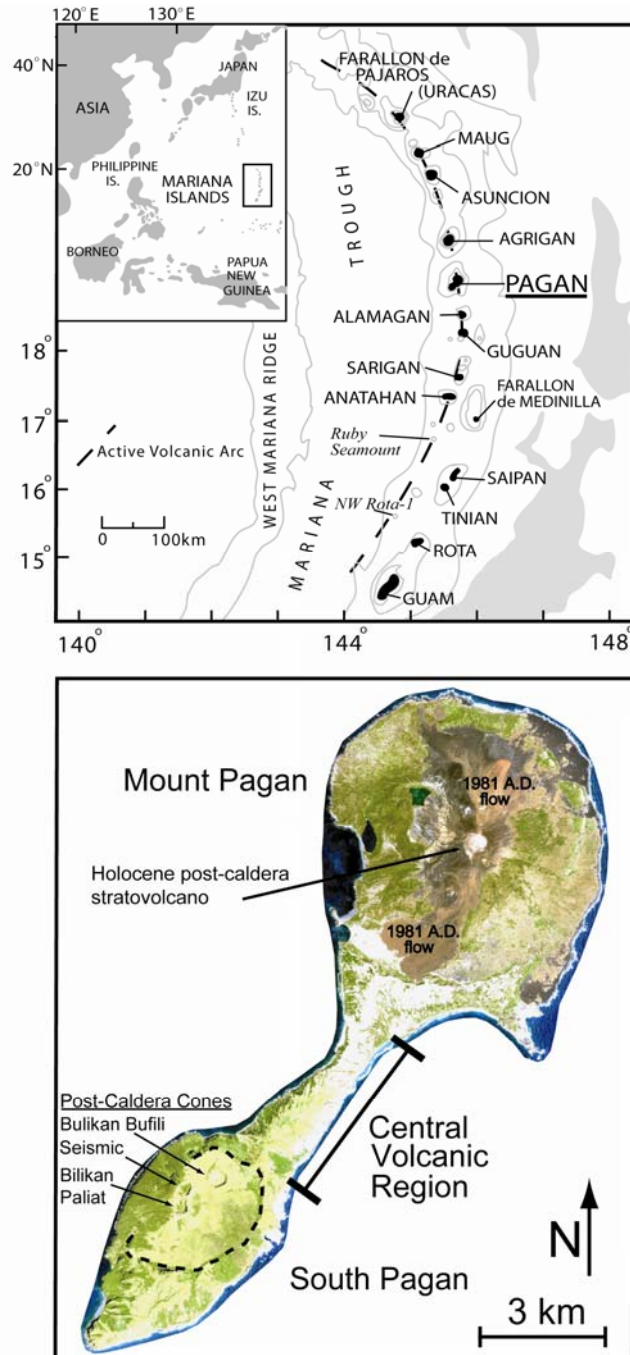


Fig. 2.1 a. Location map of the Northern Mariana Islands modified from Karig (1971). The nine islands extending from Anatahan to Farallon de Parajos outline the active subaerial volcanic arc. The inset map shows the regional location of the Northern Mariana Islands. The shaded gray areas to the right of the active arc denote the location of the Mariana trench. Ocean Drilling Project Site 801 is located ~900 km east of the Mariana trench at $18^{\circ} 38.538'N$ $156^{\circ} 21.588'E$. b. Annotated satellite image of Pagan Island showing the locations of Mt. Pagan, CVR, and South Pagan volcanoes, and young volcanic features. Source: National Oceanic and Atmospheric Administration IKONOS image (http://coris.noaa.gov/metadata/records/html/image_mosaic_pagan_2003.html).

effects of crustal contamination is likely minimal compared to continental convergent settings (Elliott et al., 1997).

The relative contribution of slab-derived components is generally described in a regional context for multiple island-arc volcanoes or along-arc variations (e.g., Peate and Pearce, 1998; Ishikawa and Tera, 1999; Kent and Elliott, 2002; George et al., 2003). Moreover, most temporal geochemical studies of arc volcanoes (including the Marianas) describe the evolution of arc systems over tens of millions years (e.g., Hickey-Vargas and Reagan, 1987; Romick et al., 1990; Elburg and Foden, 1998; Reagan et al., 2008). In contrast, temporal geochemical studies of individual or closely-spaced arc volcanoes over shorter time periods (e.g., hundreds to tens of thousands of years) are rare (e.g., Tataru-San Pedro volcanic complex, Dungan et al., 2001; Arenal, Bolge et al., 2006). These studies provide valuable insight into fine-scale changes in mantle source compositions and melting conditions related to variable fluxes of sediment (melts) and aqueous fluid to the mantle wedge. Mariana arc lavas have been well studied making this intra-oceanic convergent margin an ideal location to investigate the slab-derived components involved in arc magma genesis. Previous whole-rock and melt inclusion studies have identified the fluid-rich (Guguan Volcano) and sediment-rich (Agrigan Volcano) end-members for Mariana arc lavas (Elliott et al., 1997; Tollstrup and Gill, 2005). No clear systematic along-arc geochemical variations have been recognized for Mariana volcanoes. Rather, the compositional differences are thought to reflect varying proportions of aqueous fluid and sediment contributions to individual melting regions beneath these volcanoes (Kent and Elliott, 2002).

Here we present a comprehensive geochemical study of lavas from two adjacent volcanoes on Pagan Island, one of the most active volcanic centers in the Mariana arc located between the sediment-rich Agrigan and fluid-rich Guguan volcanoes (Fig. 2.1). Stratigraphically-controlled Quaternary to Holocene lavas from South Pagan and the CVR were collected and analyzed for major- and trace-element abundances, and Pb, Sr, and Nd isotopic ratios to

investigate small-scale spatial and temporal compositional variations between these adjacent volcanoes. The goals of this paper are to assess and identify the slab contributions (fluid and sediment components) involved in arc magma genesis, evaluate the nature and extent of mantle partial melting, and examine crustal magmatic processes beneath Mariana volcanoes.

2.3 Results

2.3.1 Pagan geology and sampling

Pagan has the largest subaerial surface area ($\sim 48 \text{ km}^2$) and volume (2160 km^3 ; Bloomer et al. 1989) among the active Mariana volcanic islands. The island consists of two stratovolcanoes, South Pagan (548 m) and Mt. Pagan (570 m), that are joined by the CVR, an eroded remnant of an extinct Quaternary stratovolcano (Fig. 2.1). This volcano is a 4 km long, 70-580 m high ridge consisting of steeply to moderately dipping, 0.3-10 m thick basaltic a'a lavas interbedded with rare ash deposits. The CVR is older than both Mt. Pagan and South Pagan based on stratigraphic relationships and the deeply eroded nature of the volcanic edifice (Banks et al., 1984). Mount Pagan and South Pagan have Holocene cones within their 6 and 4 km wide Quaternary calderas, respectively (Corwin et al., 1957). Lavas from these two volcanoes were emplaced over two main eruptive periods termed the pre- and post-caldera stages (Fig. 2.2), which are defined as having erupted before or after the formation of their respective calderas.

South Pagan Volcano has three intra-caldera Holocene cones (Bulikan Bulifli, Seismic, and Bilikan Paliat) with 100-150 m deep summit craters (Figs. 2.1 and 2.2). Bulikan Bulifli is a broad, low-lying cone that produced the oldest exposed post-caldera flows that surface the northeast floor of the caldera. The most recent post-caldera flows cover most of the western flank and floor of the caldera. They originated from the Seismic and Bilikan Paliat cones, which are coalesced along a NE-SW axis (Fig. 2.2). South Pagan's historical eruptive record is relatively short and intermittently recorded. The only verified historical South Pagan eruption occurred in

1864 A.D., although the volcano may have erupted in 1929 A.D. (Simkin et al., 1981). New carbon-14 dating of charcoal beneath a Seismic cone lava within the caldera (not analyzed in this study) yielded an age of 305 ± 35 years BP (F. Trusdell, unpublished data, 2009). Three samples (TM-06-214, TM-06-275, and TM-06-911) were collected from two flows that are stratigraphically younger than the 305 ± 35 years BP lava. Samples TM-06-275 and TM-06-911 are from the same lava flow collected 0.5 km apart. These three lavas are termed “historical” because they likely post-date the first recorded eruption from Mt. Pagan in 1669 A.D. (Simkin et al., 1981).

Mount Pagan has a single symmetrical cone and two maars within its ~ 9.4 ka caldera (Trusdell et al., 2006). A prominent tuff breccia (“Mount Pagan tuff breccia”; Fig. 2.2), thought to have been produced during the formation of Mt. Pagan caldera (Trusdell et al., 2006), caps much of the CVR (Fig. 2.2). Lavas at the base of the inner caldera wall of Mt. Pagan are < 780 kyr based on paleomagnetic measurements (Larson et al. 1974). Mount Pagan is the most historically active Mariana volcano with 15 eruptions in ~ 350 years (Simkin et al., 1981). Its most explosive historical eruption (VEI = 4) in May 1981 produced basaltic a’a flows and air-fall deposits totaling ~ 0.2 km³ (Banks et al., 1984).

Forty-two samples (37 flows and 5 dikes) that encompass a wide geographical and temporal range for South Pagan and the CVR were analyzed. A majority of these lavas were sampled stratigraphically along the steeply eroded east side of the CVR, and on the flanks, inner walls, and floor of South Pagan caldera (Fig. 2.2). Most CVR lavas are thought to be significantly older than South Pagan pre-caldera lavas. However, the two youngest CVR flows sampled (TM-06-03 and TM-06-34) termed “late-stage CVR” (Table 2.1) are closer in age to the oldest South Pagan pre-caldera lavas based on stratigraphic relationships. Sample TM-06-34 is overlain by South Pagan pre-caldera flows at the base of the northern flank of the South Pagan caldera, whereas sample TM-06-03 is a flow located near the top of the CVR that directly

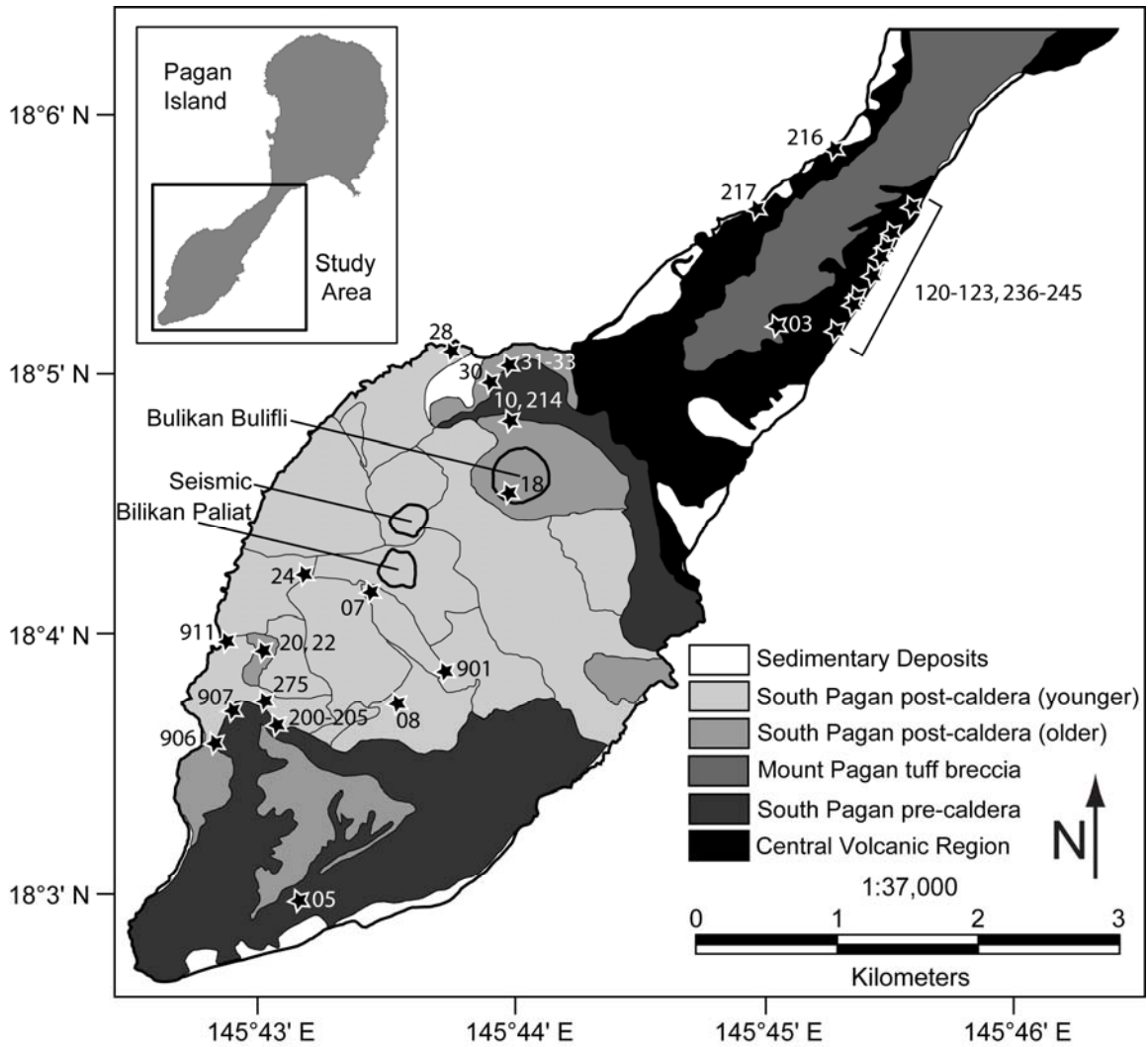


Fig. 2.2 Simplified geologic map of southern Pagan Island showing the distribution of CVR, and South Pagan pre-caldera and post-caldera stage lavas, the Mt. Pagan tuff breccia unit and sedimentary deposits. South Pagan post-caldera units are divided in two age groups, older and younger Holocene units, based on stratigraphy. The thin lines within the South Pagan post-caldera (younger) field delineate individual lava flows and tephra deposits. Sample locations are plotted and are listed in Table A.2. South Pagan post-caldera cones are outlined in black. Geology compiled by F. Trusdell and R. McGimsey (2008).

underlies the ~9.4 ka Mt. Pagan tuff breccia (Fig. 2.2). Relative stratigraphic order for four suites of lavas from the CVR and South Pagan was determined by geologic mapping (Table 2.1; Fig. 2.2). In order from oldest to youngest, these suites are: (1) Ten lavas sampled from a ~830 m section along the east coast of the CVR. These lavas were sampled ~300 vertical meters below the Mt. Pagan tuff breccia unit. (2) A late-stage CVR lava (TM-06-03; described above) that predates South Pagan pre-caldera lavas. (3) Nine South Pagan pre-caldera lavas from a ~175 m section along the volcano's southwest flank and caldera wall. (4) Five South Pagan post-caldera lavas originating from the Holocene cones that surface the caldera floor. In addition, five dikes (three from the CVR and two from South Pagan) were analyzed. The ages of the dikes are unknown, but the observation that they crosscut CVR and South Pagan pre-caldera lavas suggests they likely predate South Pagan post-caldera lavas.

2.3.2 Analytical methods

Major and trace element (Rb, Sr, Y, Zr, Ni, Cr, V, and Ba) abundances for 42 samples (Table 2.1) were determined using X-ray fluorescence spectrometry (XRF) at Washington State University (WSU) using methods described by Johnson et al. (1999). Estimates of analytical precision for XRF major and trace element abundances are based on duplicate analyses of samples TM-06-10 and TM-06-30, which agree to within 2% for all elements (Table 2.1). All estimates of precision in this paper are given as $\pm 2\sigma$. Hawaiian basaltic rock in-house reference material (Kil1919) was analyzed with the samples to evaluate the accuracy of the XRF data. Comparison XRF Kil1919 values (n=6) from Rhodes and Vollinger (2004) show that all element abundances agree within 4% except for MnO (6%), Ba (9%), Y (9%), V (11%), and Na₂O (23%).

Fifteen samples were analyzed for Sc, Cs, Rb, Ba, Sr, Th, U, Pb, Nb, Ta, Hf, Zr, Y, and REE abundances using inductively coupled plasma mass spectrometry (ICP-MS) at WSU (Table 2.2). Analytical methods for the ICP-MS analyses are described in Knaack et al. (1994).

Estimates of analytical precision based on the TEB in-house reference material (n=54; Knaack et al. 1994) show that all elements agree within 5% except for Sc (8%), Nb (9%), Ta (12%), U (13%), Pb (15%), Rb (16%), Th (16%), and Cs (17%), which are in low concentrations (0.1-4.0 ppm) in the TEB reference. Kil1919 (n=2) was analyzed with the samples and comparison ICP-MS Kil1919 values (n=11) from Pietruszka and Garcia (1999) show that all element concentrations agree within 2% (Table 2.2) except for Dy (3%), Nb (3%), and Hf (13%). However, Sc, Sr, Pb, and Ta were not analyzed by Pietruszka and Garcia (1999). No inter-laboratory bias corrections were made to Mariana literature ICP-MS trace element data discussed in this paper due to the absence of common rock standards. Prior to both XRF and ICP-MS analyses, the samples were crushed between tungsten carbide coated plates, ultrasonically washed three times in deionized water for 2-4 minutes, and hand-picked under a binocular microscope to avoid chips with any signs of alteration. The selected chips (~35 g) were then powdered for analysis using either a tungsten carbide swing mill (XRF) or an agate mortar and pestle (ICP-MS).

Fifteen South Pagan and CVR lavas were analyzed from hand-picked rock chips for Pb, Sr, and Nd isotopic ratios (Table 2.3) at San Diego State University (SDSU) using the chemical and mass spectrometric procedures described in Marske et al. (2007). Isotopic ratios of Pb and Nd were measured with a Nu Plasma multi-collector inductively coupled plasma mass spectrometer (MC-ICP-MS), whereas Sr isotopic ratios were measured using a VG Sector 54 thermal ionization mass spectrometer (TIMS; Table 2.3). All literature isotopic data shown on the figures and discussed in the text has been corrected relative to the isotopic standards listed in Table 2.3.

Table 2.1 Whole-rock XRF analyses of southern Pagan lavas. Total iron is given as FeO*. Oxide abundances are in wt. %; trace element contents are in ppm. Loss on ignition (LOI) values are in %. Abbreviations are given for the Central Volcanic Region (CVR), late-stage CVR (CVR late), CVR dikes, South Pagan pre-caldera (SPPre) and post-caldera (SPPost), South Pagan dikes (SP dike). Negative LOI values indicate gain on ignition. Relative stratigraphic position (Strat #) is known for some lavas in which older to younger lavas correspond to increasing values (1-24). Replicate analyses (r) are given for TM-06-10 and TM-06-30. (a) The in-house reference material Kil1919, analyzed with the Pagan samples, was collected from the same lava as the BHVO-1 and -2 standards. (b) Reference values for Kil1919 are from Rhodes and Vollinger (2004). Element concentrations below detection limit noted as “b.d.”.

Sample	TM-06-15A	TM-06-16	TM-06-10	TM-06-10r	TM-06-901
Location	SPPost	SPPost	SPPost	SPPost	SPPost
Strat #	—	—	—	—	—
SiO ₂	52.05	61.76	53.5	53.49	53.86
TiO ₂	0.787	0.725	0.808	0.808	0.809
Al ₂ O ₃	17	15.44	17.08	17.08	17.08
FeO*	9.23	6.79	9.04	9.16	9.04
MnO	0.18	0.17	0.18	0.18	0.18
MgO	5.5	1.97	4.93	4.93	4.8
CaO	10.79	4.84	10.08	10.08	9.97
Na ₂ O	2.29	3.92	2.79	2.8	2.82
K ₂ O	0.824	2.16	1.01	1.01	1.08
P ₂ O ₅	0.141	0.218	0.155	0.157	0.155
Total	98.79	98	99.58	99.7	99.79
LOI	0.85	1.12	-0.13	-0.13	-0.1
Y	21.9	38	23.2	23	23.9
Sr	322	277	317	316	316
Rb	15.1	41.2	18.5	18.5	19.8
Zr	78	172	85	86	89
Ni	21	b.d.	13	12	12
Cr	32	b.d.	25	25	21
V	268	111	269	269	269
Sample	TM-06-28	TM-06-08	TM-06-07	TM-06-275	TM-06-911
Location	SPPost	SPPost	SPPost	SPPost	SPPost
Strat #	—	—	—	24	24
SiO ₂	53.83	53.89	52.48	53.88	53.98
TiO ₂	0.797	0.793	0.781	0.78	0.791
Al ₂ O ₃	16.88	16.79	17.23	16.73	16.95
FeO*	9.13	9.08	9.25	9.1	9.1
MnO	0.18	0.18	0.18	0.18	0.18
MgO	4.83	4.92	4.92	4.96	4.92
CaO	9.9	9.94	9.9	10.06	10.1
Na ₂ O	2.8	2.75	2.62	2.73	2.77
K ₂ O	1.09	1.1	0.971	1.09	1.1
P ₂ O ₅	0.16	0.16	0.154	0.155	0.153
Total	99.6	99.6	98.49	99.66	100.04
LOI	-0.02	-0.09	0.99	-0.04	-0.23
Y	24.4	24.5	22.7	24.4	24.4
Sr	308	302	303	303	307
Rb	20	20.1	17.8	20.3	20.2
Zr	90	91	87	90	89
Ni	11	12	12	13	13
Cr	16	20	20	22	22
V	269	268	267	269	271

Table 2.1 (Continued)

Sample	TM-06-214	TM-06-24	TM-06-18	TM-06-20	TM-06-22
Location	SPPost	SPPost	SPPost	SP dike	SP dike
Strat #	23	22	21	—	—
SiO ₂	53.6	52.68	60.12	52.27	52.2
TiO ₂	0.796	0.785	0.785	0.792	0.842
Al ₂ O ₃	16.76	17.19	16.03	17.17	17.64
FeO*	9.32	9.17	6.85	9.18	9.4
MnO	0.18	0.18	0.16	0.18	0.18
MgO	4.89	5.15	2.25	5.33	4.82
CaO	10	10.47	5.82	10.49	10.34
Na ₂ O	2.76	2.61	3.85	2.61	2.76
K ₂ O	1.07	0.914	1.93	0.859	0.87
P ₂ O ₅	0.158	0.144	0.233	0.145	0.155
Total	99.54	99.29	98.04	99.03	99.2
LOI	-0.13	0.09	0.83	0.32	0.27
Y	24	22.7	34.6	22.1	22.8
Sr	306	317	286	341	351
Rb	19.3	17.1	36.7	14.5	14.9
Zr	88	78	158	71	72
Ni	12	13	b.d.	19	15
Cr	15	26	3	39	23
V	271	271	148	279	295
Sample	TM-06-30	TM-06-30r	TM-06-31	TM-06-32	TM-06-33
Location	SPPre	SPPre	SPPre	SPPre	SPPre
Strat #	—	—	—	—	—
SiO ₂	61.21	61.18	52.28	54.33	55.09
TiO ₂	0.905	0.902	0.778	0.759	0.786
Al ₂ O ₃	15.6	15.61	16.98	16.87	17.02
FeO*	7.49	7.42	9.39	8.9	8.82
MnO	0.18	0.18	0.18	0.18	0.18
MgO	1.99	1.99	5.6	4.75	4.27
CaO	5.15	5.16	10.89	9.58	8.86
Na ₂ O	4.23	4.23	2.47	2.84	3.06
K ₂ O	2.08	2.08	0.899	1.12	1.23
P ₂ O ₅	0.31	0.309	0.136	0.164	0.175
Total	99.15	99.06	99.6	99.49	99.49
LOI	-0.09	-0.09	-0.04	0.03	-0.11
Y	41.5	40	21.4	23.7	26.4
Sr	322	321	321	378	377
Rb	36.7	38	16.9	18.6	20.9
Zr	161	163	77	87	97
Ni	b.d.	b.d.	21	16	14
Cr	b.d.	b.d.	37	20	15
V	114	116	272	265	255

Table 2.1 (Continued)

Sample	TM-06-05	TM-06-205	TM-06-204	TM-06-203	TM-06-202
Location	SPPre	SPPre	SPPre	SPPre	SPPre
Strat #	20	19	18	17	16
SiO ₂	54.71	53.28	53.17	52.85	52.97
TiO ₂	0.868	0.765	0.761	0.763	0.768
Al ₂ O ₃	18.26	17.39	17.51	17.38	17.36
FeO*	8.42	8.83	8.85	8.9	8.93
MnO	0.17	0.18	0.17	0.18	0.18
MgO	3.23	5.24	5.12	5.19	5.22
CaO	8.81	10.65	10.6	10.43	10.57
Na ₂ O	3.15	2.66	2.51	2.67	2.49
K ₂ O	1.14	0.871	0.868	0.851	0.84
P ₂ O ₅	0.181	0.131	0.129	0.125	0.124
Total	98.93	100	99.69	99.34	99.44
LOI	0.37	-0.19	-0.14	0.2	0.15
Y	26.6	22	21.8	21.3	22.4
Sr	341	330	333	328	330
Rb	21.5	15.4	14.5	15.2	14.1
Zr	98	76	76	75	75
Ni	4	18	18	19	19
Cr	8	50	47	48	48
V	246	273	270	254	273
Sample	TM-06-201	TM-06-200	TM-06-907	TM-06-906	TM-06-241
Location	SPPre	SPPre	SPPre	SPPre	CVR dike
Strat #	15	14	13	12	—
SiO ₂	52.46	52.7	61.6	57.56	50.42
TiO ₂	0.778	0.766	0.696	0.859	0.76
Al ₂ O ₃	17.24	17.21	16.62	16.27	19.27
FeO*	9.1	8.89	6.07	8.75	9.06
MnO	0.18	0.18	0.15	0.19	0.18
MgO	5.15	5.07	2.04	3.26	4.8
CaO	10.28	10.28	5.54	7.12	11.71
Na ₂ O	2.65	2.61	4.46	3.61	2.59
K ₂ O	0.855	0.891	1.62	1.6	0.584
P ₂ O ₅	0.12	0.127	0.214	0.227	0.109
Total	98.81	98.72	99.01	99.45	99.49
LOI	0.72	0.65	0.17	0.17	-0.15
Y	21.1	22.4	34.8	31.2	17.8
Sr	325	326	326	298	379
Rb	14.7	15.3	26.8	28.9	9.8
Zr	76	75	127	128	50
Ni	18	17	b.d.	5	16
Cr	46	44	3	17	19
V	251	266	131	197	298

Table 2.1 (Continued)

Sample	TM-06-217	TM-06-120	TM-06-03	TM-06-34	TM-06-216
Location	CVR dike	CVR dike	CVR late	CVR late	CVR
Strat #	—	—	11	—	10
SiO ₂	48.25	48.99	56.15	52.41	49.48
TiO ₂	0.769	0.804	0.736	0.811	0.804
Al ₂ O ₃	19.31	17.86	18.26	18.93	17.21
FeO*	10.15	10.9	7.69	8.91	10.78
MnO	0.19	0.21	0.17	0.17	0.21
MgO	5.66	5.64	2.89	3.73	6.28
CaO	13.22	11.92	8.19	10.37	11.89
Na ₂ O	2.08	2.43	3.67	2.83	2.31
K ₂ O	0.456	0.628	1.18	0.87	0.555
P ₂ O ₅	0.098	0.134	0.155	0.146	0.13
Total	100.18	99.51	99.1	99.17	99.66
LOI	-0.32	-0.23	-0.02	0.19	-0.09
Y	13.4	18.2	26.1	22.6	20.2
Sr	387	447	365	388	400
Rb	7.5	8.9	19	14.2	8.1
Zr	32	43	92	71	41
Ni	11	16	3	6	16
Cr	17	17	3	10	19
V	353	345	213	281	324
Sample	TM-06-236	TM-06-237	TM-06-123	TM-06-122	TM-06-121
Location	CVR	CVR	CVR	CVR	CVR
Strat #	9	8	7	6	5
SiO ₂	48.63	48.93	48.38	49.11	49.24
TiO ₂	0.833	0.803	0.804	0.785	0.787
Al ₂ O ₃	17.92	17.5	17.58	17.72	18.39
FeO*	11.32	11.08	11.07	10.98	10.88
MnO	0.21	0.21	0.21	0.21	0.21
MgO	5.55	5.87	5.88	5.89	5.51
CaO	12.04	12.13	12.06	12.02	11.81
Na ₂ O	2.35	2.33	2.3	2.26	2.4
K ₂ O	0.594	0.603	0.554	0.627	0.608
P ₂ O ₅	0.145	0.132	0.13	0.132	0.136
Total	99.58	99.6	98.98	99.73	99.97
LOI	-0.22	-0.3	-0.03	-0.04	-0.08
Y	18.8	18.2	17.9	17.5	18.1
Sr	453	436	442	445	469
Rb	7.4	7	6.7	9.5	7.7
Zr	40	41	43	40	40
Ni	14	17	17	18	17
Cr	8	17	14	18	25
V	362	351	342	339	333

Table 2.1 (Continued)

Sample	TM-06-238	TM-06-239	TM-06-245	TM-06-243	Kil1919 ^a	Kil1919 ^b
Location	CVR	CVR	CVR	CVR	Kīlauea	Kīlauea
Strat #	4	3	2	1	—	—
SiO ₂	49.56	49.16	49.18	51.58	50.26	50.61
TiO ₂	0.765	0.741	0.761	0.724	2.832	2.8
Al ₂ O ₃	18.65	17.76	18.53	16.78	13.83	13.91
FeO*	10.65	10.61	10.61	9.54	11.08	11.01
MnO	0.2	0.2	0.2	0.18	0.17	0.18
MgO	5.31	5.95	5.39	5.66	7.15	6.96
CaO	11.76	12.12	11.75	10.81	11.65	11.56
Na ₂ O	2.42	2.24	2.36	2.58	2.32	1.8
K ₂ O	0.635	0.571	0.612	0.86	0.532	0.536
P ₂ O ₅	0.14	0.132	0.134	0.142	0.27	0.277
Total	100.09	99.48	99.52	98.85	100.1	99.65
LOI	-0.15	0.04	-0.16	0.28	-0.48	—
Y	17.2	17.2	17	19.4	27	24.7
Sr	476	448	473	395	405	395
Rb	8.7	8.3	7.4	14.3	9.3	9
Zr	39	39	40	59	176	177
Ni	18	24	18	20	103	101
Cr	28	54	26	49	261	266
V	327	328	337	302	320	284

Table 2.2 ICP-MS trace element analyses of southern Pagan lavas. Values are in ppm. (a) Kil1919 (n=2) was analyzed as an unknown with these analyses. (b) Reference values for Kil1919 are from Pietruszka and Garcia (1999).

Sample	Rb	Cs	Ba	La	Ce	Pr	Nd	Sm	Eu	Gd	Tb	Dy	Ho	Er
South Pagan Post-Caldera														
TM-06-275	21.9	0.660	217.3	8.07	17.58	2.61	12.03	3.41	1.02	3.97	0.69	4.34	0.92	2.59
TM-06-214	22.3	0.645	216.2	8.05	17.63	2.62	12.04	3.39	1.05	4.05	0.69	4.38	0.93	2.59
TM-06-24	19.4	0.570	198.2	7.56	16.44	2.46	11.23	3.20	1.03	3.75	0.65	4.06	0.88	2.45
TM-06-18	38.5	1.157	373.3	13.98	30.06	4.36	19.51	5.24	1.39	5.96	1.02	6.47	1.37	3.91
South Pagan Pre-Caldera														
TM-06-05	22.7	0.688	238.4	9.10	19.97	2.98	13.78	3.85	1.19	4.54	0.78	4.96	1.05	2.95
TM-06-202	15.3	0.361	201.9	7.47	16.07	2.38	11.06	3.15	0.99	3.69	0.63	4.05	0.85	2.42
CVR Dike														
TM-06-217	8.1	0.180	100.5	4.27	9.18	1.44	6.93	2.12	0.83	2.60	0.44	2.80	0.57	1.61
Late-Stage CVR														
TM-06-03	20.7	0.305	252.1	9.17	19.58	2.92	13.27	3.70	1.20	4.30	0.75	4.74	1.01	2.86
TM-06-34	15.3	0.416	196.0	7.40	15.74	2.41	11.14	3.20	1.08	3.78	0.64	4.11	0.86	2.46
Central Volcanic Region														
TM-06-216	9.1	0.221	148.8	5.87	12.90	1.95	9.50	2.86	1.02	3.41	0.58	3.70	0.77	2.17
TM-06-236	7.5	0.124	146.9	6.14	12.95	1.96	9.38	2.71	0.98	3.15	0.53	3.34	0.70	1.97
TM-06-237	7.7	0.151	150.9	5.91	12.76	1.93	9.28	2.73	0.97	3.23	0.55	3.48	0.73	2.05
TM-06-239	9.3	0.258	167.3	6.16	13.02	1.94	9.06	2.65	0.94	3.12	0.52	3.27	0.70	1.94
TM-06-245	7.8	0.074	159.7	5.84	12.35	1.87	8.83	2.56	0.94	3.00	0.50	3.20	0.68	1.90
TM-06-243	14.5	0.239	208.2	7.36	15.37	2.27	10.49	2.96	0.99	3.43	0.58	3.66	0.77	2.19
In-house basaltic reference material (Kīlauea volcano)														
Kil1919 ^a	9.5	0.095	132.6	15.85	38.36	5.54	25.02	6.40	2.14	6.54	1.01	5.65	1.05	2.59
±2σ	0.1	0.002	0.2	0.04	0.02	0.06	0.12	0.04	0.06	0.01	0.01	0.05	0.01	0.01
Kil1919 ^b	9.8	0.093	131	15.4	38.2	5.51	24.5	6.12	2.08	6.26	0.91	5.29	0.98	2.53

Table 2.2 (Continued)

Sample	Tm	Yb	Lu	Th	Y	Nb	Hf	U	Pb	Ta	Zr	Sr	Sc
South Pagan Post-Caldera													
TM-06-275	0.38	2.46	0.39	1.24	24.7	1.94	2.16	0.611	3.23	0.13	96.2	294	23.1
TM-06-214	0.38	2.48	0.39	1.23	25.0	1.98	2.13	0.625	3.30	0.13	95.7	315	24.0
TM-06-24	0.36	2.34	0.37	1.09	23.8	1.82	1.95	0.550	2.93	0.12	87.8	337	21.7
TM-06-18	0.58	3.78	0.60	2.30	36.7	3.53	3.83	1.120	4.49	0.24	169.8	256	15.0
South Pagan Pre-Caldera													
TM-06-05	0.44	2.80	0.45	1.30	27.6	2.20	2.39	0.639	1.29	0.14	103.8	322	17.5
TM-06-202	0.36	2.29	0.37	1.01	23.0	1.80	1.82	0.474	2.51	0.12	78.5	318	22.7
CVR Dike													
TM-06-217	0.24	1.43	0.23	0.45	15.1	0.69	0.78	0.198	1.24	0.04	31.8	369	33.7
Late-Stage CVR													
TM-06-03	0.43	2.80	0.46	1.27	27.6	2.09	2.17	0.608	2.25	0.14	96.8	347	17.0
TM-06-34	0.36	2.33	0.37	0.92	23.4	1.68	1.71	0.432	2.70	0.11	74.9	367	22.8
Central Volcanic Region													
TM-06-216	0.32	2.01	0.32	0.69	20.8	1.03	1.08	0.282	2.14	0.06	44.5	408	27.2
TM-06-236	0.29	1.79	0.29	0.73	18.6	0.97	0.96	0.282	1.78	0.06	39.8	441	27.1
TM-06-237	0.30	1.88	0.30	0.69	19.3	0.99	1.03	0.300	2.59	0.06	42.1	435	28.5
TM-06-239	0.28	1.80	0.29	0.74	18.6	1.07	0.99	0.325	2.66	0.06	42.1	496	22.2
TM-06-245	0.28	1.76	0.28	0.69	18.1	1.00	0.95	0.312	2.26	0.06	39.7	487	22.1
TM-06-243	0.32	2.08	0.33	1.02	20.7	1.56	1.47	0.476	2.96	0.10	64.0	420	21.0
In-house basaltic reference material (Kīlauea volcano)													
Kil1919 ^a	0.34	1.95	0.29	1.30	26.9	19.4	3.77	0.460	1.11	1.47	179.8	406	24.3
±2σ	0.00	0.01	0.00	0.00	0.4	0.2	0.02	0.003	0.00	0.00	1.8	0.2	0.4
Kil1919 ^b	0.35	2.02	0.28	1.25	28.0	18.2	4.47	0.441	—	—	178	—	—

Table 2.3 Pb, Sr, and Nd isotopic data for southern Pagan lavas. Lead isotopic ratios were corrected for instrumental mass fractionation using the measured isotopic ratio of Tl (NBS 997) added to the sample compared to an assumed $^{205}\text{Tl}/^{203}\text{Tl}=2.3889$ for this standard from Thirlwall (2002). The average Tl-corrected value for NBS981 Pb (n=20) was $^{206}\text{Pb}/^{204}\text{Pb}=16.9419\pm 16$ (2σ), $^{207}\text{Pb}/^{204}\text{Pb}=15.4991\pm 18$ (2σ), and $^{208}\text{Pb}/^{204}\text{Pb}=36.7216\pm 53$ (2σ). All of the Pb isotopic data are reported relative to the NBS 981 Pb standard values of Galer & Abouchami (1998): $^{206}\text{Pb}/^{204}\text{Pb}=16.9405$, $^{207}\text{Pb}/^{204}\text{Pb}=15.4963$, and $^{208}\text{Pb}/^{204}\text{Pb}=36.7219$. Sr and Nd isotopic ratios were corrected for instrumental mass fractionation relative to $^{86}\text{Sr}/^{88}\text{Sr}=0.1194$ and $^{146}\text{Nd}/^{144}\text{Nd}=0.7219$, respectively. The average measured values for Sr and Nd standards were $^{87}\text{Sr}/^{86}\text{Sr}=0.710244\pm 10$ (2σ ; n=10) for SRM987 (by TIMS) and $^{143}\text{Nd}/^{144}\text{Nd}=0.512097\pm 8$ (2σ ; n=8) for Ames Nd (by MC-ICP-MS). All Sr and Nd isotopic data are reported relative to constant standard values for SRM987 ($^{87}\text{Sr}/^{86}\text{Sr}=0.710250$) and Ames Nd ($^{143}\text{Nd}/^{144}\text{Nd}=0.512130$). After correcting to this value for Ames Nd, multiple analyses of the La Jolla Nd standard (n=4) run as an unknown averaged $^{143}\text{Nd}/^{144}\text{Nd}=0.511843\pm 7$. Averages of multiple analyses of Kil1919 for Pb (n=8) and Nd (n=7) isotopic ratios are given. Strontium isotopic ratios are an average of duplicate analyses of each sample (except TM-06-911; n=3). Total procedural blanks were negligible compared to the amount of sample used (>0.6 g) and the concentrations of Pb, Sr, and Nd in the samples.

Sample	$^{206}\text{Pb}/^{204}\text{Pb}$	$^{207}\text{Pb}/^{204}\text{Pb}$	$^{208}\text{Pb}/^{204}\text{Pb}$	$^{87}\text{Sr}/^{86}\text{Sr}$	$^{143}\text{Nd}/^{144}\text{Nd}$	ϵ_{Nd}
South Pagan Post Caldera						
TM-06-275	18.8246	15.5639	38.4184	0.703495	0.512999	+7.05
TM-06-911	18.8228	15.5646	38.4190	0.703494	0.512996	+6.98
TM-06-214	18.8238	15.5625	38.4155	0.703479	0.513006	+7.17
TM-06-24	18.8231	15.5619	38.4137	0.703455	0.513007	+7.20
TM-06-18	18.8234	15.5657	38.4283	0.703467	0.512998	+7.02
South Pagan Pre-Caldera						
TM-06-05	18.8241	15.5656	38.4278	0.703447	0.513011	+7.28
TM-06-202	18.8294	15.5658	38.4333	0.703460	0.513004	+7.13
TM-06-205	18.8272	15.5634	38.4259	0.703457	0.513012	+7.30
CVR Dike						
TM-06-217	18.8506	15.5589	38.4168	0.703436	0.512976	+6.59
Late-Stage CVR						
TM-06-03	18.8092	15.5664	38.4233	0.703401	0.513001	+7.09
TM-06-34	18.8632	15.5606	38.4378	0.703407	0.513004	+7.14
Central Volcanic Region						
TM-06-216	18.8219	15.5653	38.4278	0.703441	0.513000	+7.06
TM-06-237	18.8308	15.5674	38.4357	0.703419	0.512982	+6.70
TM-06-245	18.8361	15.5672	38.4390	0.703466	0.512967	+6.41
TM-06-243	18.8490	15.5690	38.4568	0.703467	0.512980	+6.67
In-house basaltic reference material (Kīlauea volcano)						
Kil1919	18.6550	15.4896	38.2062	—	0.512974	+6.52

2.3.3 Major element chemistry

South Pagan and CVR lavas range from subalkaline, medium-K basalts to high-silica andesites (48-62 wt. % SiO₂) with low to moderate MgO contents (2.0-6.3 wt. % MgO; Fig. 2.3). These lavas have major element compositions that mostly lie within the range of lavas from other Mariana volcanoes. The CVR lavas are basalts with a relatively narrow MgO range (4.8-6.3 wt. %), except for the two evolved late-stage samples (2.9 and 3.7 wt. %). South Pagan lavas are basaltic andesites to high-silica andesites with 2.0-5.6 wt. % MgO. South Pagan and CVR lavas generally plot on distinct major element trends (Fig. 2.3). The CVR lavas have higher CaO, FeO, and Al₂O₃ (not shown), and lower SiO₂ and K₂O contents (at a given MgO) except for the oldest stratigraphically controlled CVR lava (TM-06-243) and a South Pagan pre-caldera flow (TM-06-05) that lie along the South Pagan and CVR trends, respectively (Fig. 2.3). South Pagan and CVR lavas display overlapping TiO₂, P₂O₅, and Na₂O contents at a given MgO (Table 2.1).

Most South Pagan and Mt. Pagan lavas have a similar and narrow range of MgO contents (~4.5-5.5 wt. %), although several South Pagan lavas are more evolved (Fig. 2.3). The major element abundances of Mt. Pagan lavas (at a given MgO) are similar to South Pagan and CVR lavas. In detail, Mt. Pagan pre-caldera lavas typically overlap with CVR lavas, whereas most Mt. Pagan post-caldera lavas lie along trends (except for FeO which is highly variable) that are similar to South Pagan lavas (Fig. 2.3).

2.3.4 Trace element chemistry

Normalized trace element patterns for South Pagan and CVR lavas relative to average normal mid-oceanic ridge basalt (N-MORB; Hofmann, 1988) are similar to other Mariana arc lavas (Fig. 2.4a). South Pagan and CVR lavas are enriched in Th, U, Pb, and large ion lithophile elements (LILE: Rb, Ba, K, Sr), and depleted in high field strength elements (HFSE: Nb, Ta, Hf, Zr) with respect to N-MORB. South Pagan and CVR lavas are slightly enriched in most of the light rare-

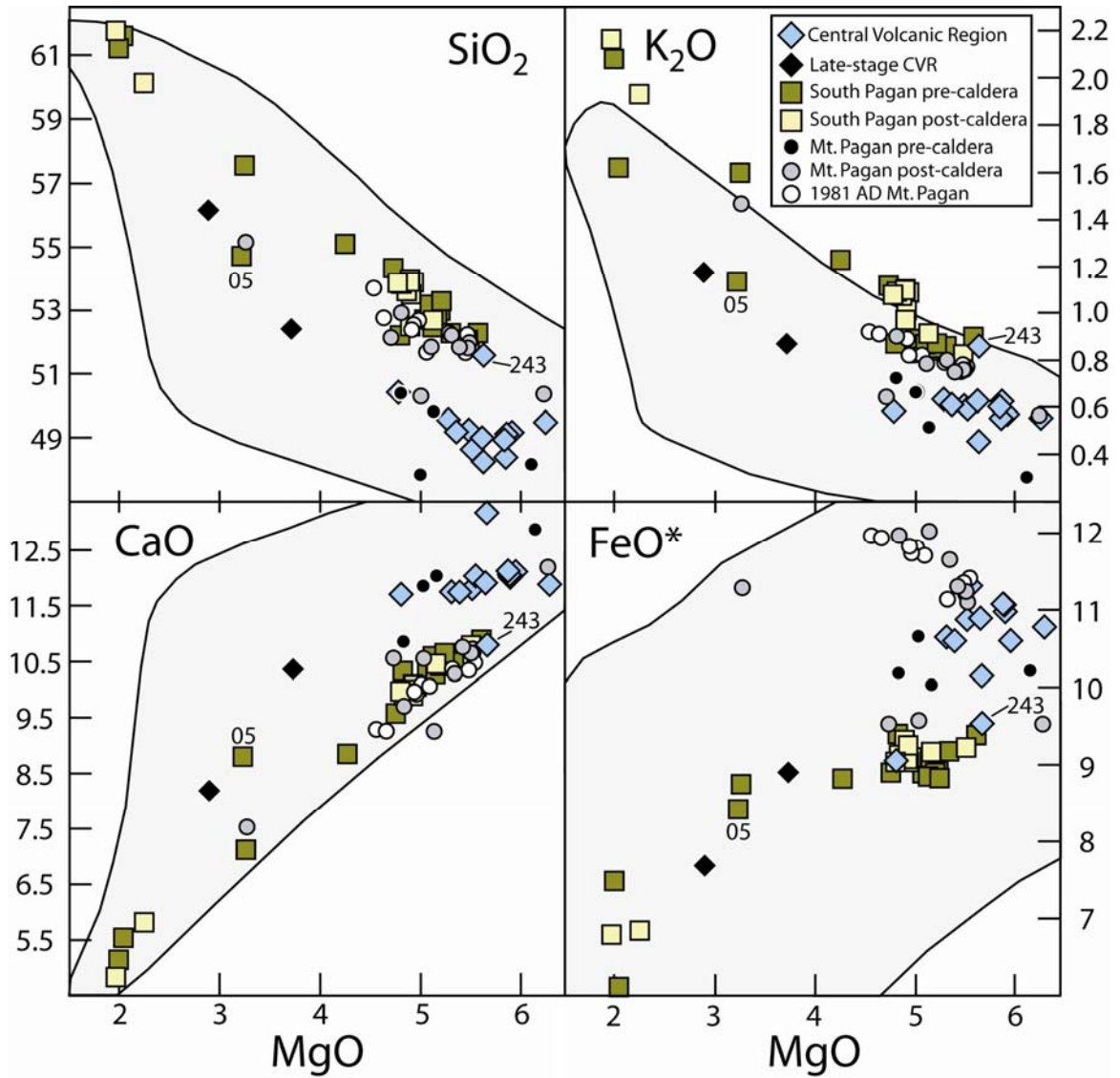


Fig. 2.3 Whole-rock MgO variation diagrams for Pagan lavas (South Pagan, CVR, and Mt. Pagan). The compositional field of other Mariana arc lavas is shown in the light gray area. Mount Pagan, South Pagan, and CVR lavas are grouped according to eruptive stages (see inset for symbols). Samples TM-06-243 and TM-06-05 are shown on the plots for reference. All values are in wt. %. The data sources for Mt. Pagan and Mariana lavas are from Larson et al. (1974), Dixon and Batiza (1979), Meijer and Reagan (1981), Woodhead (1989) and Elliott et al. (1997). The 2σ error bars are equal to or less than the size of the symbols.

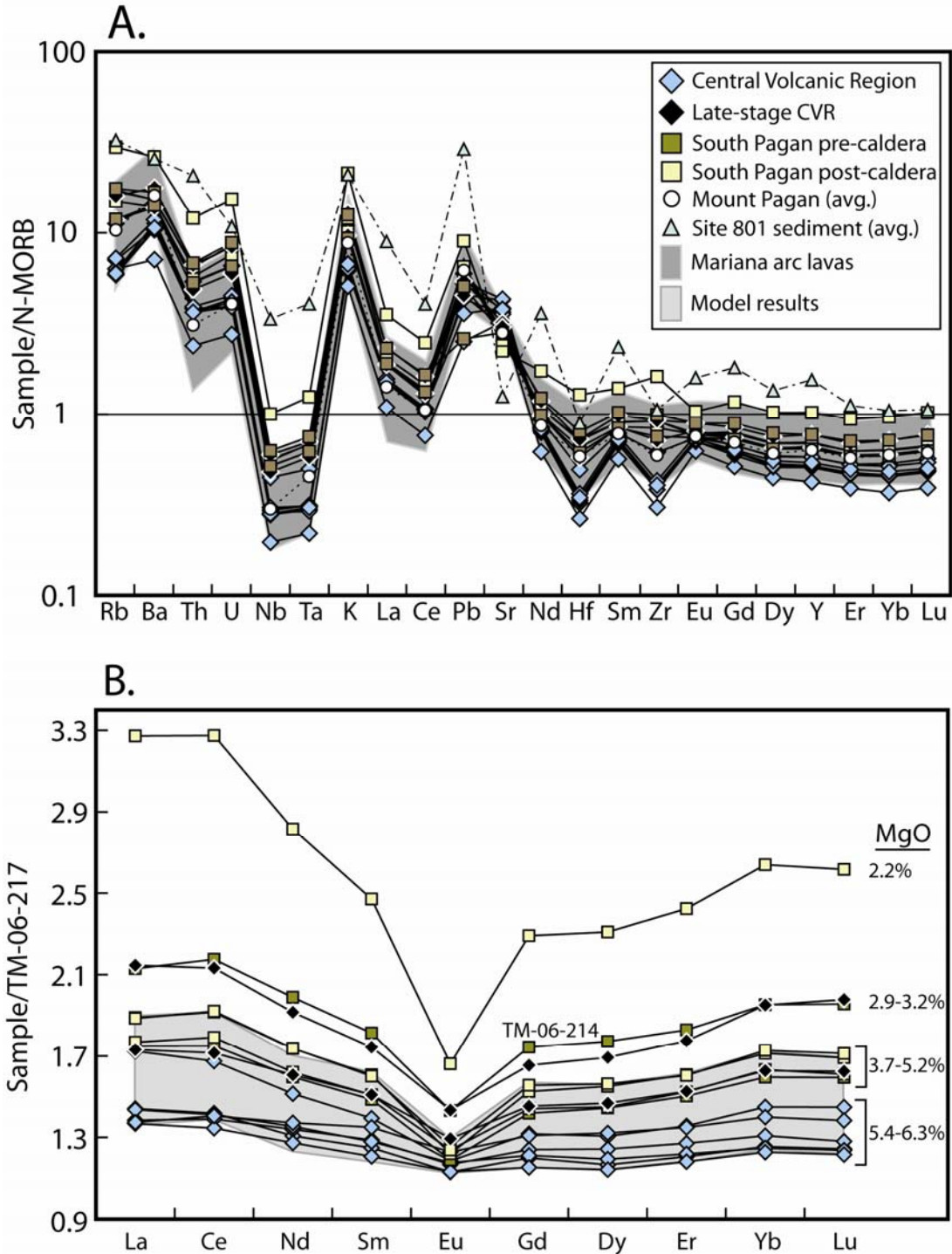


Fig. 2.4 Normalized trace element patterns for Pagan lavas. (a) Trace element concentrations normalized to N-MORB (Hofmann 1988). The Mt. Pagan pattern (open circles) is an average of six pre-and post-caldera lavas from Woodhead (1989) and Elliott et al. (1997). The normalized trace element abundances of average ODP Site 801 sediment (triangles) are from Plank and Langmuir (1998). The range of normalized trace element abundances of other Mariana lavas is shown in the dark gray field (Woodhead, 1989; Elliott et al., 1997; Woodhead et al., 2001). (b) Rare-earth element abundances in CVR and South Pagan lavas normalized to a relatively mafic CVR sample (TM-06-217). The light gray field shows the range of the mass-balance melting model results (Table 2.5) for CVR and South Pagan lavas with >3.5% MgO.

earth elements (LREE: La, Ce, Pr, Nd), but have relatively constant or slightly decreasing abundances of the middle (MREE: Sm, Eu, Gd, Tb, Dy, Ho, Er) to heavy (HREE: Tm, Yb, Lu) rare-earth elements, which are slightly more depleted than N-MORB, but typical of Mariana arc lavas (Fig. 2.4a). South Pagan and late-stage CVR lavas have greater incompatible trace element abundances compared to most CVR lavas, reflecting their more evolved compositions (Figs. 2.3 and 4). Most South Pagan and CVR lavas display negative Eu anomalies, which are largest for the lower MgO samples (Fig. 2.4b).

South Pagan and CVR lavas display small but systematic differences in key trace element ratios (Fig. 2.5). The CVR lavas (excluding late-stage lavas) have higher Ba/Th, Sm/Yb, La/Nb, Th/Nb, Nb/Zr, and Ba/Nb (not shown) on average than South Pagan lavas. In contrast, ratios of LREE to MREE or HREE (e.g., La/Sm) in South Pagan lavas typically overlap with CVR lavas. In addition, some of these ratios (e.g., Ba/Th and Nb/Zr) have generally decreased over the eruptive history of both volcanoes (Fig. 2.6). Mount Pagan lavas show differences in many of these key trace element ratios compared to South Pagan and CVR lavas, despite the close proximity of the volcanoes (all within ~10 km). For example, South Pagan and CVR lavas have higher La/Sm and Nb/Zr ratios, and significantly lower Ba/Th and Ba/La than Mt. Pagan lavas (Fig. 2.5).

2.3.5 Pb, Sr, and Nd isotope ratio variations

South Pagan and CVR lavas lie mostly within the Pb, Nd, and Sr (not shown) isotopic range of other Mariana lavas (Fig. 2.7a). The Pb isotopic ratios of CVR ($^{206}\text{Pb}/^{204}\text{Pb}=18.81-18.86$) and South Pagan ($^{206}\text{Pb}/^{204}\text{Pb}=18.82-18.83$) lavas display an extremely limited range, compared to Mt. Pagan lavas ($^{206}\text{Pb}/^{204}\text{Pb}=18.62-18.86$). The ranges of $^{143}\text{Nd}/^{144}\text{Nd}$ in South Pagan (0.51300-0.51301) and CVR (0.51297-0.51300) lavas (Fig. 2.7c) are also smaller and lower (on average) than Mt. Pagan lavas (0.51300-0.51306). South Pagan and CVR lavas show overall decreases in

$^{208}\text{Pb}/^{204}\text{Pb}$ ratios over time (Fig. 2.7b). This long-term decrease is superimposed on shorter-term Pb isotopic fluctuations (Fig. 2.6). South Pagan and CVR lavas are isotopically distinct (in $^{206}\text{Pb}/^{204}\text{Pb}$ vs. $^{143}\text{Nd}/^{144}\text{Nd}$ space) from Mt. Pagan lavas, except for three Mt. Pagan pre-caldera lavas that lie within analytical uncertainty (Fig. 2.7c). Mount Pagan pre-caldera and 1981 A.D. lavas display relatively high $^{143}\text{Nd}/^{144}\text{Nd}$ and low $^{206}\text{Pb}/^{204}\text{Pb}$ ratios, whereas CVR lavas have relatively low $^{143}\text{Nd}/^{144}\text{Nd}$ and high $^{206}\text{Pb}/^{204}\text{Pb}$ ratios (Fig. 2.7c). South Pagan and late-stage CVR lavas, and most Mt. Pagan post-caldera flows have relatively high $^{206}\text{Pb}/^{204}\text{Pb}$ and intermediate $^{143}\text{Nd}/^{144}\text{Nd}$ that lie between the fields of CVR and Mt. Pagan pre-caldera lavas. The $^{87}\text{Sr}/^{86}\text{Sr}$ ratios for South Pagan and CVR lavas (0.70340-0.70350) partially overlap with the range of Mt. Pagan lavas (0.70345-0.70354, Woodhead, 1989; Elliott et al., 1997), but no systematic temporal variations were observed (Table 2.3).

2.4 Discussion

2.4.1 Magmatic differentiation

The relatively wide range of MgO (2.0-6.3 wt. %) and SiO₂ (48-62 wt. %) contents, and the presence of olivine, clinopyroxene, plagioclase, and titanomagnetite phenocrysts in South Pagan and CVR lavas suggest that their parental magmas were modified by variable amounts of crystal fractionation. Moreover, the abundance of complexly zoned and sieved plagioclase phenocrysts (~15-40 vol. %), and minor plagioclase xenocrysts in most of these lavas indicates that magma mixing was also important. South Pagan and CVR lavas show a strong decrease of CaO/Al₂O₃, Sr/La and Eu/Eu*, and FeO and TiO₂/Y with increasing SiO₂ (Figs. 2.3 and 2.8), which is consistent with the overall fractionation of clinopyroxene, plagioclase, and titanomagnetite, respectively. Although plagioclase fractionation or accumulation can modify the CaO/Al₂O₃ ratios of the lavas, mass-balance calculations indicate that the effect of plagioclase fractionation on the CaO/Al₂O₃ ratio is only ~25% that of an equivalent amount of clinopyroxene fractionation.

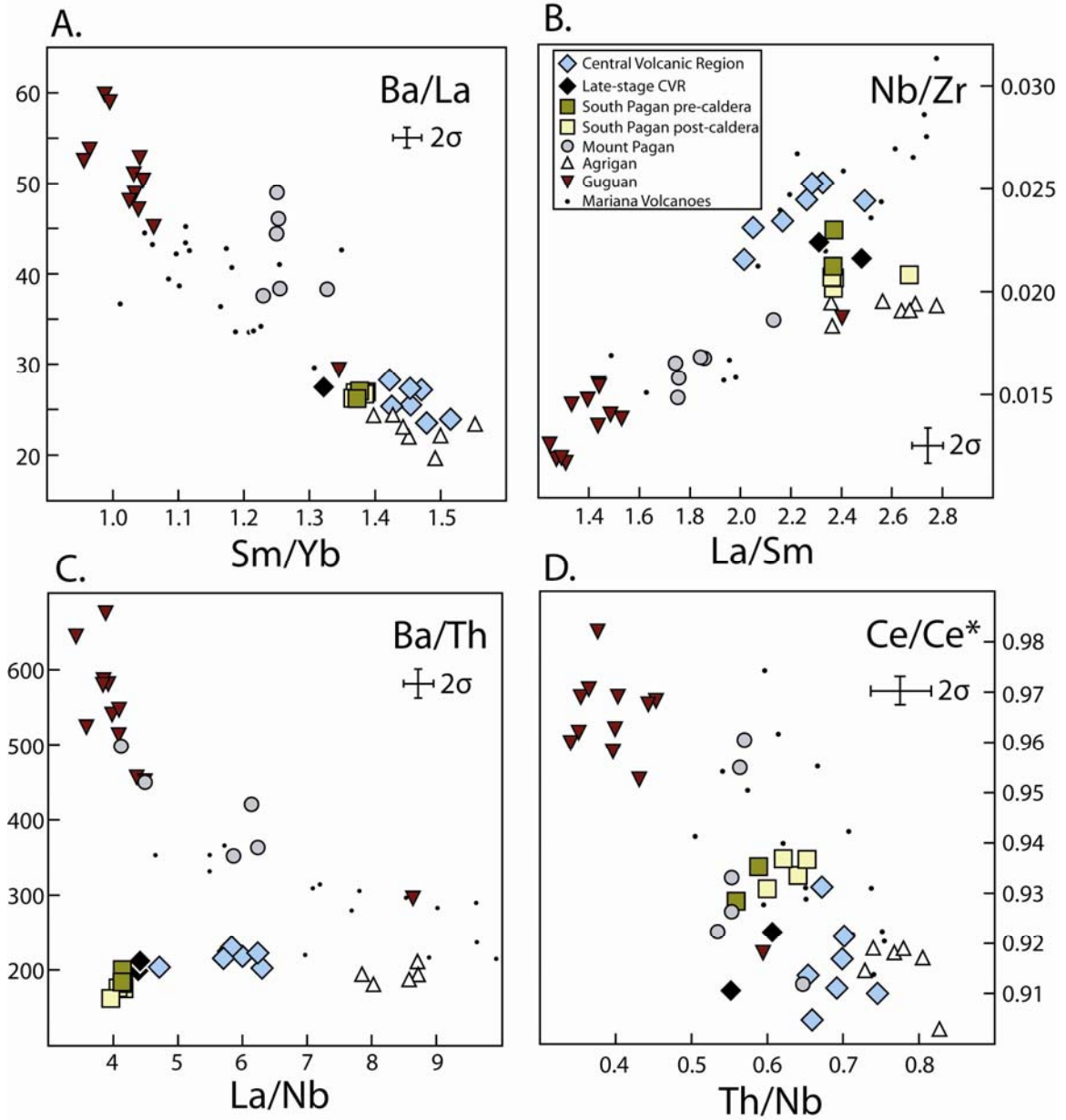


Fig. 2.5 Trace element ratio-ratio plots for Pagan lavas. The compositions of Mt. Pagan (gray circles), Guguan (upside down triangles), Agrigan (white triangles), and Mariana volcanoes (small black circles) are included (Woodhead, 1989; Elliott et al., 1997; Stern et al., 2006). The Ce/Ce* ratio is the measured Ce concentration over the expected Ce concentration (Ce*). Ce* is calculated from the interpolation of primitive mantle-normalized abundances of the rare earth elements La and Pr (Sun and McDonough, 1989). Pacific pelagic clays have prominent negative Ce anomalies (Lin, 1992) and the larger Ce/Ce* deviation from unity reflecting greater contribution from subducted sediment to the subarc mantle (Elliott et al., 1997). The 2σ error bars for South Pagan and CVR lavas are shown in each plot.

The CaO/Al₂O₃ values in South Pagan and CVR lavas also correlate strongly with Sc/Y ratios (Fig. 2.9), a tracer of clinopyroxene fractionation (e.g., Naumann and Geist, 1999). The good linear correlation between these two ratios ($R^2=0.92$) suggests CaO/Al₂O₃ is dominantly controlled by clinopyroxene fractionation. The amount of clinopyroxene fractionation in South Pagan (7-26%) and CVR (0.5-5%) lavas was calculated based on mass-balance calculations assuming a clinopyroxene-free parental magma with a CaO/Al₂O₃ value equal to the highest value observed for Pagan lavas (0.7; Woodhead, 1989). The composition of clinopyroxene used in the calculation (CaO=22 wt. %, Al₂O₃=1.9 wt. %) is an average of multiple mineral core analyses from Guguan lavas (Kohut et al., 2006). The extent of plagioclase and titanomagnetite crystallization in Pagan lavas was estimated using an equilibrium crystallization model (Shaw, 1970) assuming that the highest Sr/La (0.9; Woodhead, 1989) and TiO₂/Y (0.045; this study) ratios observed in Pagan lavas represent a plagioclase- and titanomagnetite-free parental melt. The mineral/melt partition coefficients used for Sr, La, Ti, and Y are listed in Table 2.4. The results show that the greatest amounts of plagioclase fractionation occurred in the more evolved South Pagan lavas (36-47%, excluding sample TM-06-18 with 70%) and late-stage CVR lavas (31 and 44%), compared to more mafic CVR lavas (2-14%). Although plagioclase accumulation could also be an important process based on the relatively high modal abundance of this mineral in Pagan lavas, most Pagan lavas have Eu/Eu* <1, which indicated that plagioclase fractionation dominates. The calculated amount of titanomagnetite crystallization is higher in South Pagan lavas (3-16%) than CVR lavas (0-3%). The abundances of incompatible elements (e.g., HFSE, LREE, and LILE) in South Pagan and CVR lavas increase with the extent of differentiation (e.g., K₂O vs. MgO; Fig. 2.3), although ratios of most incompatible elements show little or no correlation with indices of differentiation (Tables 2.1 and 2.2).

The effects of crystal fractionation and magma mixing in Pagan lavas are superimposed on geochemically distinct parental magma compositions delivered to each volcano. For example,

most CVR and Mt. Pagan pre-caldera lavas have higher CaO and FeO, and lower SiO₂ and K₂O (at a given MgO) that lie on separate compositional trends compared to Mt. Pagan post-caldera and South Pagan lavas (Fig. 2.3). These individual trends have persisted over the eruptive history of each volcano and during the Mt. Pagan pre- and post-caldera stages. These trends suggest that Pagan lavas differentiated from parental magmas that have been compositionally distinct from each other over relatively long time periods (>10 kyr). This interpretation is supported by small, but significant differences in ratios of key incompatible trace elements (e.g., Ba/Th, La/Sm, and Nb/Zr), and Pb and Nd isotopic ratios between CVR, South Pagan, and Mt. Pagan lavas (Figs. 2.5 and 2.7). In the next sections, we relate these parental magma differences to subduction contributions and melting processes.

2.4.2 The role of slab contributions

2.4.2.1 *Aqueous fluid component*

Dehydration reactions in the downgoing slab are expected to transfer elements that are mobile in the aqueous fluid phase into the overlying mantle wedge (Arculus and Johnson, 1981). Large ion lithophile elements are fluid mobile and are readily partitioned into this aqueous phase within the subduction zone (Gill, 1981; Hawkesworth et al., 1991; Keppler, 1996; Johnson and Plank, 1999), whereas REE, HFSE, and Th are relatively immobile in aqueous fluids (Brenan et al., 1995; Keppler, 1996; Ayers et al., 1997; Kessel et al., 2005). Partial melting of the mantle wedge (enriched in these fluid mobile elements) produces magmas with elevated ratios of highly incompatible LILE over HFSE, LREE, or Th (e.g., Ba/Nb, Ba/La, or Ba/Th). For example, South Pagan and CVR lavas display relatively high Ba/Nb ratios (105-159; Table 2.2) that greatly exceed the values for N-MORB and DMM (<9, Sun and McDonough, 1989; Workman and Hart, 2005), average altered upper Pacific oceanic crust (61; Alt and Teagle, 2003), and average bulk subducted sediment from Ocean Drilling Project (ODP) Site 801 (57; Plank and Langmuir, 1998)

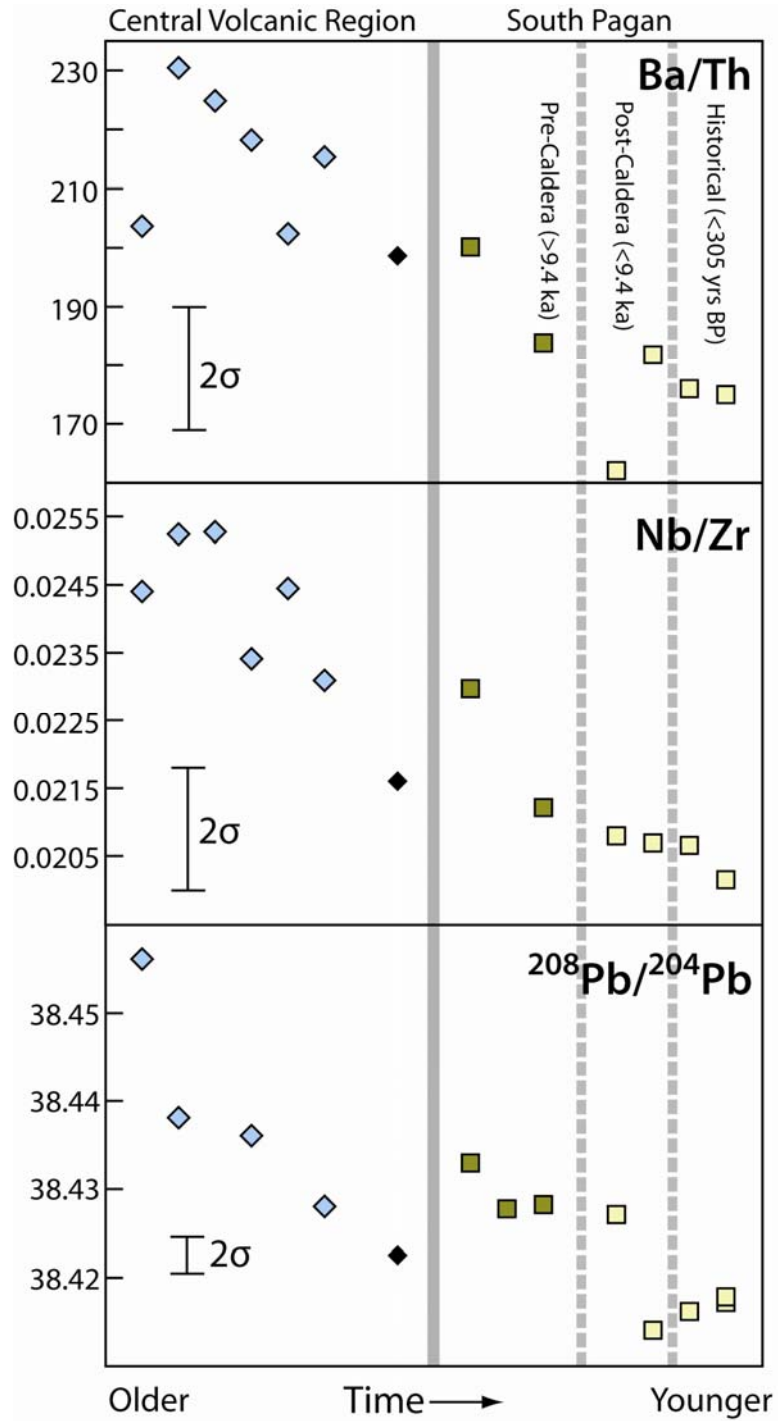


Fig. 2.6 Temporal geochemical variations of South Pagan and CVR lavas. The solid gray vertical lines denote the boundaries between the South Pagan pre-caldera stage, post-caldera stage, and historical period. The dashed line marks the boundary between CVR and South Pagan pre-caldera lavas. The 2σ error bars are shown on each plot.

Table 2.4 Mineral/melt partition coefficients for the mass-balance model calculations. Magnetite, olivine, and spinel. The mineral/melt partition coefficients (D) for the REE are expected to be very low in these minerals (Nielsen et al. 1992) and are assumed to be zero. For magnetite, D_{Ti} comes from Nielsen (1992), and D_Y is from Nielsen et al. (1992). Clinopyroxene. D_{Ce} , D_{Nd} , D_{Sm} , D_{Er} , D_{Yb} , D_{Lu} used in the model were selected to lie within the range of the experiment results from Salters and Longhi (1999). Orthopyroxene. D_{La} , D_{Sm} , and D_{Gd} are average values from Nielsen et al. (1992). Plagioclase. D_{La} , D_{Ce} , D_{Sm} , D_{Gd} , and D_{Yb} are from the experimental results of Phinney and Morrison (1990). D_{Sr} and D_{Eu} is from Pietruszka and Garcia (1999). All other partition coefficients are interpolated or extrapolated from these values.

	Magnetite	Clinopyroxene	Orthopyroxene	Plagioclase
La	0	0.12	0.02	0.036
Ce	0	0.12	0.03	0.031
Nd	0	0.22	0.04	0.025
Sm	0	0.31	0.05	0.020
Eu	0	0.31	0.06	0.330
Gd	0	0.39	0.07	0.016
Dy	0	0.53	0.11	0.013
Er	0	0.63	0.13	0.010
Yb	0	0.70	0.15	0.007
Lu	0	0.70	0.16	0.005
Ti	8	—	—	—
Y	0.004	—	—	—
Sr	—	—	—	1.8

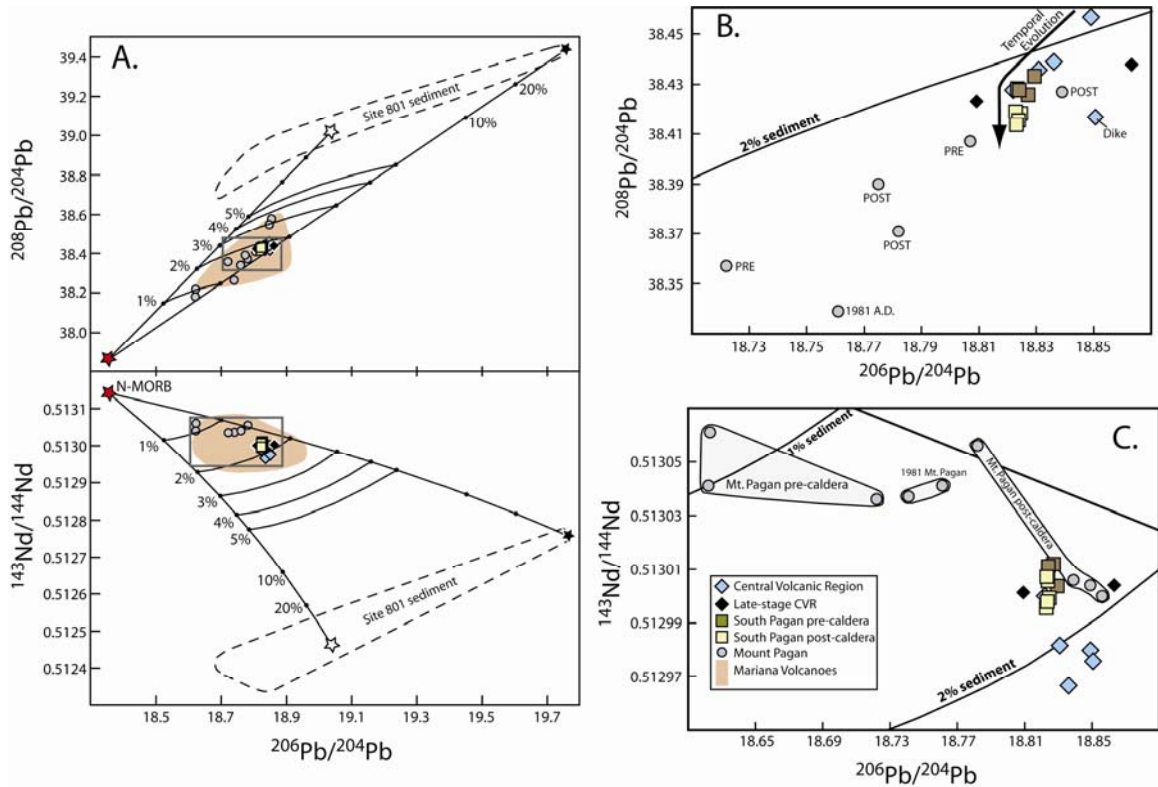


Fig. 2.7 Plots of $^{206}\text{Pb}/^{204}\text{Pb}$ vs. $^{208}\text{Pb}/^{204}\text{Pb}$ and $^{143}\text{Nd}/^{144}\text{Nd}$ ratios for Pagan lavas. South Pagan and CVR lavas, and the fields Mt. Pagan (gray circles), Mariana (tan fields) lavas, and subducted sediment from ODP Site 801 (Plank and Langmuir, 1998) are shown. The rectangles in (a) outline the enlarged view for (b) and (c). Mount Pagan samples labeled PRE and POST refer to pre-caldera and post-caldera stage lavas, respectively. The N-MORB composition (filled star) is an average of Pacific N-MORB compiled from Bach et al. (1994); Mahoney et al. (1994); Vlastevic et al. (1999); Wendt et al. (1999); Chauvel and Blichert-Toft (2001). The data sources for Mt. Pagan and Mariana lavas are given in the caption to Fig. 2.5. Mixing lines between regional subducted sediment (black and open stars) and Pacific N-MORB are shown. The sediment end-members include averaged bulk sediment from ODP Site 801 (open star at $^{206}\text{Pb}/^{204}\text{Pb}=19.04$, $^{208}\text{Pb}/^{204}\text{Pb}=39.01$, $^{143}\text{Nd}/^{144}\text{Nd}=0.51247$) and a volcanic turbidite sample from ODP Site 801 with the most radiogenic Pb isotopic ratios (black star at $^{206}\text{Pb}/^{204}\text{Pb}=19.76$, $^{208}\text{Pb}/^{204}\text{Pb}=39.44$, $^{143}\text{Nd}/^{144}\text{Nd}=0.51276$). The Pb and Nd concentrations used in the mixing model are 10 and 90 ppm, respectively, for the sediment end-members, and 0.3 and 4 ppm, respectively, for the N-MORB end-member. These concentrations lie within the ranges observed for ODP Site 801 sediment and Pacific N-MORB. The amount of sediment mixing with N-MORB is shown in 1% increments. The arrow illustrates the systematic variation of CVR and South Pagan lavas towards lower Pb isotopic ratios with time. The 2σ error bars on each panel are the size of the symbols or smaller.

located ~900 km east of the Mariana trench. It is unlikely that the high Ba/Nb, Ba/La, or Ba/Th ratios in Mariana arc lavas are controlled by variations in the degree of partial melting (~6-30% observed for Mariana volcanoes, Bloomer et al., 1989; Peate and Pearce, 1998; Turner et al., 2006), because ratios of these highly incompatible elements (Ba, Nb, La, Th) are only affected at much lower degrees of mantle melting (e.g., Hofmann, 1997). Thus, variations in Ba/Nb, Ba/La, and Ba/Th ratios for Pagan and other Mariana lavas are thought to be dominantly controlled by the relative amount of the aqueous fluid component in the mantle source region (e.g., Elliott et al., 1997; Stern et al., 2006).

South Pagan and CVR lavas have low Ba/Nb, Ba/La, and Ba/Th ratios compared to most other Mariana lavas (Fig. 2.5), indicating these lavas originated from a source that experienced less fluid addition. In contrast, Mt. Pagan lavas display Ba/Th and Ba/La ratios that are 2 to 3 times higher than the values for CVR and South Pagan lavas. Some Mt. Pagan lavas overlap with lavas from Guguan (Fig. 2.5), the fluid-rich end-member for Mariana lavas (Kent and Elliott, 2002). These observations suggest that Mt. Pagan magmas originated from a source with a larger fluid component than CVR and South Pagan lavas. South Pagan and CVR lavas have similarly low ratios of highly incompatible LILE over HFSE, LREE, or Th, however these lavas display small temporal decreases in Ba/Th and Ba/Nb suggesting that the fluid contribution component has diminished during the eruptive history of southern Pagan (Fig. 2.6).

2.4.2.2 Sediment Component

The amount of subducted sediment transferred to the mantle wedge is generally <2-3% for intra-oceanic arcs (e.g., Tonga, Turner et al., 1997; Izu, Chauvel et al., 2009). Previous studies suggest <3% sediment mixing with a depleted source is required to explain the isotopic variability in Mariana lavas (Meijer, 1976; Wade et al., 2005; Stern et al., 2006). These estimates are primarily based on ratios of fluid-immobile incompatible elements (i.e., HFSE, REE, and Th), and Pb, Hf,

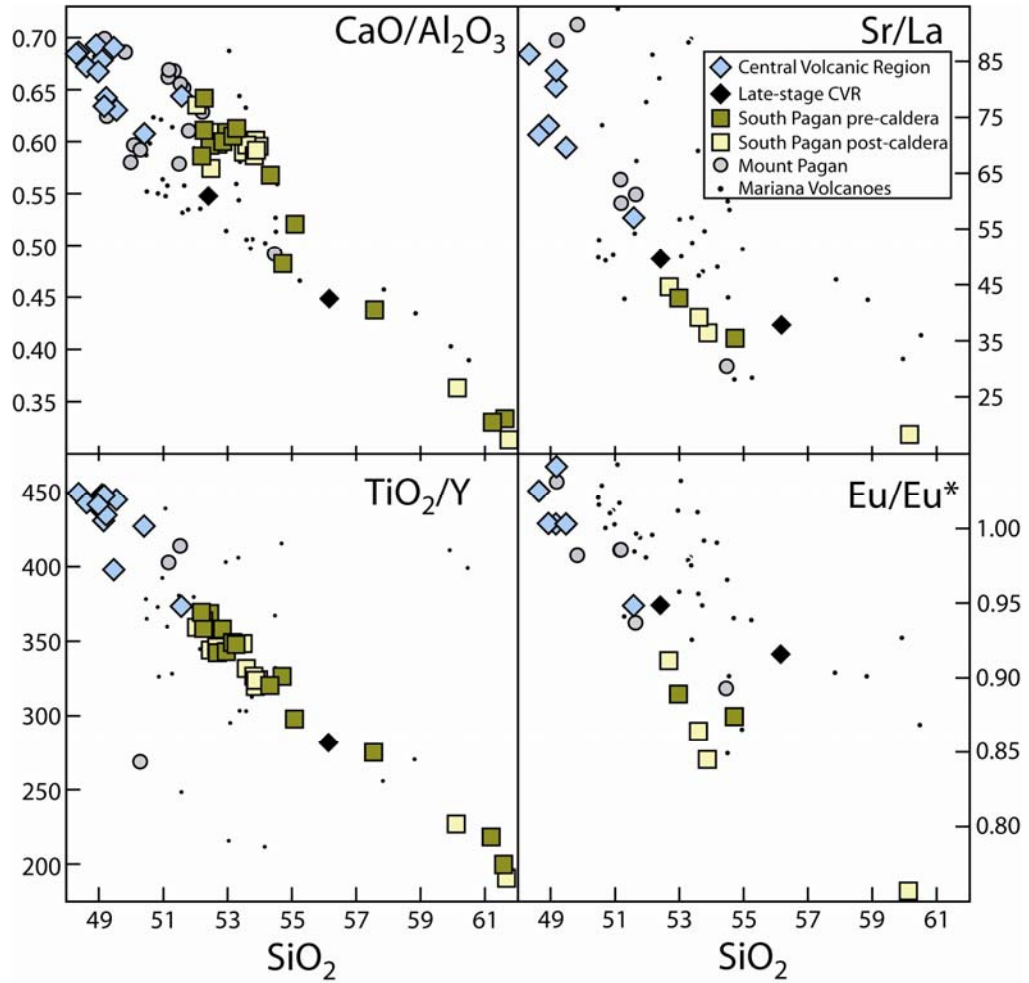


Fig. 2.8 SiO_2 vs. $\text{CaO}/\text{Al}_2\text{O}_3$, Sr/La , TiO_2/Y , and Eu/Eu^* (Eu anomaly) for Mariana lavas. The Eu/Eu^* ratio is the measured Eu concentration over the expected Eu concentration (Eu^*). The expected Eu concentration is calculated from the interpolation of chondrite-normalized abundances of the rare earth elements Sm and Gd. Data sources for Mariana lavas are given in the Fig. 2.5 caption. The 2σ error bars are the size of the symbols or smaller.

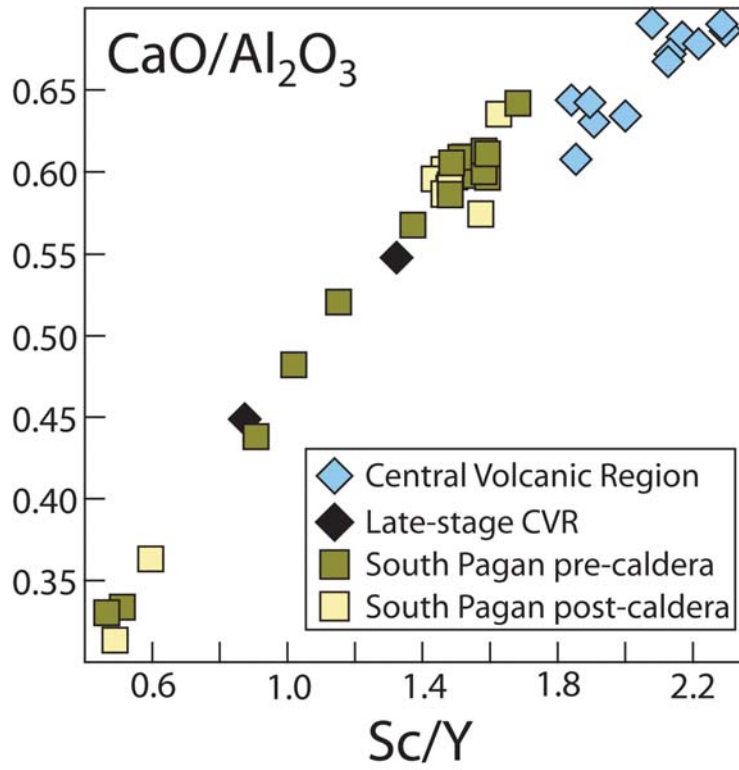


Fig. 2.9 Sc/Y vs. $\text{CaO}/\text{Al}_2\text{O}_3$ for South Pagan, and CVR lavas. Decreasing $\text{CaO}/\text{Al}_2\text{O}_3$ and Sc/Y values reflect increasing clinopyroxene fractionation. The 2σ error bars are smaller than the size of the symbols.

and Nd isotopic ratios. Regional bulk subducted sediment (e.g., ODP Site 801) has low $^{143}\text{Nd}/^{144}\text{Nd}$, high Pb isotopic ratios (Fig. 2.7) and abundances of highly incompatible elements (Fig. 2.4a), and has a prominent negative Ce anomaly (Elliott et al. 1997) compared to N-MORB. Consequently, elevated ratios of highly to moderately incompatible elements (i.e., La/Sm and Nb/Zr) and $^{208}\text{Pb}/^{204}\text{Pb}$, low $^{143}\text{Nd}/^{144}\text{Nd}$ ratios, and negative Ce anomalies in Mariana arc lavas (Figs. 2.5 and 2.10) are thought to result from increased sediment contribution (or sediment addition as a partial melt) to the mantle wedge (Elliott et al., 1997; Elburg and Foden, 1998; Kohut et al., 2006). In addition, rutile is thought to be an important accessory mineral in Mariana subducted sediment (Elliott et al., 1997; Tollstrup and Gill, 2005). Partial melting of rutile-bearing sediment in the mantle source would fractionate HFSE (from REE and Th) if this mineral remains in the residue of partial melting. This process would lead to higher Th/Nb and La/Nb ratios in lavas derived from a more sediment-rich source (Kent and Elliott, 2002; George et al., 2003).

The CVR lavas have the lowest $^{143}\text{Nd}/^{144}\text{Nd}$ and Ce/Ce* ratios, and highest Th/Nb and Nb/Zr ratios among Pagan lavas (Figs. 2.7 and 2.10), which probably reflect greater amounts of sediment in their source. Furthermore, CVR lavas are compositionally similar to Agrigan lavas, which are thought to represent the sediment-rich end-member for Mariana volcanoes (Kent and Elliott, 2002). Although some sediment indicators overlap between South Pagan and CVR lavas (i.e., La/Sm), South Pagan lavas have (on average) higher $^{143}\text{Nd}/^{144}\text{Nd}$ ratios, lower $^{208}\text{Pb}/^{204}\text{Pb}$, Th/Nb, Nb/Zr, and La/Nb ratios, and Ce/Ce* values closer to unity, indicating a smaller sediment contribution compared to CVR lavas. Mount Pagan lavas display higher $^{143}\text{Nd}/^{144}\text{Nd}$ ratios, and lower Nb/Zr, Th/Nb, La/Sm, and radiogenic Pb isotopic ratios compared to South Pagan and CVR lavas. Mount Pagan lavas also partially overlap with the compositional field of Guguan lavas, which are thought to represent the sediment-poor end-member (<0.05% sediment addition; Stern et al., 2006) for Mariana volcanoes. Overall, these observations suggest that most Mt.

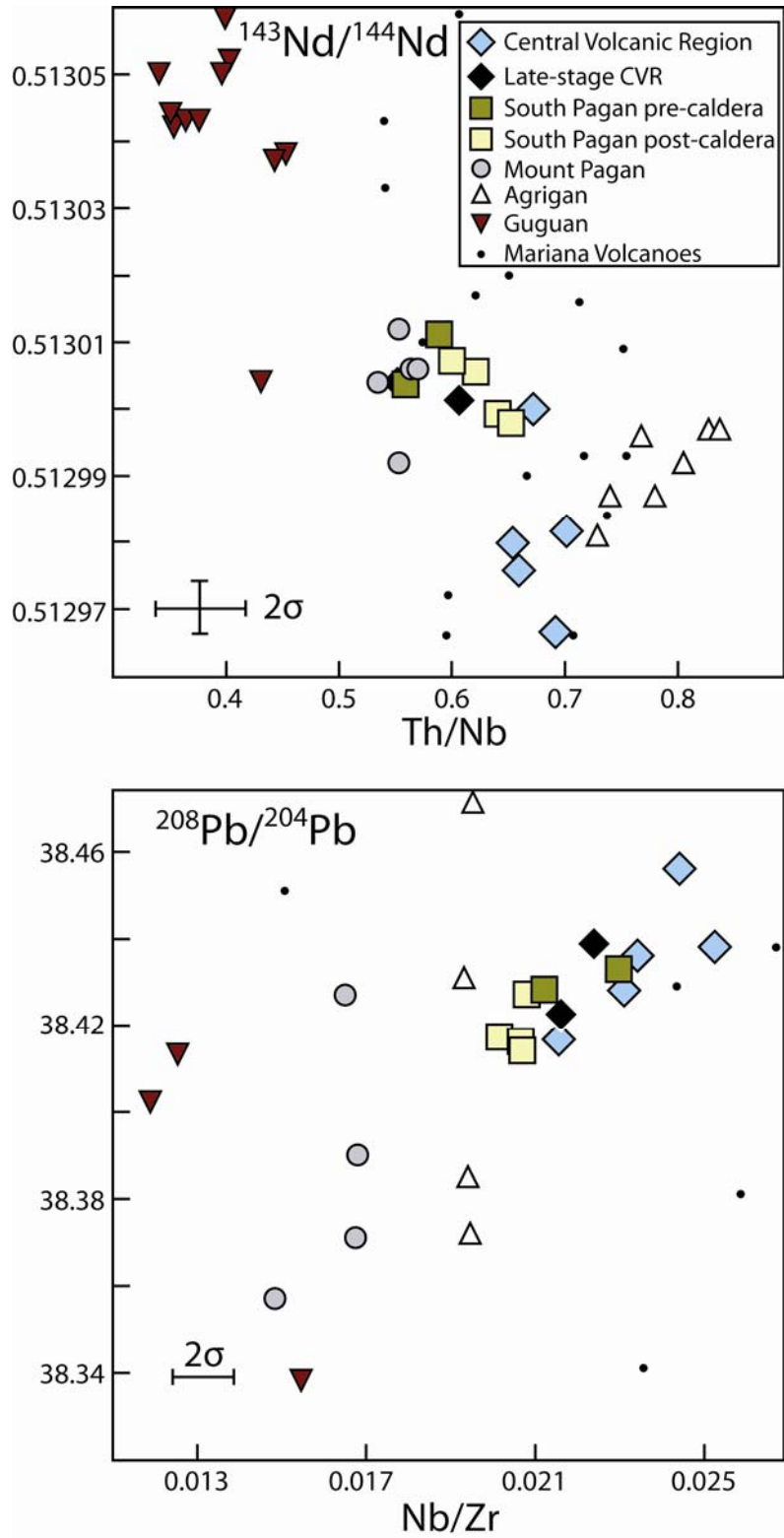


Fig. 2.10 Nb/Zr vs. $^{208}\text{Pb}/^{204}\text{Pb}$ and Th/Nb vs. $^{143}\text{Nd}/^{144}\text{Nd}$ for Pagan lavas (South Pagan, CVR, Mt. Pagan, and other Mariana volcanoes). The data sources for the Mariana lavas are given in the caption to Fig. 2.5. The 2σ error bars are shown unless they are smaller than the size of the symbols.

Pagan lavas were derived from a more sediment-poor source than CVR and South Pagan lavas (Figs. 2.5 and 2.7).

Lead, Hf, and Nd isotopic arrays of arc lavas that trend from MORB-like compositions towards average local sediment compositions have been recognized at several arcs (Aleutian, Jicha et al., 2004; Marianas, Tollstrup and Gill, 2005; Antilles, Marchesi et al., 2007). These trends are thought to result from partial melting of a variably mixed depleted mantle-sediment source. To quantify the extent of sediment addition to Pagan, Agrigan, and Guguan lavas, mixing lines were calculated between two sediment end-members (average bulk sediment from ODP Site 801 and a volcanic turbidite sample with highly radiogenic Pb isotopic ratios), and average Pacific N-MORB (Fig. 2.7). The results suggest that the sediment contribution to CVR lavas (~1.8-2.2%, with an average of 2.0%) is slightly higher on average than South Pagan lavas (~1.8-1.9%, with an average of 1.8%). This observation is consistent with the temporal decreases in some sediment indicators (e.g., Nb/Zr and $^{208}\text{Pb}/^{204}\text{Pb}$) over the sampled history of South Pagan and CVR volcanoes (Fig. 2.6). Mount Pagan lavas generally have a smaller amount of sediment (~0.9-2.0%, with an average of 1.4%), excluding two post-caldera lavas that require ~3% addition (Fig. 2.7b). These two post-caldera lavas also have relatively high Th/Nb, La/Sm, Nb/Zr, La/Nb, and lower $^{143}\text{Nd}/^{144}\text{Nd}$ and Ce/Ce* ratios compared to other Mt. Pagan lavas, which is consistent with greater amounts of sediment. These sediment estimates for Pagan lavas generally lie within the range of sediment-poor Guguan (~0.9-1.7%, with an average of 1.3%) and sediment-rich Agrigan (~1.4-2.8%, with an average of 2.2%) endmember lavas.

2.4.3 Mantle source and melting model for Mariana lavas

Recent studies have noted the importance of amphibole fractionation in the crust and/or magmatic interaction with amphibole-bearing crustal gabbro cumulates as a control on the REE variability in arc lavas (e.g., Macpherson et al., 2006; Davidson et al., 2007). For example, MREE (e.g.,

$D_{Dy}=1.5$; Sisson, 1994) are more compatible in hornblende than HREE ($D_{Yb}=1.0$) and LREE ($D_{La}=0.2$), suggesting that the saucer-shaped REE patterns observed in some arc lavas (e.g., Jolly et al., 2002; Figueroa et al., 2009) are related to parental magmas interacting with, or fractionating amphibole. The REE abundances of Pagan lavas normalized to a relatively mafic CVR sample (TM-06-217; 5.7 wt. % MgO) show saucer-shaped REE patterns (Fig. 2.4b). No modal amphibole is observed in Pagan lavas and this mineral is absent or only minimally present in other Mariana lavas and xenoliths (Dixon and Batiza, 1979; Meijer and Reagan, 1981; Kent and Elliott, 2002). Given the lack of petrographic evidence for amphibole in Pagan lavas, we present a mass-balance model that considers the role of sediment contribution to the depleted mantle wedge, variations in the degree of partial melting, and crystal fractionation of an amphibole-free mineral assemblage to explain the saucer-shaped REE patterns of Pagan lavas (Fig. 2.4b). Representative lavas from the fluid-rich (Guguan) and sediment-rich (Agrigan) end-members for Mariana arc lavas were also modeled. The model assumptions and parameters are described in Table 2.5. Briefly, this two-step model attempts to match the REE abundances of these lavas by: (1) partial melting a variably mixed source consisting of a small amount of subducted sediment (ODP Site 801) and depleted mantle (DMM), and (2) fractionating or accumulating clinopyroxene, plagioclase, olivine, and titanomagnetite from these parental melts. The model results match the REE abundances of the least evolved Pagan, Agrigan, and Guguan lavas (with >3.5 wt. % MgO) within 8%, with an average difference of 2% for the modeled REE.

The model results demonstrate that the saucer-shaped REE patterns in Pagan lavas can arise from partial melting of mixed mantle-sediment source (Figs. 2.4b and 2.11), and that amphibole is not required to depress the MREE relative to the LREE and HREE. Two different factors create the saucer-shaped pattern. First, the addition of sediment to the DMM source creates a mixed source that is slightly less depleted in LREE (Fig. 2.11a) compared to DMM. Second, partial melting of this mixed source generates a melt that is slightly enriched in LREE,

Table 2.5 Representative results of the REE melting model for Mariana lavas. Representative model results for the CVR, late-stage CVR (L-S CVR), South Pagan pre-caldera (SP PRE) and post-caldera (SP POST), Mt. Pagan pre-caldera (MP PRE) and post-caldera (MP POST), Agrigan, and Guguan lavas. The mantle source is assumed to be a mixture of ODP Site 801 sediment and depleted mantle (represented by DMM). The assumed sediment composition (SED) used for the model is an average of three Site 801 stratigraphic units (chert, radiolarite, and volcanoclastic sediment) from Plank and Langmuir (1998). The pelagic clay unit from Site 801 (Plank and Langmuir 1998) was not included because it gave unreasonable model results (i.e., unusually small amounts of sediment, excessive crystal fractionation, and poor ΣR^2 values). The REE abundances of DMM comes from Workman and Hart (2005). The compositions of partial melts were calculated using a modal mineralogy (60% olivine, 20% clinopyroxene, 15% orthopyroxene, and 5% spinel) using the batch melting equation from Shaw (1970). Oliv/Mt (%) is the sum of olivine (Oliv) and titanomagnetite (Mt) fractionation and/or accumulation. These two minerals are grouped together in the model because the D values for the REE are assumed to be zero in these minerals. The model could not distinguish between clinopyroxene (Cpx) fractionation and melting of clinopyroxene-bearing source. Thus, the amount of clinopyroxene fractionation was calculated from the CaO/Al₂O₃ value of each lava (Fig. 2.3), assuming a parental magma with a CaO/Al₂O₃ value is equal to the highest value observed for Pagan lavas (0.7; Woodhead 1989). The composition of clinopyroxene used for the model is an average of multiple mineral core analyses from Kohut et al (2006). The model melt compositions were allowed to undergo equilibrium crystallization in steps. First, the calculated amount of clinopyroxene crystallization (calculated from CaO/Al₂O₃ as described above) was removed from the melt. Second, the residual melt was allowed to undergo equilibrium fractionation or accumulation of plagioclase (Plag) followed by olivine/titanomagnetite. The model parameters (mantle-sediment mixing proportions, degree of partial melting of the mixed source, and the amount of olivine/titanomagnetite and plagioclase fractionation or accumulation were varied to minimize the sum of the residuals squared (ΣR^2 value) on the REE abundances for each sample. Model results for lavas that fractionated or accumulated minerals are noted by negative and plus signs, respectively. For comparison, the expected ΣR^2 equals $\sim 123 (\pm 2\sigma)$ based on the analytical uncertainty of the REE data. The model results for each sample are given with the residuals (% difference) on the concentration of each REE shown as $100 \times [(\text{calculated abundance}/\text{observed abundance}-1)]$. Frac/accum (%) is the sum of olivine/titanomagnetite, clinopyroxene, and plagioclase fractionation and/or accumulation for the model results of each sample. Four REE (Pr, Tb, Ho, and Tm) are excluded from the model because Site 801 sediment was not analyzed for these elements. The more evolved Mariana lavas with <3.5 wt. % MgO were not modeled. The mineral/melt partition coefficients used for the model calculations are shown in Table 2.4.

Sample	SED	DMM	TM-06-243	TM-06-236	TM-06-34
Description	—	—	CVR	CVR	L-S CVR
La	12.8	0.19	7.41 (0.7)	6.12 (-0.2)	7.54 (0.9)
Ce	20.5	0.55	15.5 (0.3)	13.5 (4.4)	15.9 (-0.7)
Nd	13.3	0.58	10.3 (-1.9)	8.96 (-4.5)	10.9 (-1.6)
Sm	2.88	0.24	2.94 (-0.5)	2.62 (-3.6)	3.17 (0.5)
Eu	0.75	0.10	0.99 (0.0)	0.98 (0.14)	0.99 (0.0)
Gd	2.63	0.36	3.46 (1.0)	3.10 (-1.6)	3.77 (2.1)
Dy	2.38	0.51	3.69 (0.8)	3.29 (-1.5)	4.04 (0.0)
Er	1.27	0.35	2.20 (0.6)	1.96 (-0.3)	2.42 (-0.2)
Yb	1.12	0.37	2.09 (0.5)	1.86 (3.7)	2.30 (0.5)
Lu	0.17	0.06	0.33 (-1.5)	0.29 (2.5)	0.36 (-1.4)
Sediment (%)	—	—	2.1	1.3	1.9
Melting (%)	—	—	4.3	2.9	5.5
Oliv/Mt (%)	—	—	-0.9	+9.7	+4.5
Cpx (%)	—	—	-4.4	-2.2	-12.0
Plag (%)	—	—	-22.6	-0.1	-21.6
Frac/Accum (%)	—	—	-10.7	+6.8	-29.0
ΣR^2	—	—	9.1	77	7.7

Table 2.5 (Continued)

Sample	TM-06-202	TM-06-214	TM-06-24	PA-5	PAF3B
Description	SP PRE	SP POST	SP POST	MP POST	MP PRE
La	7.53 (0.8)	8.12 (0.8)	7.63 (1.0)	5.03 (-0.1)	3.49 (-0.1)
Ce	16.0 (-0.3)	17.5 (-0.8)	16.3 (-1.1)	11.2 (2.2)	8.18 (2.5)
Nd	10.9 (-1.8)	11.8 (-1.8)	11.1 (-1.5)	8.42 (-2.4)	6.12 (-2.8)
Sm	3.16 (0.1)	3.45 (1.6)	3.22 (0.6)	2.64 (-3.1)	1.94 (-3.0)
Eu	0.99 (0.0)	1.05 (0.0)	1.03 (0.0)	0.97 (0.0)	0.73 (0.1)
Gd	3.76 (1.9)	4.10 (1.2)	3.83 (2.2)	3.30 (0.4)	2.41 (2.1)
Dy	4.04 (0.0)	4.37 (-0.2)	4.10 (1.0)	3.74 (4.1)	2.69 (1.0)
Er	2.42 (-0.2)	2.60 (0.7)	2.45 (-0.3)	2.29 (1.3)	1.64 (-2.3)
Yb	2.30 (0.6)	2.47 (-0.3)	2.33 (-0.6)	2.21 (-0.3)	1.58 (-1.3)
Lu	0.36 (-1.1)	0.39 (-1.3)	0.37 (-1.3)	0.35 (-2.6)	0.25 (3.5)
Sediment (%)	1.9	1.7	1.8	1.4	1.0
Melting (%)	4.7	4.0	4.4	7.3	5.1
Oliv/Mt (%)	+19.5	+20.7	+16.3	-13.2	-18.9
Cpx (%)	-7.2	-8.2	-7.2	-2.4	0.0
Plag (%)	-34.6	-39.2	-31.6	-9.6	-3.5
Frac/Accum (%)	-22.3	-26.6	-22.4	-25.2	+15.4
ΣR^2	11	11	13	46	48

Table 2.5 (Continued)

Sample	AGR5	AGR4B	GU9	GU21
Description	Agrihan	Agrihan	Guguan	Guguan
La	7.72 (3.1)	7.72 (2.2)	2.89 (1.5)	3.18 (1.9)
Ce	15.7 (-1.4)	16.4 (2.4)	7.48 (-1.9)	7.95 (-2.1)
Nd	10.2 (-6.5)	10.2 (-7.7)	6.36 (-3.2)	6.95 (-3.7)
Sm	2.86 (0.6)	2.85 (-3.3)	2.20 (3.0)	2.45 (1.2)
Eu	0.93 (-0.1)	1.04 (0.0)	0.81 (-0.1)	0.88 (0.0)
Gd	3.31 (3.5)	3.29 (0.7)	2.90 (1.3)	3.28 (3.4)
Dy	3.48 (5.4)	3.41 (3.2)	3.39 (3.0)	3.96 (3.9)
Er	2.06 (0.8)	2.00 (2.7)	2.10 (-0.4)	2.50 (-3.0)
Yb	1.94 (-2.3)	1.88 (-0.9)	2.04 (-1.2)	2.46 (-2.7)
Lu	0.31 (-4.1)	0.30 (-0.3)	0.32 (-2.4)	0.39 (0.3)
Sediment (%)	2.4	1.7	0.4	0.6
Melting (%)	4.2	2.4	9.3	14.6
Oliv/Mt (%)	+28.4	-17.0	-3.9	-21.7
Cpx (%)	-8.9	-6.2	-11.2	-12.3
Plag (%)	-25.8	-5.3	-16.1	-18.0
Frac/Accum (%)	-6.3	+5.5	31.2	-52.0
ΣR^2	118	100	44	66

but the MREE better preserve the original source pattern and remain more depleted than the HREE (Fig. 2.11b). Subsequent crystallization or accumulation of olivine, clinopyroxene, plagioclase, and titanomagnetite raises or lowers the REE patterns, although clinopyroxene removal can cause further LREE to HREE fractionation (Table 2.4) and plagioclase fractionation can create negative Eu anomalies (Fig. 2.11b). The calculated amount of crystal fractionation (5-29%) or accumulation (3-8%, excluding one CVR lava with 29%) in Pagan lavas correlates with their SiO₂ (Fig. 2.12) and MgO (not shown) contents, which suggests that the model successfully accounts for the effects of magmatic differentiation on the abundances of the REE.

The model results suggest (on average) that the amount of sediment addition to Guguan (~0.6%) and Mt. Pagan lavas (~0.9%) is lower than CVR (~1.4%), South Pagan (~1.8%), and Agrigan (~2.0%) lavas (Table 2.6). Overall, these calculated amounts correlate positively with other sediment indicators (e.g., La/Sm or the model-independent ratio, Th/Nb) indicating the model successfully accounts for the effects of sediment addition to the mantle source region (Fig. 2.13). The amount of sediment addition for Pagan lavas based on the REE melting model and the Pb and Nd isotopic mixing model agrees well for Mt. Pagan lavas (0.6-1.4% vs. ~0.9-1.9%, excluding the post-caldera lavas with ~3% sediment addition) and South Pagan lavas (~1.7-1.9% for both models). In contrast, the model results for CVR lavas (0.9-2.1% vs. ~1.8-2.2%) do not agree as well. This apparent discrepancy can also be seen in some of the geochemical tracers of sediment addition. For example, CVR lavas have lower ¹⁴³Nd/¹⁴⁴Nd and Ce/Ce* values, and higher Nb/Zr, Th/Nb, and ²⁰⁸Pb/²⁰⁴Pb ratios than South Pagan or Mt. Pagan lavas, which probably reflect a relatively large amount of sediment in the source of the CVR lavas. In contrast, most CVR lavas have La/Sm ratios that are lower than South Pagan lavas which seems to conflict with the other sediment indicators. This difference might result from variations in the composition of the subducted sediment. The REE model assumes a single composition of sediment for all lavas. However, ODP Site 801 sediments are compositionally and mineralogically heterogeneous (Plank

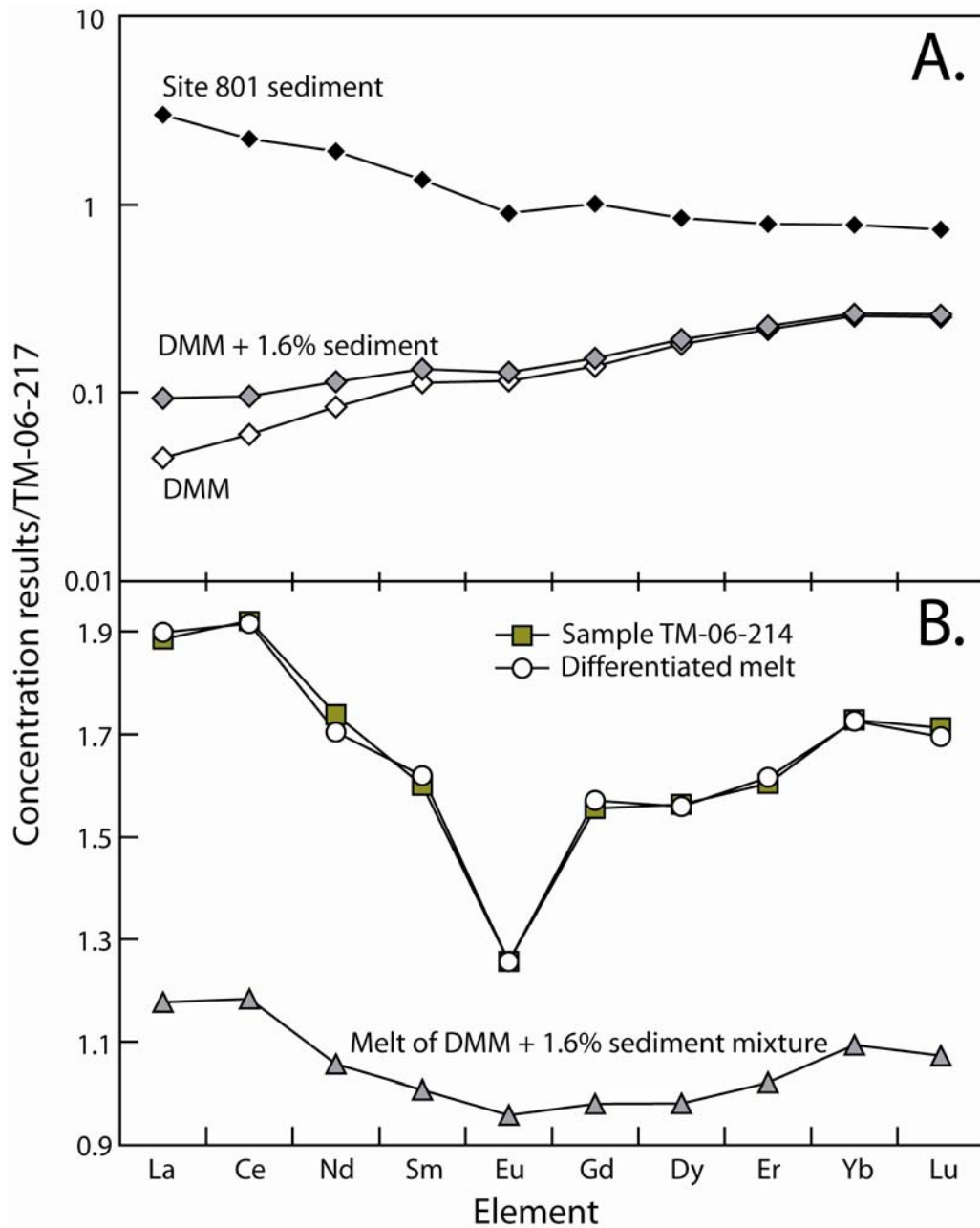


Fig. 2.11 Mass-balance REE melting model results for a representative South Pagan sample, TM-06-214. An explanation of the model calculations and parameters (mantle-sediment mixing proportions, degree of partial melting of the mixed source, and the amount of crystal fractionation or accumulation) is given in Table 2.5. All REE patterns are normalized to a relatively mafic CVR sample (TM-06-217). (a) The REE profiles for DMM (open diamonds), ODP Site 801 sediment (black diamonds), and the calculated mixture of the two sources (DMM+1.6% sediment; gray diamonds). (b) Partial melting of the DMM+1.6% sediment source (triangles) and subsequent crystal fractionation (open circles) produces a saucer-shaped REE pattern that closely matches the REE profile of sample TM-06-214 (squares).

Table 2.6 Summary of REE melt model results. The ranges in amount of sediment and degree of melting calculated for Mariana lavas are shown. Averages for these ranges are in the parentheses. The volcanoes are listed by location from north to south.

Location	Sediment	Melting	Fluid content
Agrigan	1.6-2.4% (2.0%)	2.4-4.7% (3.5%)	low
Mt. Pagan	0.6-1.4% (0.9%)	4.0-7.3% (5.0%)	high
CVR	0.9-2.1% (1.4%)	3.0-4.3% (3.6%)	low
South Pagan	1.7-1.9% (1.8%)	4.0-4.7% (4.3%)	low
Guguan	0.3-0.9% (0.6%)	9.0-14.6% (11.0%)	high

and Langmuir 1998). These sediments have a wide range in La/Sm (17-61) and other REE ratios, but much less variable ratios involving HFSE, such as Th/Nb (2.5-3.0). This observation suggests that the La/Sm ratios of the lavas will be more strongly affected by the composition of the subducted sediment. Thus, it is possible that the source of the CVR lavas had a relatively large amount of less LREE-enriched sediment (compared to the source of other Pagan lavas). Based on these observations, the calculated amount sediment addition to Mariana lavas based on the Pb and Nd isotopic mixing model is thought to be more accurate than the REE model estimates.

The calculated degree of partial melting based on the REE melting model for Pagan (3-7%), Agrigan (2-5%), and Guguan (9-15%) lavas is similar to, or lower than previous estimates for Mariana lavas (6-30%; Bloomer et al., 1989; Peate and Pearce, 1998; Turner et al., 2006). The melt fractions required to match the REE abundances of the CVR lavas (3.0-4.3%, excluding a late-stage lava with 5.5%) and South Pagan lavas (4.0-4.7%) are generally lower (Table 2.5; Fig. 2.13) than those for Mt. Pagan lavas (4.0-7.3%). Some REE ratios (i.e., Sm/Yb and La/Yb) have been used to decipher melting variations within the subarc mantle (e.g., Asimov and Langmuir, 2003; Kelemen et al., 2003; Stern et al., 2006). The calculated degree of partial melting from the REE melting model correlates ($R^2 = 0.88$) with the Sm/Yb ratios of Mariana lavas, and broadly correlates with their Ba/La (not shown) and Ba/Th ratios (Fig. 2.13). In detail, Mt. Pagan and Guguan lavas have the highest Ba/Th and Ba/La ratios and lowest Sm/Yb ratios among Mariana lavas, which are consistent with a relatively large fluid contribution and high degree of partial melting, respectively (Figs. 2.5a and 2.13). In contrast, South Pagan, CVR, and Agrigan lavas have some of the highest Sm/Yb ratios and lowest Ba/La and Ba/Th ratios reflecting a smaller fluid contribution and lower degree of partial melting. These observations indicate that the fluid flux to the subarc mantle may be the dominant control on the extent of partial melting for Mariana arc volcanoes. Similar correlations between the amount of fluid

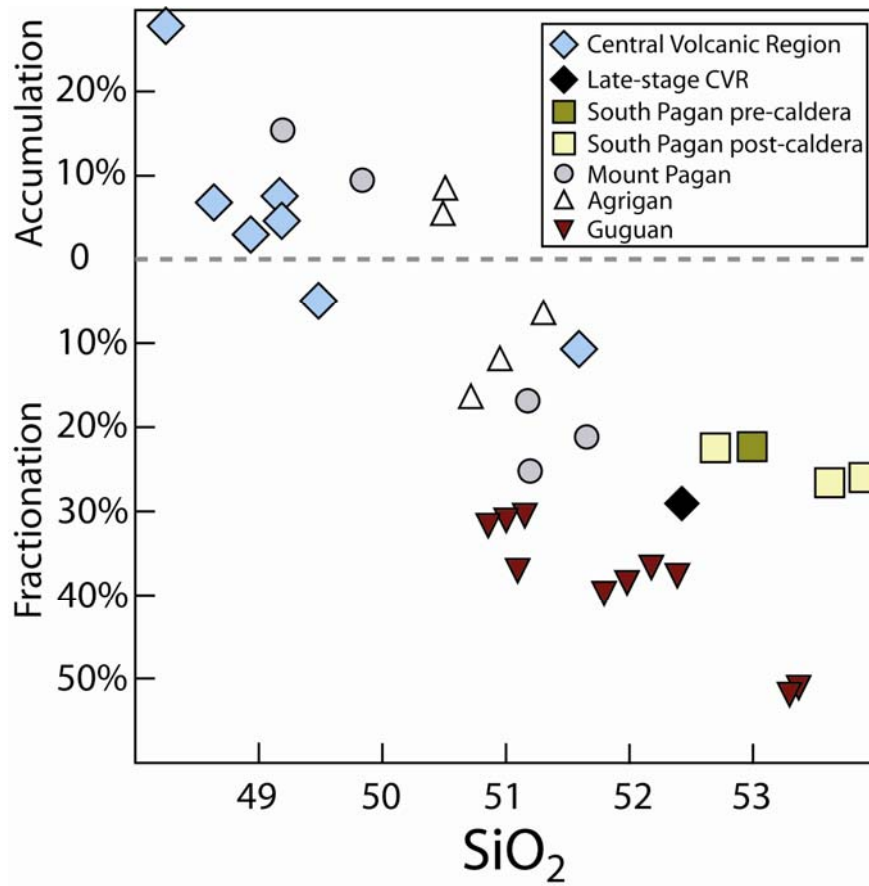


Fig. 2.12 SiO₂ vs. the estimated amount of crystallization and accumulation for Mariana lavas. The amount of crystallization or accumulation (in %) was calculated using the REE melting model presented in Table 2.5. Data sources for Mariana lavas are given in the caption to Fig. 2.5. The 2σ error bar for SiO₂ is smaller than the size of the symbols.

supplied to the mantle wedge and the degree of partial melting have also been recognized along other arc fronts (e.g., Izu-Bonin, Ishizuka et al., 2007; Kamchatka, Portnyagin et al., 2007; Central America, Rychert et al., 2008).

2.4.4 Dynamics of the partial melting processes beneath Pagan

Geochemical variations of cross-arc volcanoes (oriented perpendicular to the strike of the magmatic front) provide a unique constraint on the nature of the mantle source (fluid and sediment components), and melting conditions within arc systems (Gill, 1981; Ryan et al., 1996; Stern et al., 2006). For example, systematic geochemical variations of lavas from the Guguan cross-arc volcanoes could reflect a westward decrease in the fluid component (and the extent of melting) and/or an increase in the melting of subducted sediment due to the sampling of melts from increasing depth in the subduction zone (Stern et al., 2006). These variations in lava chemistry were observed for cross-arc Guguan volcanoes separated by 8-29 km (Stern et al., 2006). South Pagan caldera lies ~6 km farther west than Mt. Pagan caldera (Fig. 2.2) and it is located slightly west of the main arc axis defined by active Mariana volcanoes (dashed line; Fig. 2.1). This ~6 km offset is only slightly smaller than the range for Guguan volcanoes. Thus, the lower Ba/Th, Sm/Yb, and $^{143}\text{Nd}/^{144}\text{Nd}$, and higher Nb/Zr, La/Sm, Th/Nb, and Pb isotopic ratios at Mt. Pagan compared to South Pagan that could reflect a decrease in the fluid contribution and melt fraction, and/or an increase in sediment melting (respectively), with increasing distance from the trench.

The range of sediment contents (calculated by the Pb and Nd isotopic mixing model and REE melting model) in Mt. Pagan lavas is four times greater than the range for South Pagan lavas (Figs. 2.7 and 2.13). In detail, the $^{206}\text{Pb}/^{204}\text{Pb}$ and $^{143}\text{Nd}/^{144}\text{Nd}$ variability in Mt. Pagan lavas is equivalent to 64% and 45% of the total range observed in Mariana lavas (Fig. 2.7a). There is considerably less $^{206}\text{Pb}/^{204}\text{Pb}$ and $^{143}\text{Nd}/^{144}\text{Nd}$ variability for South Pagan (2% and 12%) lavas.

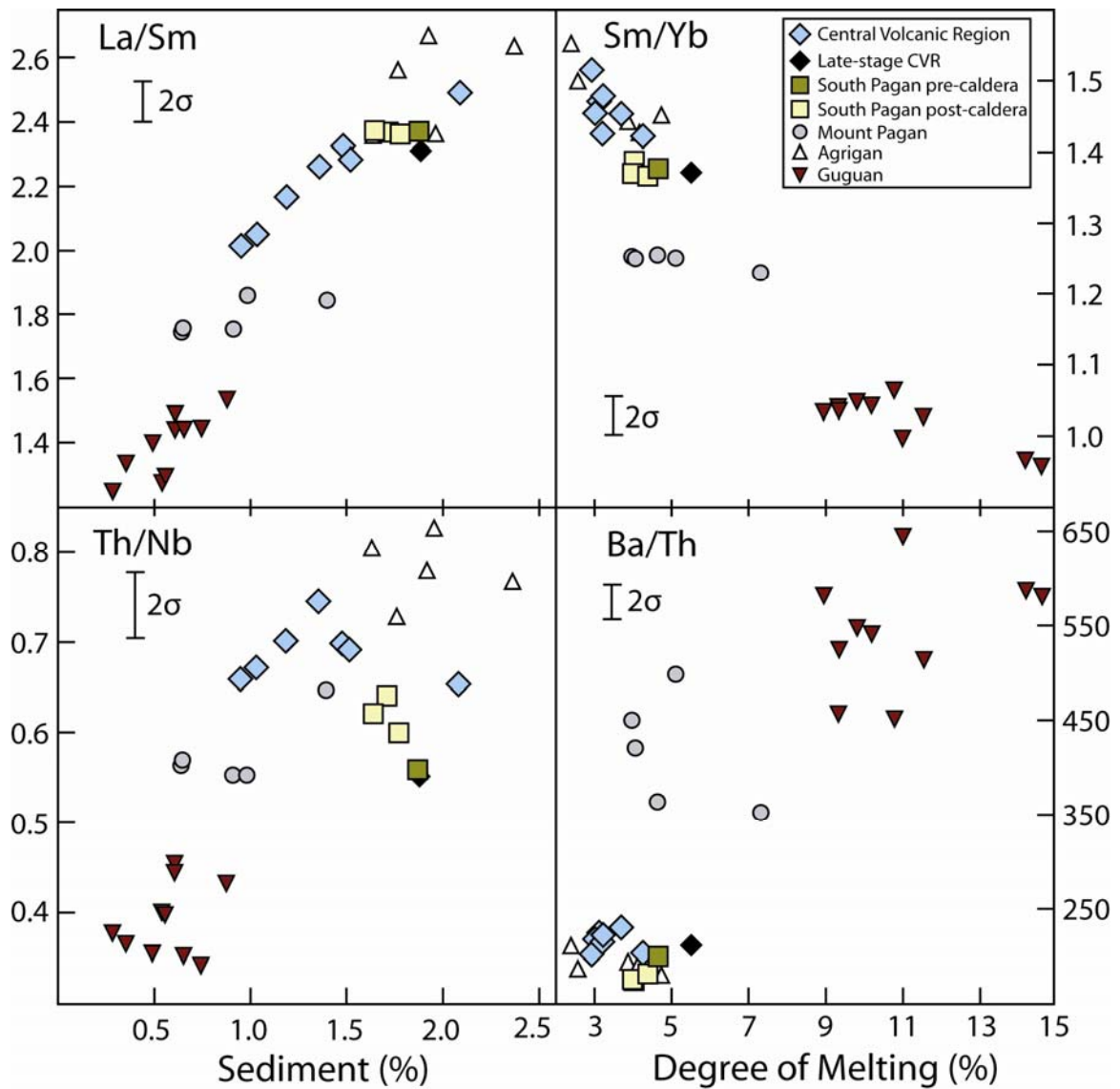


Fig. 2.13 Incompatible trace element ratios vs. the amount of sediment addition to the mantle source and the degree of partial melting for selected Mariana arc lavas. The amount of sediment addition and degree of partial melting was calculated using the REE melting model presented in Table 2.5. The sources for the Mariana lavas are given in the caption to Fig. 2.5. The 2σ error bars for the trace element ratios are shown in each panel.

These observations might be explained if greater extents of partial melting in the source region of Mt. Pagan (compared to South Pagan) facilitated melting over a wider region. Partial melting over a larger area is more likely to sample a greater range in the amount of subducted sediment. Moreover, the highly variable sediment content observed in Mt. Pagan lavas (compared to South Pagan lavas), and the significant differences in the amounts of fluid and sediment components between these volcanoes, suggest that the length scale of compositional heterogeneity in the mantle wedge is small with respect to the distance between their summits (~10 km).

2.5 Conclusions

Pagan Island is one of the most historically active volcanic centers in the Mariana Arc. Two main eruptive sequences, the pre-caldera (<780-9.4 ka) and post-caldera (<9.4 ka) stages, have been recognized for South Pagan and Mt. Pagan volcanoes based on geologic mapping. Holocene South Pagan lavas originated from three post-caldera cones located within the volcano's caldera. South Pagan and CVR lavas are relatively evolved (2-6 wt. % MgO) and lie along distinct fractionation trends. Olivine, clinopyroxene, titanomagnetite, and plagioclase fractionation, plagioclase accumulation, and magma mixing are important crustal processes for these lavas. Despite its proximity, Mt. Pagan has erupted mostly geochemically distinct lavas compared to CVR and South Pagan reflecting variations in slab contributions (i.e., sediment and aqueous fluid) to the mantle wedge and the extent of partial melting. South Pagan and CVR lavas have lower Ba/Th and Ba/La than Mt. Pagan lavas reflecting a smaller flux of aqueous fluid to the subarc mantle beneath these volcanoes. The CVR lavas have the lowest $^{143}\text{Nd}/^{144}\text{Nd}$ and Ce/Ce* ratios, and highest Nb/Zr and Th/Nb ratios among Pagan lavas due to a greater amount of sediment addition to the mantle source below this volcano. Lead and Nd isotopic mixing calculations indicate the average sediment contribution to Agrigan (~2.2%), CVR (~2.0%), and South Pagan (~1.8%) lavas is slightly higher than Mt. Pagan (~1.4%) and Guguan (~1.3%) lavas.

The overall temporal decreases in Ba/Th, Nb/Zr, and $^{208}\text{Pb}/^{204}\text{Pb}$ ratios in CVR and South Pagan lavas suggest the fluid and sediment contributions to the mantle source have progressively diminished during the known eruptive history of southern Pagan volcanoes. Melt modeling of Mariana lavas demonstrates that saucer-shaped normalized REE patterns observed in some arc lavas can arise from partial melting of a mixed mantle-sediment source, and do not require amphibole interaction or fractionation to depress the middle REE abundances of the lavas. The calculated degree of mantle partial melting based on the REE melting model for Pagan (3-7%), Agrigan (2-5%), and Guguan (9-15%) lavas is similar to, or lower than previous estimates for Mariana lavas (6-30%). The correlation between the Ba/Th and Sm/Yb ratios of the lavas, (and the degree of partial melting) suggests that the fluid contribution to the mantle wedge is the dominant control on the extent of partial melting beneath Mariana arc volcanoes. A decrease in the amount of fluid addition (lower Ba/Th and Ba/La) and extent of melting (higher Sm/Yb), and increase in the sediment contribution (higher Th/Nb, La/Sm, Nb/Zr, and $^{208}\text{Pb}/^{204}\text{Pb}$) from Mt. Pagan to South Pagan could reflect cross-arc melting variations within the Mariana arc. This might reflect a decrease in the fluid component (and the extent of melting) and/or an increase in the amount of subducted sediment due to the sampling of melts from increasing depth in the subduction zone. The range of sediment contents in Mt. Pagan lavas is significantly greater than the range for South Pagan lavas, suggesting that the length scale of compositional heterogeneity in the mantle wedge is small with respect to the distance between their summits (~10 km).

CHAPTER 3

EVOLUTION OF KĪLAUEA VOLCANO'S SHALLOW MAGMATIC PLUMBING SYSTEM: A GEOCHEMICAL PERSPECTIVE FROM HISTORICAL RIFT LAVAS (1790-1980 A.D.)

3.1 Abstract

Over 200 years of frequent, voluminous ($\sim 4.3 \text{ km}^3$), and compositionally variable (5-18 wt. % MgO) eruptions at Kīlauea's summit, and east (ERZ) and southwest (SWRZ) rift zones provide an excellent opportunity to explore the magmatic connection between the volcano's summit and rift zones, and to determine shallow magma storage times. Here, we present new Pb, Sr, and Nd isotopic ratios, and major- and trace-element abundances for 48 historical Kīlauea rift lavas (1790-1980 A.D.). Overall, historical Kīlauea rift and summit lavas display overlapping temporal geochemical variations (e.g., $\text{K}_2\text{O}/\text{TiO}_2$, Nb/Y, $^{87}\text{Sr}/^{86}\text{Sr}$, and $^{206}\text{Pb}/^{204}\text{Pb}$) indicating that they originated from similar parental magmas for a given time period (i.e., months to years). Strongly evolved ($< 6 \text{ wt. \% MgO}$) ERZ lavas plot off these temporal trends suggesting they were rift-stored magmas. The compositional variation in most Kīlauea rift eruptions (e.g., 1790, 1840, 1868, 1919-23, 1955, and 1960-74) is a consequence of mixing new mantle-derived magma with stored or hybrid magmas residing in the volcano's summit and rift zone reservoirs. Olivine, clinopyroxene, and plagioclase fractionation and/or accumulation are superimposed on these magmatic processes. MELTS modeling indicates most ERZ and SWRZ magmas fractionate over a range of pressures (0.5-1.5 kbars) equivalent to the depth of Kīlauea's $\sim 2\text{-}5 \text{ km}$ deep summit reservoir. Many historical ERZ and SWRZ magmas are delivered to the volcano's summit reservoir before entering and erupting along the rift zones, excluding lavas from the prolonged 1969-74 Mauna Ulu ERZ eruption. The rate of $^{206}\text{Pb}/^{204}\text{Pb}$ variation in the Mauna Ulu lavas ($\sim 0.015 \text{ year}^{-1}$) is ~ 4 times greater than observed for late 20th century Kīlauea historical summit

lavas ($\sim 0.004 \text{ year}^{-1}$). This rapid change indicates these lavas may have partially or completely bypassed the summit reservoir. The MgO-variable (6.7-11.5 wt. %) 1971 and 1974 caldera rim and floor lavas reflect the eruption of stored, moderately evolved magmas from the volcano's summit reservoir that were hydraulically forced to the surface by more mafic magmas that also bypassed the summit reservoir. Magma storage times for late 20th century lavas in the ERZ (~ 12 -165 years) are significantly shorter than most estimates for Kīlauea's summit and middle ERZ (~ 23 -160 years), lower ERZ (>550 years), and the interconnected volume beneath the volcano (~ 100 -3000 years).

3.2 Introduction

Spatial and temporal geochemical variations during long-lived eruptions yield valuable insight into the shallow magmatic processes within active volcanoes (e.g., Cerro Azul, Galapagos, Teasdale et al., 2005; El Hierro, Canary Islands, Stroncik et al., 2009; Etna, Italy, Andronico et al., 2005; Hekla, Iceland, Sigmarsson et al., 1992; Vulcano, Italy, Peccerillo et al., 2006). These studies provide a detailed view of the size, shape, and location of magma reservoirs, and magma transport, mixing, storage, and differentiation processes within the crust and volcanic edifice (e.g., summit, flanks, and rift zones). Kīlauea volcano, located on the island of Hawai'i (Fig. 3.1) has been prolific in its eruption frequency (Fig. 3.2) and volume ($\sim 4.3 \text{ km}^3$) during the past 220 years (Macdonald et al., 1983; Sutton et al., 2003) making it an ideal location to investigate the processes that operate in an interconnected magmatic plumbing network on timescales of hours to decades.

The basic magmatic architecture of Kīlauea volcano is well known. Seismic and petrologic studies suggest that Kīlauea magmas originate from partial melting at mantle depths (>60 -80 km) within the upper Hawaiian plume (e.g., Eaton and Murata, 1960; Watson and McKenzie, 1991; Tilling and Dvorak, 1993). Rapid melt extraction from the mantle source

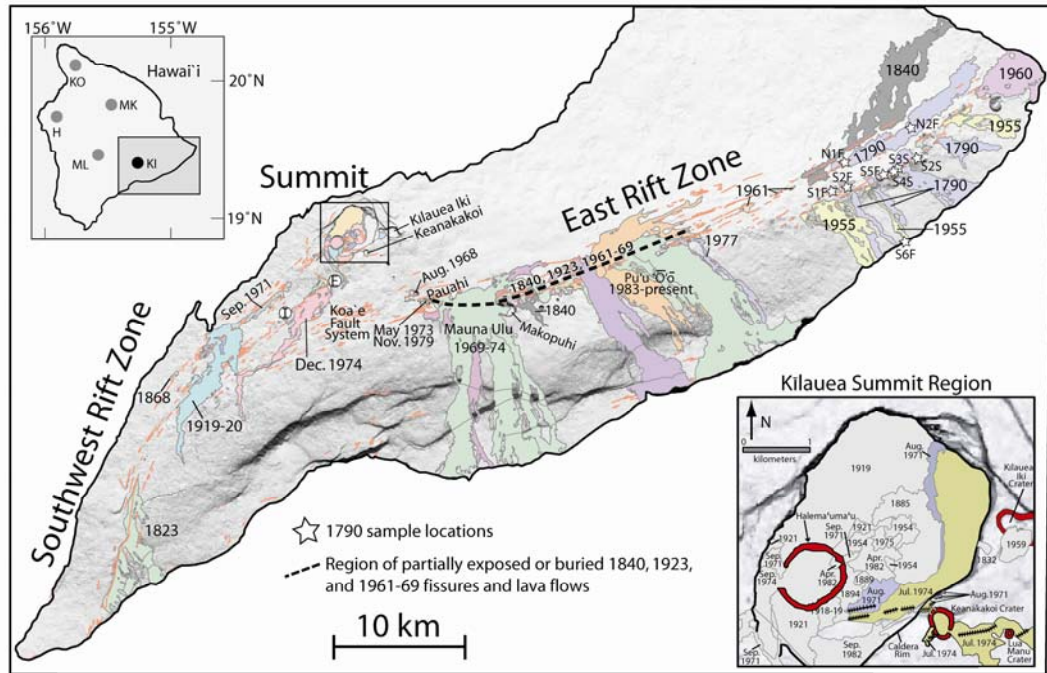


Fig. 3.1 Location map of historical SWRZ, ERZ, and summit eruptions, and ERZ pit craters (Kīlauea Iki, Keanakakoi, Pauahi, and Makopuhi) modified from Trusdell et al. (2005). The inset map shows the island of Hawai'i with the summit locations of Kīlauea (KI), Hualalai (H), Mauna Loa (ML), Mauna Kea (MK), and Kohala (KO). The sampling locations of the 1790 lavas are noted with white stars and partial sample number (e.g., S2F). The dashed black line represents the general locations of the 1961-69 fissures and vents that were subsequently buried by younger lavas. The white circles represent the vent locations (E and I) for the December 1974 eruption. The outlined box corresponds to the enlarged area of Kīlauea's summit region. The location of the August 1971 and July 1974 caldera floor and rim fissures and lava flows are shown. Historical summit extracaldera lavas, and lavas that surface the caldera floor are also labeled with the year they erupted.

region into chemically isolated channels (e.g., McKenzie, 1985; Williams and Gill, 1989) is probably the dominant melt transport mechanism beneath Kīlauea because it provides a relatively large amount of melt for sustained, high volume eruptions (Pietruszka et al., 2006). These melts are thought to ascend through a primary conduit to Kīlauea's shallow (~2-5 km deep) magma reservoir and its two rift zones (e.g., Tilling and Dvorak, 1993; Wright and Klein, 2006). The magmatic core of these rifts may extend to depths of 9-10 km, near the volcano's basal decollement (Delaney et al., 1990).

The magmatic connection between Kīlauea's primary magma conduit and rift zones is only broadly defined, leading to considerable uncertainty in the depth and scale of magma interconnectivity between the summit and rift zone regions (e.g., Fiske and Kinoshita, 1969; Decker, 1987; Denlinger, 1997). Seismicity studies indicate that magma primarily intrudes both rift zones as sheeted dikes at depths of <5 km (Klein et al., 1987; Ryan, 1988; Wright and Klein, 2006), although aseismic magma transport to the ERZ may occur at greater depths (Koyanagi et al., 1987; Delaney et al., 1998; Wright and Klein, 2008). This ambiguity has led to contrasting ideas regarding the way magmas are 'processed' through Kīlauea's plumbing system. Previous studies suggest: (1) all magmas reside in the summit reservoir before intruding into the rift zones (Duffield et al., 1982; Wright and Klein, 2006), (2) magmas first appear along the ERZ before erupting at the summit (Wright and Fiske, 1971), and (3) magmas partially or completely bypass the summit reservoir before intruding into the ERZ (Garcia et al., 1996) or erupting near the summit (Helz, 1987).

The residence time of magma in volcanic or crustal reservoirs has implications for the rates of magmatic differentiation and the thermal regime of magmatic systems (e.g., Cooper et al., 2001). Magma residence times in the upper plumbing system of some highly active volcanoes (e.g., Etna, Italy, Condomines et al., 1995; Piton de Fournaise, Reunion, Sigmarsson et al., 2005; Stromboli, Italy, Francalanci et al., 1999) can be relatively short (~15 to 30 years). Although

Kīlauea is also highly active ($\sim 0.06\text{-}0.18 \text{ km}^3/\text{year}$ magma supply rate during the late 20th century; Dvorak and Dzurisin, 1993; Heliker et al., 1998; Cayol et al., 2000; Sutton et al., 2003), there is a wide range in estimates for magma residence times in Kīlauea's summit reservoir, ERZ, and the interconnected volume beneath the volcano. For example, a 10-year storage time for 1959 summit lavas was calculated based on crystal size distributions (Mangan, 1990), although magma supplying this eruption may have bypassed the summit reservoir (Helz, 1987; Anderson and Brown, 1993). Magma residence times in the summit reservoir of $\sim 70\text{-}160$ years from 1820-94, $\sim 20\text{-}90$ years from 1894-1921, ~ 12 years from 1921-34, and $\sim 29\text{-}43$ years from 1961-82 were estimated based on the temporal geochemical variations of summit lavas (Pietruszka and Garcia, 1999b; Garcia et al., 2003). The January 1997 lavas from the Pu'u 'Ō'ō ERZ eruption (1983-present; Fig. 3.1) are thought to represent hybrid magmas, some of which were stored in the ERZ for $\sim 29\text{-}34$ years based on geochemical mixing modeling (Thornber et al., 2003). A >550 year residence time was calculated for the phenocrysts in the strongly evolved 1955 ERZ lavas (implying a similarly long magma residence time) based on uranium-series disequilibria (Cooper et al., 2001). A residence time of $\sim 100\text{-}3000$ years for the entire interconnected volume of Kīlauea's magmatic network was estimated based on magma supply rates during the late 20th century (Decker, 1987; Denlinger, 1997). These variable time estimates may result from the different methods used to determine average residence times over different time scales (years to centuries). This geochemical study aims to resolve the ambiguity and uncertainty related to Kīlauea's magmatic plumbing network and magma storage time estimates.

New major- and trace-element abundances and high-precision Pb, Sr, and Nd isotopic ratios for a representative suite of historical (1790-1980 A.D.) rift zone lavas are used here to investigate the small-scale spatial and temporal compositional variations between historical rift and summit lavas. Although major element analyses have been previously reported for many historical rift lavas (e.g., Macdonald and Eaton, 1964; Wright, 1971; Wright and Fiske, 1971),

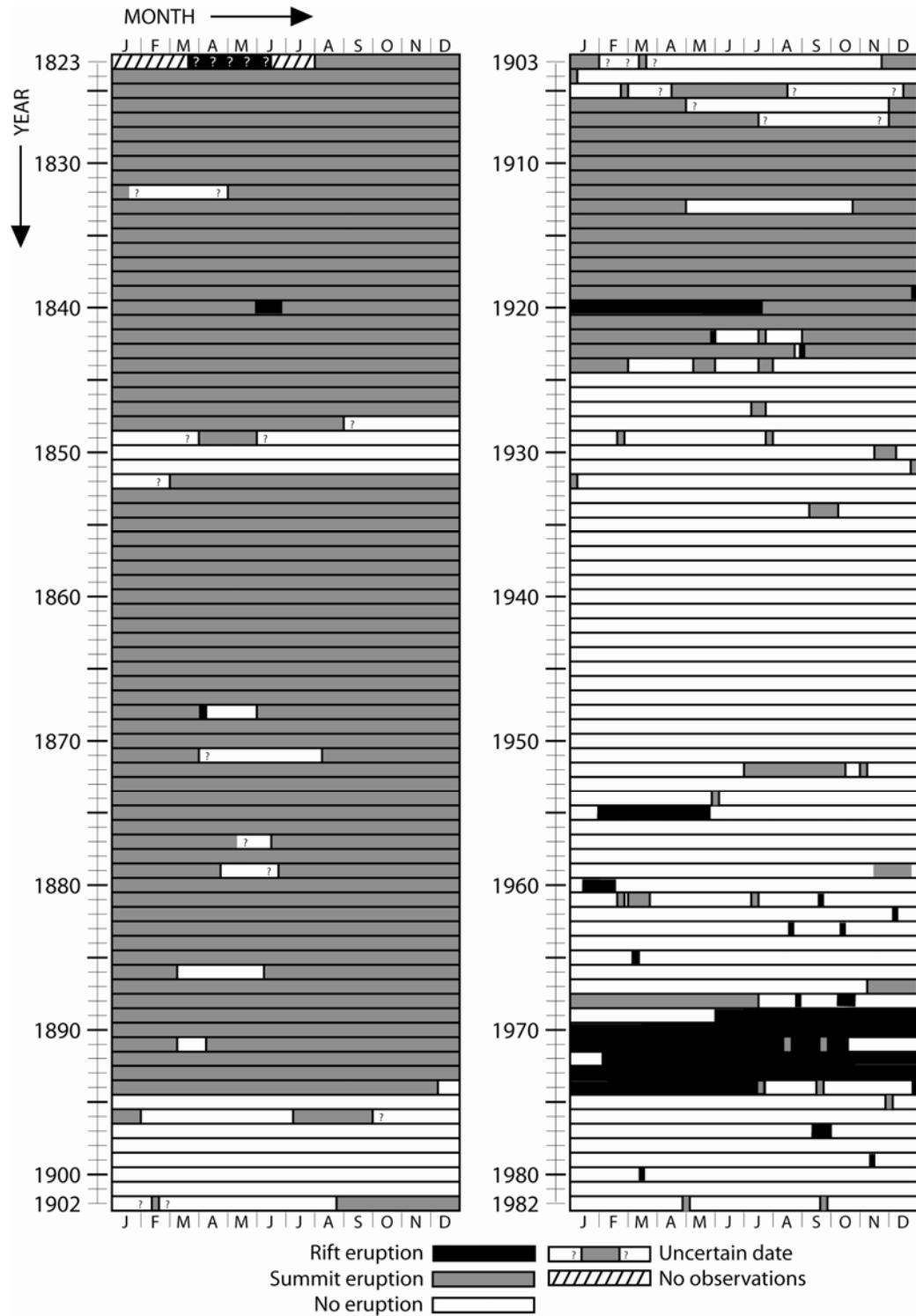


Fig. 3.2 Graphic summary of the historical eruptive activity at Kīlauea Volcano from 1823 to 1982. Rift eruptions are depicted by the black bars. Summit eruptions (gray bars) include the lava lake activity prior to the explosive 1924 eruption, caldera eruptions, and eruptions that occurred between the caldera and Kīlauea Iki crater. This figure was modified from Garcia et al. (2003) based on descriptions from Dana (1889), Brigham (1909), Fiske et al. (1987), Bevens et al. (1988), and Macdonald et al. (1983).

we present the first comprehensive geochemical characterization of the historical rift eruptions (excluding the 1955, 1960, 1969-71 Mauna Ulu, and 1983-present Pu‘u ‘Ō‘ō eruptions, Hofmann et al., 1984; Helz and Wright, 1992; Wright and Helz, 1996; Garcia et al., 2000; Cooper et al., 2001).

Historical Kīlauea summit lavas display systematic temporal variations of highly to moderately incompatible element ratios (e.g., Nb/Y and La/Yb) and Pb isotopic ratios (Fig. 3.3) with an abrupt reversal after 1924 (Pietruszka and Garcia, 1999a; Garcia et al., 2003). These variations are thought to result from the partial melting of small-scale compositional heterogeneities within the Hawaiian plume based on the short-term fluctuations of Pb, Sr, and Nd isotope ratios on a time-scale of years to centuries (Pietruszka and Garcia, 1999a; Marske et al., 2007). The degree of partial melting decreased from the early 19th century until the mid-20th century, which correlates with a lower eruption rate for the volcano between 1840-1959 (Pietruszka and Garcia, 1999a). This interval of declining magma supply rate culminated with a series of explosive summit eruptions in 1924. These reversed trends continued into the late 20th century (Fig. 3.3b) reflecting an increase in the degree of partial melting and eruption rate (Pietruszka and Garcia, 1999a). These systematic geochemical variations in historical summit lavas provide an excellent opportunity to ‘fingerprint’ the composition of the parental magma delivered to Kīlauea’s rift zones and summit for a given time interval. Thus, the historical variations for summit lavas can be used as a template for comparison with the temporal compositional record for historical rift lavas.

In this study we compare the temporal geochemical variations of historical rift and summit lavas to: (1) establish the petrogenetic relationship between summit and rift parental magmas, (2) evaluate the magmatic link between the summit and rift zones, and, (3) determine the timescales of magma transport, mixing, and differentiation processes within the shallow plumbing system, and (4) estimate magma storage times in the rift zones (prior to eruption)

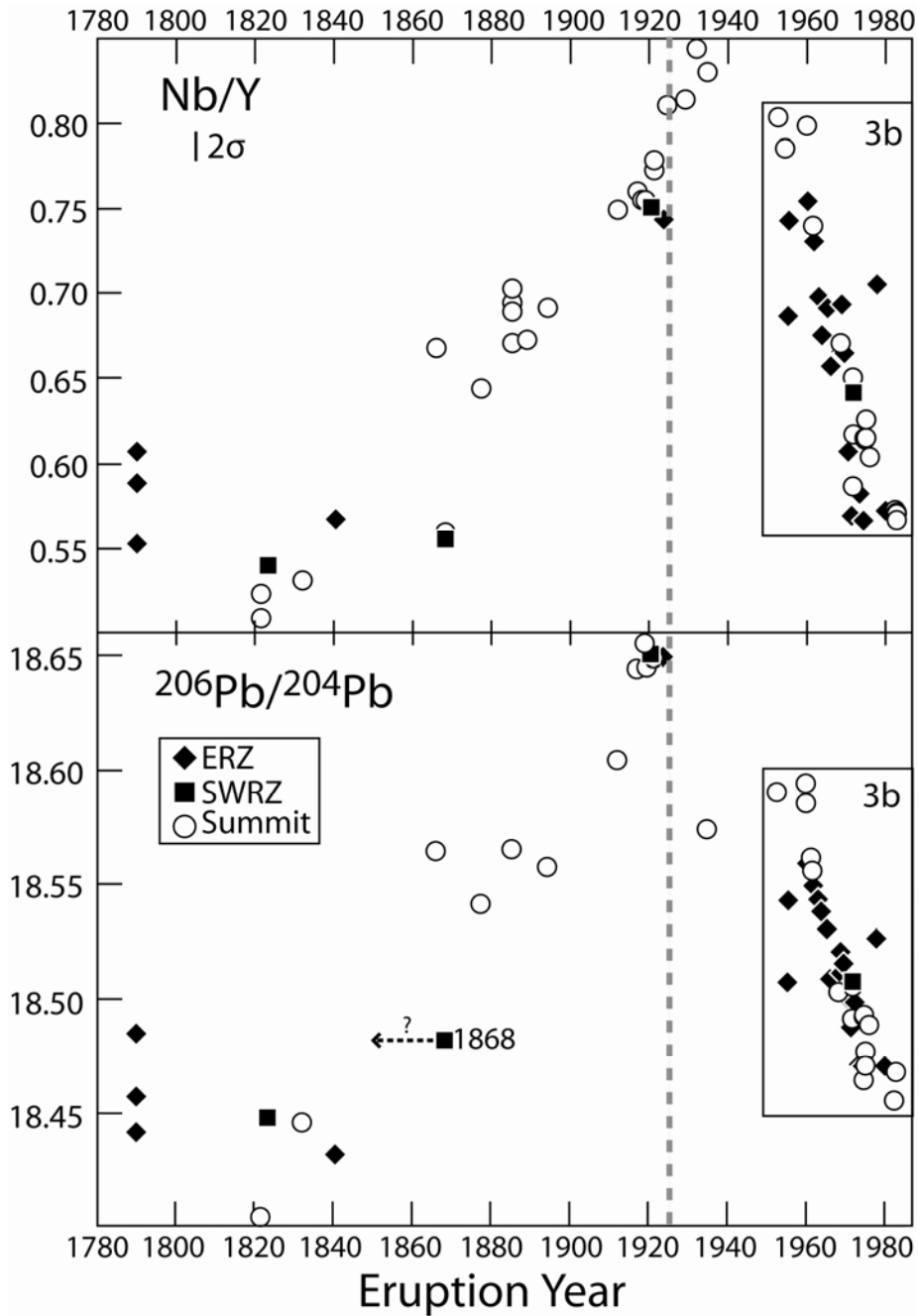


Fig. 3.3 Temporal variation in Nb/Y and $^{206}\text{Pb}/^{204}\text{Pb}$ ratios for Kīlauea historical rift and summit lavas. The lavas are subdivided by eruption location (see inset for symbols). Dashed vertical bar denotes the 1924 summit phreatic eruption. The low precision Pb isotopic historical summit data from Pietruszka and Garcia (1999a) is not used in this study (excluding the 1866, 1894, and 1912 lavas) due to the large differences in analytical uncertainty compared to our high precision Pb isotopic data. Rather, the Pb isotopic values for summit lavas presented here and in subsequent figures is unpublished high precision data from D. Heaton (2009). (a.) The 1868 SWRZ lava may have been stored for several decades before erupting (dashed arrow). The rectangles outline the enlarged views for (b.). (b.) The March and May labels correspond to the 1955 ERZ lavas. The 1977 ERZ lava may have been stored since ~1965 (dashed arrows). The 2σ error bars are presented unless they are smaller than the size of the symbols.

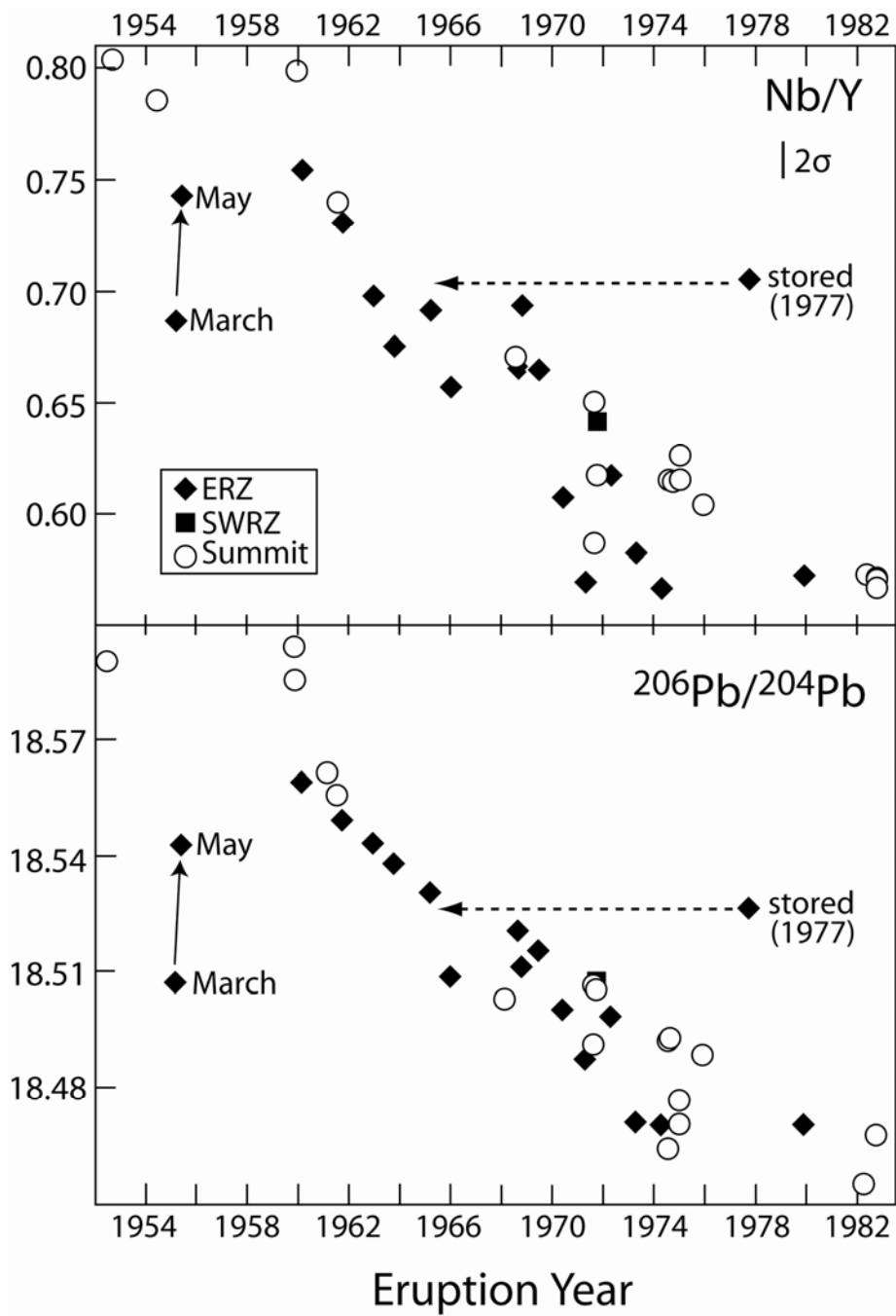


Fig. 3.3 (Continued)

based on the apparent time ‘lag’ for a given magma composition to erupt at the summit vs. rift zone, or vice versa. This study is useful because it is based on a consistent geochemical method to evaluate these processes for the entire historical period.

3.3 Results

3.3.1 Overview of Kīlauea’s historical rift zone eruptions

This overview is based on Macdonald et al. (1983) unless otherwise noted. The historical period had 23 ERZ and 5 SWRZ eruptions (lasting hours to years; Fig. 3.2) which produced a larger volume ($\sim 0.5 \text{ km}^3$) of lava than the ~ 32 summit eruptions ($\sim 0.3 \text{ km}^3$). This period began with a series of phreatomagmatic and phreatic summit eruptions in 1790 that followed ~ 300 years of explosive summit activity (Swanson, 2008). The earliest historical rift eruptions also occurred around ~ 1790 (hereafter referred to as 1790) along Kīlauea’s lower ERZ (Fig. 3.1). The exact age is uncertain because there is no written record of it, and radiocarbon dates for charcoal under several flows yielded ages of less than 200 years before present (relative to 1950 A.D.; Moore and Trusdell, 1991). However, Hawaiian oral accounts indicate that an eruption occurred along the lower ERZ around 1790 (Swanson, 2008). The next known Kīlauea eruption occurred sometime between 1820 and 1823, producing high lava-fountaining within the caldera (Sharp et al., 1987), just prior to the start of written descriptions of Kīlauea’s volcanic activity in August 1823.

From ~ 1823 to 1924 volcanism at the summit was dominated by nearly continuous lava lake activity within the caldera (Fig. 3.2). Three brief (< 1 day) eruptions in 1832, 1868, and 1877 from vents between Kīlauea caldera and Kīlauea Iki (a pit crater adjacent to the summit caldera; Fig. 3.1) were accompanied by caldera floor collapses and brief hiatuses in lava lake activity. Three rift eruptions also occurred in the 19th century including two along the SWRZ in 1823 (~ 12 weeks) and 1868 (~ 1 day), and one along the middle and lower ERZ in 1840 (~ 4 weeks; Fig. 3.1).

The 42-week Mauna Iki eruption took place from 1919-20 along the upper SWRZ, followed by ~1-2 day eruptions along the upper ERZ in May 1922 and August 1923. In 1924, the lava lake within the caldera drained, its floor and walls collapsed, and numerous violent phreatic explosions occurred.

Following the 1924 explosive activity, summit eruptions were sporadic and short-lived (hours to several months). Seven short-lived (days to weeks) summit eruptions that took place from 1924 to 1934 were followed by an eruptive hiatus until the 1952 summit eruption (Fig. 3.2). The 1954 summit eruption (3 days) and 1959 Kīlauea Iki eruption (~7 weeks) were succeeded by three short-lived summit eruptions in 1961 (1-22 days) and one prolonged summit eruption from 1967-68 (~36 weeks). Two prolonged eruptions in February 1955 (~13 weeks) and January 1960 (~5 weeks) marked the first lower ERZ eruptions since 1840 (Figs. 3.1 and 3.2). The main locus of eruptive activity at Kīlauea shifted to the ERZ beginning with the 1955 eruption (Figs. 3.1 and 3.2). Nine short-lived (1-15 day) eruptions took place along the middle and upper ERZ between September 1961 and February 1969.

The 1969-74 Mauna Ulu eruption along the upper ERZ (Fig. 3.1) is the second longest Kīlauea historical rift eruption after the ongoing Pu‘u ‘Ō‘ō eruption (1983-present). Mauna Ulu had two eruptive periods (May 1969 to October 1971 and February 1972 to July 1974) separated by a 4-month pause (Fig. 3.2). In May 1973, a seismic swarm began under Mauna Ulu at a depth of 2-4 km, and travelled westward and upward, followed by a short-lived eruption at Pauahi crater (Fig. 3.1). Three brief summit eruptions in August 1971 (10 hours), September 1971 (2 days), and July 1974 (3 days), and one SWRZ eruption in September 1971 (5 days) occurred during the Mauna Ulu eruption, towards the end of each eruptive phase (Figs. 3.1 and 3.2). Three short-lived (hours) eruptions subsequently took place at the summit (September 1974 and November 1975) and between the Koa‘e fault system and SWRZ (December 1974). In September 1977, a ~3 week eruption occurred along the middle ERZ, followed by one day

eruptions in Pauahi crater in December 1979 and near Mauna Ulu in 1980 (Fig. 3.1). Two brief (<1 day) summit eruptions took place in 1982. The Pu‘u ‘Ō‘ō eruption is the most voluminous (~3.5 km³; Sutton et al., 2003) historical Kīlauea rift eruption (Fig. 3.1).

3.3.2 Analytical methods

Forty-eight historical Kīlauea rift samples were analyzed for major- and trace-element (Rb, Sr, Y, Nb, Zr, Zn, Ni, Cr, V, Ba, and Ce) abundances over a four-week period using X-ray fluorescence spectrometry (XRF) at the University of Massachusetts (Table 3.1). Details of methods used and estimates of analytical precision for the XRF analyses are given by Rhodes (1996) and Rhodes and Vollinger (2004). The Kīlauea basalt standard BHVO-1 (n=5) and the in-house reference sample Kil1919 (n=1), were run as internal controls for trace element abundances during this period (Table 3.1). In addition, Kil1919 was also analyzed once with the samples to evaluate the accuracy of the XRF major element data. Comparison XRF Kil1919 values (n=6) from Rhodes and Vollinger (2004) show that all element abundances agree within 2% except Rb, V, and Ce (6%), and Na₂O (19%). The low Na₂O content of the Kil1919 reference sample analyzed by Rhodes and Vollinger (2004) is thought to result from the loss of semi-volatile Na after multiple analyses were performed on the same fused disk. All estimates of precision in this paper are given as $\pm 2\sigma$.

Twenty-seven samples were analyzed over two days for Sc, V, Cr, Co, Ni, Cu, Zn, Sr, Cs, Rb, Ba, Th, U, Pb, Nb, Zr, Hf, Y, and rare earth element (REE) abundances using inductively coupled plasma mass spectrometry (ICP-MS) at the Australian National University (Table 3.2). Analytical methods and estimates of precision for the ICP-MS trace element analyses are given in Table 3.2 and by Norman et al. (1998). Estimates of analytical precision based on the Kīlauea basaltic reference material Kil93 (n=4) show that all elements agree within 6% except for Co, Rb, and Pb (7%), Sc (8%), Zr (9%), and Cr (13%). Prior to both XRF and ICP-MS analyses,

Table 3.1 Whole-rock XRF analyses of historical Kilauea rift lavas. * Total iron given as Fe₂O₃. Date refers to the day and/or year the sample was erupted. Oxide abundances are in wt. %; trace element contents are in ppm. The Kil1919a (n=1) reference material analyzed with the samples was collected from the same lava flow as BHVO-2. Comparison values (Kil1919b) from Rhodes and Vollinger (2004) are given. BHVO-2 (n=5) was run as a standard by XRF for trace element abundances.

Sample	1790N-1F	1790N-2F	1790S-1F	1790S-3S	1790S-5F
Date	1790	1790	1790	1790	1790
Loc.	ERZ	ERZ	ERZ	ERZ	ERZ
SiO ₂	51.11	50.85	51.12	50.61	50.64
TiO ₂	2.724	3.13	3.334	2.203	2.193
Al ₂ O ₃	13.52	13.44	13.30	13.91	13.61
Fe ₂ O ₃ *	12.43	13.43	13.77	11.17	11.20
MnO	0.19	0.19	0.19	0.17	0.17
MgO	6.77	5.60	5.31	8.05	8.38
CaO	10.56	9.62	9.33	11.06	11.15
Na ₂ O	2.19	2.67	2.30	1.88	2.15
K ₂ O	0.468	0.629	0.671	0.373	0.378
P ₂ O ₅	0.266	0.331	0.363	0.204	0.207
Total	100.23	99.89	99.69	99.63	100.08
Y	27.0	27.8	34.7	21.8	22.2
Sr	334	355	357	322	318
Rb	7.4	8.6	11.4	5.9	6.1
Nb	14.8	16.1	20.3	11.9	11.8
Zr	171	183	234	137	135
Ni	83	105	59	133	139
Cr	189	204	17	354	406
V	280	286	326	238	243
Zn	116	120	138	103	101
Ba	107	123	157	90	91
Sample	1790S-2F	1790S-2S	1790S-4S	1790S-6F	1823SW-F
Date	1790	1790	1790	1790	1823
Loc.	ERZ	ERZ	ERZ	ERZ	SWZ
SiO ₂	50.66	50.60	50.79	51.13	50.73
TiO ₂	2.766	2.272	2.285	3.121	2.468
Al ₂ O ₃	13.56	13.45	13.81	13.6	13.43
Fe ₂ O ₃ *	12.45	11.50	11.33	12.81	12.17
MnO	0.18	0.17	0.18	0.18	0.19
MgO	6.88	8.47	7.86	5.65	7.21
CaO	10.38	10.86	11.03	9.51	10.91
Na ₂ O	1.82	2.10	1.61	2.64	2.20
K ₂ O	0.539	0.401	0.381	0.679	0.447
P ₂ O ₅	0.288	0.220	0.218	0.363	0.243
Total	99.52	100.04	99.49	99.68	100.00
Y	32.5	22.9	23.1	33.8	24.7
Sr	354	316	327	361	330
Rb	10.3	6.3	6.2	11.6	6.8
Nb	18.4	12.3	12.3	20	13.1
Zr	214	142	142	232	156
Ni	62	140	126	75	107
Cr	50	378	347	83	380
V	318	250	250	301	269
Zn	127	102	99	129	111
Ba	145	89	91	143	102

Table 3.1 (Continued)

Sample	FT89-10	FT89-21	FT89-22	1868SW	MI-07-09
Date	1840	1840	1840	7-Apr-1868	1919
Loc.	ERZ	ERZ	ERZ	SWZ	SWZ
SiO ₂	50.85	48.83	47.35	50.87	49.58
TiO ₂	2.355	2.101	1.813	2.554	2.653
Al ₂ O ₃	12.88	10.94	9.49	13.49	13.06
Fe ₂ O ₃ *	11.82	11.86	12.17	11.67	12.11
MnO	0.18	0.17	0.17	0.17	0.18
MgO	8.91	14.58	18.41	7.6	7.79
CaO	10.46	9.08	7.89	10.65	11.23
Na ₂ O	2.15	1.71	1.58	1.75	2.46
K ₂ O	0.395	0.374	0.323	0.459	0.506
P ₂ O ₅	0.178	0.196	0.158	0.248	0.259
Total	100.18	99.84	99.37	99.46	99.83
Y	31.7	17.9	18.1	25.6	24.2
Sr	352	240	251	334	378
Rb	9.4	5.2	5.2	7.5	8.2
Nb	17.8	9.3	9.7	13.8	17.7
Zr	209	112	115	158	171
Ni	71	833	745	140	133
Cr	62	1224	1134	362	383
V	325	199	209	258	269
Zn	133	110	108	107	107
Ba	127	76	87	107	118
Sample	MI-07-06	MI-07-05	MI-07-04	MI-07-08	MI-07-02
Date	1919	1919	1919	1920	1920
Loc.	SWZ	SWZ	SWZ	SWZ	SWZ
SiO ₂	49.59	49.77	49.69	49.92	50.23
TiO ₂	2.628	2.636	2.635	2.692	2.759
Al ₂ O ₃	13.01	13.12	13.16	13.42	13.59
Fe ₂ O ₃ *	12.00	11.98	11.96	11.88	11.79
MnO	0.18	0.18	0.18	0.18	0.18
MgO	8.22	7.92	8.07	7.46	6.91
CaO	11.08	11.23	11.13	11.30	11.57
Na ₂ O	2.06	2.12	2.17	1.91	1.81
K ₂ O	0.498	0.492	0.502	0.517	0.521
P ₂ O ₅	0.257	0.256	0.259	0.266	0.267
Total	99.52	99.70	99.76	99.55	99.63
Y	23.7	23.7	24.1	24.5	24.7
Sr	374	377	378	383	391
Rb	8.2	8.2	8.1	8.4	8.5
Nb	17.6	17.4	17.5	17.9	18.0
Zr	169	169	169	173	175
Ni	158	144	151	131	104
Cr	429	419	423	441	397
V	272	274	269	280	280
Zn	108	107	109	106	105
Ba	120	114	124	122	121

Table 3.1 (Continued)

Sample	MI-07-01	MI-07-03	8	1A	2E
Date	1920	1920	25-Aug-1923	25-Feb-1955	3-Mar-1955
Loc.	SWZ	SWZ	ERZ	ERZ	ERZ
SiO ₂	50.08	49.77	49.20	50.72	50.82
TiO ₂	2.690	2.631	2.492	3.527	3.611
Al ₂ O ₃	13.36	13.0	12.57	13.32	13.18
Fe ₂ O ₃ *	11.84	12.00	12.11	13.34	13.56
MnO	0.18	0.19	0.18	0.19	0.20
MgO	7.53	8.43	9.77	5.60	5.32
CaO	11.38	11.15	10.82	9.44	9.25
Na ₂ O	2.21	2.19	2.02	2.65	2.62
K ₂ O	0.504	0.492	0.466	0.742	0.785
P ₂ O ₅	0.262	0.255	0.243	0.399	0.427
Total	100.04	100.11	99.87	99.93	99.75
Y	24.1	23.6	22.6	35.6	38.1
Sr	384	376	356	386	391
Rb	8.4	8.1	7.7	12.4	13.6
Nb	17.7	17.3	16.5	25.3	25.3
Zr	170	167	161	254	270
Ni	129	159	273	78	68
Cr	431	476	647	85	74
V	277	272	261	337	336
Zn	104	107	111	138	140
Ba	119	117	106	173	184
Sample	6T	8Y	10Z	19-Feb-60	K-61-30
Date	25-Mar-1955	28-Mar-1955	25-May-1955	19-Feb-1960	22-Sep-1961
Loc.	ERZ	ERZ	ERZ	ERZ	ERZ
SiO ₂	50.42	50.29	50.54	49.73	50.20
TiO ₂	3.286	3.253	3.182	2.704	2.913
Al ₂ O ₃	13.37	13.34	13.43	12.52	13.14
Fe ₂ O ₃ *	13.08	13.01	12.82	12.26	12.27
MnO	0.20	0.19	0.19	0.19	0.19
MgO	6.06	6.13	6.20	9.68	7.65
CaO	9.95	9.94	10.16	10.15	10.42
Na ₂ O	2.53	2.49	2.49	2.02	2.15
K ₂ O	0.691	0.684	0.669	0.532	0.609
P ₂ O ₅	0.356	0.351	0.344	0.283	0.311
Total	99.93	99.68	100.01	100.07	99.85
Y	32.3	31.8	31.5	25.7	28.0
Sr	397	392	398	356	380
Rb	12.1	12.2	11.8	9.4	10.4
Nb	23.5	24.1	22.5	18.1	20.2
Zr	231	228	224	176	197
Ni	84	88	86	273	148
Cr	121	124	137	525	322
V	322	319	313	274	291
Zn	127	126	120	112	117
Ba	168	171	166	136	145

Table 3.1 (Continued)

Sample	H-304	H-441	M-40	Aloi65-5a	HI-68-02
Date	7-Dec-1962	5-Oct-1963	5-Mar-1965	24-Dec-1965	22-Aug-1968
Loc.	ERZ	ERZ	ERZ	ERZ	ERZ
SiO ₂	50.46	50.16	50.23	50.16	47.89
TiO ₂	2.864	2.743	2.744	2.645	2.108
Al ₂ O ₃	13.32	13.37	13.28	13.20	10.78
Fe ₂ O ₃ *	12.05	12.05	12.24	12.10	12.88
MnO	0.18	0.18	0.19	0.18	0.19
MgO	7.25	7.34	7.62	7.66	14.2
CaO	10.69	10.75	10.77	10.91	9.19
Na ₂ O	2.27	2.18	2.17	2.23	1.74
K ₂ O	0.588	0.559	0.558	0.541	0.417
P ₂ O ₅	0.304	0.288	0.284	0.274	0.213
Total	99.98	99.62	100.09	92.24	99.61
Y	27.5	26.1	25.8	25.0	20.0
Sr	380	383	384	378	304
Rb	9.9	9.4	9.5	9.0	6.7
Nb	19.0	17.4	17.5	16.0	12.9
Zr	193	184	183	176	137
Ni	114	110	109	108	396
Cr	312	288	294	328	975
V	289	287	289	283	248
Zn	116	119	119	117	117
Ba	142	137	135	124	100
Sample	N68-14	N68-11	DAS69-3-2	DAS70-1213-41	DAS71-1213-134
Date	7-Oct-1968	14-Oct-1968	13-Jun-1969	24-May-1970	12-Apr-1971
Loc.	ERZ	ERZ	ERZ	ERZ	ERZ
SiO ₂	50.29	50.06	49.55	49.55	50.27
TiO ₂	2.721	2.614	2.465	2.381	2.372
Al ₂ O ₃	13.78	13.13	12.54	12.63	13.18
Fe ₂ O ₃ *	12.23	12.22	12.32	12.48	12.19
MnO	0.18	0.19	0.19	0.19	0.19
MgO	6.67	8.03	9.43	9.46	7.96
CaO	10.85	10.78	10.56	10.45	10.95
Na ₂ O	2.24	2.17	2.05	2.02	2.04
K ₂ O	0.548	0.523	0.493	0.448	0.426
P ₂ O ₅	0.280	0.267	0.250	0.232	0.225
Total	99.79	99.97	99.85	99.84	99.80
Y	25.9	24.8	23.2	23.5	24.0
Sr	386	369	353	329	326
Rb	8.8	8.7	8.2	7.1	6.8
Nb	17.7	16.3	15.1	13.8	13.4
Zr	180	172	161	151	147
Ni	85	137	197	155	124
Cr	184	358	508	494	431
V	297	282	274	276	273
Zn	120	118	118	116	115
Ba	129	122	116	106	100

Table 3.1 (Continued)

Sample	S1971SW-2	MU472-32	MU473-108	MU474-163	J1974-EV
Date	1-Sep-1971	14-Apr-1972	10-Apr-1973	8-Apr-1974	19-Jul-1974
Loc.	SWZ	ERZ	ERZ	ERZ	ERZ
SiO ₂	50.09	49.79	49.36	49.25	50.40
TiO ₂	2.522	2.371	2.267	2.149	2.485
Al ₂ O ₃	13.14	12.53	12.28	11.82	13.57
Fe ₂ O ₃ *	12.22	12.44	12.46	12.53	12.30
MnO	0.18	0.19	0.19	0.19	0.18
MgO	7.71	9.76	10.23	11.72	7.14
CaO	10.93	10.50	10.26	9.91	10.81
Na ₂ O	2.14	2.11	1.81	1.90	2.33
K ₂ O	0.508	0.453	0.421	0.397	0.472
P ₂ O ₅	0.259	0.234	0.221	0.206	0.246
Total	99.70	90.62	99.50	100.07	99.93
Y	24.1	23.0	23	21.6	25.0
Sr	362	330	316	297	344
Rb	7.9	7.1	6.9	6.4	7.6
Nb	15.2	13.9	13.1	12.1	14.3
Zr	164	150	144	135	157
Ni	110	225	205	312	99
Cr	334	628	633	804	275
V	272	253	269	257	276
Zn	115	114	116	114	117
Ba	119	103	101	97	108
Sample	KL-77-11	16-Nov-79	11-Mar-80	Kil1919a	Kil1919b
Date	18-Sep-1977	16-Nov-1979	11-Mar-1980	—	—
Loc.	ERZ	ERZ	ERZ	—	—
SiO ₂	50.82	49.63	49.92	50.07	50.00
TiO ₂	3.438	2.238	2.376	2.755	2.766
Al ₂ O ₃	13.43	12.11	12.52	13.54	13.74
Fe ₂ O ₃ *	13.22	12.53	12.26	12.04	12.09
MnO	0.20	0.19	0.19	0.18	0.18
MgO	5.41	10.48	9.94	6.86	6.88
CaO	9.47	10.24	10.17	11.25	11.42
Na ₂ O	2.69	1.50	2.04	2.20	1.78
K ₂ O	0.746	0.408	0.445	0.536	0.530
P ₂ O ₅	0.397	0.218	0.237	0.268	0.274
Total	99.82	99.54	100.10	99.70	99.65
Y	35.2	22.4	23.5	24.7	24.7
Sr	393	308	326	394	395
Rb	12.9	6.6	7.4	8.5	9.0
Nb	24.9	12.4	14.5	18.5	18.4
Zr	254	138	151	178	177
Ni	67	256	281	101	101
Cr	63	693	528	261	266
V	338	247	264	269	284
Zn	141	112	115	108	107
Ba	173	92	106	123	124

Table 3.1 (Continued)

Sample	BHVO-2 avg.	$\pm 2\sigma$
Date	—	—
Loc.	—	—
SiO ₂	—	—
TiO ₂	—	—
Al ₂ O ₃	—	—
Fe ₂ O ₃ *	—	—
MnO	—	—
MgO	—	—
CaO	—	—
Na ₂ O	—	—
K ₂ O	—	—
P ₂ O ₅	—	—
Total	—	—
Y	24.6	0.2
Sr	386	3
Rb	8.3	0.2
Nb	18.1	0.1
Zr	177	1
Ni	117	17
Cr	290	8
V	279	2
Zn	111	2
Ba	126	5

Table 3.2 ICP-MS trace element analyses of Kīlauea rift lavas. Values are in ppm. Kil93 (n=4), an in-house reference material, was analyzed with these samples. Eruption year for the samples are presented in Table 3.1.

Sample	Rb	Cs	Ba	La	Ce	Pr	Nd	Sm	Eu	Gd	Tb
1790S-2F	12.0	0.116	160	16.9	43.2	6.24	29.1	7.62	2.53	8.03	1.25
1790S-4S	7.3	0.070	104	11.3	29.3	4.32	20.4	5.46	1.88	5.83	0.90
1790S-6F	12.8	0.129	166	17.9	46.2	6.65	30.6	7.97	2.61	8.29	1.29
1823SW-F	8.1	0.082	112	11.9	31.3	4.62	21.6	5.82	1.98	6.07	0.96
FT89-10	10.8	0.107	148	15.8	41.1	6.02	27.9	7.44	2.49	7.84	1.21
1868SW	8.7	0.086	122	12.7	32.8	4.83	22.6	6.05	2.08	6.41	1.02
MI-07-02	10.0	0.100	139	15.6	39.8	5.70	25.8	6.41	2.16	6.42	0.99
8	9.4	0.092	131	14.7	37.5	5.38	24.2	6.05	2.07	6.15	0.95
2E	15.6	0.147	202	22.5	57.5	8.19	37.1	9.38	3.02	9.62	1.50
10Z	13.7	0.131	183	19.9	50.3	7.12	31.9	7.90	2.60	8.03	1.24
19-Feb-1960	11.7	0.116	161	17.5	44.0	6.24	27.9	6.93	2.27	7.01	1.08
K-61-30	12.5	0.115	165	17.8	44.7	6.36	28.6	7.16	2.36	7.29	1.12
H-304	11.8	0.115	155	16.7	42.0	5.99	27.1	6.85	2.28	7.01	1.09
H-441	11.0	0.109	148	15.6	39.5	5.65	25.7	6.58	2.19	6.73	1.02
M-40	10.6	0.105	148	15.5	39.2	5.60	25.5	6.52	2.16	6.61	1.01
Aloi65-5a	10.0	0.097	140	14.6	37.0	5.33	24.3	6.26	2.09	6.33	0.97
HI68-02	8.2	0.082	117	12.4	31.3	4.51	20.6	5.32	1.78	5.38	0.83
N68-11	9.7	0.094	135	14.2	36.0	5.16	23.6	6.12	2.04	6.20	0.96
DAS69-3-2	9.1	0.088	127	13.5	34.1	4.88	22.4	5.84	1.93	5.87	0.91
DAS70-1213-41	8.2	0.080	116	12.2	31.2	4.52	20.8	5.49	1.85	5.69	0.89
DAS71-1213-1348.1	0.081	113	12.0	30.6	4.47	20.6	5.42	1.86	5.77	0.91	
S1971SW-2	9.1	0.088	128	13.3	34.0	4.91	22.5	5.78	1.97	6.01	0.92
MU472-32	8.5	0.082	120	12.6	32.1	4.64	21.3	5.47	1.89	5.85	0.90
MU473-108	7.6	0.077	107	11.3	28.8	4.17	19.3	5.06	1.75	5.44	0.84
MU474-163	7.1	0.070	100	10.5	26.9	3.90	18.2	4.78	1.65	5.13	0.80
KL-77-11	13.6	0.129	179	19.5	49.0	6.96	31.5	7.90	2.62	8.12	1.25
16-Nov-1979	7.8	0.074	109	11.6	29.5	4.27	19.9	5.21	1.78	5.54	0.86
In-house basaltic reference material (Kīlauea volcano)											
Kil93 avg.	7.0	0.072	102	11.0	28.5	4.20	19.7	5.28	1.81	5.69	0.89
±2σ	0.4	0.004	1.4	0.2	0.6	0.08	0.45	0.19	0.05	0.13	0.03

Table 3.2 (Continued)

Sample	Th	Y	Nb	Hf	U	Pb	Dy	Ho	Er	Yb	Lu
1790S-2F	1.36	33.5	19.7	5.34	0.441	1.32	7.01	1.35	3.27	2.76	0.382
1790S-4S	0.87	24.2	13.4	3.69	0.286	0.86	5.06	0.98	2.40	1.99	0.279
1790S-6F	1.47	34.7	21.1	5.76	0.476	1.38	7.14	1.39	3.32	2.77	0.388
1823SW-F	0.91	25.8	13.9	3.95	0.311	0.94	5.35	1.04	2.46	2.06	0.294
FT89-10	1.25	33.0	18.7	5.26	0.407	1.31	6.83	1.33	3.17	2.64	0.371
1868SW	1.00	27.3	15.2	4.16	0.332	0.97	5.68	1.10	2.63	2.19	0.310
MI-07-02	1.29	25.8	19.4	4.43	0.432	1.10	5.48	1.05	2.51	2.02	0.286
8	1.21	24.4	18.1	4.15	0.406	1.06	5.21	1.00	2.36	1.93	0.269
2E	1.86	39.9	27.4	6.72	0.611	1.66	8.11	1.56	3.76	3.15	0.447
10Z	1.66	33.2	24.7	5.62	0.529	1.44	6.80	1.30	3.15	2.58	0.372
19-Feb-1960	1.45	28.6	21.6	4.92	0.469	1.26	5.93	1.14	2.74	2.27	0.319
K-61-30	1.47	29.8	21.8	4.98	0.472	1.29	6.13	1.18	2.83	2.32	0.328
H-304	1.38	28.8	20.1	4.77	0.447	1.24	5.93	1.12	2.72	2.23	0.317
H-441	1.28	27.4	18.5	4.54	0.416	1.18	5.66	1.07	2.58	2.12	0.299
M-40	1.28	26.3	18.2	4.52	0.412	1.17	5.61	1.07	2.55	2.11	0.302
Aloi65-5a	1.21	25.3	16.6	4.31	0.375	1.13	5.46	1.04	2.47	2.03	0.293
HI68-02	1.01	21.6	14.4	3.66	0.321	0.96	4.62	0.89	2.10	1.75	0.250
HI68-11	1.16	25.1	17.4	4.24	0.362	1.22	5.33	1.02	2.43	2.02	0.286
DAS69-3-2	1.10	23.7	15.7	3.99	0.351	1.12	5.06	0.97	2.31	1.91	0.270
DAS70-1213-41	1.00	23.8	14.4	3.75	0.311	0.97	5.01	0.97	2.31	1.94	0.271
DAS71-1213-1340.95	24.9	14.2	3.74	0.305	0.96	5.15	1.00	2.42	2.04	0.285	
S1971SW-2	1.09	24.5	15.7	4.00	0.347	1.03	5.12	1.00	2.39	1.97	0.276
MU472-32	1.03	24.0	14.8	3.82	0.320	0.99	5.05	0.98	2.37	1.95	0.273
MU473-108	0.91	22.8	13.3	3.53	0.282	0.89	4.77	0.92	2.25	1.87	0.261
MU474-163	0.84	21.9	12.4	3.28	0.269	0.84	4.54	0.88	2.15	1.79	0.251
KL-77-11	1.61	33.2	23.4	5.63	0.508	1.46	6.89	1.32	3.18	2.64	0.369
16-Nov-1979	0.94	23.7	13.6	3.61	0.293	1.02	4.84	0.93	2.30	1.94	0.278
In-house basaltic reference material (Kīlauea volcano)											
Kil93 avg.	0.86	23.7	12.7	3.64	0.278	0.91	5.02	0.98	2.37	1.99	0.279
$\pm 2\sigma$	0.03	0.8	0.5	0.03	0.006	0.06	0.07	0.01	0.03	0.03	0.007

Table 3.2 (Continued)

Sample	Zr	Sr	Sc	V	Cr	Co	Ni	Cu	Zn	Ga
1790S-2F	—	368	31.0	352	35	46.5	70	150	138	24.2
1790S-4S	147	341	31.3	273	332	44.1	120	97	104	20.5
1790S-6F	—	378	29.8	318	75	41.7	81	129	124	23.4
1823SW-F	160	350	33.1	283	350	45.1	102	127	107	20.8
FT89-10	—	375	32.2	347	58	45.7	73	134	128	23.5
1868SW	166	351	32.6	283	363	43.9	139	143	109	21.1
MI-07-02	180	413	33.9	308	378	46.5	116	143	112	21.9
8	168	401	34.0	298	454	52.9	206	140	112	21.5
2E	—	409	30.9	371	72	44.7	81	137	140	25.4
10Z	—	427	31.1	337	118	46.2	103	143	129	24.4
19-Feb-1960	—	402	31.4	311	376	47.1	171	49	113	22.4
K-61-30	—	418	32.0	321	278	48.3	152	135	122	23.4
H-304	—	405	32.2	314	315	48.3	136	128	120	22.7
H-441	189	415	32.4	305	290	49.8	135	137	120	22.6
M-40	184	398	31.7	287	273	45.4	127	124	111	21.0
Aloi65-5a	175	393	32.6	281	321	45.9	120	121	106	20.4
HI68-02	147	336	29.6	247	600	62.3	375	115	109	17.8
HI68-11	171	383	32.2	297	3282	70.9	1680	140	149	21.1
DAS69-3-2	160	365	31.5	271	466	53.6	215	123	111	19.8
DAS70-1213-41	150	340	31.8	268	397	54.4	208	122	107	19.4
DAS71-1213-134	150	345	32.8	279	367	48.7	134	128	108	20.5
S1971SW-2	163	373	32.8	281	340	48.0	127	121	108	20.4
MU472-32	154	350	31.7	270	503	52.4	196	120	109	19.8
MU473-108	141	321	30.3	250	475	55.5	251	114	102	18.1
MU474-163	132	306	29.7	244	517	64.8	439	113	106	17.8
KL-77-11	—	420	30.3	334	86	43.8	81	139	127	24.3
16-Nov-1979	145	331	31.2	254	444	51.1	196	117	103	18.9
In-house basaltic reference material (Kīlauea volcano)										
Kil93 avg.	138	314	30.7	260	394	50.4	151	120	102	18.7
±2σ	11	17	2.1	6	51	2.8	9	6	5	0.6

Table 3.3 Pb, Sr, and Nd isotopic data for Kīlauea rift lavas. Lead isotope ratios were corrected for instrumental mass fractionation using the measured isotope ratio of Tl (SRM 997) added to the sample compared to an assumed $^{205}\text{Tl}/^{203}\text{Tl}=2.3889$ for this standard from Thirlwall (2002). The average Tl-corrected value for NBS981 Pb (n=14) was $^{206}\text{Pb}/^{204}\text{Pb}=16.9405\pm 15$ (2σ), $^{207}\text{Pb}/^{204}\text{Pb}=15.4963\pm 15$ (2σ), and $^{208}\text{Pb}/^{204}\text{Pb}=36.7219\pm 44$ (2σ). All of the Pb isotopic data are reported relative to the NBS 981 Pb standard values of Galer & Abouchami (1998): $^{206}\text{Pb}/^{204}\text{Pb}=16.9405$, $^{207}\text{Pb}/^{204}\text{Pb}=15.4963$, and $^{208}\text{Pb}/^{204}\text{Pb}=36.7219$. Sr and Nd isotope ratios were corrected for instrumental mass fractionation relative to $^{86}\text{Sr}/^{88}\text{Sr}=0.1194$ and $^{146}\text{Nd}/^{144}\text{Nd}=0.7219$, respectively. The average measured values for Sr and Nd standards were $^{87}\text{Sr}/^{86}\text{Sr}=0.710245\pm 14$ (2σ ; n=80) for SRM987 (by TIMS) and $^{143}\text{Nd}/^{144}\text{Nd}=0.512117\pm 8$ (2σ ; n=56) for Ames Nd (by MC-ICP-MS). All Sr and Nd isotopic data are reported relative to constant standard values for SRM987 ($^{87}\text{Sr}/^{86}\text{Sr}=0.710250$) and Ames Nd ($^{143}\text{Nd}/^{144}\text{Nd}=0.512130$). After correcting to this value for Ames Nd, multiple analyses of the La Jolla Nd standard ran as an unknown averaged $^{143}\text{Nd}/^{144}\text{Nd}=0.511842\pm 7$ (2σ ; n=11). The average of multiple analyses of the Kil1919 reference material for Pb (n=23), Sr (n=26), and Nd (n=15) isotopic ratios and the Menehune reference material for Pb (n=15), Sr (n=26) and Nd (n=11) isotopic ratios are given. The uncertainties on the Kil1919 and Menehune Pb, Sr, and Nd isotopic ratios are the $\pm 2\sigma_m$ errors of the replicate analyses. Total procedural blanks were negligible compared to the concentrations of Pb, Sr, and Nd in the samples. Eruption year for the samples are presented in Table 3.1.

Sample	$^{206}\text{Pb}/^{204}\text{Pb}$	$^{207}\text{Pb}/^{204}\text{Pb}$	$^{208}\text{Pb}/^{204}\text{Pb}$	$^{87}\text{Sr}/^{86}\text{Sr}$	$^{143}\text{Nd}/^{144}\text{Nd}$
1790S-2F	18.4415	15.4732	38.0841	0.703591	0.512958
1790S-4S	18.4847	15.4779	38.1194	0.703599	0.512962
1790S-6F	18.4570	15.4751	38.0919	0.703592	0.512960
1823SW-F	18.4478	15.4762	38.0785	0.703612	0.512956
FT89-10	18.4317	15.4735	38.0822	0.703607	0.512954
1868SW	18.4818	15.4761	38.0986	0.703571	0.512959
MI-07-02	18.6506	15.4856	38.2056	0.703469	0.512974
8	18.6493	15.4857	38.2033	0.703470	0.512973
2E	18.5072	15.4775	38.1348	0.703575	0.512958
10Z	18.5429	15.4804	38.1707	0.703566	0.512949
19-Feb-1960	18.5590	15.4825	38.1853	0.703574	0.512954
K-61-30	18.5493	15.4808	38.1726	0.703572	0.512954
H-304	18.5433	15.4800	38.1659	0.703578	0.512953
H-441	18.5380	15.4801	38.1616	0.703581	0.512960
M-40	18.5304	15.4794	38.1568	0.703578	0.512954
Aloi65-5a	18.5087	15.4777	38.1379	0.703580	0.512956
HI68-02	18.5205	15.4789	38.1469	0.703566	0.512955
N68-14	18.5112	15.4785	38.1411	0.703575	0.512956
DAS69-3-2	18.5154	15.4782	38.1418	0.703566	0.512958
DAS70-1213-41	18.5002	15.4775	38.1294	0.703555	0.512957
DAS71-1213-134	18.4874	15.4771	38.1200	0.703544	0.512960
S1971SW-2	18.5075	15.4784	38.1383	0.703569	0.512959
MU472-32	18.4984	15.4776	38.1312	0.703563	0.512959
MU473-108	18.4711	15.4750	38.1075	0.703552	0.512960
MU474-163	18.4704	15.4766	38.1112	0.703552	0.512959
KL-77-11	18.5263	15.4791	38.1528	0.703570	0.512957
16-Nov-1979	18.4705	15.4752	38.1072	0.703548	0.512960
In-house basaltic reference material (Kīlauea volcano)					
Kil1919	18.6556 \pm 9	15.4899 \pm 6	38.2076 \pm 14	0.703471 \pm 3	0.512973 \pm 3
Menehune	18.4073 \pm 5	15.4714 \pm 5	38.0625 \pm 15	0.703617 \pm 3	0.512950 \pm 2

the Kīlauea lava samples were crushed between tungsten carbide plates, washed repeatedly in an ultrasonic bath of deionized water for 2-3 minutes, hand picked (~40 g) to remove any chips with signs of alteration, and powdered in a tungsten carbide swing mill for the XRF analyses or an agate mill for the ICP-MS analyses.

The same 27 samples analyzed for trace elements by ICP-MS were analyzed for Pb, Sr, and Nd isotopic ratios (Table 3.3) at San Diego State University (SDSU) using the chemical and mass spectrometric procedures and analytical methods described in Marske et al. (2007). Isotopic ratios of Pb and Nd were measured with a Nu Plasma 1700 multi-collector inductively coupled plasma mass spectrometer (MC-ICP-MS), whereas Sr isotopic ratios were measured using a VG Sector 54 thermal ionization mass spectrometer (TIMS) at SDSU (Table 3.3). All literature isotopic data shown on the figures and discussed in the text have been corrected relative to the isotopic standards listed in Table 3.3.

3.3.3 Sampling

The historical Kīlauea lavas presented in this study were sampled along the SWRZ (n=11) and ERZ (n=37). We collected from exposed surface flows along the two rift zones (sample locations are presented in Table A.3). Additional samples were obtained from the collections of the Smithsonian Institution and the University of Hawai‘i for some eruptions whose products are now covered by younger lava flows. A list of referenced Kīlauea rift samples obtained from the Smithsonian Institution is presented in Table A.4. Samples with known eruption dates are labeled with the date they were erupted (e.g., 22-Aug-1968). Samples with previous field numbers (e.g., MU472-32) are also given (Table 1). At least one sample from each historic SWRZ and ERZ eruption was analyzed (excluding May 1922 and August 1963, which are covered by more recent flows). Multiple samples were analyzed for the prolonged rift eruptions in 1790 (n=9), 1840 (n=3), 1919-20 Mauna Iki (n=8), 1955 (n=5), October 1968 (n=2), and 1969-74 Mauna Ulu (n=6)

eruptions (Table 3.1). Temporal control is known for these eruptions excluding 1790. The 1790 lavas were sampled along two parallel fissures that are separated by 1-2 km. Two vent lavas from the north fissure (e.g., 1790N) were sampled 5 km apart, six lavas from vents along the south fissure (e.g., 1790S) were sampled along a 6 km section, and a lava flow (1790S-6F) originating from the southern fissure was collected near the coast (Fig. 3.1). The 8 lavas from the 1919-20 SWRZ eruption are linked to a temporal history for this eruption (Table A.5) as described by Rowland and Munro (1993).

3.3.4 Whole-rock geochemistry

Historical Kīlauea rift lavas display a slightly wider range in MgO contents (5.3-18.4 wt. %) compared to historical summit lavas (6.0-17.8 wt. %; Garcia et al., 2003). The most evolved (<6.0 wt. % MgO) lavas erupted along the middle (1977, 1983, and 1997) and lower ERZ (1790 and 1955), whereas the more mafic lavas (>10 wt. % MgO) have erupted along the entire ERZ (1840, 1968, 1969-74, and 1979; Fig. 3.1). Historical SWRZ eruptions are less frequent and produced lavas with a relatively restricted range in MgO contents (6.9-8.4 wt. %; Table 3.1). Most historical rift lavas are compositionally similar to historical summit lavas (Fig. 3.4). At a given MgO content, the Al₂O₃, K₂O, TiO₂, Fe₂O₃* (i.e., total iron), and SiO₂ abundances in historical rift lavas (excluding the 1790 flows and lavas with <6.0 wt. % MgO) overlap with the field of historical summit lavas (Fig. 3.4). The 1790 rift lavas have relatively high SiO₂ and Al₂O₃, and low K₂O, TiO₂ and Fe₂O₃ abundances (at a given MgO) that expand the compositional range for historical Kīlauea lavas. Incompatible major elements (e.g., K₂O) in historical rift and summit lavas generally form curved trends when plotted against MgO (Fig. 3.4). Kīlauea rift and summit lavas display a linear increase of CaO and Al₂O₃ abundances with decreasing MgO contents to ~7.2 and ~6.8 wt. %, respectively, where there is a kink in the trends (Fig. 3.4). There are small, but significant short-term variations (years to decades) in major element

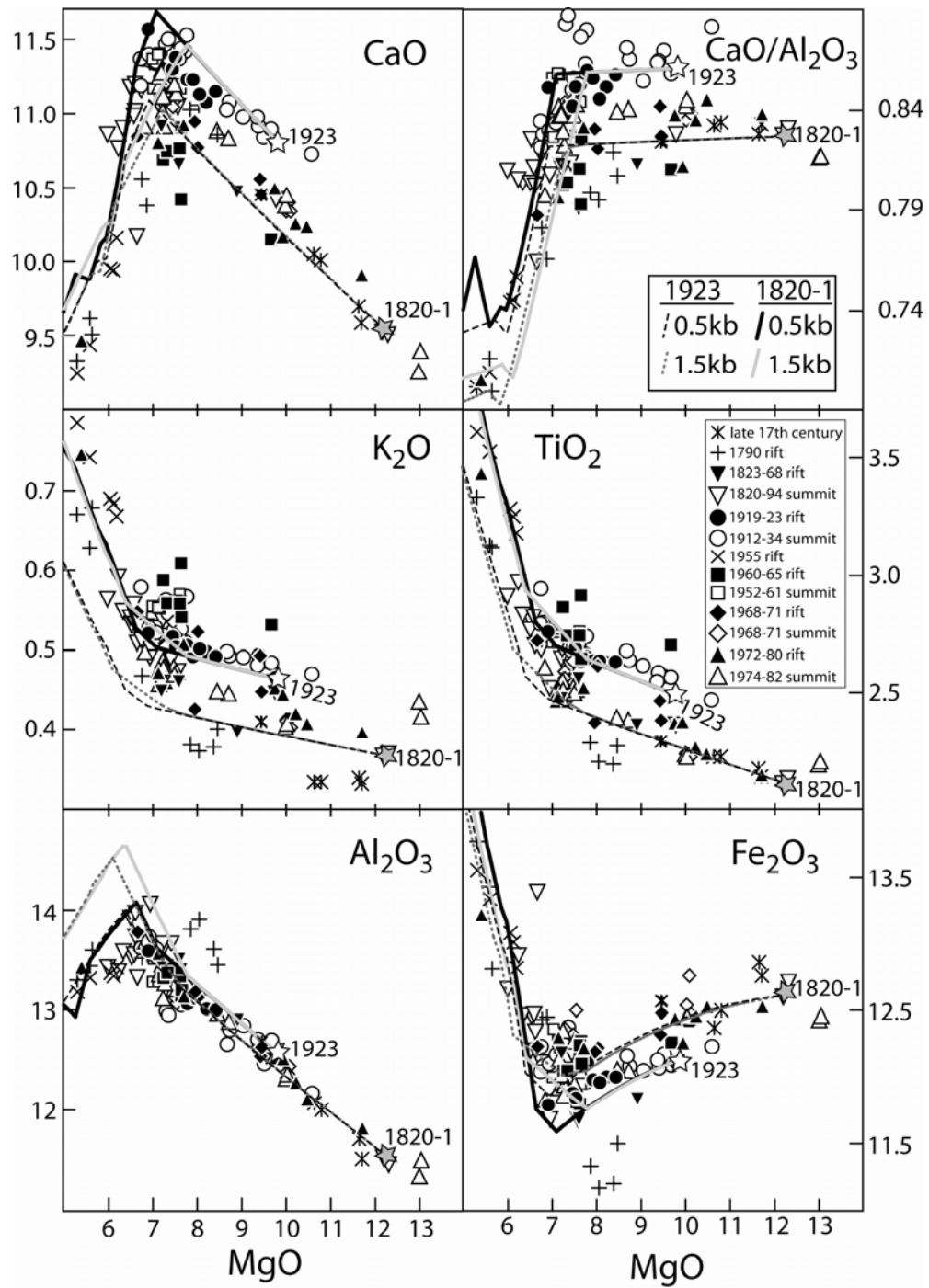


Fig. 3.4 Whole-rock MgO variation diagrams for historical Kīlauea rift and summit lavas. The Kīlauea lavas are grouped according to eruption date (see inset for symbols). (a.) The dashed and solid lines are the liquid lines of descent determined from MELTS modeling (see text for details). The LLD were calculated from two potential parent magmas (1820-1 and 25-Aug-1923) at 0.5 and 1.5 kbars. (b.) The gray field highlights the linear mixing trends oblique to the LLD (discussed in the text). Arrows illustrate the general crystallization paths for olivine, clinopyroxene (cpx), and plagioclase (plag) based on the calculated LLD. Three rift samples (22-Aug-1968, FT89-21, and FT89-22) are not plotted because they have >14 wt. % MgO. Summit data is from Garcia et al. (2003). All values are in wt. % (except CaO/Al₂O₃).

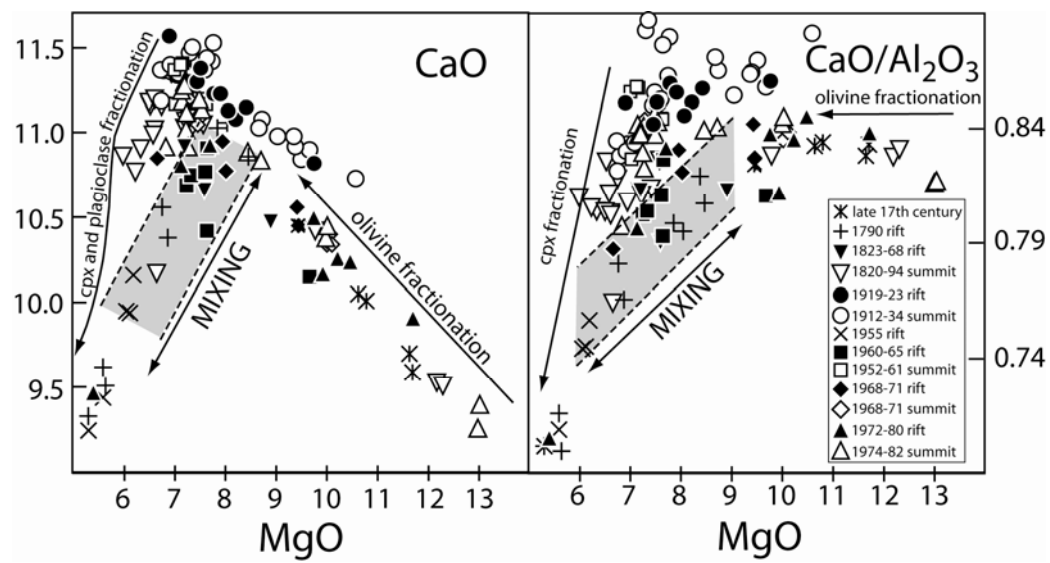


Fig. 3.4 (Continued)

abundances in these lavas (Fig. 3.4). For example, 1790-1868 lavas and 1919-23 lavas show considerable differences in SiO₂, CaO, and K₂O (at a given MgO) that cannot be explained by crystal fractionation of the observed minerals in these lavas. These variations were previously observed for historical summit lavas and were attributed to compositionally distinct mantle-derived parental magmas (e.g., Wright, 1971; Garcia et al., 2003).

Historical rift lavas display a relatively wide range of incompatible trace element abundances (e.g., Nb or Rb) that generally overlap with historical Kīlauea summit lavas (Fig. 3.5). Overall, the compositional fields of historical rift and summit lavas overlap in ratios of highly to moderately incompatible trace elements (e.g., La/Yb, Nb/Y, and Ba/Sm) and Pb and Sr isotopic ratios (Figs. 3.5 and 3.6). Kīlauea lavas lie along two distinct arrays in ²⁰⁶Pb/²⁰⁴Pb vs. ²⁰⁸Pb/²⁰⁴Pb and ⁸⁷Sr/⁸⁶Sr space (Fig. 3.6). The 1820-1923 rift and summit lavas form a linear trend defined by lower ²⁰⁸Pb/²⁰⁴Pb (for a given ²⁰⁶Pb/²⁰⁴Pb), whereas lavas erupted after the 1924 explosive summit eruption form a trend characterized by higher ²⁰⁸Pb/²⁰⁴Pb (at a given ²⁰⁶Pb/²⁰⁴Pb). These trends intersect close to the 1820-23 summit sample. The ²⁰⁶Pb/²⁰⁴Pb and ⁸⁷Sr/⁸⁶Sr ratios in 1820-1923 Kīlauea lavas make an inversely correlated trend, whereas 1955-82 lavas show a positive trend (Fig. 3.6). Overall, the compositional fields of Kīlauea rift and summit lavas generally overlap. However, there are multiple rift eruptions (i.e., 1868, 1955, 1960, 1968, 1971, 1974, and 1977) that are geochemically and isotopically distinct compared to summit lavas that erupted during similar time intervals (Figs. 3.5 and 3.6). These differences and their implications for magmatic processes are described below.

3.3.5 Temporal and spatial compositional variations

Historical Kīlauea rift and summit lavas display systematic temporal variations in ratios of highly to moderately incompatible elements (e.g., Nb/Y and K₂O/TiO₂), and ²⁰⁶Pb/²⁰⁴Pb ratios (Fig. 3.3).

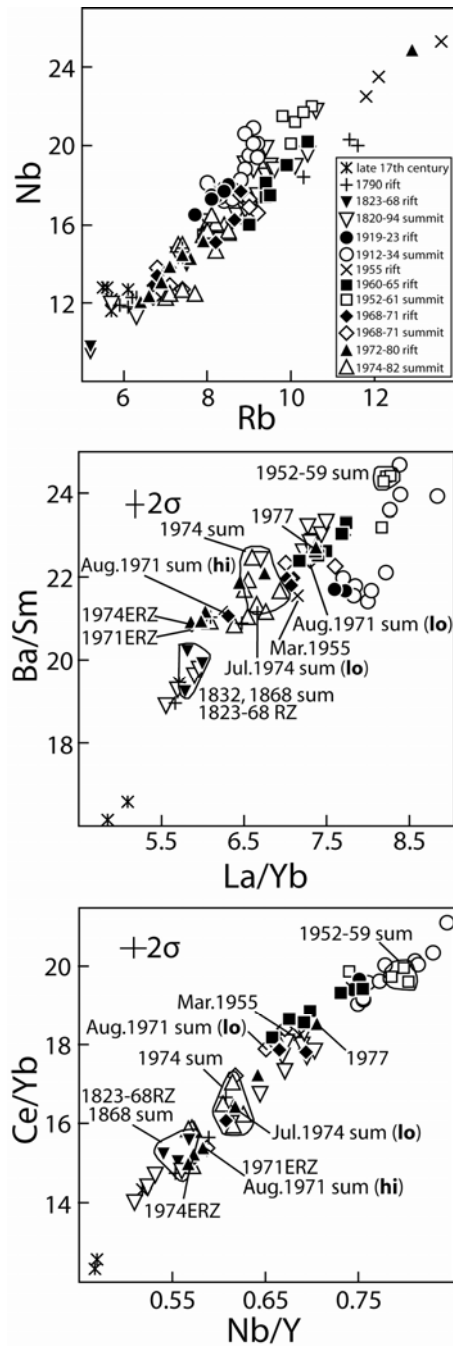


Fig. 3.5 Trace element geochemical variations for historical Kīlauea rift (RZ or ERZ) and summit (sum) lavas. The ‘hi’ and ‘lo’ labels refer to the higher and lower MgO August 1971 and July 1974 summit lavas discussed in the text. Kīlauea summit ICP-MS trace element data from Pietruszka and Garcia (1999a) were corrected by normalizing the average Kil1919 reference sample (n=11) used for summit lavas to the BHVO-2 standard values for this study (Kil1919 and BHVO-2 come from the same lava flow). Estimates for the analytical precision of the summit lavas analyzed by ICP-MS can be found in Pietruszka and Garcia (1999a). The 2σ error bars are shown in the corner of each plot unless they are smaller than the size of the symbols. The values are in ppm except for the ratios.

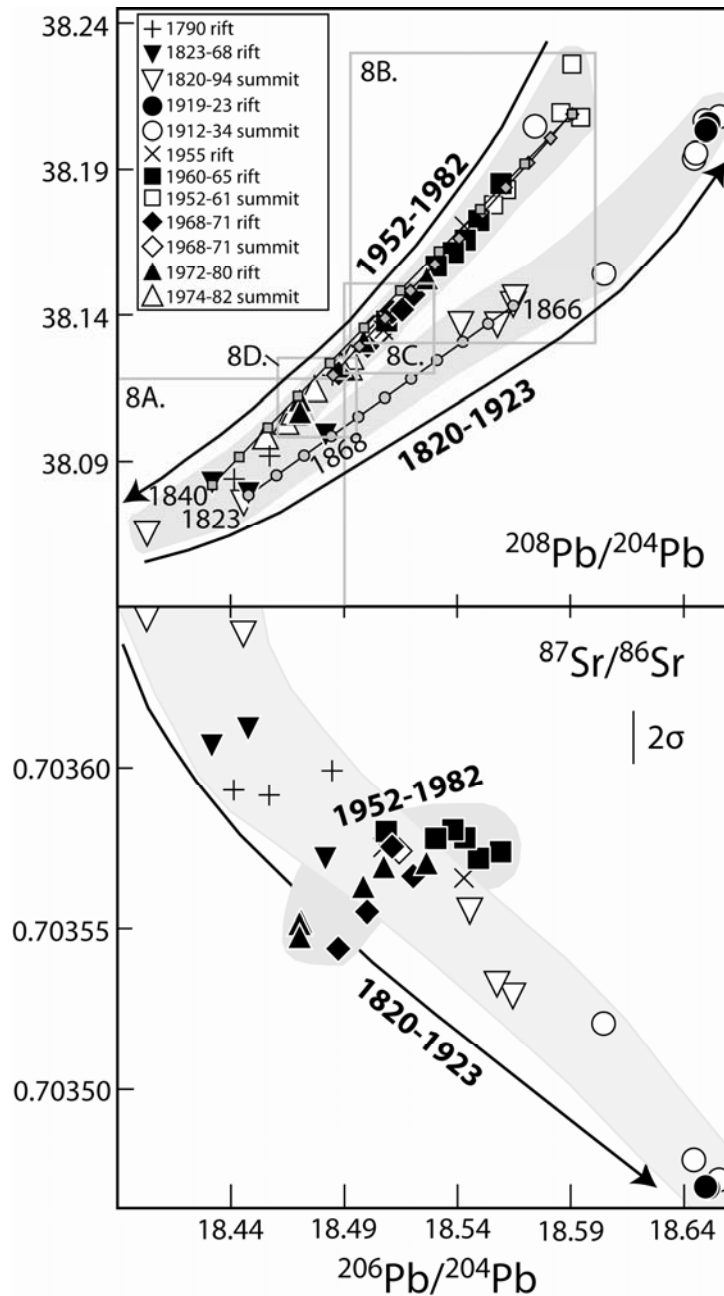


Fig. 3.6 Plots of $^{206}\text{Pb}/^{204}\text{Pb}$ vs. $^{208}\text{Pb}/^{204}\text{Pb}$ and $^{87}\text{Sr}/^{86}\text{Sr}$ ratios for historical Kīlauea rift and summit lavas. Three mixing lines are shown between the 1823 SWRZ (1823SW-F; $^{206}\text{Pb}/^{204}\text{Pb}=18.448$, $^{208}\text{Pb}/^{204}\text{Pb}=38.079$) and 1866 summit ($^{206}\text{Pb}/^{204}\text{Pb}=18.564$, $^{208}\text{Pb}/^{204}\text{Pb}=38.143$) lavas (line with gray circles), the 1840 ERZ (FT89-10, $^{206}\text{Pb}/^{204}\text{Pb}=18.432$, $^{208}\text{Pb}/^{204}\text{Pb}=38.082$) and 1959 Kīlauea Iki ($^{206}\text{Pb}/^{204}\text{Pb}=18.590$, $^{208}\text{Pb}/^{204}\text{Pb}=38.209$) lavas (line with gray squares), and the 1790 ERZ (1790S-4S; $^{206}\text{Pb}/^{204}\text{Pb}=18.485$, $^{208}\text{Pb}/^{204}\text{Pb}=38.119$) and 1959 Kīlauea Iki ($^{206}\text{Pb}/^{204}\text{Pb}=18.590$, $^{208}\text{Pb}/^{204}\text{Pb}=38.209$) lavas (lines with gray diamonds). The 1959 Kīlauea Iki end members are an average of two analyses from this eruption [IKI-58 (S-1) and IKI-01 (S-2)]. The Pb abundances assumed for the mixing model are 1 ppm (1866 and 1959 lavas), and 1.3 and 0.9 ppm for the 1840 and 1790 lavas, respectively (Table 3.2). Mixing results are plotted in 10% increments. Panels (8a., 8b., 8c., and 8d.) are shown in Fig. 3.8. The 2σ error bars are shown unless they are smaller than the size of the symbol.

From 1790 to 1923, rift and summit lavas show temporal trends characterized by overall increases in these ratios. The slopes of these variations reversed following the 1924 explosive summit eruptions. These reversed trends continued into the late 20th century (Fig. 3.3b). Overall, the rift temporal trends generally overlap with summit trends indicating that these lavas originated from a common parental magma(s) for a given time period. However, superimposed on the long-term historical trends are short-term compositional variations during individual rift eruptions and/or differences between contemporaneous summit and rift lavas in the 1868, 1955, 1960, 1968, 1969-74, and 1977 eruptions.

The 1868 SWRZ and summit lavas have significantly lower $^{206}\text{Pb}/^{204}\text{Pb}$, $^{87}\text{Sr}/^{86}\text{Sr}$, La/Yb, and Nb/Y ratios than the 1866 and 1877 summit lavas, and lie close to, or overlap with early 19th century Kīlauea lavas (Fig. 3.3a). The evolved 1955 ERZ lavas (Table 3.1) lie off the main 20th century geochemical trends (Fig. 3.3b). The early March and late May 1955 lavas have significantly lower $^{206}\text{Pb}/^{204}\text{Pb}$ and Nb/Y ratios compared to 1952-59 summit lavas (Fig. 3.3b), although the late May 1955 lava is less distinct. The late May 1955 lava has higher Nb/Y and $^{206}\text{Pb}/^{204}\text{Pb}$ values, and lower $^{87}\text{Sr}/^{86}\text{Sr}$ ratios that are closer in composition to 1952-59 summit lavas (Figs. 3.3b, 3.6, and 3.8b). The 1960 ERZ lava has significantly lower $^{206}\text{Pb}/^{204}\text{Pb}$ and Nb/Y compared to the 1959 Kīlauea Iki lavas that erupted ~12 weeks prior (Fig. 3.3b). The August 1968 ERZ picritic lava (14.2 wt. % MgO) has higher $^{206}\text{Pb}/^{204}\text{Pb}$, and lower Nb/Y and La/Yb ratios compared to the February and July 1968 summit lavas (7.5 wt. % MgO; Pietruszka and Garcia, 1999a).

The 1969-74 Mauna Ulu lavas are compositionally distinct from some summit and SWRZ lavas that erupted contemporaneously in August and September 1971, and July 1974 (Figs. 3.2 and 3.7). The two main phases of the Mauna Ulu eruption produced mostly mafic lavas (7-18 wt. % MgO; Wright et al., 1975; Hofmann et al., 1984) that record systematic temporal decreases in $\text{K}_2\text{O}/\text{TiO}_2$, Nb/Y, and $^{206}\text{Pb}/^{204}\text{Pb}$ ratios from 1969 to 1971 and 1972 to 1974 (Fig.

3.7). The temporal geochemical decreases during the two phases are more rapid than the late 20th century summit variations (Fig. 3.7). For example, the rate of decrease in ²⁰⁶Pb/²⁰⁴Pb ratios during the 1969-71 (0.015 year⁻¹) and 1972-74 (0.014 year⁻¹) intervals is 3-4 times greater than observed for 1952-82 summit lavas (0.004 year⁻¹), based on a linear regression of the data. The Mauna Ulu eruption was punctuated by contemporaneous, compositionally variable (6.9-11.5 wt. % MgO, Duffield et al., 1982; Lockwood et al., 1999; Garcia et al., 2003) summit eruptions in August (10 hours) and September (2 days) 1971, and July 1974 (3 days), and a SWRZ eruption in September 1971 (5 days; Fig. 3.2). During the August 1971 and July 1974 eruptions, higher MgO lavas (10.0-11.5 wt. %) erupted from fissures on the southeast caldera rim (Fig. 3.1), whereas lower MgO lavas (6.7-7.6 wt. %) issued from fissures on the caldera floor (Duffield et al., 1982; Lockwood et al., 1999; Garcia et al., 2003). Lower MgO lavas were also erupted in July 1974 along a 1.5 km-long fissure system located just south and east of Keanakakoi crater (Lockwood et al., 1999; Fig. 3.1).

The sharp drop in MgO contents during the August 1971 and July 1974 summit eruptions coincides with higher K₂O/TiO₂, Nb/Y, and ²⁰⁶Pb/²⁰⁴Pb ratios in the lavas (Fig. 3.7). The MgO-rich August 1971 caldera rim lavas have relatively low K₂O/TiO₂, Nb/Y, and ²⁰⁶Pb/²⁰⁴Pb ratios that are similar to the April 1971 Mauna Ulu lava (Figs. 3.5, 3.6, and 3.7). In contrast, these ratios are significantly higher in the lower MgO August 1971 caldera floor lavas, and are similar to 1968 summit lavas (Figs. 3.5, 3.6, and 3.7). A similar pattern is observed for the July 1974 summit eruption. The higher MgO July 1974 caldera rim lavas (10.0-11.5 wt. %) have K₂O/TiO₂, Nb/Y, and ²⁰⁶Pb/²⁰⁴Pb ratios that are similar to, or lower than the April 1974 Mauna Ulu lava (Figs. 3.6 and 3.7). In contrast, the lower MgO July 1974 summit lavas are geochemically similar to the higher MgO August 1971 caldera rim lavas (Fig. 3.7).

The September 1974 summit eruption yielded moderately evolved lavas (7.2-7.5 wt. % MgO, Duffield et al., 1982; Lockwood et al., 1999; Garcia et al., 2003) that are compositionally

similar to the July 1974 caldera floor lavas. In contrast, the 6-hour December 1974 eruption that occurred between the Koa'e fault system and the upper SWRZ (Fig. 3.1) produced mafic lavas (12.2-15.7 wt. % MgO, Lockwood et al., 1999; Garcia et al., 2003) with variable Pb isotopic compositions (D. Heaton, pers. comm., 2010), with respect to the analytical error ($\pm 2\sigma=0.0015$). Lavas erupted at 04:30 a.m. ($^{206}\text{Pb}/^{204}\text{Pb}=18.477$) and 06:40 a.m. ($^{206}\text{Pb}/^{204}\text{Pb}=18.471$) local time have lower Pb isotopic ratios than the July 1974, September 1974, and November 1975 summit lavas (Figs. 3.7 and 3.8d). The 06:40 a.m. lava displays Pb isotopic ratios that are identical to 1973-74 Mauna Ulu lavas (Fig. 3.8d). The evolved 1977 ERZ lava (5.4 wt. % MgO) has significantly higher $^{206}\text{Pb}/^{204}\text{Pb}$, La/Yb, and Nb/Y ratios than the 1975 and 1982 summit and 1979 and 1980 ERZ lavas.

3.4 Discussion

3.4.1 Magma mixing vs. crystal fractionation in rift zone magmas

Magma mixing is an important process in historical Kīlauea rift and summit magmas (Wright and Fiske, 1971; Trusdell, 1991; Helz and Wright, 1992; Garcia et al., 2003). It is thought to be partly responsible for the progressive compositional variation of Kīlauea lavas (Wright and Fiske, 1971; Tilling and Dvorak, 1993; Garcia et al., 2003). New mantle-derived magma is almost continuously delivered to the summit reservoir where it is thought to mix relatively rapidly (<10 years) before erupting (Pietruszka and Garcia, 1999a; Garcia et al., 2003). This interpretation is based on the systematic short-term changes in ratios of incompatible elements and Pb, Sr, and Nd isotopic ratios of summit lavas (Fig. 3.3). In contrast, rift magmas are thought to represent hybrids of compositionally distinct magma 'batches' that intruded from the summit reservoir, or magmas that bypassed the summit reservoir entirely (Wright and Fiske, 1971; Wright et al., 1975; Jackson et al., 1975; Ryan et al., 1981; Duffield et al., 1982). Previous mineral chemistry studies identified clear evidence for magma mixing (i.e., resorbed and/or reversely zone crystals of

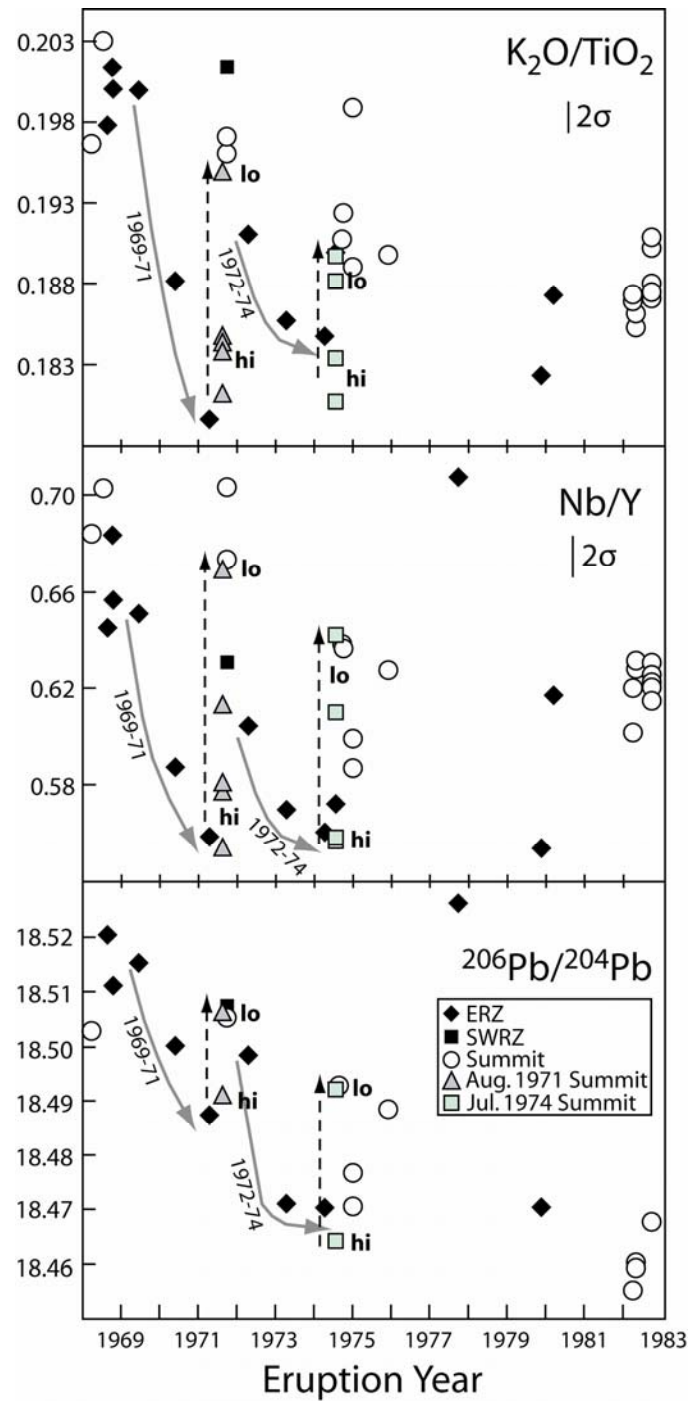


Fig. 3.7 Temporal geochemical variations for Kīlauea rift and summit lavas between 1968 and 1983. The Nb/Y values are XRF data. The solid arrows show the systematic temporal geochemical decreases observed during the two phases of the Mauna Ulu eruption (1969-71 and 1972-74). The dashed arrows depict the rapid geochemical changes during the short-lived August 1971 (triangles) and July 1974 (light squares) caldera rim and floor eruptions. The 'hi' label reflects the higher MgO caldera rim lavas, whereas the 'lo' refers to the lower MgO caldera floor lavas. Historical summit data sources: Pietruszka and Garcia (1999a) and Garcia et al. (2003). The 2σ error bars are presented unless they are smaller than the size of the symbols.

olivine, clinopyroxene, and plagioclase) in the 1840, 1955, and 1960 ERZ lavas, and 1983 and 1997 Pu‘u ‘Ō‘ō lavas (Trusdell, 1991; Helz and Wright, 1992; Wright and Helz, 1996; Garcia et al., 1989; Thornber et al., 2003). These eruptions (excluding 1997 Pu‘u ‘Ō‘ō) generally began with extrusion of stored, evolved and/or hybrid magmas followed later by more mafic compositions. This eruptive pattern is attributed to the intrusion of higher MgO summit-derived magma that enters the rift zone and mixes with stored magma before or during the eruption (e.g., Wright and Fiske, 1971; Wright and Helz, 1996; Garcia et al., 1992).

The effects of crystal fractionation are superimposed on the compositions produced by magma mixing (Fig. 3.4). The importance of olivine crystallization and accumulation in historical rift lavas is evident from their wide range of MgO contents (5.3-18.7 wt. %; Wright and Fiske, 1971; Wright et al., 1975; Moore et al., 1980). Moreover, the compositional variation in unmixed rift lavas with >7.2 wt. % MgO (e.g., Pu‘u ‘Ō‘ō ERZ lavas, Garcia et al., 2000; Marske et al., 2008) is primarily related to olivine fractionation and/or accumulation (i.e., olivine control, Powers, 1955; Wright, 1971). The kinked and curved major element trends in rift lavas (Fig. 3.4) also suggest that crystal fractionation is an important process in controlling their major element compositional variations (e.g., Wright and Fiske, 1971; Garcia et al., 1996).

MELTS modeling (using Adibat_1ph version; Ghiorso and Sack, 1995; Smith and Asimov, 2005) was undertaken to calculate liquid lines of descent (LLD) for the observed rift and summit compositional trends (Fig. 3.4). Two potential parental magma compositions (historical Kīlauea samples, 25-Aug-1923; Table 3.1 and 1820-1; Garcia et al., 2003) were used as endmembers because they have high MgO contents and span most of the range of observed summit and rift zone lava compositions (Fig. 3.4). Sample 25-Aug-1923 was chosen because it lies along the trend of early 20th century summit and SWRZ lavas. Sample 1820-1 was selected because it lies along early 19th and late 20th century rift and summit trends. The modeling conditions were fractional crystallization, an oxygen fugacity of QFM-1 (one log unit below the

quartz-fayalite-magnetite buffer), which is within the range of Rhodes and Vollinger (2005) and Roeder et al. (2003), and water contents of 0.20-0.33 wt. %, which lie within the ranges expected for Hawaiian magmas (Clague et al., 1995; Wallace and Anderson, 1998). The data were modeled over a range of pressures (0.5-2 kbars, equivalent to ~1.5-6 km) that encompass the shallow (~2-5 km deep) magma storage reservoirs beneath the summit (e.g., Eaton and Murata, 1960; Fiske and Kinoshita, 1969; Yang et al., 1992; Tilling and Dvorak, 1993) and ERZ (Wolfe et al., 1987).

The calculated LLD generally parallel the major element abundances of the lavas suggesting these overall variations are related to crystal fractionation (Fig. 3.4). For example, the kinks in the Al_2O_3 (at ~6.8 wt. % MgO) and CaO (at ~7.2 wt. % MgO) trends mark the onset of plagioclase and clinopyroxene fractionation, respectively. The overall curved trends on plots of K_2O and TiO_2 vs. MgO (Fig. 3.4) also indicate that the compositional variations of the rift lavas are dominated by the effects of crystal fractionation because magma mixing would produce linear trends (e.g., Garcia et al., 2003). However, some rift lavas lie below the modeled LLD (on the MgO vs. CaO and $\text{CaO}/\text{Al}_2\text{O}_3$ plots) that likely reflect a magma mixing trend. For example, 1790, 1868, 1955, 1960, and 1961-68 ERZ lavas make linear trends that span evolved and mafic compositions (Fig. 3.4b). These variations can be explained by mixing of evolved rift-stored magma and a more mafic magma. The importance of magma mixing is further explored in the next section based on geochemical variations of individual summit and rift eruptions.

3.4.2 Magmatic plumbing network beneath Kīlauea volcano

Deciphering the short-term (hours to years) compositional differences between rift and summit lavas observed during individual eruptions or eruptive intervals are critical to our understanding of the magmatic interplay beneath Kīlauea's summit and rift zones. This section considers the origin of these differences over four time periods (1790-1923, 1955-68, 1969-74, and 1974-79),

and the implications they have for the shallow plumbing network and magma residence times beneath Kīlauea volcano.

3.4.2.1 1790-1923 eruptive interval

The MgO-variable 1790 lavas erupted from two parallel fissures along the lower ERZ separated by 1-2 km (Fig. 3.1). The six 1790 lavas sampled along a 6 km section of the south fissure (e.g., 1790S) show an overall downrift increase in MgO contents (5.3-8.5 wt. % MgO; Fig. 3.1). In contrast, the two lavas sampled from vents along the north fissure (e.g., 1790N) spaced 5 km apart show a decrease in MgO contents moving downrift (6.8 to 5.6 wt. %). Magma mixing is an important process for the 1790 lavas based on the linear trends in plots of MgO vs. CaO and CaO/Al₂O₃ (oblique to the LLD), in which these lavas span differentiated (~6 wt. % MgO) and more mafic (~8.5 wt. % MgO) compositions (Fig. 3.4b). Plagioclase accumulation in the relatively mafic 1790 lavas (7.9-8.5 wt. % MgO) may also be an important process based on the elevated Al₂O₃ contents (at a given MgO) and presence of plagioclase phenocrysts and microphenocrysts (~2-9 vol. %) in the lavas. The extent of plagioclase accumulation was estimated by the addition of plagioclase in 1% steps to match the major element abundances of the 1790 lavas. The composition of plagioclase used in the calculation is an average of multiple mineral core analyses from rift-stored 1997 Pu‘u ‘Ō‘ō lavas (Garcia et al., 2000). This mass-balance model indicates that the relatively high Al₂O₃ and low K₂O, TiO₂ and Fe₂O₃ abundances (at a given MgO) in 1790 lavas can be explained if they accumulated ~6-8 vol. % plagioclase, which is consistent with the observed modal abundances of this mineral.

The 1823 SWRZ and 1832 summit lavas (7.2-7.6 wt. % MgO, Wright, 1971; Garcia et al., 2003; Table 3.1) are geochemically and isotopically identical (Figs. 3.3a and 3.8a) suggesting that they fractionated from a common parental magma. This parental magma cannot be explained by mixing of compositions erupted shortly before (e.g., 1790, 1820-23) and/or after (1840-77)

because they lie outside of analytical error of the mixing lines (not shown). The failure of these mixing end-members indicates that the 1823 SWRZ and 1832 summit magmas represent an unmodified mantle-derived magma that was distinct from summit lavas erupted immediately before (1820-23) and after (1866). This also suggests the parental magma of the 1823 and 1832 lavas entered the SWRZ and/or summit reservoir during the time period between the eruption of the 1820-23 tephra and the 1823 rift eruption. The 9-year sampling gap between the compositionally identical 1823 SWRZ and 1832 summit eruptions suggests that the magma residing in the summit reservoir did not mix with new parental melts from the mantle during this time period. However, no Kīlauea samples erupted between 1823 and 1832 are available to verify this.

The 1840 ERZ eruption is characterized by mixing of differentiated, rift-stored magma and picrite magma that intruded the ERZ (5-19 wt. % MgO; Trusdell, 1991). The 1840 ERZ lava (FT89-10; 8.9 wt. % MgO) lies along the trend defined by higher $^{208}\text{Pb}/^{204}\text{Pb}$ (at a given $^{206}\text{Pb}/^{204}\text{Pb}$), whereas 19th century rift and summit lavas erupted before (1823 and 1832) and after (1866-77) lie along the lower Pb isotopic trend (Figs. 3.6 and 3.8a). This indicates that the 1840 lavas cannot be explained by variable mixing of any known 19th century lavas. However, the 1840 lava is isotopically similar to 1790 ERZ lavas and lavas from both eruptions lie along the same trend in $^{206}\text{Pb}/^{204}\text{Pb}$ vs. $^{208}\text{Pb}/^{204}\text{Pb}$ space (Fig. 3.8a). These observations could suggest that rift-stored 1790 magma was a possible mixing component to create some of the hybrid 1840 lavas. For example, the 1840 ERZ lava lies within the error of mixing lines between 1790 ERZ and 900-1400 or 1820-1823 A.D. summit lavas (not shown). Thus it is possible that the 1840 ERZ lava could reflect a hybrid of rift-stored magmas and/or summit-derived magmas (Fig. 3.9a).

On April 2, 1868, a ~M7.9 earthquake apparently triggered a ~4 hour eruption at Kīlauea Iki crater (Brigham, 1909; Wyss and Koyanagi, 1992). The active summit lava lake began to drain shortly after the earthquake and emptied by April 5 (Brigham, 1909). Approximately two

days later, a short-lived eruption occurred along the SWRZ (Fig. 3.1). Despite erupting ~17 km apart, the 1868 SWRZ and Kīlauea Iki lavas are geochemically identical (Figs. 3.3a and 3.5), suggesting that they originated from a similar parental magma. The 1868 SWRZ and Kīlauea Iki lavas display distinctively lower Nb/Y ratios (Figs. 3.5 and 3.6) than summit lavas erupted just prior (1866) and after (1877-94). Pietruszka and Garcia (1999a) also noted the moderately evolved 1868 Kīlauea Iki lavas (~6.7 wt. % MgO) had geochemical similarities to early 19th century lavas, and may have been stored for decades. The 1868 SWRZ lava also displays relatively low Pb isotopic ratios that lie between the 1823 SWRZ and 1866-77 summit lavas (Figs. 3.5 and 3.6). No isotopic data exist for the 1868 Kīlauea Iki lavas. Mixing calculations confirm that the 1868 SWRZ lava falls on a binary mixing line between the 1823 (~70%) and 1866 (~30%) lavas (Fig. 3.6). Thus, the 1868 SWRZ lavas may represent a mixture of stored 1823 SWRZ and 1866 summit magma. The 1868 SWRZ and Kīlauea Iki lavas lie below the calculated LLD (Fig. 3.4), also suggesting they were hybrid magmas. This mixing relationship can be explained if the active lava lake (with a composition similar to the 1866 lavas) drained and mixed with 1823 magma that was stored in the shallow summit region or within the rift zone.

Alternatively, the 1868 SWRZ lava may reflect an unmixed, stored magma from the mid 19th century (Fig. 3.3a). This assumes that the systematic ²⁰⁶Pb/²⁰⁴Pb and Nb/Y increase in summit lavas between 1820 and 1923 track the progressive change in parental magma delivered to the summit reservoir rather than mixing of compositionally distinct magmas over a period of decades (e.g., Pietruszka and Garcia, 1999a). For example, the intermediate Pb isotopic ratios in the 1868 SWRZ lava could simply reflect the eruption of stored magma that intruded into the rift zone between 1832 and 1866. For example, the collapse of the summit caldera and magma drainage that shortly followed the 1840 ERZ eruption (Macdonald et al., 1983) may have facilitated this magma storage event. This is the only known major summit collapse and lava lake drainage event that occurred during this time period. In this scenario, the 1868 ~M7.9

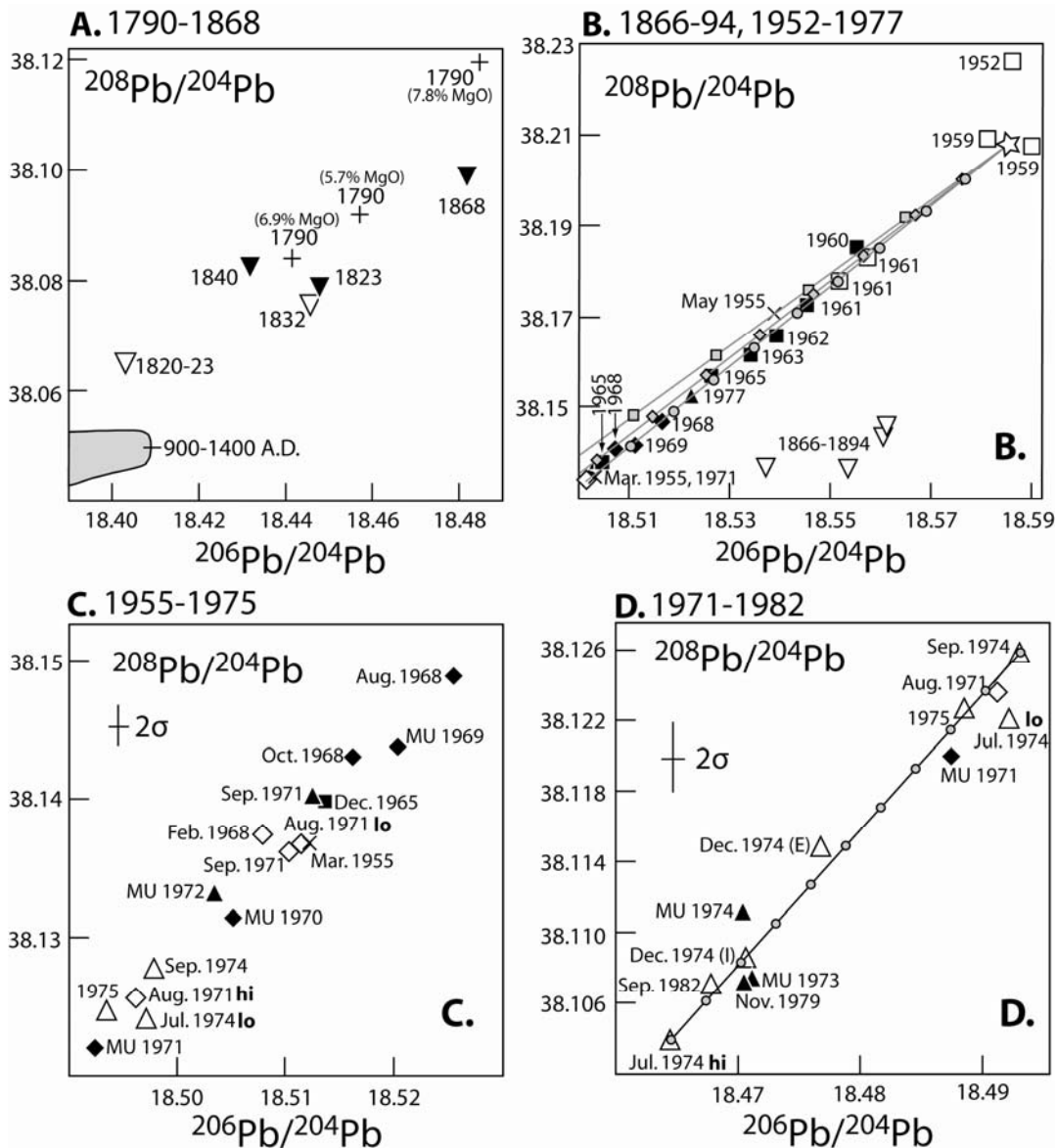


Fig. 3.8 Plots of $^{206}\text{Pb}/^{204}\text{Pb}$ vs. $^{208}\text{Pb}/^{204}\text{Pb}$ ratios for historical Kīlauea rift and summit lavas, and late prehistoric (900-1400 A.D.) summit lavas (data from Marske et al., 2007). The square outlines in Fig. 3.6 correspond to the four panels presented here. Eruption year is labeled beside the symbols. Symbol descriptions are given in the Fig. 3.6 caption. (a.) MgO content is plotted next to the 1790 ERZ lavas. Late 20th century lavas were excluded from this plot. (b.) A mixing line between August 1971 summit (Kil71-6; $^{206}\text{Pb}/^{204}\text{Pb}=18.506$, $^{208}\text{Pb}/^{204}\text{Pb}=38.135$) and 1959 Kīlauea Iki ($^{206}\text{Pb}/^{204}\text{Pb}=18.590$, $^{208}\text{Pb}/^{204}\text{Pb}=38.209$) lavas (line with gray circles) is shown. The 1959 Kīlauea Iki end member (open star) is an average of two analyses from this eruption [IKI-58 (S-1) and IKI-01 (S-2)]. One ppm Pb for the 1959 and 1971 lavas is assumed for the mixing model. Mixing calculations between 1840 ERZ (line with gray squares) and 1790 ERZ (line with gray diamonds) lavas with 1959 Kīlauea Iki end member are described in the Fig. 3.6 caption. (d.) The December 1974 lavas are labeled with the vents (E or I) from which they erupted from. A mixing line (line with gray circles) between the July 1974 (Kil774-1; $^{206}\text{Pb}/^{204}\text{Pb}=18.464$, $^{208}\text{Pb}/^{204}\text{Pb}=38.104$) and September 1974 (Kil-974-8; $^{206}\text{Pb}/^{204}\text{Pb}=18.493$, $^{208}\text{Pb}/^{204}\text{Pb}=38.126$) summit lavas is plotted. A Pb content of 1 ppm was assumed for the July and September 1974 lava. Mixing results shown in 10% increments. The ‘hi’ and ‘lo’ labels refer to the higher and lower MgO August 1971 and July 1974 lavas.

earthquake and subsequent drainage of the active summit lake into the SWRZ in 1868 may have acted as a hydraulic plunger that triggered the eruption of magma that had been stored in the SWRZ since ~1840.

The 1919-23 eruptive period at Kīlauea is the only other historical interval (besides the 1971-74 period) when contemporaneous eruptions took place along the SWRZ (1919-20), ERZ (1922 and 1923), and summit (1919-23). This eruptive interval also provides an important snapshot of the state of Kīlauea's plumbing system just prior to the 1924 summit explosions. The SWRZ, ERZ, and summit lavas erupted between 1919 and 1923 show little geochemical variability. For example, the 42-week 1919-20 Mauna Iki SWRZ eruption produced lavas with ratios of highly to moderately incompatible elements (e.g., Nb/Y) that lie within analytical uncertainty (Table 3.1). No systematic temporal variations were observed for major and trace element abundances or ratios during this eruption. Similarly, the 1919-20 (SWRZ), 1921 (summit), and 1923 (ERZ) lavas have identical $^{206}\text{Pb}/^{204}\text{Pb}$ and $^{87}\text{Sr}/^{86}\text{Sr}$ ratios (relative to analytical uncertainty) indicating that they originated from a common parental magma during this period (Fig. 3.6). The 1919-23 ERZ, SWRZ, and summit lavas generally lie along a single LLD defined by relatively high CaO abundances (at a given MgO), also indicating that they fractionated from a compositionally similar parental magma (Fig. 3.4).

The compositional homogeneity among 1919-23 summit, ERZ and SWRZ has implications for the nature of the magmatic plumbing system during this period. For example, the Mauna Iki eruption was shallowly fed from the upper summit reservoir and directly from the active lava lake in the caldera based on visual observations, geologic mapping, and deformation studies (Jaggard, 1920; Rowland and Munro, 1993). Moreover, the one-day August 25, 1923 ERZ eruption was preceded by rapid draining of the active summit lake that began on August 24 and emptied by August 28. These observations suggest that a strong hydraulic magmatic connection

existed between the summit area and upper SWRZ and ERZ prior to the 1924 explosive summit eruption (Fig. 3.9b).

3.4.2.2 1955-1968 eruptive interval

The parentage and magmatic history of lavas from the 3-month 1955 lower ERZ eruption is controversial. The eruption is subdivided into early, more evolved lavas (February 28 to March 20; 5.0-5.7 wt. % MgO) and late, less evolved lavas (March 25 to May 26; 6.2-6.7 wt. % MgO; Wright and Fiske, 1971). There are conflicting explanations for the origin of the early 1955 lavas including: (1) young prehistoric to 1924 era magmas that were intruded and stored beneath the lower ERZ (Wright and Fiske, 1971), (2) differentiates of the magmas that erupted later in 1955 (Ho and Garcia, 1988), and (3) stored magmas containing phenocrysts that had resided in the lower ERZ for at least 550 years, with the implication that the magmas are similarly old (Cooper et al., 2001). The origin of the late 1955 lavas is somewhat better constrained. Least squares modeling of major- and trace-element abundances indicate that the early, rift-stored 1955 magmas mixed with a mafic magma similar to 1952 summit lavas to create the late 1955 lavas (Wright and Fiske, 1971; Helz and Wright, 1992).

Our new high precision Pb isotopic data provide a sensitive geochemical fingerprint for determining the parental magmas of the 1955 lavas. The 1955 lavas lie on the trend defined by high $^{208}\text{Pb}/^{204}\text{Pb}$ at a given $^{206}\text{Pb}/^{204}\text{Pb}$ (Figs. 3.6 and 3.8b), and are distinct from young prehistoric lavas (900-1400A.D.; Marske et al., 2007) and historical summit lavas erupted before 1955 (Pietruszka and Garcia, 1999a). This indicates that no known pre-1955 lava compositions are suitable parental magmas for the 1955 lavas. Moreover, the early 1955 lavas cannot be simple differentiates of the more mafic late 1955 lavas (e.g., Ho and Garcia, 1988) because they are geochemically and isotopically distinct (Figs. 3.5 and 3.8b). Alternately, the early 1955 lava is isotopically and geochemically similar to the 1968-71 summit lavas (Figs. 3.5, 3.6, and 3.8c), that

could suggest the parental magma of the 1968-71 summit lavas was present in the plumbing system prior to the 1955 eruption. The presence of ‘future’ magmas was invoked by Wright and Fiske (1971) in which ‘summit compositions’ were erupted along the ERZ (between 1955 and 1968) ~2-8 years before they were extruded at the summit. However, this process is probably unreasonable to explain the early 1955 lavas because it would require that magma was stored ~16 years, which is 2-8 times longer than the estimate in Wright and Fiske (1971).

The origin of the early and late 1955 lavas can be explained by mixing of evolved, rift stored (900 to 1840 A.D.) magma and mafic 1950s summit derived magmas. Mixing calculations based on Pb isotopic ratios indicate that the 1955 lavas lie within analytical error of mixing lines between the 1959 Kīlauea Iki lavas and some 900-1400 A.D. summit lavas (not shown) or 1790 or 1840 ERZ lavas (Figs 3.6 and 3.8b). However, 1790 or 1840 ERZ magmas are a more likely mixing endmembers because the 1955 eruption occurred along a system of fissures that partially overlaps the 1790 fissure system, and is located ~2.5 km south of the 1840 lower ERZ fissures (Fig. 3.1). Furthermore, it is unknown if the 900-1400 A.D. summit magmas intruded the ERZ, because this is a period of time when Kīlauea’s activity was focused at the volcano’s summit (Holcomb, 1987). The 1952 and 1954 summit lavas are unsuitable mixing end members with the 1840 and lower MgO 1790 ERZ lavas because some of the 1955 lavas do not pass within analytical error of the mixing lines. The presence of the 1959 summit component in the 1955 ERZ lavas suggest that this composition was delivered to the lower ERZ ~4 years before erupting at the summit. The most Fo-rich olivines ($F_{0.85}$) in the late 1955 lavas originally crystallized from a melt containing 8.0-8.5 wt. % MgO (Helz and Wright, 1992), suggesting that the 1959 mixing end member was relatively mafic. This is also supported by the high MgO lavas (> 9 wt. %; Macdonald and Katsura, 1961) of the 1959 Kīlauea Iki eruption.

The absence of mixing textures (i.e., resorbed and/or reversely zone crystals of olivine, clinopyroxene, and plagioclase; Ho and Garcia, 1988) in the early 1955 lavas could be explained

if the minerals re-equilibrated relatively rapidly (hours to weeks; Helz and Wright, 1992) after mixing occurred. The early 1955 lavas originated from a lower contribution (~20-55%) of the mafic 1959 mixing end member (compared to the ~75% contribution for late 1955 lavas; Fig. 3.6), that would also probably result in less significant resorption and zoning in the crystals with faster mineral re-equilibration times. The lower MgO contents of the early 1955 lavas (5.0-5.7 wt. % MgO) are also consistent with a minor contribution of the 1959 mafic end member.

Magma mixing is clearly evident in the late 1955 lavas based on resorbed and reversely zoned crystals of olivine, clinopyroxene, and plagioclase (Wright and Helz, 1992), and the mixing trends (oblique to the LLD) on the MgO vs. CaO and CaO/Al₂O₃ plots (Fig. 3.4b). The presence of disequilibrium textures in the late 1955 lavas (unlike the early 1955 lavas) can be explained if a greater contribution of the mafic 1959 summit component (75%) mixed with the stored 1790 and/or 1840 (25%) magmas (Figs. 3.6 and 3.8b). Thus, mafic 1959 summit magma was fed to the lower ERZ, mixed in greater proportions with stored 1790 and/or 1840 magmas (Fig. 3.9c), resulting in stronger chemical disequilibrium between the crystals and melt. A larger summit magma contribution for the late 1955 lavas is also supported by the period of summit deflation that began eight days into the 1955 eruption (Macdonald and Eaton, 1964). This deflation event is interpreted as magma migration into the lower ERZ (Wright and Fiske, 1971).

The 1960s ERZ eruptions displayed similar characteristics (excluding the 1960 and Mauna Ulu): (1) they were relatively short-lived (hours to 15 days, lasting an average of ~5 days) and volumetrically minor (0.00013-0.17 km³; Macdonald et al., 1983), (2) they produced lavas with a narrow range of MgO contents (6.8-8.5 wt. %, excluding the August 1968 picrites), (3) they took place over the upper and middle ERZ and often erupted from the same fissure systems (Fig. 3.1), and (4) each eruption was preceded by a period of summit deflation. Based on these characteristics, some previous studies used major element modeling to conclude these ERZ lavas represent variable mixtures of geochemically distinct summit magmas from the 1950s and 1960s

(Wright and Fiske, 1971; Jackson et al., 1975; Wright et al., 1975). In contrast, all of 1960-68 lavas may have originated from a single magma 'batch' based on Pearce major-element ratios (Nicholls and Russell, 1991).

The 1960-68 ERZ lavas cannot be derived from a single magma batch because they show a temporal decrease in $^{206}\text{Pb}/^{204}\text{Pb}$ and Nb/Y ratios (Fig. 3.3b). Rather, these variations represent either progressive changes in the parental magma compositions delivered to Kīlauea (Pietruszka and Garcia, 1999a; Garcia et al., 2003), or reflect variable mixing between multiple, compositionally distinct magmas in the summit reservoir and shallow ERZ (Wright and Fiske, 1971; Wright et al., 1975). The 1960-68 rift lavas could also be explained by two-component magma mixing because they lie along a tight linear trend ($R^2=0.99$) in $^{206}\text{Pb}/^{204}\text{Pb}$ vs. $^{208}\text{Pb}/^{204}\text{Pb}$ space (Fig. 3.8b). Lead isotopic mixing calculations indicate that all 1960-68 rift and summit lavas lie within analytical error of a mixing line between 1959 Kīlauea Iki and 1971 summit lavas (Fig. 3.8b). The 1968 lavas are not a suitable mixing endmember because the 1965 ERZ lava has lower Pb isotopic ratios than the 1968 summit lavas. Moreover, the 1974-82 summit lavas are unsuitable mixing end members because some of the 1960-68 lavas do not pass within analytical error of the mixing lines. The 1959 Kīlauea Iki end member, thought to be an important mixing component in the 1960 lower ERZ eruption (Wright and Helz, 1996), probably represents the composition of the resident magma. In this mixing model, the $^{206}\text{Pb}/^{204}\text{Pb}$ decreases from 1960-68 (Fig. 3.8b) document the progressive increase of the 1971 component in lavas from 1960 (~35%) to October 1968 (~90%). These variations likely reflect binary mixing in the summit reservoir followed by periodic withdrawals based on the episodes of summit deflation that accompanied each eruption (Fig. 3.9c). Simple two component magma mixing to explain the geochemical variations for the 1960-68 ERZ lavas implies that the input composition to the summit reservoir (i.e., 1971 summit) remained homogeneous for ~10 years. However, the systematic temporal variations could also reflect changes in the melt delivered from the mantle

source region to the summit reservoir (e.g., Pietruszka and Garcia 1999a), followed by periodic withdrawals to the rift.

The August 1968 upper ERZ eruption produced picritic lavas (>12 wt. % MgO; Jackson et al., 1975), the origin of which is controversial. These picrites are thought to represent primitive melts from the upper mantle (Nicholls and Stout, 1988) or a shallow, mixed magma that accumulated olivine (Jackson et al., 1975; Wright et al., 1975). Nicholls and Stout (1988) concluded that the August 1968 picrites represent primitive magmas (no olivine accumulation) based on the high MgO contents and mineral chemistry of the lavas. These authors also noted the similar incompatible element ratios between August 1968 ERZ and early 1968 summit lavas demonstrate a comagmatic origin in which August 1968 picrites fractionated to form the early 1968 summit lavas (7.5 wt. % MgO; Garcia et al., 2003). However, olivine phenocrysts in the early August 1968 lavas have relatively low Fo contents (81-87%; Nicholls and Stout, 1988) with respect to their whole-rock Mg # of 72 (Jackson et al., 1975), indicating that the olivines are not equilibrium with their bulk composition (e.g., Roeder and Emislie 1970; Dungan and Rhodes, 1978). Thus, the August 1968 picrites represent olivine-accumulated magmas rather than primitive compositions. Moreover, the August 1968 picrites display higher $^{206}\text{Pb}/^{204}\text{Pb}$ and Nb/Y values (outside of analytical uncertainty) compared to February and June 1968 summit lavas suggesting that they originated from compositionally distinct magmas (Fig. 3.7). Previous studies suggested that the August 1968 picrites originated by mixing of 1969-71 Mauna Ulu and 1967-68 summit magmas that experience olivine accumulation (Jackson et al., 1975; Wright et al., 1975). However, the August 1968 lava has Pb isotopic ratios that are higher than both the 1969-71 Mauna Ulu and early 1968 summit lavas (Fig. 3.8c), indicating these are unsuitable mixing endmembers. Rather, binary mixing between the 1959 and 1971 end member compositions could explain the August 1968 lavas (Fig. 3.8b), as proposed for the other 1960s eruptions.

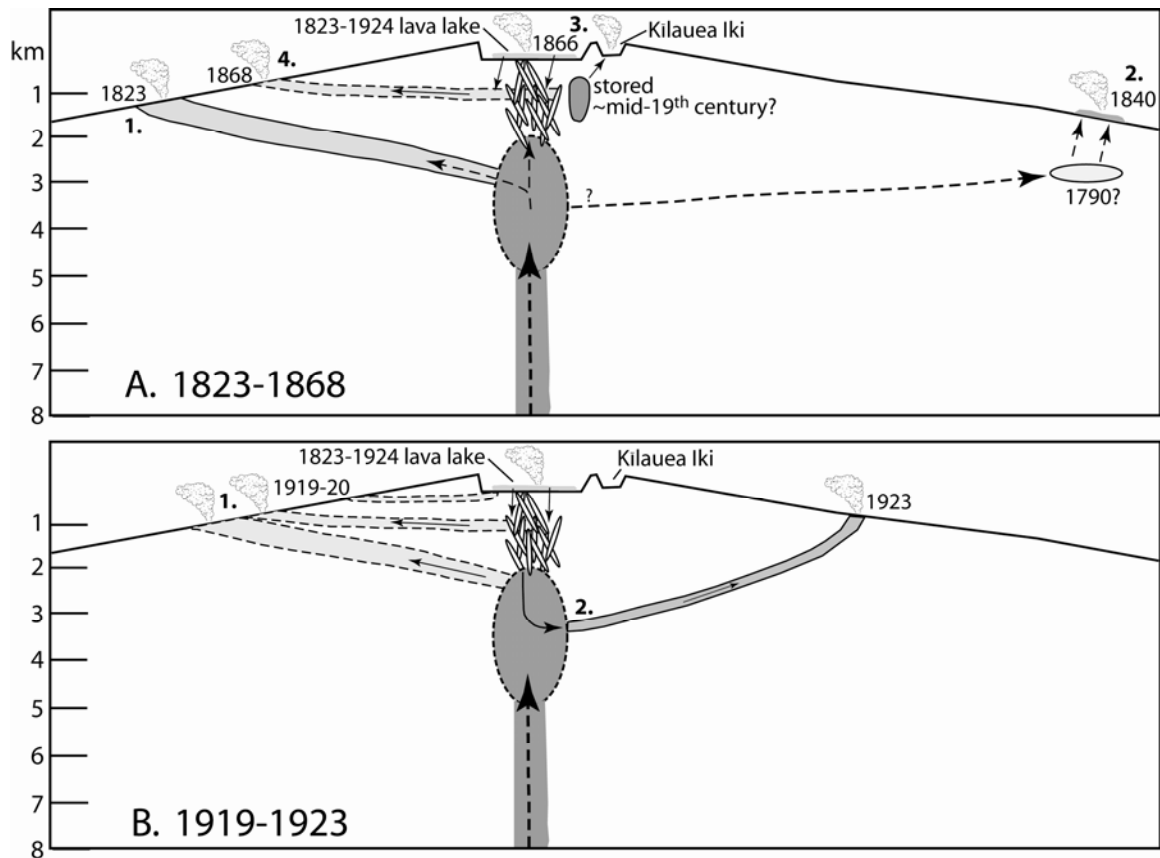


Fig. 3.9 Hypothetical cross-section of Kilauea's upper magmatic plumbing system during four time periods (1823-68, 1919-23, 1952-69, and 1969-74). The ~2-5 km deep summit magma reservoir is represented by the dashed oval. The bold numbers (e.g., 1. to 5.) represent the chronology of events for each panel where 1. is the earliest event and 5. is the latest event. The stretched ovals and blobs above the summit reservoir reflect a plexus of dikes, shallow magma bodies, or conduits that feed the summit eruptions. Dashed and solid arrows track the movement of magma. (a.) The solid arrows illustrate the draining of the active lava lake that may have been a mixing component and/or trigger for the 1868 SWRZ eruption (see text for details). (b.) The dashed gradational oval represents a relatively compositionally homogeneous, yet density stratified summit reservoir during this period. The 1919-20 Mauna Iki SWRZ eruption was fed shallowly from the top of the summit reservoir and active summit lake. Drainage of the summit reservoir (down-going arrows) may have occurred in response to the 1923 ERZ eruption. (c.) The 1959 magma intruded the ERZ and mixed with rift-stored 1790 and/or 1840 magmas to produce the 1955 lower ERZ lavas. The 1971 summit magmas mixed with 1959 summit magma compositions (corkscrew-shaped arrows) to create the 1961-69 hybrid magmas. (d.) The Mauna Ulu eruption may have been fed from a conduit that bypasses the summit reservoir (dashed arrows), possibly through an upper ERZ 'pipe' (Ryan et al., 1981). The early stages of the Mauna Ulu eruption may have mixed with rift-stored magma. December 1974 vent E and I lavas are hybrids of July and September 1974 ERZ magmas (corkscrew-shaped arrows).

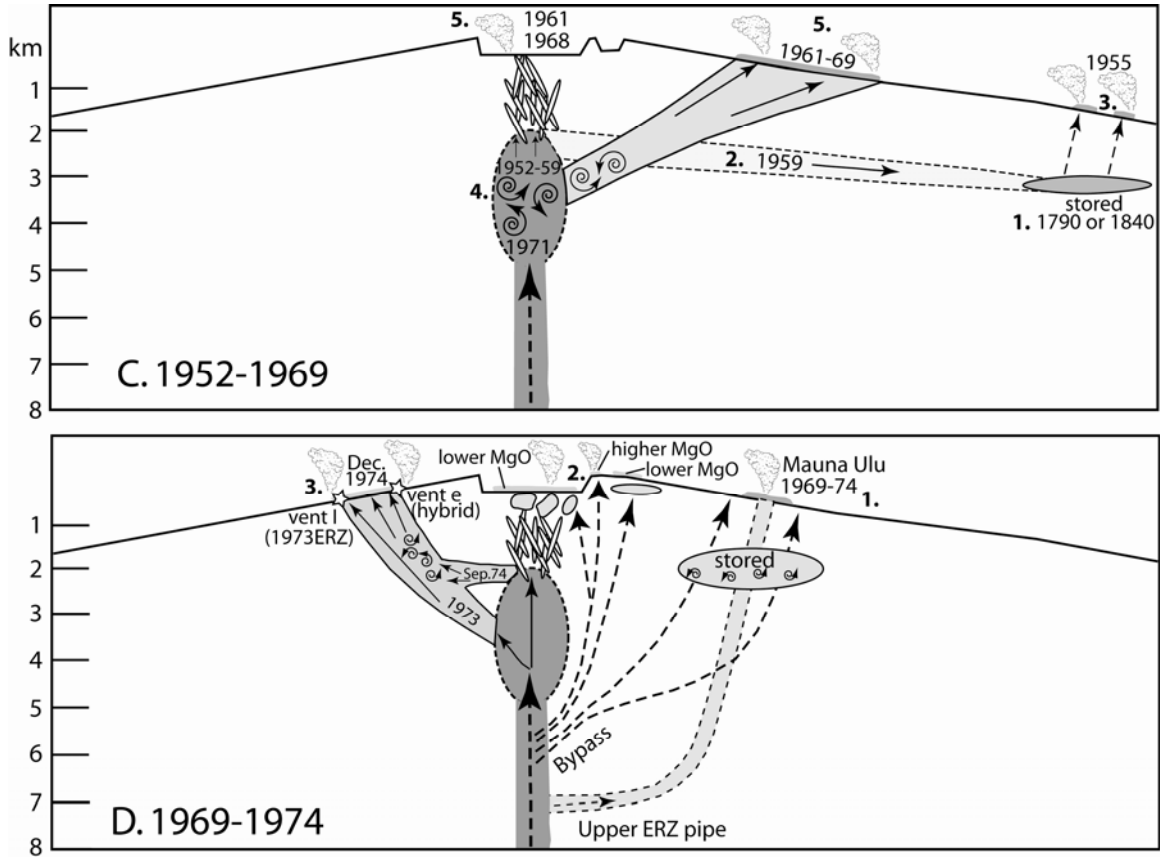


Fig. 3.9 (Continued)

3.4.2.3 1969-1974 eruptive interval

There is considerable debate regarding the compositional origin of the 1969-74 Mauna Ulu magmas, and how they were transported through Kīlauea's shallow plumbing system. For example, least squares major element modeling of the 1969-74 lavas identified 10 magma 'variants' that were suggested to have variably mixed in the summit reservoir before erupting at Mauna Ulu (Wright et al., 1975; Wright and Tilling, 1980). In contrast, Nd and Sr isotopic, and trace element studies indicate Mauna Ulu lavas originated from variable degrees of partial melting of a relatively homogeneous mantle source (Hofmann et al., 1984). The 1969-74 Mauna Ulu magmas may have also partially or completely bypassed the summit reservoir before intruding the ERZ (Fig. 3.9d) based on the following observations. The precursory seismic swarm that preceded the Mauna Ulu eruption was centered downrift from the vent, just south of Makopuhi crater (Fig. 3.1; Klein et al., 1987), rather than the summit region (typical for most ERZ eruptions during the 1960's). During the 1969-71 Mauna Ulu eruption, the summit region did not deflate (Swanson et al., 1979), unlike the 1960-68 eruptions that were accompanied by summit deflation as magma moved from the summit reservoir into the ERZ (Wright and Fiske, 1971; Jackson et al., 1975). The absence of summit deflation during the 1969-71 Mauna Ulu eruption could indicate that magma was not exclusively supplied from the summit reservoir. Seismicity studies suggest magma was fed to Mauna Ulu from 1969-74 through a steeply inclined, physically isolated 7-km-deep magma 'pipe' extending from Kīlauea's primary conduit to the upper ERZ (Ryan et al., 1981; Ryan, 1988). The origin and magmatic plumbing network for Mauna Ulu lavas is re-evaluated here with the new isotopic and trace element data.

The 1969 Mauna Ulu lava has Pb isotopic and incompatible trace element ratios similar to ERZ lavas erupted nearby in August and October 1968 (Figs. 3.1, 3.7, and 3.8c), suggesting the early part of the Mauna Ulu eruption expelled stored 1968 ERZ magmas. The rapid temporal decreases in Nb/Y, $^{206}\text{Pb}/^{204}\text{Pb}$, and $^{87}\text{Sr}/^{86}\text{Sr}$ ratios over the next two years (Fig. 3.7) cannot be

explained by partial melting of a homogeneous mantle source (e.g., Hofmann et al., 1984). Rather, this decrease likely reflects progressive mixing of a new mantle-derived input magma with stored magma similar in composition to the 1968 ERZ lavas (Fig. 3.7). A similar pattern occurred during the 1972-74 Mauna Ulu eruption. The April 1972 lava has Pb isotopic ratios that lie between the 1971 Mauna Ulu and summit lavas (Fig. 3.8c). These intermediate Pb isotopic ratios could be explained if mantle-derived magma (with low Pb isotopic ratios) encountered a stored pocket of ERZ magma (with relatively high Pb isotopic ratios) and mixed to create the hybrid that erupted in April 1972. Alternately, the intermediate Pb isotopic ratios could be explained if 1971 summit magma entered the Mauna Ulu conduit (during the early part of the 1972-74 eruption), and mixed with 1971 Mauna Ulu resident magma to form the April 1972 hybrid magma (Figs. 3.7 and 3.8d). This is supported by the period of summit deflation during the first two months of the 1972-74 eruption (Tilling et al., 1987). Thus, the Nb/Y, $^{206}\text{Pb}/^{204}\text{Pb}$, and $^{87}\text{Sr}/^{86}\text{Sr}$ decreases observed during the 1972-74 Mauna Ulu eruption can be explained by mixing of a new mantle-derived input magma with this hybrid magma (Figs. 3.7 and 3.8c). The 1969-71 and 1972-74 lavas lie along linear trends on a plot of $^{208}\text{Pb}/^{204}\text{Pb}$ vs. $^{206}\text{Pb}/^{204}\text{Pb}$ (Figs. 3.6 and 3.8), with respect to analytical uncertainty. This suggests a minimum of two mixing end members are required to explain the compositional variability during these phases.

The MgO-variable August 1971 and July 1974 summit lavas, and 1969-74 Mauna Ulu lavas can be explained if magma both bypassed and entered the summit reservoir during this time period (Fig. 3.9d). The August 1971 and July 1974 caldera rim lavas are compositionally similar to the April 1971 and 1974 Mauna Ulu lavas, respectively (Figs. 3.5, 3.7, and 3.8). This suggests these caldera rim lavas originated from the same parental magmas that were supplied to Mauna Ulu. These observations indicate that lavas erupted near the end of both Mauna Ulu phases represent the composition of the (unmixed) mantle-derived endmember because the 1971 and 1974 Mauna Ulu lavas match the compositions of the magma that supplied the August 1971 and

July 1974 caldera rim lavas. Furthermore, the decrease in Pb isotopic ratios between the 1971 and 1974 caldera rim lavas suggests that the Pb isotopic ratios of the mantle-derived end member decreased over ~3 years between 1971 to 1974 (Fig. 3.7).

The presence of Mauna Ulu-like compositions in the August 1971 and July 1974 caldera rim lavas can be explained if they represent mantle-derived magmas that were directly fed from Kīlauea's primary conduit (below the summit reservoir) to the caldera rim and upper ERZ (Fig. 3.9d). The relatively high MgO contents in mid-1970 to 1974 Mauna Ulu and caldera rim lavas (10-18 wt. % MgO, Wright et al., 1975; Hofmann et al., 1984; Garcia et al., 2003) also suggest the magmas were processed more rapidly (i.e., less time to fractionate) through Kīlauea's plumbing system. However, some Mauna Ulu magmas may have accumulated olivine in transit based on their high MgO contents. The 3-4 times faster $^{206}\text{Pb}/^{204}\text{Pb}$ variation observed during the 1969-71 and 1972-74 phases ($\sim 0.015 \text{ year}^{-1}$) than the 1952-82 summit period ($\sim 0.004 \text{ year}^{-1}$) is further evidence that Mauna Ulu magmas bypassed, or did not thoroughly mix with the summit reservoir. Unusually rapid geochemical variations were also observed for 1986-92 Pu'u Ō'ō ERZ lavas, which were thought to partially bypass the summit reservoir (Garcia et al., 1996).

The August 1971 and July 1974 caldera floor lavas have $\text{K}_2\text{O}/\text{TiO}_2$, Nb/Y, and $^{206}\text{Pb}/^{204}\text{Pb}$ ratios similar to 1968 summit and August 1971 caldera rim lavas, respectively (Figs. 3.5, 3.7, and 3.8). The compositional similarity of the 1968 and August 1971 caldera floor lavas suggest that summit reservoir magma remained relatively homogenous between these eruptions because both lavas are thought to have been supplied directly from the summit reservoir. The September 1971 SWRZ lava displays Pb isotopic ratios that identical to the August 1971 caldera floor lavas (Fig. 3.8c) supporting a previous interpretation that the SWRZ lavas were directly supplied from the upper part of the summit reservoir (Duffield et al., 1982). In contrast, the Pb isotopic ratios of the July 1974 caldera floor lavas (derived from the summit reservoir) are similar to the August 1971 caldera rim lava (mantle-derived input). This suggest that it took <3 years for

the mantle-derived input magma to thoroughly mix with the magma in the summit reservoir. In this scenario, a given magma composition might enter the lower portion of the summit reservoir and ERZ at the same time. The magma that partially or completely bypasses the summit reservoir is transported more quickly and erupts at the ERZ, whereas this same magma is buffered in the summit reservoir.

The lower MgO (6.7-7.6 wt. %) eruptions along the caldera floor fissures and the fissures south and east of Keanakakoi crater during the August 1971 and July 1974 eruptions can be explained if moderately evolved magmas were forced to the surface by the intrusion of higher MgO caldera magmas into the summit reservoir. The MgO-rich August 1971 and July 1974 caldera rim lavas have two types of olivine: lower Fo content olivines with narrow, reversely zoned rims and higher forsterite olivines with normal zoning, indicating mixing of lower and higher MgO content magmas also occurred during these eruptions (Garcia et al., 2003). Significant magma mixing between the higher MgO 1971 and 1974 Mauna Ulu compositions (lower $^{206}\text{Pb}/^{204}\text{Pb}$ and Nb/Y values) and the stored August 1968 and higher MgO August 1971 summit magmas (higher $^{206}\text{Pb}/^{204}\text{Pb}$ and Nb/Y values), respectively, should produce lavas with intermediate $^{206}\text{Pb}/^{204}\text{Pb}$ and Nb/Y contents. However, the August 1971 and July 1974 caldera rim lavas have Nb/Y and $^{206}\text{Pb}/^{204}\text{Pb}$ ratios similar to their Mauna Ulu counterparts (Figs. 3.7 and 3.8), indicating only minor mixing occurred. Extensive magma mixing during the 1971 and 1974 summit eruptions is also unlikely based on the lack of intermediate MgO contents between the caldera rim (10.0-11.5 wt. %) and floor (6.7-7.6 wt. %) lavas. Thus, the higher MgO magma probably acted as a hydraulic plunger that forced (and only slightly mixed with) stored lower MgO magma (residing below the caldera floor and along the fissures south and east of Keanakakoi crater) to the surface (Fig. 3.9d). The width of the summit reservoir probably does not exceed the southeast caldera rim in order to preserve the compositional signature August 1971 and July 1974 caldera rim lavas (Fig. 3.9d). Moreover, a sharp spatial boundary between the

summit reservoir and upper ERZ probably existed to explain the close proximity of the 1971 and 1974 caldera rim and floor vents (~30-1100 meters apart).

3.4.2.4 1974-1979 eruptive interval

The 6-hour December 31, 1974 eruption that occurred between the Koa'e fault system and upper SWRZ (Fig. 3.1) produced high MgO lavas (12.2-15.7 wt. %, Lockwood et al., 1999; Garcia et al., 2003) with heterogeneous Pb isotopic compositions (Figs. 3.7 and 3.8d). Lavas from this eruption have olivine phenocrysts (~15 vol. %) with forsterite contents too low to be in equilibrium with their bulk compositions (K. Kolysko-Rose unpublished data, 2010), indicating that the olivines were accumulated. The 04:30 a.m. lava erupted from the northernmost fissure (vent E; Lockwood et al., 1999) located 1.3 km south of Kīlauea's southeastern rim (Fig. 3.1), whereas the 06:40 a.m. lava erupted 3.5 km southwest of vent E along the southernmost fissure (vent I; Lockwood et al., 1999). Some olivines within vent E lavas have narrow, reversely zoned rims (K. Kolysko-Rose unpublished data, 2010) indicating mixing occurred shortly before or during the December 1974 eruption. Two important seismic precursors discussed in Klein et al. (1987) help elucidate the origin of the December 1974 lavas. First, the September 1974 summit eruption was shortly preceded by a slow intrusion of magma south of the summit reservoir ~3 km beneath the site of the December 1974 eruption location. Second, the December 1974 eruption was preceded by slow migration of magma from the summit region into the SWRZ on December 24. On December 30, a 2 km wide seismic swarm located 2.5 km beneath the eruption site was recorded. Hours before the eruption, earthquakes migrated upwards reflecting a propagating dike to the December 1974 eruption site.

The Pb isotopic variations during the December 1974 eruption can be explained by magma mixing (within the SWRZ) of compositions similar to the high MgO July 1974 caldera rim lavas and September 1974 summit lavas. The September 1974 lava is likely a mixing

endmember that resided beneath the December 1974 eruption site based on seismicity. The magma delivered from the summit region to the SWRZ during late December 1974 was probably similar in composition to the high MgO July 1974 mantle-derived magma. This magma was thought to have been present in Kīlauea's summit reservoir because it erupted at Mauna Ulu and the summit caldera rim only a few months before the December 1974 eruption. Mixing calculations confirm that the December 1974 lavas lies within analytical error on a binary mixing line between the high MgO July 1974 and September 1974 lavas (Fig. 3.8d). The 04:30 a.m. sample erupted along fissures closest to the summit (Fig. 3.1) originated from a greater contribution (~50%) of the September 1974 eruption compared to a ~20% contribution for the 06:40 a.m. that erupted farthest away from the summit (Fig. 3.8d).

The evolved 1977 ERZ lavas (5.3-5.9 wt. % MgO; Moore et al., 1980) are isotopically and geochemically similar to the March 1965 ERZ lavas (Figs. 3.3b, 3.5, and 3.8b), and were erupted only ~1-2 km downrift from the easternmost March 1965 fissure (Fig. 3.1; Holcomb, 1987). Moore et al. (1980) reported no evidence of magma mixing in the 1977 lavas and concluded that its highly evolved composition was produced by crystal fractionation. Thus, the 1977 lavas probably represent differentiated 1965 magma that was stored in the ERZ ~12 years before erupting. This ~12 year storage time for the 1977 lavas is shorter than the ~29-34 year rift-storage time estimate for Pu'u Ō'ō magmas that erupted ~12 km uprift in January 1997 (Thornber et al., 2003). The 1979 ERZ Pauahi crater rim eruption occurred along fissures located ~100 m north of May 1973 eruption vents on the floor of Pauahi crater (Fig. 3.1), which was not analyzed in this study. The 1979 ERZ lava has Pb isotopic ratios that are identical to the 1973 Mauna Ulu lava that erupted only 3 weeks after the 1973 Pauahi eruption (Fig. 3.8d). Assuming the May 1973 Pauahi (not analyzed) and Mauna Ulu lavas have similar Pb isotopic ratios, the 1973 and 1979 Pauahi lavas may have originated from the same parental magma.

3.5 Summary of magmatic processes in Kīlauea's rift zones

There appears to be no single magmatic process (i.e., magma transportation, storage, and mixing) that can account for the chemical and isotopic variations of Kīlauea's historical rift zone lavas. Instead, a range of processes are important. Overall, most ERZ and SWRZ magmas are delivered to the volcano's summit reservoir before intruding the rift zones. This indicates that: (1) a strong magmatic connection exists between the summit reservoir and rift zones, (2) most magmas are similarly 'processed' through Kīlauea's shallow plumbing system, (3) magma storage times in the summit reservoir and rift zones are generally similar. Some historical SWRZ rift eruptions (i.e., 1823, 1919-20, and 1971) were fed shallowly from the upper summit reservoir and/or directly from active lava lakes in the summit caldera (Rowland and Munro, 1993; Duffield et al., 1982; Klein et al., 1987), suggesting that magmas are not stored in the SWRZ for prolonged periods prior to eruption. In contrast, the 1868 and 1974 SWRZ lavas may have originated from rift-stored magma. Historical ERZ lavas originated from new mantle-derived magma and/or magma that may have been stored in the rift zone for decades to centuries. Prolonged (weeks-years) historical ERZ eruptions (i.e., 1840, 1955, 1960, 1969-71 and 1972-74 Mauna Ulu, 1983-present Pu'u Ō'ō) generally began with extrusion of stored, evolved and/or hybrid magmas followed later by more mafic compositions. This appears to be a typical eruptive pattern in which higher MgO summit-derived magma intrudes the ERZ and mixes with stored magma before or during an eruption (e.g., Wright and Fiske, 1971; Wright and Helz, 1996; Garcia et al., 1992). Most short-lived (hours to weeks), volumetrically-minor rift eruptions (i.e., 1868, 1923, 1961-68, December 1974, 1979) were preceded or accompanied by a period of summit deflation or drainage of the summit lava lake suggesting magma from the summit reservoir was withdrawn to supply these ERZ eruptions.

Most Kīlauea magmas are processed through the summit reservoir before intruding the rift zones. However, magmas that supplied the longest-lived (years to decades) historical ERZ

eruptions (Pu‘u ‘Ō‘ō and Mauna Ulu) partially or completely bypassed the summit reservoir. Thus, magma bypass may be an important process to sustained long-lived high-volume ERZ eruptions. The 1971 and 1974 summit eruptions expelled magma that both bypassed the summit reservoir (caldera rim lavas) and magma that was processed through the summit reservoir (caldera floor lavas) providing an important snapshot of the state of Kīlauea’s plumbing system. The July 1974 caldera floor lavas (derived from the summit reservoir) and August 1971 caldera rim lava (mantle-derived magma that bypassed the summit reservoir) originated from a common parental magma. This suggest that it took <3 years for the mantle-derived input magma to thoroughly mix with the magma in the summit reservoir. This estimate is significantly shorter than previous estimates for late 20th century Kīlauea summit lavas (~23-43 years, Pietruszka and Garcia 1999b; Garcia et al., 2003). The width of the summit reservoir probably does not exceed the southeast caldera rim in order to preserve the compositional signature August 1971 and July 1974 caldera rim lavas. Moreover, a sharp spatial boundary between the summit reservoir and upper ERZ probably existed to explain the close proximity of the 1971 and 1974 caldera rim and floor vents (~30-1100 meters apart).

The magma storage times estimates prior to eruption for the evolved 1977 middle (~12 years) and 1955 lower (~115-165 years) ERZ lavas are significantly shorter than the >550 year age inferred for the early 1955 lavas (Cooper et al., 2001), but closer to the ~29-34 year storage estimate for the January 1997 Pu‘u ‘Ō‘ō ERZ lavas (Thornber et al., 2003). The overall increase in magma residence time moving down rift likely reflects lower magma supply rates to the lower ERZ (Dzurisin et al., 1984).

APPENDIX

A.1 Individual Sr isotope ratios for Pu‘u ‘Ō‘ō lavas. Multiple analyses for a given sample are from a single dissolution. The average $^{87}\text{Sr}/^{86}\text{Sr}$ value for each sample is presented in Table 1.5. Samples 26-Mar-89, 12-May-91, 29-Dec-92 (#1 and #2), and 27-Apr-95 were re-run to further improve the precision of these analyses compared to the data presented by Garcia *et al.* (1989, 2000) and Pietruszka *et al.* (2006). Samples 29-Dec-92 #1 and #2 represent separate dissolutions performed by Pietruszka *et al.* (2006). The $^{87}\text{Sr}/^{86}\text{Sr}$ values of the SRM987 standard by TIMS were 0.710255 ± 17 (2σ ; $n=60$) for the 1999-2004 Pu‘u ‘Ō‘ō lavas, and 0.710246 ± 17 (2σ ; $n=18$) for Kill1919 and the 1989-1998 and 2005 Pu‘u ‘Ō‘ō lavas. Multiple analyses of the SRM987 standard by MC-ICP-MS with the 1998-2004 lavas gave $^{87}\text{Sr}/^{86}\text{Sr} = 0.710220 \pm 13$ (2σ ; $n=35$). The in-run errors are less than the external reproducibility of SRM987. All Sr isotope ratios are reported relative to $^{87}\text{Sr}/^{86}\text{Sr}=0.710250$ for SRM 987.

Sample	$^{87}\text{Sr}/^{86}\text{Sr}$ (TIMS)	$^{87}\text{Sr}/^{86}\text{Sr}$ (MC-ICP-MS)	Sample	$^{87}\text{Sr}/^{86}\text{Sr}$ (TIMS)	$^{87}\text{Sr}/^{86}\text{Sr}$ (MC-ICP-MS)
26-Mar-89	0.703586		12-Apr-03	0.703634	0.703641
	0.703582			0.703643	
	0.703581			0.703644	
12-May-91	0.703586		15-Jan-04	0.703625	0.703642
29-Dec-92 #1	0.703606			0.703634	
	0.703585			0.703638	
	0.703598			0.703623	
29-Dec-92 #2	0.703609		7-Jun-04	0.703623	0.703635
	0.703591			0.703627	
	0.703594			0.703621	
27-Apr-95	0.703594			0.703612	
	0.703612		31-Jan-05	0.703622	
	0.703598			0.703627	
7-Sep-98	0.703607			0.703616	
	0.703592			0.703622	
	0.703607			0.703616	
	0.703602			0.703634	
	0.703592			0.703629	
	0.703608		8-Aug-05	0.703620	
13-Feb-99		0.703616		0.703631	
27-Oct-99	0.703610	0.703627		0.703611	
	0.703619			0.703613	
	0.703630			0.703641	
19-Feb-00	0.703617	0.703634	Kil1919	0.703472	
	0.703623			0.703476	
	0.703621			0.703483	
21-Jun-00		0.703644			
8-Jan-01		0.703639			
7-Jul-01	0.703616	0.703635			
	0.703631				
	0.703621				
9-Feb-02	0.703636	0.703628			
	0.703646				
	0.703639				
20-Aug-02	0.703642	0.703633			
	0.703638				
	0.703643				

A.2 Pagan sample locations. Longitude and latitude values are given in decimal degrees.

Sample	Longitude (N)	Latitude (E)
South Pagan Post-Caldera		
TM-06-15A	—	—
TM-06-16	—	—
TM-06-10	18.0800	145.7318
TM-06-901	18.0638	145.7286
TM-06-28	18.0840	145.7273
TM-06-08	18.0622	145.7251
TM-06-07	18.0686	145.7238
TM-06-275	18.0627	145.7167
TM-06-911	18.0663	145.7142
TM-06-214	18.0810	145.7322
TM-06-24	18.0703	145.7198
TM-06-18	18.0750	145.7322
South Pagan Dikes		
TM-06-20	18.0648	145.7161
TM-06-22	18.0651	145.7161
South Pagan Pre-Caldera		
TM-06-30	18.0825	145.7280
TM-06-31	18.0845	145.7311
TM-06-32	18.0844	145.7314
TM-06-33	18.0850	145.7328
TM-06-05	18.0511	145.7191
TM-06-205	18.0613	145.7170
TM-06-204	18.0613	145.7169
TM-06-203	18.0617	145.7173
TM-06-202	18.0617	145.7173
TM-06-201	18.0618	145.7173
TM-06-200	18.0618	145.7174
TM-06-907	18.0627	145.7149
TM-06-906	18.0598	145.7132
CVR dikes		
TM-06-241	18.0872	145.7552
TM-06-217	18.0940	145.7493
TM-06-120	18.0929	145.7588
Late-stage CVR		
TM-06-03	18.0873	145.7508
TM-06-34	—	—
Central Volcanic Region (CVR)		
TM-06-216	18.0975	145.7545
TM-06-236	18.0920	145.7583
TM-06-237	18.0951	145.7602
TM-06-123	18.0938	145.7591
TM-06-122	18.0935	145.7593
TM-06-121	18.0935	145.7593
TM-06-238	18.0929	145.7585
TM-06-239	18.0920	145.7583
TM-06-245	18.0896	145.7572
TM-06-243	18.0888	145.7567

A.3 Kīlauea rift sample locations. Longitude and latitude values are given in decimal degrees. Other rift samples were obtained from the collections of the Smithsonian Institution and the University of Hawai'i.

Sample	Longitude (N)	Latitude (W)
1790N-1F	19.4579	154.9404
1790N-2F	19.4832	154.9015
1790S-1F	19.4432	154.9491
1790S-3S	19.4581	154.9065
1790S-5F	19.4547	154.9156
1790S-2F	19.4460	154.9418
1790S-2S	19.4661	154.8944
1790S-4S	19.4569	154.9097
1790S-6F	19.4126	154.8979
1823SW-F	19.2402	155.4196
1868SW	19.3219	155.3902
MI-07-09	19.3646	155.3371
MI-07-06	19.3188	155.3777
MI-07-05	19.3326	155.3725
MI-07-04	19.3279	155.3645
MI-07-08	19.3491	155.3483
MI-07-02	19.3234	155.3643
MI-07-01	19.3478	155.3550
MI-07-03	19.3248	155.3639
S1971SW-2	19.3339	155.3722
J1974-EV	19.3995	155.2517
NOV. 1979	19.3718	155.2258

A.4 Kīlauea rift sample labels. Sample field numbers with corresponding catalogued Smithsonian Institution (S.I.) numbers.

Field #	S.I. number
8	116253-36
K-61-30	116082-23
H-304	116083-8
H-441	116085-5
M-40	116299-32
Aloi-65-05a	116087-4
HI68-02	116089-2
N68-14	116090-14
N68-11	116090-11
DAS69-3-2	116092-14
DAS70-1213-041	116093-41
DAS71-1213-134	116094-12
MU472-32	116097-32
MU473-108	116098-27
MU474-163	116099-40
KL-77-11	116129-8

A.5 1919-20 Mauna Iki sample descriptions. The eruptive stages and dates from Rowland and Munro (1993) correspond to the 1919-20 samples collected for this study.

- Late stage 1 (MI-07-09 and MI-07-06; December 16 to 23)
- Stage 2a (MI-07-05; December 24 to 29)
- Stage 2b (MI-07-04; December 2 to January 17)
- Stage 3 (MI-07-08; January 18 to April 16)
- Stage 4 (MI-07-02 and MI-07-03; April 17 to August 3)
- Last lava erupted 2-3 weeks after cessation of the active flow field (MI-07-01)

REFERENCES

- Abouchami W., Hofmann A.W., Galer S.J.G., Frey F.A., Eisele J., & Feigenson, M. (2005) Lead isotopes reveal bilateral asymmetry and vertical continuity in the Hawaiian mantle plume. *Nature* 434:851-856.
- Alt J.C. & Teagle D.A.H. (2003) Hydrothermal alteration of upper oceanic crust formed at fast-spreading ridge: mineral, chemical and isotopic evidence from ODP Site 801. *Chemical Geology* 201:191-211.
- Anderson A.T. & Brown G.G. (1993) CO₂ contents and formation pressures of some Kilauean melt inclusions. *American Mineralogist* 78:794-803.
- Andronico D., Branca S., Calvari S., Burton M., Caltabiano T., Corsaro R.A., Del Carlo P., Garfi G., Lodato L., Miraglia L., Mure F., Neri M., Pecora E., Pompilio M., Salerno G., & Spampinato L. (2005) A multi-disciplinary study of the 2002-03 Etna eruption: insights into a complex plumbing system. *Bulletin of Volcanology* 67:314-330.
- Arculus R.J. & Johnson R.W. (1981) Island arc magma sources: a geochemical assessment of the roles of slab-derived components and crustal contamination. *Geochemical Journal* 15:109-133.
- Asimow P.D. & Langmuir C.H. (2003) The importance of water to oceanic mantle melting regimes. *Nature* 421:815-820.
- Ayers J.C., Dittmer S.K., & Layne G.D. (1997) Partitioning of elements between peridotite and H₂O at 2.0-3.0 GPa and 900-1100°C and application to models of subduction zone processes. *Earth and Planetary Science Letters* 150:381-398.
- Bach W., Hegner E., Erzinger J., & Satir M. (1994) Chemical and isotopic variations along the superfast spreading East Pacific Rise from 6 to 30°S. *Contributions to Mineralogy and Petrology* 116:365-380.

- Banks N.G., Koyanagi R.Y., Sinton J.M., & Honma K.T. (1984) The eruption of Mount Pagan volcano, Mariana Islands, 15 May 1981. *Journal of Volcanology and Geothermal Research* 22:225-269.
- Bevens D., Takahashi T.J., & Wright T.L., eds. (1988) The early serial publications of the Hawaiian Volcano Observatory. Hawaii Natural History Association, vol. 1-3, 1224 p.
- Blichert-Toft J., Albarede F., & Frey F. (1999) Hf isotopic evidence for pelagic sediments in the source of Hawaiian basalts. *Science* 285:879-882.
- Blichert-Toft J., Weis D. Maerschalk C., & Albarede F. (2003) Hawaiian hotspot dynamics as inferred from the Hf and Pb isotopic evolution of Mauna Kea volcano. *Geochemistry, Geophysics, Geosystems* 4, doi:10.1029/2002GC000340.
- Bloomer S.H., Stern R.J., & Smoot N.C. (1989) Physical volcanology of the submarine Mariana and volcano arcs. *Bulletin of Volcanology* 51:210-224.
- Bolge L.L., Carr M.J., Feigenson M.D., & Alvarado G.E. (2006) Geochemical stratigraphy and magmatic evolution at Arenal volcano, Costa Rica. *Journal of Volcanology and Geothermal Research* 157:34-48.
- Brenan J.M., Shaw H.F., Ryerson F.J., & Phinney D.L. (1995) Mineral-aqueous fluid partitioning of trace elements at 900°C and 2.0 GPa: constraints on the trace element chemistry of mantle and deep crustal fluids. *Geochimica et Cosmochimica Acta* 59:3331-3350.
- Brigham W.T. (1909) The volcanoes of Kilauea and Mauna Loa on the island of Hawaii, their variously recorded history to the present time. *Memoirs of the Bernice Pauahi Bishop museum* 2. Honolulu, HI: Bishop Museum Press. Reprinted 1974, Kraus Reprint Company, Millwood, NY, 608 p.
- Bryce J. G., DePaolo D. J., & Lassiter J. C. (2005) Geochemical structure of the Hawaiian plume: Sr, Nd, and Os isotopes in the 2.8 km HSDP-2 section of Mauna Kea volcano. *Geochemistry, Geophysics, Geosystems* 6, doi:10.1029/2004GC000809.

- Byers C.D., Garcia M.O., & Muenow D.W. (1985) Volatiles in pillow rim glasses from Loihi and Kilauea volcanoes, Hawaii. *Geochimica et Cosmochimica Acta* 49:1887-1896.
- Cayol V., Dieterich J.H., Okamura A.T., & Miklius A. (2000) High magma storage rates before the 1983 eruption of Kilauea, Hawaii. *Science* 288:2343-2346.
- Chauvel C. & Blichert-Toft J. (2001) A hafnium isotope and trace element perspective on melting of the depleted mantle. *Earth and Planetary Science Letters* 190:137-151.
- Chauvel C., Marini J-C., Plank T., & Ludden J.N. (2009) Hf-Nd input flux in the Izu-Mariana subduction zone and recycling of subducted material in the mantle. *Geochemistry, Geophysics, Geosystems* 10, doi:10.1029/2008GC002101.
- Chen C.-Y. & Frey F.A. (1985) Trace element and isotopic geochemistry of lavas from Haleakala volcano, East Maui, Hawaii: implications for the origin of Hawaiian basalts. *Journal of Geophysical Research* 90:8743-8768.
- Chen C.-Y., Frey F.A., Rhodes J.M. & Eaton R.M. (1996) Temporal geochemical evolution of Kilauea volcano: comparison of Hilina and Puna Basalt. *Geophysical Monograph, American Geophysical Union* 95:161-181.
- Clague D.A., Moore J.G., Dixon J.E., & Friesen W.B. (1995) Petrology of submarine lavas from Kilauea's Puna Ridge, Hawaii. *Journal of Petrology* 36:299-349.
- Cohen A.S. & O'Nions R.K. (1993) Melting rates beneath Hawaii: evidence from uranium series isotopes in recent lavas. *Earth and Planetary Science Letters* 120:169-175.
- Condomines M., Tanguy J.C., & Michaud V. (1995) Magma dynamics at Mt. Etna: constraints from U-Th-Ra-Pb radioactive disequilibria and Sr isotopes in historical lavas. *Earth and Planetary Science Letters* 132:25-41.
- Cooper K.M., Reid M.R., Murrell M.T., & Clague, D.A. (2001) Crystal and magma residence at Kilauea volcano, Hawaii. *Earth and Planetary Science Letters* 184:703-718.

Corwin G., Bonham L.D., Terman M.J., & Viele G.W. (1957) Military geology of Pagan, Mariana Islands: U.S. Army Corps of Engineers, Intelligence Dossier, 259 p.

Dana E.S. (1889) Contributions to the petrography of the Sandwich Islands. *American Journal of Science* 37:441-467.

Davidson J., Turner S., Handley H., Macpherson C., & Dosseto A. (2007) Amphibole “sponge” in arc crust? *Geology* 35:787-790.

Decker R.W. (1987) Dynamics of Hawaiian Volcanoes: an overview. In: Decker, R.W., Wright, T.L., Stauffer P.H. (eds.), *Volcanism in Hawaii*. United States Geological Survey Professional Paper 1350:997-1018.

Delaney P.T., Fiske R.S., Miklius A., Okamura A.T., & Sako M.K. (1990) Deep magma body beneath the summit and rift zones of Kilauea Volcano, Hawaii. *Science* 247:1311-1316.

Delaney P.T., Denlinger R.P., Lisowski M., Miklius A., Okubo P.G., Okamura A.T., & Sako M.K. (1998) Volcanic spreading at Kilauea, 1976-1996. *Journal of Geophysical Research* 103:18003-18023.

Denlinger, R.P. (1997) A dynamic balance between magma supply and eruption rate at Kilauea volcano, Hawaii. *Journal of Geophysical Research* 102:18091-18100.

DePaolo D.J., Bryce J.G., Dodson A., Shuster D. L., & Kennedy B. M. (2001) Isotopic evolution of Mauna Loa and the chemical structure of the Hawaiian plume. *Geochemistry, Geophysics, Geosystems* 3, doi:10.1029/2000GC000139.

Dixon T.H. & Batiza R. (1979) Petrology and geochemistry of recent lavas in the Northern Marianas. *Contrib Mineral Petrol* 70:167-181 Drilling Project. *Journal of Geophysical Research* 101:11729-11746.

Duffield W.A., Christiansen R.L., Koyanagi R.Y., & Peterson D.W. (1982) Storage, migration, and eruption of magma at Kilauea Volcano, Hawaii, 1971-1972. *Journal of Volcanology and Geothermal Research* 13:273-307.

Dungan M.A. & Rhodes J.M. (1978) Residual glasses and melt inclusions in basalts from DSDP legs 45 and 46: evidence for magma mixing. *Contributions to Mineralogy and Petrology* 67:417-431.

Dungan M.A., Wulff A., & Thompson R. (2001) Eruptive stratigraphy of the Tatara-San Pedro Complex, 36°S, Southern Volcanic Zone, Chilean Andes: reconstruction method and implications for magma evolution at long-lived arc volcanic centers. *Journal of Petrology* 42:555-626.

Dvorak J.J. & Dzurisin D. (1993) Variations in magma supply rate at Kilauea volcano, Hawaii. *Journal of Geophysical Research* 98:22255-22268.

Dzurisin D., Koyanagi R.Y., & English T.T. (1984) Magma supply and storage at Kilauea Volcano, Hawaii, 1956-1983. *Journal of Volcanology and Geothermal Research* 21:177-206.

Eaton J.P. & Murata K.J. (1960) How volcanoes grow [Hawaii]. *Science* 132, 925-938.

Eiler J.M., Farley K.A., Valley J.W., Hofmann A.W., & Stolper E.M. (1996) Oxygen isotope constraints on the sources of Hawaiian volcanism. *Earth and Planetary Science Letters* 144:453-468.

Eisele J., Abouchami W., Galer S.J.G., & Hofmann A.W. (2003) The 320 kyr Pb isotope evolution of Mauna Kea lavas recorded in the HSDP-2 drill core. *Geochemistry, Geophysics, Geosystems* 4, doi:10.1029/2002GC000339.

Elburg M & Foden J (1998) Temporal changes in arc magma geochemistry, northern Sulawesi, Indonesia. *Earth and Planetary Science Letters* 163:381-398.

Elliott T., Plank T., Zindler A., White W., & Bourdon B. (1997) Element transport from slab to volcanic front at the Mariana arc. *Journal of Geophysical Research* 102:14991-15019.

Farnetani C.G., Legras B., & Tackley P.J. (2002) Mixing and deformation in mantle plumes. *Earth and Planetary Science Letters* 196:1-15.

Fekiacova A., Abouchami W., Galer S.J.G., Garcia M.O., & Hofmann A.W. (2007) Origin and temporal evolution of Koolau volcano, Hawaii: inferences from isotope data on the Koolau

Scientific Drilling Project (KSDP), the Honolulu Volcanics and ODP Site 843. *Earth and Planetary Science Letters* 261:65-83.

Figueroa O., Deruelle B., & Demaiffe D. (2009) Genesis of adakite-like lavas of Licancabur volcano (Chile-Bolivia, Central Andes) *Comptes Rendus Geoscience* 341:310-318.

Fiske R.S. & Kinoshita W.T. (1969) Inflation of Kilauea Volcano prior to its 1967-1968 eruption. *Science* 165:341-349.

Fiske R.S., Simkin T., & Nielsen E. A. (1987) *The Volcano Letter*. Washington, DC: Smithsonian Institution Press, 530 p.

Francalanci L., Tommasini S., Conticelli S., & Davies G.R. (1999) Sr isotope evidence for short magma residence time for the 20th century activity at Stromboli Volcano, Italy. *Earth and Planetary Science Letters* 167:61-69.

Frey F.A. & Rhodes J.M. (1993) Intersield geochemical differences among Hawaiian volcanoes: implications for source compositions, melting process and magma ascent paths. *Philosophical Transactions of the Royal Society of London* 342:121-136.

Gaffney A.M., Nelson B.K., & Blichert-Toft J. (2004) Geochemical constraints on the role of oceanic lithosphere in intra-volcano heterogeneity at West Maui, Hawaii. *Journal of Petrology* 45:1663–1687.

Gaffney A.M., Nelson B.K., & Blichert-Toft J. (2005) Melting in the Hawaiian plume at 1-2 Ma as recorded at Maui Nui: The role of eclogite, peridotite, and source mixing. *Geochemistry, Geophysics, Geosystems* 6, doi:10.1029/2005GC000927.

Galer S.J.G. & Abouchami W. (1998) Practical application of lead triple spiking for correction of instrumental mass discrimination. *Mineralogical Magazine* 62A:491-492.

Garcia M.O., Ho R.A., Rhodes J.M., & Wolfe E.W. (1989) Petrologic constraints on rift zone processes: results from episode 1 of the Puu Oo eruption of Kilauea volcano, Hawaii. *Bulletin of Volcanology* 52:81-96.

- Garcia M.O., Rhodes J.M., Ho R.A., Ulrich G., & Wolfe E.W. (1992) Petrology of lavas from episodes 2-47 of the Puu Oo eruption of Kilauea volcano, Hawaii: evaluation of magmatic processes. *Bulletin of Volcanology* 55:1-16.
- Garcia M.O., Rhodes J.M., Trusdell F.A., & Pietruszka A.P. (1996) Petrology of lavas from the Puu Oo eruption of Kilauea volcano: III. The Kupaianaha episode (1986-1992) *Bulletin of Volcanology* 58:359-379.
- Garcia M.O., Ito E., Eiler J., & Pietruszka A. (1998) Crystal contamination of Kilauea volcano magmas revealed by oxygen isotope analysis of glass and olivine from the Puu Oo eruption lavas. *Journal of Petrology* 39:803-817.
- Garcia M.O., Pietruszka A.J., Rhodes J.M., & Swanson K. (2000) Magmatic processes during the prolonged Puu Oo eruption of Kilauea volcano, Hawaii. *Journal of Petrology* 41: 967-990.
- Garcia M.O. (2002) Submarine picritic basalts from Koolau volcano, Hawaii: implications for parental magma composition and mantle source. In Takahashi, E., Lipman, P. W., Garcia, M. O., Naka, J., Aramaki, S. (eds.) *Hawaiian Volcanoes: Deep Underwater Perspectives*. Geophysical Monographs, American Geophysical Union 128:391-401.
- Garcia M.O., Pietruszka A.J., & Rhodes J.M. (2003) A petrologic perspective of Kilauea volcano's summit magma reservoir. *Journal of Petrology* 44:2313-2339.
- Garcia M.O., Ito E., & Eiler J.M. (2008) Oxygen isotope evidence for chemical interaction of Kilauea historical magmas with basement rocks. *Journal of Petrology*, 49:757-769.
- George R., Turner S., Hawkesworth C., Morris J., Nye C., Ryan J., & Zheng S-H. (2003) Melting processes and fluid and sediment transport rates along the Alaska-Aleutian arc from an integrated U-Th-Ra-Be isotope study. *Journal of Geophysical Research* 108 (B5), doi 10:1029/2002JB001916.
- Ghiorso M.S. & Sack R.O. (1995) Chemical mass transfer in magmatic systems IV. A revised and internally consistent thermodynamic model for the interpolation and extrapolation of liquid-

solid equilibria in magmatic systems at elevated temperatures and pressures. *Contributions to Mineralogy and Petrology* 119:197-212.

Gill J.B. (1981) *Orogenic andesite and plate tectonics*. Springer, Berlin Heidelberg New York 390 p.

Harris A.J.L., Keszthelyi L., Flynn L.P., Mougini-Mark P.J., Thornber C., Kauahikaua J., Sherrod D., Trusdell F., Sawyer M.W., & Flament P. (1997) Chronology of the episode 54 eruption at Kilauea volcano, Hawaii, from GOES-9 satellite data. *Geophysical Research Letters*, 24:3281-3284.

Hauri E.H. (1996) Major-element variability in the Hawaiian mantle plume. *Nature* 382, 415-419.

Hawkesworth C.J., Hergt J.M., Ellam R.M., & McDermott F (1991) Element fluxes associated with subduction related magmatism. *Philosophical Transactions of the Royal Society of London* 335:393-405.

Heliker C., Mangan M.T., Mattox T.N., Kauahikaua J.P., & Helz R.T. (1998) The character of long-term eruptions: inferences from episodes 50-53 of the Puu Oo-Kupaianaha eruption of Kilauea volcano. *Bulletin of Volcanology* 59:381-393.

Heliker C. & Mattox, T.N. (2003) The first two decades of the Puu Oo-Kupaianaha eruption; chronology and selected bibliography in: Heliker, C., Swanson, D. A., Takahashi, T. J. (eds.), *The Puu Oo-Kupaianaha Eruption of Kilauea volcano, Hawaii: The first 20 years*, United States Geological Survey Professional Paper 1676:121-136.

Helz R.T. (1987) Differentiation behavior of Kilauea Iki lava lake, Kilauea Volcano, Hawaii: an overview of past and current work. *The Geochemical Society, Special Publication* 1:241-258.

Helz R.T. & Wright T.L. (1992) Differentiation and magma mixing on Kilauea's east rift zone: a further look at the eruptions of 1955 and 1960. Part 1. The late 1955 lavas. *Bulletin of Volcanology* 54:361-384.

Hemond, C., Hofmann, A.W., Heusser, G., Condomines, M., Raczek, I. & Rhodes, J.M. (1994)

U-Th-Ra systematics in Kilauea and Mauna Loa tholeiites. *Chemical Geology* 116:163-180.

Herzberg C. (2006) Petrology and thermal structure of the Hawaiian plume: a view from Mauna Kea. *Nature* 444:605-609.

Hickey-Vargas R. & Reagan M.K. (1987) Temporal variation of isotope and rare earth element abundances in volcanic rocks from Guam: implications for the evolution of the Mariana Arc. *Contributions to Mineralogy and Petrology* 97:497-508.

Hirose K. & Kushiro I. (1993) Partial melting of dry peridotites at high pressure: determination of composition of melts segregated from peridotite using aggregates of diamonds. *Earth and Planetary Science Letters* 114:477-489.

Ho R. & Garcia M.O. (1988) Origin of differentiated lavas at Kilauea Volcano, Hawaii: implications from the 1955 Eruption. *Bulletin of Volcanology* 50:35-46.

Hofmann A.W., Feigenson M.D., & Raczek I. (1984) Case studies on the origin of basalt, III, Petrogenesis of the Mauna Ulu eruption, Kilauea, 1969-1971. *Contributions to Mineralogy and Petrology* 88:24-35.

Hofmann A.W. (1988) Chemical differentiation of the Earth: the relationship between mantle, continental crust, and oceanic crust. *Earth and Planetary Science Letters* 90:297-314.

Hofmann A.W. (1997) Mantle geochemistry: the message from oceanic volcanism. *Nature* 385:219-229.

Holcomb R.T. (1987) Eruptive history and long-term behavior of Kilauea Volcano. In: Decker, R.W., Wright, T.L., Stauffer P.H. (eds.), *Volcanism in Hawaii*. United States Geological Survey Professional Paper 1350:261-350.

Huang S. & Frey F.A. (2005) Recycled oceanic crust in the Hawaiian plume: evidence from temporal geochemical variations within the Koolau Shield. *Contributions to Mineralogy and Petrology* 149:556-575.

Ishikawa T. & Tera F. (1999) Two isotopically distinct fluid components involved in the Mariana arc: evidence from Nb/B ratios and B, Sr, Nd, and Pb isotope systematics. *Geology* 27:83-86.

Ishizuka O., Taylor R.N., Yuasa M., Milton J.A., Nesbitt R.W., Uto K., & Sakamoto I. (2007) Processes controlling along-arc isotopic variation of the southern Izu-Bonin arc. *Geochemistry, Geophysics, Geosystems* 8, doi:10.1029/2006GC001475.

Jackson D.B., Swanson D.A., Koyanagi R.Y., & Wright T.L. (1975) The August and October 1968 East Rift Eruptions of Kilauea Volcano, Hawaii. United States Geological Survey Professional Paper 890. 33 p.

Jaggard T.A. (1920) Monthly bulletin of the Hawaiian Volcano Observatory 8:89-95.

Jicha B.R., Singer B.S., Brophy J.G., Fournelle J.H., Johnson C.M., Beard B.L., Lapen T.J., & Mahlen N.J. (2004) Variable impact of the subducted slab on Aleutian Island arc magma sources: evidence from Sr, Nd, Pb, and Hf isotopes and trace element abundances. *Journal of Petrology* 45:1845-1875.

Jicha B.R., Hart G.L., Johnson C.M., Hildreth W., Beard B.L., Shirey S.B., & Valley J.W. (2008) Isotopic and trace element constraints on the petrogenesis of lavas from the Mount Adams volcanic field, Washington. *Contributions to Petrology and Mineralogy* 157:189-207.

Johnson D.M., Hooper P.R., & Conrey R.M. (1999) XRF analysis of rocks and minerals for major and trace elements on a single low dilution Li-tetraborate fused bead. *Advances in X-ray Analysis* 41:843-867.

Johnson M.C. & Plank T. (1999) Dehydration and melting experiments constrain the fate of subducted sediments. *Geochemistry, Geophysics, Geosystems* 1, doi:10.1029/1999GC000014.

Jolly, W.T., Lidiak E.G., Dickin A.P., & Wu T-W. (2001) Secular geochemistry of central Puerto Rican island arc lavas: constraints on Mesozoic tectonism in the eastern Greater Antilles. *Journal of Petrology* 42:2197-2214.

- Jolly W.T., Lidiak E.G., Dickin A.P., & Way T-W. (2002) Recycling in the Puerto Rican mantle wedge, Greater Antilles island arc. *The Island Arc* 11:10-24.
- Karig D.E. (1971) Structural history of the Mariana Island Arc system. *Geological Society of American Bulletin* 82:323-344.
- Kelemen P.B., Yogodzinski G.M., & Scholl D.W. (2003) Along-strike variations in the Aleutian island arc: genesis of high Mg# andesite and implications for continental crust. Tracers of the slab. In: Eiler J (ed) *Inside the subduction factory*, vol 138. American Geophysical Union, Geophysical Monograph, Washington DC, p. 223-276.
- Kent A.J.R. & Elliott T.R. (2002) Melt inclusions from Marianas arc lavas: implications for the composition and formation of island arc magmas. *Chemical Geology* 183:263-286.
- Keppler H. (1996) Constraints from partitioning experiments on the composition of subduction-zone fluids. *Nature* 380:237-240.
- Kessel R., Schmidt M.W., Ulmer P., & Pettke T. (2005) Trace element signature of subduction-zone fluids, melts and supercritical liquids at 120-180 km depth. *Nature* 437:724-727.
- King A. J., Waggoner D. G., & Garcia M. O. (1993) Geochemistry and petrology of basalts from Leg 136, central Pacific Ocean. In: Wilkens, R. H., Firth, J., Bender, J., et al. (eds.) *Proceedings of the Ocean Drilling Program, Scientific Results 136*. College Station, TX: Ocean Drilling Program, p. 107-118.
- Klein F.W., Koyanagi R.Y., Nakata J.S. & Tanigawa W.R. (1987) The seismicity of Kilauea's magma system. *United States Geological Survey Professional Paper* 1350:1019-1185.
- Knaack C., Cornelius S.B., & Hooper P.R. (1994) Trace element analyses of rocks and minerals by ICP-MS. In: Open file report, GeoAnalytical Lab, Washington State University.
- Kohut E.J., Stern R.J., Kent A.J.R., Nielsen R.L., Bloomer S.H., & Matthew L. (2006) Evidence for adiabatic decompression melting in the southern Mariana arc from high-Mg lavas and melt inclusions. *Contributions to Mineralogy and Petrology* 152:201-221.

- Koyanagi R.Y., Chouet B., & Aki K. (1987) Origin of volcanic tremor in Hawaii: Part 1. Data from the Hawaiian Volcano Observatory, 1969-1985. In: Decker, R.W., Wright, T.L., Stauffer P.H. (eds.), *Volcanism in Hawaii*. United States Geological Survey Professional Paper 1350:1221-1257.
- Kurz M.D. & Kammer D.P. (1991) Isotopic evolution of Mauna Loa volcano. *Earth and Planetary Science Letters* 103:257-269.
- Kurz M.D., Kenna T.C., Kammer D.P., Rhodes J.M., & Garcia M.O. (1995) Isotopic evolution of Mauna Loa Volcano: a view from the submarine southwest rift zone. *Geophysical Monograph, American Geophysical Union* 92:289-306.
- Kurz M.D., Curtice J., Lott III D.E., & Solow A. (2004) Rapid helium isotopic variability in Mauna Kea shield lavas from the Hawaiian Scientific Drilling Project. *Geochemistry, Geophysics, Geosystems* 5, doi:10.1029/2002GC000439.
- Kushiro I. (1996) Partial melting of fertile mantle peridotite at high pressures: an experimental study using aggregates of diamond. *Geophysical Monograph, American Geophysical Union* 95:109-122.
- Larson E.E., Reynolds R., Merrill R., Levi S., Ozima M., Aoki Y., Kinoshita H., Zasshu S., Kawai N., Nakajima T., & Hirooka D. (1974) Major-element petrochemistry of some extrusive rocks from the volcanically active Mariana Islands. *Bulletin of Volcanology* 38:361-377.
- Lassiter J.C., DePaolo D.J., & Tatsumoto M. (1996) Isotopic evolution of Mauna Kea volcano: results from the initial phase of the Hawaii Scientific Drilling Project. *Journal of Geophysical Research* 101:11769-11780.
- Lassiter J.C. & Hauri E.H. (1998) Osmium-isotope variations in Hawaiian lavas: evidence for recycled oceanic lithosphere in the Hawaiian plume. *Earth and Planetary Science Letters* 164:483-496.

- Lin P-N. (1992) Trace element and isotopic characteristics of western Pacific pelagic sediments: implications for the petrogenesis of Mariana Arc magmas. *Geochimica et Cosmochimica Acta* 56:1641-1654.
- Lockwood J.P., Tilling R.I., Klein F., Okamura, A.T., & Peterson D.W. (1999) Magma migration and resupply during the 1974 summit eruptions of Kilauea, Volcano, Hawaii. United States Geological Survey Professional Paper 1613. 37 p.
- Longhi, J. (2002) Some phase equilibria systematics of lherzolite melting: I, *Geochemistry, Geophysics, Geosystems* 2, doi:10.1029/2001GC000204.
- Macdonald G.A. & Katsura T (1961) Variations in the lava of the 1959 eruption of Kilauea Iki. *Pacific Science* 15:358-369.
- Macdonald G.A. & Eaton J.P. (1964) Hawaiian volcanoes during 1955. *United States Geological Survey Bulletin* 1171:1-170.
- Macdonald G. A., Abbott A. T., & Peterson F. L. (1983) *Volcanoes in the Sea: the Geology of Hawaii*. Honolulu, HI: University of Hawaii Press. 517 p.
- Macpherson C.G., Dreher S.T., & Thirlwall M.F. (2006) Adakites without slab melting: high pressure differentiation of island arc magma, Mindanao, the Philippines. *Earth and Planetary Science Letters* 243:581-593.
- Mahoney J.J., Sinton J.M., Kurz M.D., Macdougall J.D., Spencer K.J., & Lugmair G.W. (1994) Isotope and trace element characteristics of a super-fast spreading ridge: East Pacific Rise, 13-23°S. *Earth and Planetary Science Letters* 121:173-193.
- Mangan M.T. (1990) Crystal size distribution systematics and the determination of magma storage times: the 1959 eruption of Kilauea volcano, Hawaii. *Journal of Volcanology and Geothermal Research* 44:295-302.
- Marchesi C., Garrido C.J., Bosch D., Proenza J.A., Gervilla F., Monie P., & Rodriguez-Vega A. (2007) Geochemistry of Cretaceous magmatism in eastern Cuba: recycling of North American

continental sediments and implications for subduction polarity in the Greater Antilles paleo-arc. *Journal of Petrology* 48:1813-1840.

Marske J.P., Pietruszka A.J., Weis D., Garcia M.O., & Rhodes, J.M. (2007) Rapid passage of a small-scale heterogeneity through the melting regions of Kilauea and Mauna Loa volcanoes, Hawaii. *Earth and Planetary Science Letters* 259:34-50.

Marske J.P., Garcia M.O., Pietruszka A.J., Rhodes J.M., & Norman M.D. (2008) Geochemical variations during Kilauea's Puu Oo eruption reveal a fine-scale mixture of mantle heterogeneities within the Hawaiian Plume. *Journal of Petrology* 49:1297-1318.

McBirney A.R., Taylor H.P. & Armstrong R.L. (1987) Paricutin re-examined; a classic example of crustal assimilation in calc-alkaline magma. *Contributions to Mineralogy and Petrology* 95:4-20.

McKenzie D. (1985) ^{230}Th - ^{238}U disequilibrium and the melting processes beneath ridge axes. *Earth and Planetary Science Letters* 72:149-157.

Meijer A (1976) Pb and Sr isotopic data bearing on the origin of volcanic rocks from the Mariana island-arc system. *Geological Society of American Bulletin* 87:45-51.

Meijer A. & Reagan M. (1981) Petrology and geochemistry of the island of Sarigan in the Mariana Arc: calc-alkaline volcanism in an oceanic setting. *Contributions to Mineralogy and Petrology* 77:337-354.

Mittelstaedt E. & Garcia M.O. (2007) Modeling the sharp compositional interface in the Puu Oo magma reservoir, Kilauea volcano, Hawaii. *Geochemistry, Geophysics, Geosystems* 8, doi:10.1029/2006GC001519.

Moore J.G. & Ault W.U. (1965) Historic littoral cones in Hawaii. *Pacific Science* 19, 3-11.

Moore R.B., Helz R.T., Dzurisin D., Eaton G.P., Koyanagi R.Y., Lipman P.W., Lockwood J.P., & Puniwai G.S. (1980) The 1977 eruption of Kilauea volcano, Hawaii. *Journal of Volcanology and Geothermal Research* 7:189-210.

- Moore R.B. & Trusdell F.A. (1991) Geologic map of the lower east rift zone of Kilauea volcano, Hawaii. United States Geological Survey Map I-2225 (1:24000).
- Nakata J.S., Heliker C. & Sherrod D.R. (2000) Hawaiian Volcano Observatory; Summary 99; Part 1, Seismic data, January to December 1999, with a chronological summary. United States Geological Survey Report OF 00-0433, 61 p.
- Naumann T.R. & Geist D.J. (1999) Generation of alkali-olivine basalts by fractionation of tholeiitic magma. *Geology* 27:423-426.
- Nicholls J. & Stout M.Z. (1988) Picritic melts in Kilauea-Evidence from the 1967-1968 Halemaumau and Hiiaka eruptions. *Journal of Petrology* 29:1031-1057.
- Nicholls J. & Russell J.K. (1991) Major-element chemical discrimination of magma-batches in lavas from Kilauea Volcano, Hawaii, 1954-1971 eruptions. *Canadian Mineralogist* 29:981-993.
- Nielsen R.L. (1992) BIGD: a FORTRAN program to calculate trace-element partition coefficients for natural mafic and intermediate composition magmas. *Computer Geoscience* 18: 773-788.
- Nielsen R.L., Gallahan W.E., & Newberger F. (1992) Experimentally determined mineral-melt partition coefficients for Sc, Y and REE for olivine, orthopyroxene, pigeonite, magnetite and ilmenite. *Contributions to Mineralogy and Petrology* 110:488-499.
- Norman M.D., Griffin W.L., Pearson N.J., Garcia M.O., & O'Reilly S.Y. (1998) Quantitative analysis of trace element abundances in glasses and minerals: a comparison of laser ablation ICPMS, solution ICPMS, proton microprobe, and electron microprobe data. *Journal of Analytical Atomic Spectrometry* 13:477-482.
- Okano O. & Tatsumoto M. (1996) Petrogenesis of ultramafic xenoliths from Hawaii inferred from Sr, Nd, and Pb isotopes. *Geophysical Monograph, American Geophysical Union* 95:135-147.

- Peate D.W. & Pearce J.A. (1998) Causes of spatial compositional variations in Mariana arc lavas: trace element evidence. *The Island Arc* 7:479-495.
- Peccerillo A., Frezzotti M.L., De Astis G., & Ventura G. (2006) Modeling the magma plumbing system of Vulcano (Aeolian Islands, Italy) by integrated fluid-inclusion geobarometry, petrology, and geophysics. *Geology* 34:17-20.
- Phinney W.C. & Morrison D.A. (1990) Partition coefficients of calcic plagioclase: implications for Archean anorthosites. *Geochimica et Cosmochimica Acta* 54:1639-1654.
- Pietruszka A.P. & Garcia M.O. (1999a) A rapid fluctuation in the mantle source and melting history of Kilauea volcano inferred from the geochemistry of its historical summit lavas (1790-1982). *Journal of Petrology* 40:1321-1342.
- Pietruszka A.P. & Garcia M.O. (1999b) The size and shape of Kilauea volcano's summit magma storage reservoir: a geochemical probe. *Earth and Planetary Science Letters* 167:311-320.
- Pietruszka A.P., Rubin K.H., & Garcia M.O. (2001) ^{226}Ra - ^{230}Th - ^{238}U disequilibria of historical Kilauea lavas (1790-1982) and the dynamics of mantle melting within the Hawaiian plume. *Earth and Planetary Science Letters* 186:15-31.
- Pietruszka A.J., Hauri E.H., Carlson R.W., & Garcia M.O. (2006) Remelting of recently depleted mantle within the Hawaiian plume inferred from the ^{226}Ra - ^{230}Th - ^{238}U disequilibria of Puu Oo eruption lavas. *Earth and Planetary Science Letters* 244:155-169.
- Plank T. & Langmuir C. (1998) The chemical composition of subducting sediment and its consequence for the crust and mantle. *Chemical Geology* 145:325-394.
- Poland M., Miklius A., Orr T., Sutton J., Thornber C. & Wilson D. (2008) New episodes of volcanism at Kilauea volcano, Hawaii. *EOS* 89:37-38.
- Portnyagin M., Hoernle K., Plechov P., Mironov N., & Khubunaya S. (2007) Constraints on mantle melting and composition, and nature of slab components in volcanic arcs from volatiles

- (H₂O, S, Cl, F) and trace elements in melt inclusions from the Kamchatka Arc. *Earth and Planetary Science Letters* 255:53-69.
- Powers H. (1955) Composition and origin of basaltic magma of the Hawaiian Islands. *Geochimica et Cosmochimica Acta* 7:77-107.
- Putirka K. (1997) Magma transport at Hawaii: inferences based on igneous thermobarometry. *Geology* 25:69-72.
- Reagan M.K., Hanan B.B., Heizler M.T., Hartman B.S., & Hickey-Vargas R. (2008) Petrogenesis of volcanic rocks from Saipan and Rota, Mariana Islands, and implications for the evolution of the Nascent Island Arcs. *Journal of Petrology* 49:441-464.
- Reiners P. W. (2002) Temporal-compositional trends in intraplate basalt eruptions: implications for mantle heterogeneity and melting processes. *Geochemistry, Geophysics, Geosystems* 3, doi:10.1029/2001GC000250.
- Ren Z.-Y., Tomoyuki S., Masako Y., Johnson K.M., & Takahashi E. (2006) Isotope compositions of submarine Hana Ridge lavas, Haleakala volcano, Hawaii: Implications for source compositions, melting process and the structure of the Hawaiian plume. *Journal of Petrology* 47:255-275.
- Rhodes J.M., Wenz K.P., Neal C.A., Sparks J.W., & Lockwood J.P. (1989) Geochemical evidence for invasion of Kilauea's plumbing system by Mauna Loa magma. *Nature* 337:257-260.
- Rhodes J.M. & Hart S.R. (1995) Episodic trace element and isotopic variations in historical Mauna Loa lavas: implications for magma and plume dynamics. *American Geophysical Union Geophysical Monograph* 92:263-286.
- Rhodes J.M. (1996) Geochemical stratigraphy of lava flows sampled by the Hawaii Scientific Drilling Project. *Journal of Geophysical Research* 101:11729-11746.

- Rhodes J.M. & Vollinger M.J. (2004) Composition of basaltic lavas sampled by phase-2 of the Hawaii Scientific Drilling Project: Geochemical stratigraphy and magma types. *Geochemistry, Geophysics, Geosystems* 5, doi:10.1029/2002GC000434.
- Rhodes J.M. & Vollinger M.J. (2005) Ferric/ferrous ratios in 1984 Mauna Loa lavas: a contribution to understanding the oxidation state of Hawaiian magmas. *Contributions to Mineralogy and Petrology* 149:666-674.
- Rizzo, A., Caracausi, A., Favara, R., Martelli, M., Paonita, A., Paternoster, M., Nuccio, P.M. & Rosciglione, A. (2006) New insights into magma dynamics during the last two eruptions of Mount Etna as inferred by geochemical monitoring from 2002 to 2005. *Geochemistry, Geophysics, Geosystems* 7, doi:10.1029/2005GC001175.
- Roeder P.L. & Emslie R.F. (1970) Olivine-liquid equilibrium. *Contributions to Mineralogy and Petrology* 29:275-289.
- Roeder P.L., Thornber C., Poustovetov A., & Grant A. (2003) Morphology and composition of spinel in Puu Oo lava (1996-1998), Kilauea volcano, Hawaii. *Journal of Volcanology and Geothermal Research* 123:245-265.
- Romick, J.D., Perfit M.R., Swanson S.E., & Schuster, R.D. (1990) Magmatism in the eastern Aleutian arc: temporal characteristics of igneous activity on Akutan island. *Contributions to Mineralogy and Petrology* 104:700–721.
- Rowland S.K. & Munro D.C. (1993) The 1919-1920 eruption of Mauna Iki, Kilauea: chronology, geologic mapping, and magma transport mechanisms. *Bulletin of Volcanology* 55:190-203.
- Ryan J.G., Morris J., Bebout G., & Leeman W.P. (1996) Describing chemical fluxes in subduction zones: insights from “depth profiling” studies of arc and forearc rocks. In: Bebout G (ed) *Subduction: Top to Bottom*, vol. 96 American Geophysical Union, Geophysical Monograph, Washington DC, p. 263-268.

- Ryan M.P., Koyanagi R.Y., & Fiske R.S. (1981) Modeling the three-dimensional structure of macroscopic magma transport systems: application to Kilauea Volcano, Hawaii: *Journal of Geophysical Research* 86:7111-7129.
- Ryan M.P. (1988) The mechanics and three-dimensional internal structure of active magmatic systems: Kilauea Volcano, Hawaii. *Journal of Geophysical Research* 93:4213-4248.
- Rychert C.A., Fischer, K.M., Abers, G.A., Plank T., Syracuse E., Protti J.M., Gonzalez V., & Strauch W. (2008) Strong along-arc variations in attenuation in the mantle wedge beneath Costa Rica and Nicaragua. *Geochemistry, Geophysics, Geosystems* 9, doi:10.1029/2008GC002040.
- Salters V.J.M. & Longhi J. (1999) Trace element partitioning during the initial stages of melting beneath mid-ocean ridges. *Earth and Planetary Science Letters* 166:15-30.
- Shamberger P.J. & Garcia M.O. (2006) Geochemical modeling of magma mixing and magma reservoir volumes during early episodes of Kilauea volcano's Puu Oo eruption. *Bulletin of Volcanology* 69:345-352.
- Sharp R.P., Dzurisin D., & Malin, M.C. (1987) An early 19th century reticulate pumice from Kilauea Volcano. In: Decker, R.W., Wright, T.L., Stauffer P.H. (eds.), *Volcanism in Hawaii*. United States Geological Survey Professional Paper 1350:997-1018.
- Shaw D.M. (1970) Trace element fractionation during anatexis. *Geochimica et Cosmochimica Acta* 34:237-243.
- Shaw A.M., Hauri E.H., Fischer T.P., Hilton D.R., & Kelley K.A. (2008) Hydrogen isotopes in Mariana arc melt inclusions: implications for subduction dehydration and the deep-Earth water cycle. *Earth and Planetary Science Letters* 275:138-145.
- Sigmarsson O., Condomines M., & Fourcade S. (1992) A detailed Th, Sr and O isotope study of Hekla; differentiation processes in an Icelandic volcano. *Contributions to Mineralogy and Petrology* 112:20-34.

- Sigmarsson O., Condomines M., & Bachelery P. (2005) Magma residence time beneath the Piton de la Fournaise Volcano, Reunion Island, from U-series disequilibria. *Earth and Planetary Science Letters* 234:223-234.
- Simkin T., Siebert L., McClelland L., Bridge D., Newhall C., & Latter J.H. (1981) *Volcanoes of the World*. Smithsonian Institution, Stroudsburg, PA 232 p.
- Sims K. W. W., DePaolo D. J., Murrell M. T., Baldrige W. S., Goldstein S., Clague D., & Jull M. (1999) Porosity of the melting zone and variations in the solid mantle upwelling rate beneath Hawaii: inferences from the ^{238}U - ^{230}Th - ^{226}Ra and ^{235}U - ^{231}Pa disequilibria. *Geochimica et Cosmochimica Acta* 63:4119-4138.
- Sisson T.W. (1994) Hornblende-melt trace-element partitioning measured by ion microprobe. *Chemical Geology* 117:331-344.
- Smith P.M. & Asimow P.D. (2005) Adibat_1ph: A new public front-end to the MELTS, pMELTS, and pHMELTS models. *Geochemistry, Geophysics, Geosystems* 6, doi:10.1029/2004GC000816.
- Sobolev A.V., Hofmann A.W., Sobolev S.V., & Nikogosian I.K. (2005) An olivine-free mantle source of Hawaiian shield basalts. *Nature* 434:590-597.
- Sobolev A.V., Hofmann A.W., Kuzmin D.V., Yaxley G.M., Arndt N.T., Chung S.-L., Danyushevsky L.V., Elliott T., Frey F.A., Garcia M.O., Gurenko A.A., Kamenetsky V.S., Kerr A.C., Krivolutskaya N.A., Matvienkov V.V., Nikogosian I.K., Rocholl A., Sigurdsson I.A., Sushchevskaya N.M. & Teklay M. (2007) The amount of recycled crust in sources of mantle-derived melts. *Science* 316:412-417.
- Stern C.R. & Kilian R. (1996) Role of the subducted slab, mantle wedge and continental crust in the generation of adakites from the Andean Austral Volcanic Zone. *Contributions to Mineralogy and Petrology* 123:263-281.

Stern R.J., Fouch M.J., & Klemperer S. (2003) An overview of the Izu-Bonin-Mariana subduction factory. In: Eiler J, Hirschmann M (eds.) Inside the subduction factory, vol 138. AGU Monograph, Washington DC, p. 175-222.

Stern R.J., Kohut E., Bloomer S.H., Leybourne M., Fouch M., & Vervoort J. (2006) Subduction factory processes beneath the Guguan cross-chain, Mariana Arc: no role for sediments, are serpentinites important? *Contributions to Mineralogy and Petrology* 151:202-221.

Stille P., Unruh D.M., & Tatsumoto M. (1986) Pb, Sr, Nd, and Hf isotopic constraints on the origin of Hawaiian basalts and evidence for a unique mantle source. *Geochimica et Cosmochimica Acta* 50:2303-2319.

Stolper E.M., DePaolo D.J., & Thomas D.M. (1996) Introduction to special section; Hawaii Scientific Drilling Project. *Journal of Geophysical Research* 101:11593-11598.

Stolper, E.M., Sherman, S., Garcia, M.O., Baker, M. & Seaman, C. (2004) Glasses in the submarine section of the HSDP-2 drill core, Hilo, Hawaii. *Geochemistry, Geophysics, Geosystems* 5, doi:10.1029/2003GC000553.

Stroncik N.A., Klugel A., & Hansteen T.H. (2009) The magmatic plumbing system beneath El Hierro (Canary Islands): constraints from phenocrysts and naturally quenched basaltic glasses in submarine rocks. *Contributions to Mineralogy and Petrology* 157:593-607.

Sun S.S. & McDonough W.F. (1989) Chemical and isotopic systematics of oceanic basalts: implications for mantle composition and processes. In: Saunders, AD, Norry MJ (eds.) *Magmatism in the Ocean Basins*. Geological Society of London Special Publication 42:315-345.

Sutton J.A., Elias T., & Kauahikaua J. (2003) Lava-effusion rates for the Puu Oo-Kupaianaha eruption derived from SO₂ emissions and very low frequency (VLF) measurements. In: Heliker, C., Swanson, D. A., Takahashi, T. J. (eds.), *The Puu Oo-Kupaianaha Eruption of Kilauea Volcano, Hawaii: The first 20 years*, United States Geological Survey Professional Paper 1676:121-136.

- Swanson D.A., Duffield W.A., Jackson D.B., & Peterson D.W. (1979) Chronological narrative of the 1969-1971 Mauna Ulu eruption of Kilauea volcano, Hawaii. United States Professional Paper 1056. 55 p.
- Swanson D.A. (2008) Hawaiian oral tradition describes 400 years of volcanic activity at Kilauea. *Journal of Volcanology and Geothermal Research* 176:427-431.
- Takahashi, E. & Nakajima, K. (2002) Melting process in the Hawaiian plume; an experimental study. In: Takahashi, E., Lipman, P. W., Garcia, M. O., Naka, J., Aramaki, S. (eds.), *Hawaiian Volcanoes: Deep Underwater Perspectives*. American Geophysical Union Geophysical Monographs 128:403-418.
- Tatsumoto M. (1978) Isotopic composition of lead in oceanic basalt and its implication to mantle evolution. *Earth and Planetary Science Letters* 38:63–87.
- Teasdale R., Geist D., Kurz M., & Harpp K. (2005) 1998 eruption at Volcan Cerro Azul, Galapagos Islands: 1. Syn-eruptive petrogenesis. *Bulletin of Volcanology* 67:170-185.
- Thirlwall M.F. (2002) Multicollector ICP-MS analysis of Pb isotopes using a ^{207}Pb - ^{204}Pb double spike demonstrates up to 400ppm/amu systematic errors in Tl-normalization. *Chemical Geology* 184:255-274.
- Thornber C.R. (2001) Olivine-liquid relations of lava erupted by Kilauea volcano from 1994 to 1998: implications for shallow magmatic processes associated with the ongoing East-Rift-Zone eruption. *The Canadian Mineralogist* 39:239-266.
- Thornber C.R. (2003) Magma-reservoir processes revealed by geochemistry of the Puu Oo-Kupaianaha eruption in: Heliker, C., Swanson, D. A., Takahashi, T. J. (eds.), *The Puu Oo-Kupaianaha Eruption of Kilauea Volcano, Hawaii: The first 20 years*, United States Geological Survey Professional Paper 1676:121-136.

Thornber C.R., Heliker C., Sherrod D.R., Kauahikaua J.P., Miklius A., Okubo P.G., Trusdell F.A., Budahn J.R., Ridley W.I., & Meeker G.P. (2003) Kilauea East Rift Zone magmatism; an episode 54 perspective. *Journal of Petrology* 44:1525-1559.

Tilling R.I., Christiansen R.L., Duffield W.A., Endo E.T., Holcomb R.T., Koyanagi R.Y., Peterson D.W., & Unger J.D. (1987) The 1972-1974 Mauna Ulu eruption, Kilauea Volcano: An example of quasi-steady-state magma transfer. In: Decker, R.W., Wright, T.L., Stauffer P.H. (eds.), *Volcanism in Hawaii*. United States Geological Survey Professional Paper 1350:405-469.

Tilling R.I., Wright T.L. & Millard, H.T., Jr (1987) Trace-element chemistry of Kilauea and Mauna Loa lava in space and time: a reconnaissance. United States Geological Survey Professional Paper 1350:641-689.

Tilling R.I. & Dvorak J.J. (1993) Anatomy of a basaltic volcano. *Nature* 363:125-133.

Tollstrup D.L. & Gill J.B. (2005) Hafnium systematics of the Mariana arc: evidence for sediment melt and residual phases. *Geology* 33:737-740.

Trusdell F.A. (1991) The 1840 eruption of Kilauea volcano: petrologic and volcanologic constraints on rift zone processes. Master Thesis, University of Hawaii, Manoa 109 p.

Trusdell F.A., Wolfe E.W., & Morris J. (2005) Digital database of the geologic map of the Island of Hawaii. United States Geological Survey Data Series 144.

Trusdell F.A., Moore R.B., & Sako M.K. (2006) Preliminary geologic map of Mount Pagan Volcano, Pagan Island, Commonwealth of the Northern Mariana Islands: U.S. Geol Survey Open-File Report 2006-1386, 32 p.

Turner S.P. & Hawkesworth C.J. (1997) Constraints on flux rates and mantle dynamics beneath island arcs from Tonga-Kermadec lava geochemistry. *Nature* 389:568-573.

Turner S.P., Regelous M., Hawkesworth C.J., & Rostami K. (2006) Partial melting processes above subducting plates: constraints from ^{231}Pa - ^{235}U disequilibria. *Geochimica et Cosmochimica Acta* 70:480-503.

- Ulmer P. (1989) The dependence of the Fe²⁺-Mg cation-partitioning between olivine and basaltic liquid on pressure, temperature and composition. *Contributions to Mineralogy and Petrology* 101:261-271.
- Vlastevic I., Aslanian D.L.D., Bougault H., Olivet J.L., & Geli L. (1999) Large-scale chemical and thermal division of the Pacific mantle. *Nature* 399:345-350.
- Vlastelic I., Staudacher T., & Semet M. (2005) Rapid change of lava composition from 1998 to 2002 at Piton de la Fournaise (Reunion) inferred from Pb isotopes and trace elements; evidence for variable crustal contamination. *Journal of Petrology* 46:79-107.
- Wade J.A., Plank T., Stern R.J., Tollstrup D.L., Gill J.B., O'Leary J.C., Eiler J.M., Moore R.B., Woodhead J.D., Trusdell F., Fischer T.P., & Hilton D.R. (2005) The May 2003 eruption of Anatahan volcano, Mariana Islands: geochemical evolution of a silicic island-arc volcano. *Journal of Geothermal and Volcanology Research* 146:139-170.
- Wallace P.J. & Anderson A.T. (1998) Effects of eruption and lava drainback on the H₂O contents of basaltic magmas at Kilauea Volcano. *Bulletin of Volcanology* 59:327-344.
- Wanless V. D., Garcia M. O., Trusdell F. A., Rhodes J. M., Norman M. D., Weis D. Fornari D. J., Kurz M. D., & Guillou H. (2006) Submarine radial vents on Mauna Loa volcano, Hawaii. *Geochemistry, Geophysics, Geosystems* 7, doi: 10.1029/2005GC001086.
- Watson S. & McKenzie D. (1991) Melt generation by plumes: a study of Hawaiian volcanism. *Journal of Petrology* 32:501-537.
- Wendt J.I., Regelous M., Niu Y., Hekinian R., & Collerson K.D. (1999) Geochemistry of lavas from the Garrett Transform Fault: insights into mantle heterogeneity beneath the eastern Pacific. *Earth and Planetary Science Letters* 173:271-284.
- West H.B. & Leeman W.P. (1987) Isotopic evolution of lavas from Haleakala volcano, Hawaii. *Earth and Planetary Science Letters* 84:211-225.
- Wilcox R.E. (1954) Petrology of Paricutin volcano, Mexico. *United States Survey Bulletin B*

0965-C, 281-354.

Williams R.W. & Gill J.B. (1989) Effects of partial melting on the uranium decay series.

Geochimica et Cosmochimica Acta 53:1607-1619.

Wolfe E.W., Garcia M.O., Jackson D.B., Koyanagi R.Y., Neal C.A. & Okamura A.T. (1987) The Puu Oo eruption of Kilauea volcano, episodes 1 through 20, January 3, 1983, to June 8, 1984. In:

Decker R.W., Wright T.L., & Stauffer P.H. (eds.), *Volcanism in Hawaii*. United States

Geological Survey Professional Paper 1350:471-508.

Woodhead J.D. (1989) Geochemistry of the Mariana arc (western Pacific): source compositions and processes. *Chemical Geology* 76:1-24.

Woodhead J.D., Hergt J.M., Davidson J.P., & Eggins S.M. (2001) Hafnium isotope evidence for 'conservative' element mobility during subduction zone processes. *Earth and Planetary Science Letters* 192:331-346.

Woodhead J.D., Trusdell F., Fischer T.P., & Hilton D.R. (2005) The May 2003 eruption of Anatahan volcano, Mariana Islands: geochemical evolution of a silicic island-arc volcano. *Journal of Volcanology Geothermal Research* 146:139-170.

Workman R.K. & Hart S.R. (2005) Major and trace element composition of the depleted MORB mantle (DMM). *Earth and Planetary Science Letters* 231:53-72.

Wright T.L. (1971) *Chemistry of Kilauea and Mauna Loa in space and time*. United States Geological Survey Professional Paper 735. 40 p.

Wright T.L. & Fiske R.S. (1971) Origin of differentiated and hybrid lavas of Kilauea Volcano, Hawaii. *Journal of Petrology* 12:1-65.

Wright T.L., Swanson, D.A., & Duffield W.A. (1975) Chemical compositions of Kilauea east-rift lava, 1968-1971. *Journal of Petrology* 16:110-133.

Wright T.L. & Tilling R.I. (1980) Chemical variation in Kilauea eruptions 1971-1974. *American Journal of Science* 280-A:777-793.

- Wright T.L. & Helz R.T. (1996) Differentiation and magma mixing on Kilauea's east rift zone: a further look at the eruptions of 1955 and 1960. Part 2. The 1960 lavas. *Bulletin of Volcanology* 57:602-630.
- Wright T.L. & Klein F.W. (2006) Deep magma transport at Kilauea Volcano, Hawaii. *Lithos* 87:50-79.
- Wright T.L. & Klein F.W. (2008) Dynamics of magma supply to Kilauea volcano, Hawaii: integrating seismic, geodetic, and eruption data. In: Annen C. & Zellmer G.F. (eds.), *Dynamics of crustal magma transfer, storage, and differentiation*. Geological Society, London Special Publications 304:83-116.
- Wyss M. & Koyanagi R.Y. (1992) Isoleismal maps, macroseismic epicenters and estimated magnitudes of historic earthquakes in the Hawaiian Islands. United States Geological Survey Bulletin 2006, 93 p.
- Xu G., Frey F.A., Clague D.A., Abouchami W., Blichert-Toft J., Cousens B. & Weisler M. (2007) Geochemical characteristics of West Molokai shield- and postshield-stage lavas: constraints on Hawaiian plume models. *Geochemistry, Geophysics, Geosystems* 8, doi:10.1029/2006GC001554.
- Yang X., Davis P.M., Delaney P.T., & Okamura A.T. (1992) Geodetic analysis of dike intrusion and motion of the magma reservoir beneath the summit of Kilauea Volcano, Hawaii; 1970-1985. *Journal of Geophysical Research* 97:3305-3324.